

Aus dem  
Centrum für Biomedizin und Medizintechnik Mannheim (CBTM)  
der Medizinischen Fakultät Mannheim  
Abteilung für Kardiovaskuläre Physiologie  
Leiter: Prof. Dr. med. Schubert

The role of vascular smooth muscle  $K_v7$  channels  
in renal perfusion

Inauguraldissertation  
zur Erlangung des medizinischen Doktorgrades  
der  
Medizinischen Fakultät Mannheim  
der Ruprecht-Karls-Universität  
zu  
Heidelberg

vorgelegt von  
Felix Stocker

aus  
Berchtesgaden  
2019

Dekan: Prof. Dr. med. Sergij Goerd  
Referent: Prof. Dr. med. Rudolf Schubert

In Dankbarkeit  
meinen Eltern

# TABLE OF CONTENTS

	Page
ABBREVIATIONS .....	1
<b>1 INTRODUCTION .....</b>	<b>4</b>
1.1 Function of the cardiovascular system.....	4
1.2 Cardiovascular function and autoregulation of the kidney.....	4
1.3 Vascular microscopic anatomy.....	4
1.4 Mechanisms of vasoconstriction .....	4
1.4.1 Vasoconstriction from a mechanistic-focused perspective .....	5
1.4.2 Vasoconstriction from an organism-focused perspective .....	6
1.5 Mechanisms of vasorelaxation.....	6
1.5.1 Vasorelaxation from a mechanistic-focused perspective .....	6
1.5.2 Vasorelaxation from an organism-focused perspective.....	7
1.5.2.1 cGMP/PKG .....	7
1.5.2.2 cAMP/PKA.....	7
1.6 Potassium channels in vascular reactivity.....	8
1.6.1 $K_{ir}$ .....	8
1.6.2 $K_{ATP}$ .....	9
1.6.3 $BK_{Ca}$ .....	9
1.6.4 $K_v$ .....	10
1.6.4.1 $K_v1-4$ .....	10
1.6.4.2 $K_v7$ .....	10
1.6.4.2.1 KCNQ genes and $K_v7$ channel structure .....	11
1.6.4.2.2 $K_v7$ expression .....	11
1.6.4.2.3 $K_v7$ pharmacology.....	12
1.6.4.2.4 $K_v7$ regulation .....	13
1.6.4.2.5 Role of $K_v7$ in vascular physiology .....	15
1.6.4.2.6 Role of $K_v7$ in vascular pathology .....	16
1.7 Objective of this thesis .....	17
<b>2 METHODS.....</b>	<b>19</b>

2.1	Animal Model .....	19
2.2	Solutions .....	19
	Source .....	20
2.3	Drugs.....	21
2.4	Myography .....	22
2.4.1	The myography setup .....	22
2.4.2	Macroscopic preparation .....	22
2.4.3	Microscopic preparation .....	23
2.4.4	Principles of measurement.....	23
2.4.5	Normalization .....	24
2.4.6	Viability testing.....	25
2.4.7	Experimental protocols .....	26
2.4.7.1	Concentration-response relationship protocols .....	26
2.4.7.2	Precontraction protocols.....	27
2.4.8	Data analysis.....	28
2.5	Isolated perfused kidney .....	29
2.5.1	Isolated perfused kidney setup .....	30
2.5.2	Macroscopic preparation .....	33
2.5.3	Microscopic preparation .....	34
2.5.4	Preparation of the isolated perfused kidney setup.....	35
2.5.5	Viability testing.....	35
2.5.6	Experimental protocols .....	36
2.5.7	Data analysis.....	37
2.6	Statistics.....	38
<b>3</b>	<b>RESULTS .....</b>	<b>39</b>
3.1	Validation of the isolated perfused kidney model .....	39
3.2	Contribution of $K_{v7.2-5}$ to agonist-induced renal vasoconstriction.....	48
3.3	Contribution of $K_{v7.1}$ to agonist-induced renal vasoconstriction .....	52
3.4	Contribution of $K_{v7}$ to the anticontractile effect of ANP in agonist-induced renal vasoconstriction .....	55
3.5	Contribution of $K_{v7}$ to the anticontractile effect of Urocortin in agonist-induced renal vasoconstriction .....	64
3.6	Contribution of $K_{v7}$ to agonist-induced vasoconstriction in isolated perfused kidneys .....	72

4 DISCUSSION.....	79
4.1 Validating the isolated perfused kidney model.....	79
4.1.1 Perfusion flow rate .....	79
4.1.2 Viability tests .....	79
4.1.3 Comparability of kidneys from different rats.....	80
4.1.4 Confounding factors .....	81
4.1.5 Organ edema .....	81
4.1.6 Limitations .....	81
4.2 Contribution of $K_v7.2-5$ to agonist-induced renal vasoconstriction.....	82
4.3 Contribution of $K_v7.1$ to agonist-induced renal vasoconstriction .....	87
4.4 Contribution of $K_v7$ to the anticontractile effect of ANP in agonist-induced renal vasoconstriction .....	90
4.5 Contribution of $K_v7$ to the anticontractile effect of Urocortin in agonist-induced renal vasoconstriction .....	93
5 SUMMARY.....	96
6 BIBLIOGRAPHY .....	97
7 APPENDIX.....	121
8 CURRICULUM VITAE .....	123
9 DANKSAGUNG.....	124

## ABBREVIATIONS

4-AP	4-aminopyridine
AC	adenylyl cyclase
ACh	acetylcholine
ADP	adenosine diphosphate
AKAP	A-kinase-anchoring protein
ANP	atrial natriuretic peptide
ATP	adenosine triphosphate
AT <sub>1</sub> R	angiotensin II receptor type 1
AUC	area under the curve
BK <sub>Ca</sub>	large conductance calcium-activated potassium channels
BSA	bovine serum albumin
Ca <sup>2+</sup>	calcium ions
[Ca <sup>2+</sup> ] <sub>i</sub>	intracellular calcium concentration
Ca <sup>2+</sup> /CaM	Ca <sup>2+</sup> -calmodulin complex
CaD	caldesmon
CaM	calmodulin
CGRP	calcitonin gene-related peptide
CO	cardiac output
CO <sub>2</sub>	carbon dioxide
cAMP	cyclic adenosine monophosphate
cGMP	cyclic guanosine monophosphate
CRR	concentration-response relationship
DAG	diacylglycerol
DMSO	dimethyl sulfoxide
DPO-1	diphenyl phosphine oxide-1
EC <sub>50</sub>	half maximal effective concentration
EDTA	ethylenediaminetetraacetic acid
EGTA	ethylene glycol-bis(β-aminoethyl ether)-N,N,N',N'-tetraacetic acid
EPAC	exchange protein directly activated by cAMP

eNOS	endothelial nitric oxide synthase
GC	guanylyl cyclase
GFR	glomerular filtration rate
GPCR	G protein coupled receptor
GTP	guanosine triphosphate
HEPES	4-(2-hydroxyethyl)-1-piperazineethanesulfonic acid
IBTX	iberiotoxin
IC	internal circumference
IC <sub>1</sub>	IC at which a maximum response to a vasoconstrictor is observed
IC <sub>50</sub>	half maximal inhibitory concentration
IC <sub>100</sub>	IC at which a transmural wall pressure of 100mmHg is observed
iNOS	inducible nitric oxide synthase
IP <sub>3</sub>	inositol 1,4,5-trisphosphate
IP <sub>3</sub> R	inositol 1,4,5-trisphosphate receptor
K <sup>+</sup>	potassium ions
K <sub>ATP</sub>	ATP-sensitive potassium channel
K <sub>ir</sub>	inward rectifier potassium channel
K <sub>v</sub>	voltage-gated potassium channel
KCl	potassium chloride
LCA	left coronary artery
L-NNA	N <sup>G</sup> -Nitro-L-arginine-methyl ester
LTCC	L-type calcium channel
MLCK	myosin light chain kinase
MLCP	myosin light chain phosphatase
Mx	methoxamine hydrochloride
MYPT1	myosin phosphatase target subunit 1
NCX	Na <sup>+</sup> /Ca <sup>2+</sup> exchanger
Na <sup>+</sup>	sodium ions
pD <sub>2</sub>	negative logarithm of the half maximal effective concentration (EC <sub>50</sub> )
PAH	pulmonary arterial hypertension
PCR	polymerase chain reaction

PKA	cAMP-dependent protein kinase
PKC	protein kinase C
PKG	cGMP-dependent protein kinase
PLC	phospholipase C
PMCA	plasma membrane Ca <sup>2+</sup> ATPase
PSS	physiological salt solution
PVAT	perivascular adipose tissue
qPCR	quantitative polymerase chain reaction
RAAS	renin-angiotensin-aldosterone system
RBC	red blood cell
RBF	renal blood flow
RPP	renal perfusion pressure
ROCK	Rho-associated protein kinase
RCA	right coronary artery
RLC	regulatory light chain
rpm	rounds per minute
RyR	ryanodine receptor
SEM	standard error of the mean
SERCA	sarco/endoplasmic reticulum Ca <sup>2+</sup> -ATPase
SHR	spontaneously hypertensive rat
SOPF	specific and opportunistic pathogen free
SPF	specific pathogen free
STX	stromatoxin
SVR	systemic vascular resistance
TGF	tubuloglomerular feedback
TRP	transient receptor potential
V <sub>50</sub>	voltage at which half maximal activation is observed
V <sub>m</sub>	membrane potential
VOCC	voltage-operated calcium channel
VSMC	vascular smooth muscle cell

## 1 INTRODUCTION

### 1.1 Function of the cardiovascular system

The circulatory system serves to enable cell homeostasis in an organism that is too large to be supplied by diffusion. Through the mechanism of convection, it contributes to cell respiration and metabolism by providing oxygen, water and nutrients while removing carbon dioxide and wasteful metabolites. Simultaneously, it acts as a transport and communication system for distributing intermediary metabolites or even cells and for delivering hormones or autacoids. Complex mechanisms are necessary for regulation of blood distribution between and within organs to match cellular demand. Convection of blood happens along blood pressure gradients; blood pressure is the product of cardiac output (CO) and systemic vascular resistance (SVR), and vascular resistance is largely determined by the tone of small arteries and arterioles<sup>1-3</sup>. Overall, the regulation of blood vessel tone is subject to involuntary systemic mechanisms. The three main players orchestrating vascular tone are the autonomic nervous system infiltrating the vessel wall, the autoregulatory mechanisms of the vessel itself, and the hormones, autacoids or other agents influencing the vessel from the luminal as well as from the abluminal side<sup>4</sup>.

### 1.2 Cardiovascular function and autoregulation of the kidney

The kidney plays a central role in the circulatory system due to its excretory, hormonal and metabolic functions contributing to intravascular fluid maintenance and blood pressure control. Most prominent among these many mechanisms the kidney contributes to is the renin-angiotensin-aldosterone system (RAAS), which relies upon secretion of the hormone renin from renal juxtaglomerular cells into systemic circulation to first stimulate formation of angiotensin I and subsequent conversion into angiotensin II through the angiotensin-converting enzyme (ACE)<sup>5</sup>. The RAAS is of central function in the regulation of blood pressure and is target of two main groups of antihypertensive drugs, ACE-inhibitors and angiotensin receptor blockers. To fulfil its complex integrative task, the kidney itself vitally depends upon fine-tuned regulation of blood supply. Renal autoregulation maintains renal blood flow (RBF) and glomerular filtration rate (GFR) independent of renal perfusion pressure (RPP) in a manner distinguished from most other organs insofar as it is intrinsic to the kidney and thus largely independent of extrinsic nervous regulation or circulating hormones<sup>6</sup>. Thus, the tone of renal resistance arteries is intrinsically determined by an interplay of two major mechanisms, the relatively quickly-acting renal myogenic response<sup>7</sup> and the more delayed macula densa tubuloglomerular feedback response<sup>8,9</sup>.

### 1.3 Vascular microscopic anatomy

Blood vessels generally consist of three distinct layers<sup>10</sup>. The innermost *tunica intima* is made up of a single layer of endothelial cells mounted on a basal lamina, which besides regulating vascular tone are involved in immunological and inflammatory processes<sup>11</sup>. Underneath it the three-dimensional *tunica media* is the thickest layer in arterial vessels and besides elastic fibers for structural support contains mostly the vascular smooth muscle cells (VSMC) responsible for active contraction and relaxation<sup>12</sup>. The outermost *tunica adventitia* consists of fibroelastic connective tissue fixating the vessel in its environment and contains nervous plexus participating in the control of vessel tone<sup>10</sup>.

### 1.4 Mechanisms of vasoconstriction

VSMCs can be stimulated by a variety of mechanisms that eventually converge to the common end point of increasing actin-myosin interaction, resulting in ATP-powered myosin lever arm rotations that cause VSMC shortening and exertion of force<sup>13</sup>. This may happen either through activation of the

motor protein myosin II via phosphorylation of its regulatory light chain (RLC) or through removal of actin filament inhibition<sup>14</sup>. First, actin-myosin interaction as a prerequisite requires the exposure of the myosin-binding sites on the actin surface through phosphorylation of Caldesmon (CaD), which otherwise inhibits myosin ATPase activity<sup>15</sup>. Second, the contractile state of VSMCs largely depends on the state of myosin RLC phosphorylation, which is increased by myosin light chain kinase (MLCK) and decreased by myosin light chain phosphatase (MLCP)<sup>16</sup>.

From a mechanistic-focused perspective, one can differentiate (i) VSMC activation through electromechanical or pharmacomechanical coupling<sup>17</sup> and (ii) Calcium ( $\text{Ca}^{2+}$ )-dependent mechanisms from  $\text{Ca}^{2+}$  sensitization<sup>16</sup>. From an organism-focused perspective, VSMC activation may be induced or supported by the autonomic nervous system, by vasoactive substances like hormones, autacoids and metabolites, or by transmural pressure<sup>18</sup>. For the sake of structural comprehensiveness, these two perspectives will in the following be elaborated consecutively, first elucidating the mechanistic elements and then drawing the bigger picture of their implementation in the organism.

#### 1.4.1 Vasocontraction from a mechanistic-focused perspective

VSMC activation can be systematized into electromechanical and pharmacomechanical coupling<sup>17</sup> or  $\text{Ca}^{2+}$ -dependent and  $\text{Ca}^{2+}$ -sensitizing mechanisms<sup>16</sup>.

Electromechanical coupling operates through membrane potential ( $V_m$ ) changes that affect the cytoplasmic  $\text{Ca}^{2+}$  level<sup>17</sup>. A depolarizing stimulus, by shifting the negative resting  $V_m$  of VSMC (-40 to -70 mV) to more positive potentials, can open voltage-operated  $\text{Ca}^{2+}$  channels (VOCC)<sup>19</sup>. Depolarization can be induced through action potentials in phasic (e.g. intestinal) smooth muscle or graded depolarization in tonic (e.g. vascular) smooth muscle<sup>19</sup>. Among the multitude of membrane-associated proteins involved in  $V_m$  regulation, ion channels like potassium ( $\text{K}^+$ ) channels are primarily important structures which when blocked contribute to VSMC depolarization<sup>1</sup>.

Pharmacomechanical coupling includes various cellular signaling mechanisms that show the common feature of changing VSMC force generation without requiring changes in  $V_m$ <sup>17</sup>. Its major two mechanisms governing contraction are increasing cytosolic  $\text{Ca}^{2+}$  [ $\text{Ca}^{2+}$ ]<sub>i</sub> in a manner not dependent on VOCC but largely on inositol 1,4,5-trisphosphate ( $\text{IP}_3$ ) and increasing the  $\text{Ca}^{2+}$  sensitivity of the contractile apparatus<sup>19</sup>.

$\text{Ca}^{2+}$ -dependent mechanisms of contraction are of central importance, since an increase of [ $\text{Ca}^{2+}$ ]<sub>i</sub> is the primary stimulus for VSMC activation<sup>20</sup>.  $\text{Ca}^{2+}$  binds to calmodulin, forming the  $\text{Ca}^{2+}$ -calmodulin complex ( $\text{Ca}^{2+}/\text{CaM}$ ) that activates MLCK to phosphorylate the myosin RLC and thus enables contractile activity<sup>21</sup>. Elevation of [ $\text{Ca}^{2+}$ ]<sub>i</sub> may result from passive transmembrane movement along electrochemical gradients, either in form of extracellular  $\text{Ca}^{2+}$  influx through plasma membrane ion channels or via release from intracellular  $\text{Ca}^{2+}$  stores<sup>20</sup>. In VSMCs, influx of extracellular  $\text{Ca}^{2+}$  is mediated primarily by voltage-gated L-type  $\text{Ca}^{2+}$  channels (LTCC), with contributions from T-type  $\text{Ca}^{2+}$  channels and  $\text{Ca}^{2+}$ -permeable ligand-gated or transient receptor potential (TRP) cation channels, whereas  $\text{Ca}^{2+}$  release from intracellular stores is mediated by sarcoplasmic membrane ryanodine receptors (RyR) and  $\text{IP}_3$ -receptors ( $\text{IP}_3\text{R}$ )<sup>22</sup>. While the  $\text{IP}_3\text{R}$  releases  $\text{Ca}^{2+}$  when activated by  $\text{IP}_3$  following activation of PLC, the RyR is activated by an increase in [ $\text{Ca}^{2+}$ ]<sub>i</sub> itself, which is referred to as  $\text{Ca}^{2+}$ -induced  $\text{Ca}^{2+}$  release<sup>23</sup>.

$\text{Ca}^{2+}$ -sensitizing mechanisms of contraction have in common the ability to induce tonic contraction with only transient increases or differing magnitudes of [ $\text{Ca}^{2+}$ ]<sub>i</sub>, which has been labeled  $\text{Ca}^{2+}$  sensitization<sup>14</sup>. Changes in  $\text{Ca}^{2+}$  sensitivity of the contractile apparatus may occur through increasing the ratio of activity of MLCK over MLCP, resulting in a higher degree of myosin RLC phosphorylation and thus myosin activity<sup>16</sup> or through increasing the activity of ERK, which by phosphorylating CaD results in a higher degree of actin availability<sup>14, 15</sup>. The former and more well-studied mechanism involves inhibition of MLCP through two different G protein coupled receptor (GPCR)-mediated pathways. One pathway involves activation of the monomeric G protein RhoA and its effector Rho-associated protein

kinase (ROCK) that may directly inhibit MLCP, while another employs the MLCP inhibitor CPI-17, which can be activated via phosphorylation through either ROCK or protein kinase C (PKC), the latter resulting from  $G_{q/11}$ -mediated activation of phospholipase C (PLC) producing the PKC activator diacylglycerol (DAG) <sup>16</sup>.

#### 1.4.2 Vasoconstriction from an organism-focused perspective

Putting things into perspective, in the organism it is an interplay of the above described fundamental mechanisms which in concert define the level of VSMC activation and vascular tone.

One key principle is endocrine and paracrine regulation through circulating vasoconstrictors including hormones like noradrenaline, angiotensin II (AII) or vasopressin and autacoids like endothelin 1 (ET-1) <sup>24</sup>. After binding to their corresponding membrane receptor, they may through  $G_{q/11}$ -mediated activation of PLC induce both  $IP_3$  formation with consecutive  $IP_3$ R-mediated  $Ca^{2+}$  release from intracellular stores and DAG formation with consecutive PKC-dependent phosphorylation of CPI-17 inhibiting MLCP <sup>25</sup>, thus combining  $Ca^{2+}$ -dependent and  $Ca^{2+}$ -sensitizing mechanisms of contraction. Additionally, PKC may activate VOCC indirectly through membrane depolarization by means of reducing  $K^+$  currents through inhibitory phosphorylation of voltage dependent  $K^+$  channels ( $K_v$ ) <sup>26, 27</sup>, large conductance  $Ca^{2+}$ -activated  $K^+$  channels ( $BK_{Ca}$ ) <sup>28-33</sup>, inward rectifier  $K^+$  channels ( $K_{ir}$ ) <sup>34-36</sup> and ATP-sensitive  $K^+$  channels ( $K_{ATP}$ ) <sup>36-41</sup>, thus also including both electromechanical and pharmacomechanical coupling in agonist-induced contraction. The autonomic nervous system releasing the neurotransmitter noradrenaline from nerve endings in the blood vessel wall to increase vascular tone <sup>42</sup> is another example involving a similar combination of mechanisms.

Another major principle relevant to the maintenance of arteriolar blood flow is the myogenic response, which is the term describing the phenomenon that an increase in transmural pressure results in arterial constriction, while a decrease in pressure is followed by dilation <sup>18, 43</sup>. Stimulated by a change in wall tension, a not yet clearly defined sensor, possibly stretch-activated cation channels from the TRP channel family, initiates cell membrane depolarization and activation of VOCCs and  $Ca^{2+}$  entry, while simultaneously mechano-transduction mechanisms independent of stretch-activated channels and/or signaling pathways including ROCK- or PKC-mediated  $Ca^{2+}$  sensitization appear to contribute <sup>14, 43</sup>. The myogenic response accordingly is also orchestrated by both  $Ca^{2+}$ -dependent and  $Ca^{2+}$ -sensitizing mechanisms, but unlike agonist-induced vasoconstriction does not require pharmacomechanical coupling yet includes electromechanical coupling.

#### 1.5 Mechanisms of vasorelaxation

Vascular relaxation may occur passively through a decrease of the contractile stimulus towards the VSMC or actively through specific vasodilatory agonists acting through the intracellular messengers cyclic guanosine monophosphate (cGMP) or cyclic adenosine monophosphate (cAMP) <sup>44</sup>. Common end point is the decrease of actin-myosin interaction, resulting from a lower level of myosin RLC phosphorylation or from lower actin availability <sup>14</sup>.

##### 1.5.1 Vasorelaxation from a mechanistic-focused perspective

Analogously to vasoconstriction, vasodilation may involve antagonization of all mechanistic elements described above (see: Chapter 1.4.1).

Counteracting electromechanical coupling may occur through VSMC hyperpolarization, which decreases the open probability of VOCC, reduces  $Ca^{2+}$  influx and lowers  $[Ca^{2+}]_i$  <sup>19</sup>. Membrane hyperpolarization most importantly involves, but is not limited to, increased outward  $K^+$  currents <sup>1</sup>.

Counteracting pharmacomechanical coupling may besides receptor antagonization of the contractile substance involve inhibition of IP<sub>3</sub>-dependent Ca<sup>2+</sup> release or decreasing Ca<sup>2+</sup> sensitivity of the contractile apparatus<sup>19</sup>.

Ca<sup>2+</sup>-dependent mechanisms of vasorelaxation reduce VSMC activity by lowering [Ca<sup>2+</sup>]<sub>i</sub> either through inhibition of Ca<sup>2+</sup> influx and/or release from intracellular stores or by actively removing Ca<sup>2+</sup> from the cytosol, both resulting in lowered CaM levels and decreased MLCK activity<sup>20,21</sup>. Outward transport of Ca<sup>2+</sup> across membranes is against its electrochemical gradient and therefore happens energy-dependently through active or secondary active transport via the plasma membrane Ca<sup>2+</sup> ATPase (PMCA) and Na<sup>+</sup>/Ca<sup>2+</sup> exchanger (NCX) or through the sarco/endoplasmic reticulum Ca<sup>2+</sup>-ATPase (SERCA)<sup>22</sup>. Both PMCA and SERCA function can be enhanced by PKC activation<sup>45</sup>.

Ca<sup>2+</sup>-desensitizing mechanisms of vasorelaxation right-shift the relation between VSMC force production and [Ca<sup>2+</sup>]<sub>i</sub> and are determined by a reduction in myosin RLC phosphorylation<sup>16</sup>. Aside from receptor antagonization of GPCR dependent vasoconstrictive agonists, these mechanisms may involve a vast array of interactions between intracellular signaling cascades, many of which target the myosin phosphatase target subunit 1 (MYPT1), a regulatory subunit of MLCP<sup>16</sup>. The RhoA/ROCK pathway is most prominent among these cascades for its phosphorylation of MYPT1 inhibiting MLCP function<sup>46</sup> and this specific inhibitory phosphorylation may be prevented by MYPT1 phosphorylation through protein kinase G (PKG)<sup>47, 48</sup>, which is thus considered a Ca<sup>2+</sup> desensitizing mechanism<sup>14</sup>. Ca<sup>2+</sup> desensitization via increased MLCP activity may also occur in form of MYPT1 dephosphorylation through protein kinase A (PKA)<sup>49,50</sup>. However, MYPT1 regulation is quite complex not only due to the vast number of kinases that may be involved, but also to its tissue-specificity<sup>14</sup>.

### 1.5.2 Vasorelaxation from an organism-focused perspective

Like in vasoconstriction, it is mostly combinations of the above mechanisms that are observed in vasodilator actions in the organism. The two key players among the intracellular second messengers involved in VSM relaxation are the cyclic nucleotides cGMP and cAMP, which (i) are generated by nucleotide cyclases – guanylate cyclase (GC) resp. adenylate cyclase (AC); (ii) exert their effect by activating cyclic nucleotide-driven kinases – cGMP-dependent kinase (PKG) resp. cAMP-dependent kinase (PKA), and (iii) are degraded by various phosphodiesterases (PDE)<sup>51</sup>.

#### 1.5.2.1 cGMP/PKG

cGMP in VSMCs can be generated by soluble cytosolic GCs activated by nitric oxide (NO)<sup>52</sup> or carbon monoxide<sup>53</sup> and by membrane-bound GCs activated by transmembrane receptors for the natriuretic peptide family<sup>54</sup>. The main, though not exclusive, effector of cGMP is PKG<sup>55</sup>. Either or both cGMP and PKG have been implemented in various anticontractile mechanisms. These involve (i) inhibition of G<sub>q/11</sub> mediated signaling<sup>56,57</sup>, (ii) lowering of [Ca<sup>2+</sup>]<sub>i</sub> through activation of PMCA<sup>58,59</sup>, SERCA<sup>60-62</sup> or NCX<sup>63,64</sup> as well as inhibition of Ca<sup>2+</sup> release through inhibition of IP<sub>3</sub>R<sup>65-68</sup> or of Ca<sup>2+</sup> influx through VOCC<sup>69</sup>; (iii) supporting Ca<sup>2+</sup> desensitization through protective phosphorylation of MYPT1 to prevent inhibition by various kinases<sup>47,48,70</sup> or phosphorylation of RhoA to prevent activation of ROCK<sup>71-73</sup> and (iv) VSMC hyperpolarization through activation of outward K<sup>+</sup> currents through K<sub>v</sub><sup>74-77</sup>, K<sub>ATP</sub><sup>78-81</sup> or BK<sub>Ca</sub><sup>76,82-85</sup>.

#### 1.5.2.2 cAMP/PKA

cAMP formation in VSM is most importantly controlled by GPCRs like the β<sub>2</sub> adrenergic receptor which is coupled to the G protein G<sub>s</sub><sup>86</sup>, but may also result from activation of corticotropin releasing factor (CRF)-receptors<sup>87</sup>, both which are linked to ACs<sup>86,88</sup>. Cross-talk exists between cAMP and cGMP signaling insofar as both cyclic nucleotides can activate both kinases at 10 times higher concentrations, although this may occur only unidirectionally since plasma concentrations of cAMP are 10-fold higher than cGMP<sup>55</sup>. This way, cAMP may also activate PKG, which has been observed in cAMP-induced PKG-

mediated inhibition of IP<sub>3</sub>R<sup>65, 66</sup> or VOCC<sup>69</sup> as well as activation of BK<sub>Ca</sub><sup>89</sup>. Otherwise, the specific implications for cAMP/PKA signaling are similar to those of cGMP/PKG and thus include (i) notably, phosphorylation of MLCK leading to decreased MLCK activity<sup>90, 91</sup>, (ii) Ca<sup>2+</sup> desensitization through protective phosphorylation of MYPT1 preventing MLCP inhibition by other kinases<sup>47, 49</sup> or through inhibition of RhoA/ROCK<sup>92, 93</sup> and (iii) activation of hyperpolarizing K<sup>+</sup> currents through K<sub>v</sub><sup>94-104</sup>, BK<sub>Ca</sub><sup>105-109</sup>, K<sub>ATP</sub><sup>1, 39, 99, 110-114</sup> and also K<sub>ir</sub><sup>115, 116</sup>.

## 1.6 Potassium channels in vascular reactivity

As can be perceived from the above, K<sup>+</sup> channels play a central role in regulating VSMC activity: with their significant influence on V<sub>m</sub> they contribute to electromechanical and Ca<sup>2+</sup>-dependent mechanisms, and due to interaction with intracellular kinases, they also participate in pharmacomechanical and Ca<sup>2+</sup>-sensitizing mechanisms. Accordingly, K<sup>+</sup> channels are involved in all vasoregulation through agonist-induced contraction, the myogenic response and cyclic nucleotide-mediated dilation.

Although the K<sup>+</sup> equilibrium potential at physiological intra- and extracellular K<sup>+</sup> concentrations according to the Nernst equation is -85 mV, V<sub>m</sub> is in general more positive due to the presence of the other permeant ions and their respective channels<sup>117</sup>. V<sub>m</sub> in VSMCs from renal interlobar artery and afferent arterioles has been reported to be in the range of -40 mV<sup>118</sup> to -55 mV<sup>119</sup>. The conductance for K<sup>+</sup> exceeds that of the other ions in VSMCs; due to their high membrane resistance<sup>120</sup> only small numbers of K<sup>+</sup> channels are necessary to influence V<sub>m</sub> and therefore small changes in K<sup>+</sup> conductance will have a rather large effect on V<sub>m</sub>, which in turn has a steep relationship to arterial tone<sup>1, 121</sup>. Thus, inhibition of relatively few K<sup>+</sup> channels may considerably decrease K<sup>+</sup> efflux, causing membrane depolarization which through increasing the open probability of VOCC leads to vasoconstriction, whereas activation of K<sup>+</sup> channels may enhance K<sup>+</sup> conductance, resulting in membrane hyperpolarization and vasodilation<sup>1, 120</sup>.

Four classes of VSMC K<sup>+</sup> channels that have been identified in the renal vasculature<sup>121</sup> and shown to affect baseline renal vascular resistance<sup>122</sup> are the inward rectifier K<sub>ir</sub>, the ATP-sensitive K<sub>ATP</sub>, the large conductance Ca<sup>2+</sup>-activated BK<sub>Ca</sub> and various voltage-gated K<sub>v</sub> channels<sup>1</sup>. A common structural theme shared by all of these are two transmembrane domains forming the ion-permeable pore which are linked by a pore-loop responsible for ion selectivity and pore regulation<sup>123</sup>.

### 1.6.1 K<sub>ir</sub>

Inward rectifier K<sup>+</sup> channels derive their name from their ability to conduct K<sup>+</sup> ions into cells at V<sub>m</sub> negative to the K<sup>+</sup> equilibrium potential, which is limited at more positive V<sub>m</sub> levels<sup>124, 125</sup>. Nonetheless, at physiological V<sub>m</sub> the electrochemical gradient will direct K<sup>+</sup> currents through K<sub>ir</sub> outwards from the cell<sup>1</sup>, while at elevated extracellular K<sup>+</sup> concentrations, for example resulting from increased metabolism, K<sub>ir</sub> conduct increased hyperpolarizing currents resulting in vessel dilation<sup>126</sup>. Currents through K<sub>ir</sub> channels contribute to resting V<sub>m</sub> in isolated VSMCs and to resting tone in isolated resistance arteries from several vascular beds, while K<sub>ir</sub> expression and function appears to be inversely related to vessel diameter<sup>123</sup>.

K<sub>ir</sub> are predominantly expressed in small resistance arteries including renal afferent arterioles<sup>127</sup> and have been found to conduct K<sup>+</sup> currents in afferent arterioles<sup>127</sup> and in distal but not proximal interlobar arteries<sup>128</sup>. Barium (Ba<sup>2+</sup>) has been shown to depolarize and constrict rat renal afferent arterioles<sup>127, 129, 130</sup> and interlobular arteries<sup>128</sup> and to increase renal vascular resistance in isolated perfused kidneys<sup>131</sup> as well as in vivo<sup>132</sup>. Regulation of K<sub>ir</sub> has in different vascular beds been shown to involve inhibition through PKC during agonist-induced contraction<sup>34-36</sup> or activation through cAMP/PKA-dependent pathways during vasodilation induced by adenosine<sup>115</sup> or hypoxia<sup>116</sup>.

### 1.6.2 $K_{ATP}$

ATP-sensitive  $K_{ATP}$  channels are named for their characteristic of being inhibited by elevated intracellular ATP<sup>133</sup>, although they display additional features like activation by adenosine diphosphate (ADP)<sup>134</sup>, independence of  $V_m$ <sup>1</sup> or regulation by a number of signaling pathways not including ADP/ATP, with the latter possibly being the more physiologically relevant feature in VSMCs<sup>123</sup>. However,  $K_{ATP}$  have initially been hypothesized to participate in the vascular response to changes in the metabolic state, amongst others serving to increase blood flow to hypoxic regions<sup>1</sup>. Besides, considerable evidence exists for involvement of  $K_{ATP}$  in both endogenous contractile and anticontractile pathways<sup>123</sup>.  $K_{ATP}$  channels in VSMCs can be inhibited by PKC<sup>36-41</sup> to support agonist-induced vasoconstriction or may participate in vasorelaxation when activated through cGMP/PKG<sup>78-81</sup> or cAMP/PKA<sup>1, 39, 99, 110-114</sup> dependent pathways.

$K_{ATP}$  have been confirmed to exist in small renal artery branches<sup>135</sup>. Pharmacologically,  $K_{ATP}$  can be blocked by sulfonylureas like glibenclamide<sup>1</sup> or higher concentrations of  $Ba^{2+}$ <sup>136</sup>. Renal arterial relaxation has been observed following pharmacological activation of  $K_{ATP}$  in isolated perfused kidneys<sup>137</sup> as well as in vivo<sup>138-140</sup> in a manner reversible by glibenclamide, whereas glibenclamide itself had no effect on RBF<sup>141</sup> but was able to reduce hypoxia-induced renal afferent arteriolar vasodilation<sup>142</sup>. Evidence for  $K_{ATP}$  implementation in cAMP/PKA signaling has also been presented in perfused hydronephrotic kidneys in form of glibenclamide inhibiting vasodilation induced by calcitonin gene-related peptide (CGRP)<sup>143</sup> or adenosine<sup>144</sup>.

### 1.6.3 $BK_{Ca}$

Large conductance  $Ca^{2+}$ -activated  $BK_{Ca}$  channels are voltage-gated  $K^+$  channels activated by both increases in intracellular  $Ca^{2+}$  and by depolarization of  $V_m$ <sup>145</sup>. They display a big single channel conductance, which is why upon discovery they have been hypothesized to serve as a negative feedback mechanism for controlling the degree of  $V_m$  depolarization and pressure-induced vasoconstriction<sup>146</sup>. When  $Ca^{2+}$  levels are low,  $BK_{Ca}$  behave as simple voltage-gated  $K^+$  channels<sup>147</sup>, while an increase in intracellular  $Ca^{2+}$  left-shifts voltage-dependence, allowing  $BK_{Ca}$  to conduct  $K^+$  currents at physiological  $V_m$  ranges<sup>148</sup>. In some vessels, presumably larger feed arteries,  $BK_{Ca}$  can be exposed to high  $Ca^{2+}$  ion concentration due to its close proximity to RyR<sup>149</sup>, which may conduct  $Ca^{2+}$  sparks<sup>146</sup> promoted by T-type VOCC mediated  $Ca^{2+}$  influx to activate hyperpolarizing  $BK_{Ca}$  currents as a negative feedback mechanism towards the myogenic response<sup>150, 151</sup>. In other vessels, supposedly smaller resistance arteries, it may be  $Ca^{2+}$  waves conducted by IP<sub>3</sub>R that promote  $BK_{Ca}$  activation<sup>152, 153</sup>. Overall, research has produced diverging results with regards to whether or not  $BK_{Ca}$  contribute to VSMC resting  $V_m$  and resting myogenic tone. Of the pore-forming  $\alpha$ -subunit of  $BK_{Ca}$ , which contains both the voltage sensor and the  $Ca^{2+}$  sensor domains, more than 20 different spliced variants displaying different functional properties have been identified in different tissues, possibly explaining some of the controversy about their physiological role<sup>123</sup>.

In the renal vasculature,  $BK_{Ca}$  presence has been confirmed structurally in small preglomerular vessels<sup>154</sup> and juxtaglomerular cells<sup>108</sup> as well as functionally in preglomerular vessels<sup>155</sup> and mesangial cells<sup>156</sup>. However, functional experiments have produced diverging results. Studies have found no effect of the highly specific  $BK_{Ca}$  blocker iberiotoxin (IBTX)<sup>157</sup> on arcuate artery VSMC  $V_m$  despite producing contractions of intact arteries<sup>158</sup> or reported no effect of IBTX on either in vivo resting RBF or agonist-induced decreases in RBF<sup>154</sup>. Contrarily, others have demonstrated application of  $BK_{Ca}$  activator NS-1619 to increase afferent arteriolar diameter<sup>159</sup> but not resting RBF<sup>154</sup> or to attenuate agonist-induced contractions<sup>159</sup> and RBF decreases<sup>154</sup>. It should be noted that these results may not be explicitly attributable to  $BK_{Ca}$  because NS-1619 can also affect  $K_v$  channels<sup>160</sup>. Such discrepancies in the renal vasculature have been suggested to be due to differences in  $[Ca^{2+}]_i$  or  $Ca^{2+}$  sensitivity of the channel<sup>122</sup>. Other than  $BK_{Ca}$ , a few studies have suggested the presence of the two

additional  $K_{Ca}$  family members that conduct intermediate ( $IK_{Ca}$ ) or small ( $SK_{Ca}$ )  $Ca^{2+}$ -dependent  $K^+$  currents in renal VSMC, but functional evidence for a role in RBF regulation is so far lacking<sup>122</sup>.

$BK_{Ca}$  are complexly regulated, with both contractile agonists and vasodilatory pathways modulating channel function<sup>33, 123, 161</sup>. They may be inhibited or internalized PKC-dependently<sup>28-31</sup> or activated during cGMP/PKG-dependent<sup>76, 82-85</sup> as well as cAMP/PKA-dependent<sup>105-109</sup> signaling cascades of endogenous dilators. In the renal vasculature,  $BK_{Ca}$  have been implemented in cGMP-dependent relaxations of glomerular mesangial cells<sup>85</sup> and cAMP-induced hyperpolarization of juxtaglomerular cells in vitro<sup>108</sup>, but not in cAMP-induced RBF increases in vivo<sup>154</sup>.

#### 1.6.4 $K_v$

Voltage-gated  $K_v$  channels are a large class of  $K^+$  channels composed of 12 families ( $K_v1-12$ )<sup>162</sup> that in general activate in response to  $V_m$  depolarization and inactivate during maintained depolarization<sup>1</sup>. Structurally,  $K_v$  channels are composed of six transmembrane  $\alpha$ -subunits (S1-S6), of which S6 along with the p-loop between S5 and S6 forms the ion-conducting pore, while S4 serves as a voltage sensor detecting changes in  $V_m$ <sup>163</sup>. Channel inactivation can happen fast through the N-terminus (N-type) or slow through the C-terminus (C-type)<sup>164</sup>. Accessory subunits may associate with the pore-forming  $\alpha$ -subunits to either themselves or through interaction with other signaling proteins modify channel properties, which along with  $\alpha$ -subunit heteromerization, alternative splicing and post-translational modification contributes to considerable heterogeneity in  $K_v$  function within and among tissues<sup>163</sup>.

In VSMCs,  $K_v$  channels are ubiquitously present<sup>165-167</sup> and among them, the  $K_v1$ ,  $K_v2$  and  $K_v7$  families are recognized for both being highly expressed and contributing to resting  $V_m$  as well as negative feedback regulation of myogenic tone<sup>167</sup>.

##### 1.6.4.1 $K_v1-4$

$K_v1-4$  were among the first  $K_v$  channels to be associated with vascular reactivity based on early observations that the unselective  $K_v1-4$  blocker 4-aminopyridine (4-AP)<sup>165</sup> caused isolated vessels contraction<sup>168, 169</sup>,  $K^+$  current inhibition at potentials close to resting  $V_m$ <sup>170, 171</sup>, VSMCs depolarization<sup>171, 172</sup> and enhancement of the myogenic response<sup>172</sup>. More recently, more specific inhibitors have revealed evidence for functional expression of  $K_v1$  and  $K_v2$ <sup>173, 174</sup> but not  $K_v3$  or  $K_v4$  family members<sup>174</sup>.  $K_v1$  channels can be specifically blocked with diphenyl phosphine oxide-1 (DPO-1)<sup>175, 176</sup> and  $K_v2$  with stromatoxin (STX)<sup>177</sup>. Regulation of 4-AP-sensitive channels appears to be predominated by  $G_s$ -coupled vasodilators acting through the cAMP/PKA pathway<sup>95, 98-104</sup>.

In the renal vasculature,  $K_v1$  channels have been identified<sup>141, 178</sup> and 4-AP sensitive  $K^+$  currents<sup>179-181</sup> have been recorded in preglomerular resistance artery VSMCs, just like 4-AP-induced vasoconstriction was observed in isolated perfused kidneys<sup>131</sup> or blood-perfused juxtamedullary nephrons<sup>130</sup>.

##### 1.6.4.2 $K_v7$

$K_v7$  channels, which are encoded by the *KCNQ* genes, have only more recently moved into focus of research on smooth muscle contractility<sup>166, 182</sup>. In contrast to 4-AP-sensitive  $K_v$  channels, which are activated at  $V_m$  around -20mV<sup>1, 165</sup>, the 4-AP-insensitive  $K_v7$  channel family members are activated at more negative  $V_m$  values<sup>183</sup> closer to the resting  $V_m$  of renal resistance artery VSMCs<sup>118-120, 129</sup>. The physiological role of  $K_v7$  in the renal vasculature may therefore likely be different from that of  $K_v1$  or  $K_v2$  channels: Under resting conditions,  $K_v7$  conduct repolarizing outward  $K^+$  currents, which reduce VSMC excitability. Closure of the  $K_v7$  channels, supposedly induced by vasoconstrictive agonists, would cause depolarization, VOCC opening and vasoconstriction, whereas 4-AP-sensitive  $K_v$  could open in response to the  $K_v7$ -blockade-induced depolarization, providing a negative feedback mechanism to limit the extent of  $V_m$  depolarization and thus minimizing contraction<sup>182</sup>.

#### 1.6.4.2.1 KCNQ genes and K<sub>v</sub>7 channel structure

The KCNQ gene family consists of five members (KCNQ1-5) located at chromosomal loci 11p15, 20q13, 8q24, 1p34 and 6q13 which express the  $\alpha$ -subunit proteins K<sub>v</sub>7.1-5 that assemble to form tetrameric K<sup>+</sup> channels<sup>183</sup>. Structurally, K<sub>v</sub>7 subunits differ from other K<sub>v</sub> families in 3 aspects<sup>184</sup>: (i) they contain a well-conserved PIP<sub>2</sub> binding domain in the proximal C-terminal region<sup>185, 186</sup> which is essential for the channel to be active<sup>186, 187</sup>; (ii) they lack the N-terminal T1 domain which controls tetramerization in K<sub>v</sub>1-4 channels<sup>188, 189</sup> and (iii) instead possess a unique C-terminal tetramerization domain<sup>190, 191</sup>. Furthermore, the K<sub>v</sub>7 C-terminal is considerably longer than that of other K<sub>v</sub> channels, providing a bigger number of interaction sites with regulatory kinases, scaffolding proteins or ubiquitin ligases<sup>183</sup>

Heteromerization of K<sub>v</sub>7  $\alpha$ -subunits produces either channel homotetramers or hetero-oligomers containing different  $\alpha$ -subunits or auxiliary  $\beta$ -subunits called KCNE<sup>192</sup>. While all K<sub>v</sub>7.1-5 may form homomeric channels in vitro, the formation of heteromers is apparently tissue-specific and restricted to certain combinations<sup>192, 193</sup>: while the neuronal K<sub>v</sub>7.3 assembles readily with K<sub>v</sub>7.2/4/5<sup>192</sup>, in VSMCs have thus far been found mostly K<sub>v</sub>7.1/K<sub>v</sub>7.5 heterotetramers<sup>194</sup> or K<sub>v</sub>7.4/K<sub>v</sub>7.5 heterotetramers<sup>195, 196</sup>. Heteromerization with the  $\beta$ -subunits KCNE is especially observed in K<sub>v</sub>7.1 channels, which can assemble with all five KCNE1-5 members, resulting in significant alterations of channel properties and suggesting different tissue-specific functions<sup>182</sup>:

Assembly of K<sub>v</sub>7.1 with KCNE1 (formerly known as minK) is most prominent for producing the K<sup>+</sup> channel conducting the cardiac slow delayed rectifier K<sup>+</sup> current (I<sub>Ks</sub>) that contributes to repolarization of action potentials in cardiac myocytes<sup>197, 198</sup>. KCNE1 drastically enhances K<sub>v</sub>7.1 current amplitudes, slows both activation and deactivation and suppresses partial inactivation<sup>199</sup>, allowing KCNQ1/KCNE1 heteromers to also contribute to endolymph production via transepithelial potassium secretion in the cochlea<sup>200, 201</sup> or to Na<sup>+</sup> absorption in the kidney<sup>202</sup> and gastrointestinal tract<sup>203, 204</sup>. By contrast, interaction with KCNE2 leads to a decreased current amplitude, instantaneous activation, rapid partial deactivation, and a linear current-voltage relationship, basically transforming K<sub>v</sub>7.1 into a voltage-independent channel<sup>205</sup>. KCNQ1/KCNE2 heteromers are present in the parietal cells of the stomach, contributing to gastric acid secretion<sup>203</sup>, as well as in thyrocytes, regulating thyroid hormone biosynthesis<sup>206</sup>. KCNE3 similarly to KCNE2 abolishes K<sub>v</sub>7.1 gating and causes instant activation, leading to constitutively open KCNQ1/KCNE3 channels<sup>207</sup> that in intestinal crypt cells contribute to chloride secretion<sup>203, 207</sup>. Heteromerization with KCNE4 is relevant in blood vessels<sup>193, 208-210</sup>. While in heterologous expression systems KCNE4 effectively suppresses K<sub>v</sub>7.1 currents at physiological V<sub>m</sub> values<sup>209</sup>, in blood vessels KCNE4 may interact with other K<sub>v</sub>7, for example with K<sub>v</sub>7.4 subunits, to sex-dependently participate in arterial tone regulation<sup>211</sup>. Finally, KCNE5 affects K<sub>v</sub>7.1 similarly as KCNE1, causing a right-shift of the K<sub>v</sub>7.1 activation threshold by 140 mV towards V<sub>m</sub> values around +40 mV and thus only allowing K<sup>+</sup> currents during strong and continued depolarization<sup>212</sup>.

In VSMCs, all five KCNE genes have been identified in various vessels including renal arteries, and apart from the ubiquitous presence of KCNE4, expression of KCNE appears to be tissue-specific<sup>193, 208, 210</sup>. Interestingly, KCNE4 depletion has been found to reduce the membrane abundance of K<sub>v</sub>7.4 channels, resulting in decreased K<sub>v</sub>7 currents and increased contractility in rat mesenteric arteries<sup>210</sup>. Association with KCNE furthermore alters K<sub>v</sub>7 channel pharmacology in a manner relevant for substances used to study or modify vascular reactivity<sup>213-217</sup>.

#### 1.6.4.2.2 K<sub>v</sub>7 expression

K<sub>v</sub>7 expression is highly tissue-specific. Important locations in which K<sub>v</sub>7 have been found to be functionally expressed are the heart, the central nervous system, the cochlea and smooth muscle (for recent review see<sup>183</sup>): K<sub>v</sub>7.1 is highly expressed in the heart and functioning as a KCNQ1/KCNE1 heterotetramer conducting the I<sub>Ks</sub> current<sup>197, 198</sup>. In the central nervous system, it is predominantly K<sub>v</sub>7.2/K<sub>v</sub>7.3 heteromers that conduct the M-current<sup>218, 219</sup> controlling neuronal action potential generation with smaller contributions from K<sub>v</sub>7.5<sup>220</sup>. The cochlea depends upon K<sub>v</sub>7.4 channels being

expressed in the outer hair cells to enable normal hearing<sup>221, 222</sup>. Smooth muscle of both vascular and intestinal type mostly expresses K<sub>v</sub>7.1, K<sub>v</sub>7.4 and K<sub>v</sub>7.5 channels<sup>166</sup>.

In the vasculature, first evidence of KCNQ expression was presented in murine portal veins, where KCNQ1 was the highest expressed subtype<sup>223, 224</sup>. Ever since, KCNQ gene products have been found in various rodent blood vessels, with either KCNQ1, KCNQ4 or less often KCNQ5 expression predominating<sup>166, 193, 194, 208, 223, 225-238</sup>. KCNQ gene products are also expressed in human arteries<sup>194, 239-241</sup>. The K<sub>v</sub>7 channel protein itself has been confirmed to be present in the cell membranes of various VSMCs<sup>96, 193, 208, 235, 238, 240</sup>.

Concerning the assembly of KCNQ subunits in order to form functional channels it has been reported for mesenteric<sup>195, 242</sup> and cerebral<sup>196</sup> artery myocytes that  $\alpha$ -subunit heteromerization results in K<sub>v</sub>7.4/K<sub>v</sub>7.5 heterotetramers rather than K<sub>v</sub>7.4 or K<sub>v</sub>7.5 homomers. Alternatively, functional K<sub>v</sub>7.1/K<sub>v</sub>7.5 heterotetramers were discovered in rat aortic myocytes, conducting currents that furthermore were enhanced by colocalization of KCNE1<sup>194</sup>. Heteromerization of K<sub>v</sub>7.1, K<sub>v</sub>7.4 and K<sub>v</sub>7.5 subunits has early been suggested based on functional studies<sup>238</sup>.

In the renal vasculature, studies on main renal arteries of rats have found expression of either KCNQ1 alone<sup>96, 243</sup> or KCNQ1 along with KCNQ4<sup>244</sup> to predominate, the latter also being the case in main renal arteries of mice<sup>245</sup>. In these vessels, KCNQ4 and KCNQ5 gene products were always, KCNQ3 only variably and KCNQ2 never detected<sup>96, 243, 244</sup>. Immunodetection has also confirmed protein translation of K<sub>v</sub>7.1, K<sub>v</sub>7.4 and K<sub>v</sub>7.5 in the rat main renal artery<sup>96</sup>. Conversely, in rat renal preglomerular arterioles, positive immunofluorescence staining was found for K<sub>v</sub>7.4 antibodies only, while K<sub>v</sub>7.1, K<sub>v</sub>7.2, K<sub>v</sub>7.3 and K<sub>v</sub>7.5 antibodies were tested negative although the same antibodies were used<sup>246</sup>.

Interestingly, KCNQ mRNA levels may change during maturation, as K<sub>v</sub>7.1 and K<sub>v</sub>7.5 expression levels are higher in muscular arteries of rats aged ~2 weeks, whereas in >2 month old rats K<sub>v</sub>7.4 mRNA predominates<sup>234</sup>. Also, K<sub>v</sub>7 channel formation may be affected by prolonged presence of vasoconstrictive agonists, since it was recently discovered that longtime-incubation (1-7 hours) of mesenteric arteries with angiotensin II decreased K<sub>v</sub>7.4 protein expression without reducing KCNQ4 transcript levels<sup>247</sup>.

#### 1.6.4.2.3 K<sub>v</sub>7 pharmacology

Several K<sub>v</sub>7-specific and even some K<sub>v</sub>7.x subunit-specific channel modulators are available. Unselective K<sub>v</sub>7 blockers or activators typically display differential half maximal inhibitory concentrations (IC<sub>50</sub>) or half maximal effective concentrations (EC<sub>50</sub>), respectively, for individual K<sub>v</sub>7.x subunits (for review, see<sup>248</sup>).

All K<sub>v</sub>7 channels are blocked by the cognitive enhancer XE991<sup>217, 219, 224, 249-253</sup>. Subunit-specific IC<sub>50</sub> values are reported to vary between K<sub>v</sub>7.1 (0.75  $\mu$ M<sup>219</sup> or 0.78  $\mu$ M<sup>217</sup>), K<sub>v</sub>7.4 (1.2  $\mu$ M<sup>249</sup> or 5.5  $\mu$ M<sup>250</sup>) and K<sub>v</sub>7.5 (61  $\mu$ M<sup>253</sup>, 65  $\mu$ M<sup>251</sup> or 75  $\mu$ M<sup>252</sup>). Another frequently used pan-K<sub>v</sub>7 blocker is the structural relative linopirdine, which also displays differential IC<sub>50</sub> values for K<sub>v</sub>7.1 (8.9  $\mu$ M<sup>219</sup> or 35  $\mu$ M<sup>223</sup>), K<sub>v</sub>7.4 (1.7  $\mu$ M<sup>249</sup> or 14  $\mu$ M<sup>250</sup>) and K<sub>v</sub>7.5 (16  $\mu$ M<sup>254</sup> or 51  $\mu$ M<sup>251</sup>). Application of XE991 or linopirdine has been demonstrated to inhibit K<sub>v</sub>7 currents in rodent<sup>96, 223, 227, 229, 238, 244, 255-258</sup> and non-rodent mammalian<sup>259</sup> VSMCs and to cause V<sub>m</sub> depolarization, active contraction and enhancement of agonist-induced vasoconstriction in various blood vessels<sup>193, 196, 208, 225-229, 232, 234, 243, 252, 256-261</sup> including renal arteries of mice<sup>245</sup> and rats<sup>77, 96, 107, 246, 255, 262</sup>.

Subunit-specific blockers are currently available for K<sub>v</sub>7.1 channels only. HMR1556 inhibits K<sub>v</sub>7.1 at an IC<sub>50</sub> of 0.54  $\mu$ M<sup>216</sup> or 0.42  $\mu$ M<sup>215</sup> and application of 10  $\mu$ M reduces K<sup>+</sup> currents through K<sub>v</sub>7.1, but not through K<sub>v</sub>7.4 or K<sub>v</sub>7.5 channels<sup>96</sup>. However, functional studies have revealed no effect on vascular reactivity in either absence<sup>196, 228, 260</sup> or presence of contractile stimuli like transmural pressure<sup>245</sup> or vasoconstrictive agonists<sup>210, 263</sup>. Likewise, systemic application in vivo did not affect vessel tone<sup>264</sup> nor heart rate, blood pressure or GFR<sup>265</sup>. Chromanol 293B is another substance that has been used to

study  $K_v7.1$  channels, although chromanol 293B may unintendedly cause inhibition of other  $K^+$  channels<sup>266-268</sup> at concentrations relatively close to its  $IC_{50}$  for  $K_v7.1$  ( $27 \mu M$ <sup>269</sup>,  $41 \mu M$ <sup>270</sup> or  $67 \mu M$ <sup>271</sup>). Nonetheless, while effectively inhibiting  $K_v7.1$  currents in VSMCs, chromanol 293B does not affect rodent<sup>193, 224, 232, 245, 263</sup>, porcine<sup>259</sup> or human<sup>239</sup> arterial contractility.

Unselective  $K_v7$  activators like the novel anticonvulsant retigabine do not affect  $K_v7.1$  channels, since KCNQ1 is lacking a single tryptophan and three leucine residues that are necessary for retigabine sensitivity in KCNQ2-5<sup>272, 273</sup>. Retigabine activates  $K_v7.4$  channels at an  $EC_{50}$  of  $\sim 1.4 \mu M$ <sup>249</sup>,  $\sim 5.2 \mu M$ <sup>273</sup> or  $\sim 5.9 \mu M$ <sup>274</sup> and  $K_v7.5$  channels at an  $EC_{50}$  of  $\sim 3.45 \mu M$ <sup>274</sup> or  $\sim 6.4 \mu M$ <sup>252</sup>. Besides left-shifting voltage-dependence  $K_v7.2-5$  to more negative  $V_m$ , retigabine also decreases their rate of deactivation and thus stabilizes the open channel configuration<sup>275-277</sup>, which is more apparent under depolarized conditions like precontraction<sup>166</sup>. Retigabine has been demonstrated to enhance  $K_v7$  currents in native vascular myocytes<sup>224, 255, 257</sup> and to cause concentration-dependent relaxations of precontracted rat renal arteries with an  $EC_{50}$  of  $9.21 \pm 2.76 \mu M$ <sup>243</sup>, while likewise relaxing other rodent<sup>194, 196, 228, 229, 232, 243, 256, 261</sup> and human<sup>239, 241</sup> arteries at similar concentrations. However, Retigabine induces normal concentration-dependent relaxations in KCNQ1<sup>-/-</sup> arteries<sup>263</sup>. Alternative substances with slightly different  $K_v7$  subtype specificities<sup>243, 248</sup> like flupirtine, S-1, ML213 or BMS204352 have also been successfully used for  $K_v7.2-5$  activation in blood vessels<sup>77, 96, 243, 246, 262</sup>.

$K_v7.1$  can be specifically activated by the benzodiazepine R-L3 (alternative name: L-364,373), which interacts with certain residues located in the S5 and S6 transmembrane domains of KCNQ1 subunits<sup>278</sup>. Pharmacological data is limited, but existing reports have suggested R-L3 to function as a partial agonist, left-shifting  $K_v7.1$  activation  $V_m$  values, slowing both activation and deactivation rate and enhancing currents with an  $EC_{50}$  of  $<1 \mu M$ <sup>213</sup>. Conversely, other reports found R-L3 to show little effect at  $1 \mu M$ , while  $10 \mu M$  increased KCNQ1 currents by  $\sim 100\%$ <sup>260</sup>. Importantly, association with KCNE1 prevents R-L3 binding to KCNQ1 subunits<sup>213</sup>, which is why R-L3 is effective on unsaturated  $(KCNQ1)_4(KCNE1)_n$  tetramers, but not on saturated  $(KCNQ1)_4(KCNE1)_4$  channels<sup>214</sup>. The effect of R-L3 on blood vessels appears to vary between arteries from different vascular beds, with some studies finding no effect<sup>196, 228, 279</sup> and others reporting concentration-dependent relaxations of agonist-induced precontraction<sup>232, 260, 263, 280</sup>. In the renal vasculature, R-L3 has been shown to cause relaxations in both rats<sup>280</sup> and mice<sup>263</sup>. However, at least in mice the anticontractile effect of R-L3 appears to rely upon mechanisms distinct from  $K_v7.1$  activation<sup>263</sup>.

#### 1.6.4.2.4 $K_v7$ regulation

Regulatory factors that may dictate  $K_v7$  function include membrane voltage, mechanical stimuli and various biochemical signals.

$K_v7$  channel activity is most importantly regulated by  $V_m$ . Half maximum activation thresholds ( $V_{50}$ ) are somewhat different between  $K_v7.x$  subfamilies, ranging from approximately  $-20$  mV ( $K_v7.1$  and  $K_v7.4$ ) over  $-30$  mV ( $K_v7.2$ ) to  $-40$  mV ( $K_v7.3$  and  $K_v7.5$ ). Single channel conductance is similar for vascular  $K_v7.1/4/5$  channels, namely  $\sim 1-4$  pS. The rate of activation of vascular  $K_v7$  channels at  $0$  mV is slower for  $K_v7.1$  ( $\sim 210$  ms) than for  $K_v7.4/5$  ( $\sim 160-180$  ms), which is reversed at more depolarized  $V_m$  ( $\sim 90$  ms for  $K_v7.1$  or  $\sim 150-160$  ms for  $K_v7.4/5$  at  $+40$  mV). At hyperpolarized  $V_m$  around  $-60$  mV,  $K_v7.1$  also display slower deactivation rates ( $\sim 455$  ms) than  $K_v7.4/5$  ( $\sim 100-125$  ms)<sup>183</sup>.

$K_v7$  channels in VSMCs have recently been implemented in transduction of mechanical stimuli like transmural pressure inducing arterial myogenic response<sup>245</sup>. It was found that activation of angiotensin II receptor type 1 (AT<sub>1</sub>R) via osmotically induced membrane stretch suppresses currents through XE991-sensitive  $K_v$  channels in mice. However, since the XE991 was used at a high concentration of  $30 \mu M$ , which is known to inhibit  $K_v$  other than  $K_v7$ <sup>208, 224, 281</sup> and since myogenic tone was still evident in arteries from KCNQ4 knockout mice and KCNQ5 mutant mice while being entirely abolished by AT<sub>1</sub>R knockout<sup>245</sup> no firm conclusion can be drawn regarding the role of  $K_v7$  channels in angiotensin II-suppressed  $K_v$  currents<sup>282</sup>.

Besides regulation through membrane voltage, the effect  $K_v7$  channels have on vascular reactivity is influenced by a remarkably large number of contractile or anticontractile biochemical signals.  $K_v7$  channels have been shown to be implemented in vasoconstrictive pathways mediated by VOCC,  $Ca^{2+}/CaM$ ,  $PIP_2$  and  $G_{q/11}$ -coupled receptor agonists as well as vasodilative pathways employing cGMP/PKG or cAMP/PKA <sup>123</sup>.

Considerable evidence exists for  $Ca^{2+}$ -dependent contractile mechanisms involving  $K_v7$  channels. Dependency on L-type  $Ca^{2+}$  channels has been demonstrated both for vasodilations induced by  $K_v7.2-5$  activator Retigabine as well as for vasoconstrictions induced by pan- $K_v7$  blockers XE991 or linopirdine in rat and murine arteries <sup>193, 225, 226, 258</sup>. Also in the renal vasculature, reversibility of XE991-induced contractions via L-type  $Ca^{2+}$  channel blockade has been found in both isometric tension recordings of rat interlobar arteries and in vivo via ultrasound flowmetry of rat renal blood flow <sup>246</sup>. Interestingly, another aspect in which  $K_v7.1$  is different from  $K_v7.4$  and  $K_v7.5$  is Calmodulin (CaM)-dependent regulation. CaM binds to the C-terminus of  $K_v7$  channels, where it is essential for correct folding of the intracellular domain <sup>283, 284</sup>. Notably, CaM confers  $Ca^{2+}$  sensitivity only to KCNQ4 and KCNQ5, which after  $Ca^{2+}$  binding to CaM show strongly reduced  $K^+$  currents, but not to KCNQ1 or KCNQ1/KCNE1 channels (Gamper et al., 2005). This might serve as a feed-forward mechanism in contraction, with  $K_v7.4$  and  $K_v7.5$  conducting  $K^+$  currents to stabilize  $V_m$  during resting state and thus preventing VOCC activation, whereas upon depolarization-induced  $Ca^{2+}$  influx and consecutive increase in  $Ca^{2+}/CaM$  resulting in inhibition of  $K_v7.4$  and  $K_v7.5$ , a decrease in these  $K^+$  currents would allow for contraction.

$K_v7$  channels are unique in that they mandatorily require  $PIP_2$  in order to conduct currents <sup>186, 187, 285, 286</sup>.  $PIP_2$  increases  $K_v7$  channel open probability by stabilizing their open configuration <sup>287, 288</sup>. This effect has been best studied in  $K_v7.1$  channels.  $PIP_2$  is required for coupling of the voltage sensing and the pore opening domain in  $K_v7.1$  channels <sup>289</sup>, slowing  $K_v7.1$  deactivation kinetics <sup>290</sup> and shifting its voltage dependency towards negative potentials <sup>290</sup> and thus overall making  $K_v7.1$  channel activation in response to  $V_m$  changes more efficient <sup>289</sup>.  $PIP_2$ -induced current enhancement has also been described for  $K_v7.4$  channels, in which furthermore  $PIP_2$  depletion reduced retigabine-induced  $K_v7.4$  current enhancement <sup>291</sup>. This  $PIP_2$ -mediated regulation of  $K_v7$  channel properties may be initiated by  $G_q$ -coupled receptor agonists like various vasoconstrictors <sup>292</sup>. Notably,  $K_v7.1$  interaction with  $PIP_2$  may be strengthened by stimulation of PKC or PKA <sup>292</sup>.

$G_{q/11}$ -coupled receptor activation, a mechanism shared by many vasoconstrictors like vasopressin, serotonin and endothelin-1, can reduce  $K_v7$  currents, leading to VSMC depolarization and contraction <sup>195, 225, 230, 257</sup>. PKC has been shown to be involved in this process, yet evidence is somewhat contradictory. On the cellular level,  $G_{q/11}$ -coupled vasoconstrictors may mediate VSMC activation by PKC-dependent inhibition of  $K_v7$  channels: In rat VSMCs, arginine vasopressin (AVP) by reducing retigabine- or flupirtine-sensitive currents causes depolarization in a manner reducible by PKC inhibitors <sup>225, 230</sup> or KCNQ5 knockdown <sup>293</sup>, DAG analogs PKC-dependently inhibit KCNQ5 currents <sup>293</sup>, direct PKC $_{\alpha}$  activation suppresses native  $K_v7$  currents <sup>195</sup> and serotonin and endothelin-1 suppress Retigabine-sensitive currents in a similar fashion as direct PKC-inhibitors <sup>257</sup>. However, on the whole-vessel level, direct evidence for PKC-dependent  $K_v7$  regulation is thus far missing: While direct PKC inhibition mimics the effect of XE991 in producing contractions in rat basilar artery <sup>257</sup>, it is inefficient in preventing linopirdine-induced contractions in either absence or presence of AVP in rat mesenteric arteries <sup>225</sup>. Indirectly suggestive for PKC involvement are existing reports of AVP-, endothelin-1- or phenylephrine-induced contractions being enhanced by XE991 <sup>193, 257</sup> or diminished by retigabine and flupirtine <sup>193, 258</sup> in rat and mice arterial vessels. Interestingly, an alternative mechanism not dependent on PKC which may serve to explain  $G_{q/11}$  mediated regulation of  $K_v7$  has lately been offered when long-term (> 1h) incubation of angiotensin II was discovered to decrease  $K_v7.4$  protein expression without reducing KCNQ4 transcript levels via interaction with HSP90 <sup>247</sup>.

More recently, cGMP-dependent regulation of  $K_v7$  channels has been discovered as a mode of  $K_v7$  participating in endogenous vasodilator action. Atrial natriuretic peptide (ANP) endothelium-

independently and cGMP-dependently relaxed methoxamine-precontracted rat aorta and renal arteries in a manner impaired by pan-K<sub>v</sub>7 blocker linopirdine, but not by specific blockers of K<sub>ir</sub>, K<sub>ATP</sub>, BK<sub>Ca</sub> or K<sub>v</sub>1-4<sup>77</sup>. Since these relaxations were unaffected by PKA-inhibition, it is likely modulations of K<sub>v</sub>7 currents are conducted by PKG. However, mechanisms may differ between species or vascular beds, since in endothelium-denuded porcine coronary arteries, relaxations to NO donor sodium nitroprusside (SNP) induced equal vasodilatation in the absence or presence of XE991<sup>259</sup>.

More vast amounts of evidence suggest cAMP-dependent regulation of vascular K<sub>v</sub>7 channels. The K<sub>v</sub>7 C-terminus contains binding domains for A-kinase-anchoring proteins (AKAP)<sup>284</sup>, indicating the possibility of K<sub>v</sub>7 channels forming signaling domains with PKA, which is commonly activated by cAMP<sup>51</sup>. Consistently, PKA has been shown to phosphorylate the K<sub>v</sub>7.1 N-terminus after forming a macromolecular complex with the KCNQ1 C-terminus, the AKAP Yoatio and protein phosphatase 1<sup>294</sup>. This mechanism may underlie the upregulation of the cardiac I<sub>Ks</sub> current achieved by β-adrenoceptor mediated cAMP elevation and PKA stimulation<sup>295</sup>. In vascular smooth muscle cells, AKAP has been found to be localized with K<sub>v</sub>7.4 channels, which in renal arteries increased with β-adrenoceptor stimulation<sup>107</sup> in a Gβγ-dependent manner<sup>262</sup>. Overall, studies have identified a number of endogenous dilators like CGRP<sup>196, 262</sup> or adenosine<sup>259</sup> as well as pharmacological substances like β-adrenoceptor agonist isoproterenol<sup>96, 97, 107, 228, 262, 280</sup> or AC stimulator forskolin<sup>97, 227, 232</sup>, which by elevating intracellular cAMP produce vasorelaxation that amongst others depend upon hyperpolarizing outward K<sub>v</sub>7 currents in various mammalian arteries including rat renal arteries<sup>96, 107, 262, 280</sup>. The individual K<sub>v</sub>7.x subtypes may be differentially affected by cAMP, since K<sub>v</sub>7.5 homotetramers in VSMC were shown to be more susceptible to PKA-dependent current enhancement than K<sub>v</sub>7.4/K<sub>v</sub>7.5 heteromers or K<sub>v</sub>7.4 homomers<sup>97</sup> and consistently forskolin-induced relaxations to be more marked in arteries with higher expression of KCNQ5 mRNA and K<sub>v</sub>7.5 protein<sup>232</sup>. Furthermore, the situation is complicated by the fact that cAMP may not only act through PKA, which appears to be the predominant mode of isoproterenol effects in renal, but not mesenteric, arteries, but may also cause relaxation by stimulating exchange protein directly activated by cAMP (EPAC), which may be the prominent mechanism in mesenteric, but not renal, arteries<sup>107</sup>. Thus, while cAMP-mediated mechanisms in general are recognized as an important modification of K<sub>v</sub>7 function, the specific pathways involved may differ between vascular beds.

Other endogenous substances that have been associated with K<sub>v</sub>7 function in blood vessels include hydrogen sulfide (H<sub>2</sub>S), which produces vasorelaxations attenuated by blockade of K<sub>v</sub>7 channels<sup>229, 259, 261, 296</sup> and enhances K<sub>v</sub>7 currents<sup>296</sup>; bradykinin, the anticontractile effect of which is reduced by application K<sub>v</sub>7 blockers<sup>279, 297</sup>; and oxygen (O<sub>2</sub>), with hypoxic vasodilation likewise being reduced by K<sub>v</sub>7 blockade<sup>233, 259</sup>.

#### 1.6.4.2.5 Role of K<sub>v</sub>7 in vascular physiology

Due to the vast number of mechanisms and players involved as well as their variation between different vascular beds, understanding K<sub>v</sub>7 channel function is very complex and thus far incomplete.

Electrophysiological features like their activation threshold being closer to the resting V<sub>m</sub> of VSMCs than that of most other K<sub>v</sub> family members<sup>183</sup> suggest a role as important determinators of resting V<sub>m</sub> and as mediators of negative-feedback regulation of mechanical or chemical signal transduction in vascular reactivity<sup>123</sup>. With K<sub>v</sub>7.1 activating faster at depolarized V<sub>m</sub> levels and deactivating slower at hyperpolarized V<sub>m</sub> compared to K<sub>v</sub>7.4 or K<sub>v</sub>7.5<sup>183</sup>, it is possible that K<sub>v</sub>7.1 may be more important for stabilizing resting V<sub>m</sub>, while K<sub>v</sub>7.4 and K<sub>v</sub>7.5 more relevantly contribute to limiting depolarization.

Other electrophysiological features like their considerably low degree of inactivation at constant V<sub>m</sub> facilitate a role as signal transduction intermediates in the actions of vasoconstrictor and vasodilator stimuli<sup>282</sup>. With K<sub>v</sub>7 currents having been shown to on the one hand be reduced by G<sub>q/11</sub>-coupled receptor activators like various vasoconstrictors, causing VSMC depolarization and contraction<sup>195, 225, 230, 257</sup> and on the other hand be activated by various endogenous vasodilators dependent on

cGMP/PKG<sup>77</sup>, cAMP-PKA<sup>96, 97, 107, 196, 227, 228, 232, 259, 262, 280</sup> or other mediators<sup>229, 233, 259, 261, 279, 296, 297</sup>, inducing VSMC hyperpolarization and vasorelaxation, K<sub>v</sub>7 channels appear to represent an important point of intersection in the fine-tuned balance of constrictive and dilative mechanisms of many arterial beds.

In the renal vasculature, Joshi et al.<sup>255</sup> were the first to discover a constrictive effect of pan-K<sub>v</sub>7 blockers XE991 and linopirdine on rat main renal arteries. Besides confirmation of these findings<sup>77, 96</sup>, also in smaller resistance vessels<sup>246</sup>, subsequent research found K<sub>v</sub>7.2-5 activators like Retigabine<sup>243</sup>, S-1<sup>96, 243</sup>, BMS204352<sup>243</sup> or flupirtine<sup>246</sup> to produce renal vasorelaxation. Consistently, KCNQ4 knockout with siRNA increases renal arterial vasoconstrictor sensitivity<sup>96</sup> and K<sub>v</sub>7 blockers increased renal perfusion pressure in rat<sup>96</sup> and murine<sup>245</sup> isolated perfused kidneys and decreased rat renal blood flow in vivo<sup>246</sup>. Notably, K<sub>v</sub>7.2-5 activator flupirtine increased in vivo rat renal blood flow, but just like XE991 showed no effect on reductions of RBF induced by vasoconstrictors norepinephrine or angiotensin II<sup>246</sup>. L-type Ca<sup>2+</sup> channel blockers like nifedipine or nifedipine completely reverse the contractions induced by linopirdine<sup>96</sup> and XE991<sup>246</sup>. The presence of linopirdine is associated with reduced renal artery relaxations to the cGMP-dependent endogenous vasodilator ANP<sup>77</sup>. Implications for an involvement of K<sub>v</sub>7 in cAMP-dependent dilation of renal arteries have been given in form of cAMP elevation stimulating linopirdine-sensitive channels<sup>96</sup>, linopirdine attenuating cAMP-dependent relaxations<sup>96, 107</sup> and K<sub>v</sub>7.4 channels colocalizing with A-kinase anchoring protein<sup>107</sup>. Overall, K<sub>v</sub>7 channels in renal arterial vessels may play a functional role by contributing to vasoconstrictor actions in a manner dependent on L-type Ca<sup>2+</sup> channels if K<sub>v</sub>7 currents are reduced, as well as in vasodilator actions possibly including cGMP- and/or cAMP-dependent mechanisms where K<sub>v</sub>7 currents are enhanced.

#### 1.6.4.2.6 Role of K<sub>v</sub>7 in vascular pathology

In the recent years, research has linked cardiovascular disease to K<sub>v</sub>7 dysfunction. While in other organs like the heart, mutations of i.e. KCNQ1 are known to lead to autosomal-dominant long QT syndrome<sup>192</sup>, short QT syndrome<sup>298</sup> or familial atrial fibrillation<sup>299</sup>, there are no known hereditary disorders of the vasculature that can be pinpointed to specific KCNQ gene mutations<sup>183</sup>. Nonetheless, K<sub>v</sub>7 dysfunction has been implemented in a multitude of vascular diseases including both hypertension and hypotension, pulmonary arterial hypertension and coronary artery disease<sup>300</sup>. Therefore, K<sub>v</sub>7 channels may be promising new drug targets for the treatment of these conditions. Giving further impetus to their relevance, the K<sub>v</sub>7 channel characteristic of being controlled by perivascular adipose tissue (PVAT)<sup>176, 229, 259, 261, 296, 301</sup> makes them an especially interesting drug target for comorbid conditions like resistant hypertension along with obesity or metabolic syndrome<sup>248</sup>.

In hypertension, downregulation of K<sub>v</sub>7 channels in VSMCs may be a contributing factor to high blood pressure<sup>300</sup>. With K<sub>v</sub>7 currents contributing to membrane hyperpolarization, decreased presence of K<sub>v</sub>7 channels would leave VSMCs more depolarized, causing vasoconstriction resulting in increased vascular resistance and elevated blood pressure. Arteries from spontaneously hypertensive rats (SHR) as well as from angiotensin-induced hypertensive mice show attenuated responses to K<sub>v</sub>7 blockers and activators and lower expression of K<sub>v</sub>7.4 compared with normotensive vessels<sup>77, 96, 228, 229, 237, 256, 302</sup>. In the aorta, of all 5 KCNQ genes only KCNQ4 was shown to be reduced<sup>256</sup>. With SHR arteries displaying reduced responsiveness to pharmacological K<sub>v</sub>7 activators, it may be questionable whether activating the remaining K<sub>v</sub>7 channels is sufficient to induce the desired therapeutic vasodilation<sup>300</sup>. However, as K<sub>v</sub>7 activators have been shown to improve vasorelaxation by PVAT, which is impaired in hypertension and obesity<sup>303</sup>, K<sub>v</sub>7 modulators may be a specific pharmacological approach for this commonly observed comorbidity.

Renovascular pathology like arteriosclerosis of small renal arterioles or glomerulosclerosis has long been known to be associated with hypertension<sup>304</sup>. Human autopsy studies have found renal afferent arteriopathy in 98% of kidneys from hypertensive subjects, contributing to the existing theory that renal resistance artery dysfunction in some cases is not only coincidental, but the primary mechanism inducing hypertension<sup>305</sup>. Goldblatt<sup>306</sup> demonstrated in 1934 that creating renal artery stenosis, which

is detected in 5-10% of patients with hypertension<sup>307</sup>, by reducing RPP leads to hypertension. Both passive renovascular stenosis and active constriction increase renal arterial resistance, which causes elevation of blood pressure via activation of the renin-angiotensin system<sup>5</sup>. In mice, genetic deletion of KCNQ3, KCNQ4, or KCNQ5 produces constriction of isolated perfused kidneys<sup>245</sup>. In SHR, KCNQ4 abundance in the renal artery is markedly reduced, and renal artery contractions or relaxations to K<sub>v</sub>7 blockers or activators is strongly diminished<sup>96</sup>. Interestingly, downregulation of K<sub>v</sub>7.4 channels in SHR occurs without a decrease in KCNQ4 mRNA and is mediated by a specific regulatory microRNA (miR153), suggesting K<sub>v</sub>7.4 abundance to be determined by post-transcriptional regulation<sup>302</sup>. Moreover, impaired ANP-induced cGMP-mediated vasorelaxation in SHR renal arteries has been implicated as a consequence of reduced VSMC K<sub>v</sub>7.4 levels<sup>77</sup>. The combination of increasing renovascular K<sub>v</sub>7 membrane abundance along with K<sub>v</sub>7 activation, the latter of which has been shown to hyperpolarize renal VSMC and relax renal arterial vessels<sup>96, 243, 246, 262</sup> as well as to increase rat renal blood flow in vivo<sup>246</sup> may be a promising therapeutic strategy in hypertension, no matter whether renovascular pathology is coincidental or causative to the elevated blood pressure.

Hypotension on the other hand can be a more acutely life-threatening condition i.e. during septic shock, in which K<sub>v</sub>7 channel blockade has been demonstrated to oppose the effect of the tryptophan metabolite and sepsis-associated vasodilator kynurenine<sup>308</sup>. Thus, targeting K<sub>v</sub>7 may pose an approach for this otherwise therapeutically challenging condition culminating in multiple organ failure<sup>300</sup>.

Pulmonary arterial hypertension (PAH) is another disease in which current treatment options can be limited, especially when PAH is secondary to cardiac dysfunction, since in this case negative side effects of the common vasodilator therapy are especially undesirable<sup>300</sup>. Tissue-specific vasodilators like activators of K<sub>v</sub>7.2-5 channels, which are found in VSMCs but not cardiac myocytes, appear as an attractive solution to this dilemma. K<sub>v</sub>7.2-5 specific activators have already been demonstrated to relax pulmonary arteries in isolated vessels<sup>255</sup> and in perfused lungs from hypoxic rats<sup>231</sup> and to attenuate PAH symptoms like cardiac hypertrophy and increased right ventricular pressure<sup>309</sup>.

In coronary artery disease, impaired hypoxia-induced coronary vasodilation is a major pathomechanism potentially to be addressed by modifying K<sub>v</sub>7 channel function<sup>300</sup>. K<sub>v</sub>7 channel activators are established to produce coronary artery relaxation<sup>194, 227, 228, 232, 259</sup> and oppositely K<sub>v</sub>7 blockers can reduce hypoxia-induced dilation of isolated coronary arteries<sup>259</sup> and reduce coronary flow rate in isolated perfused rat hearts<sup>233</sup>. Conversely though, ischemia-reperfusion experiments in these same isolated perfused rat hearts found K<sub>v</sub>7 blockers to reduce myocardial infarct size and to improve cardiac function, suggesting a direct drug effect on cardiomyocytes rather than through VSMC-mediated flow modification<sup>233</sup>.

## 1.7 Objective of this thesis

Although research has increasingly focused on K<sub>v</sub>7 in the last years, piece by piece unraveling their manifold contributions to vascular reactivity in various arterial beds, not too much is known about their role in the renal vasculature, which is of central relevance for the large number of physiological processes the kidney is involved in, most importantly blood pressure regulation. Only a handful of studies have focused on K<sub>v</sub>7 function in isolated rat main renal arteries<sup>77, 96, 107, 243, 255, 262</sup> or smaller rat and murine renal resistance vessels<sup>246</sup>, and even fewer data is available on their effect on the whole-organ vasculature<sup>96, 245</sup> or on renal blood flow in vivo<sup>246</sup>. These reports have unveiled that pharmacological blockade or activation of renal K<sub>v</sub>7 channels may influence vascular tension on the cellular, vessel segment, whole-organ and in vivo level, and implications have been given for interactions with both endogenous vasodilators and vasoconstrictive agents. However, the renal vasculature is known to intrinsically determine arterial resistance in particular through the renal myogenic response<sup>7</sup> and tubuloglomerular feedback<sup>8, 9</sup> and thus largely independently of circulating hormones<sup>6</sup>. Conclusively, some reports state that K<sub>v</sub>7 channels do not seem to mediate or buffer agonist-induced renal vasoconstriction or vasodilation<sup>121</sup>.

While some data is available on  $K_v7$  channel function in context with cGMP<sup>77</sup>- and cAMP<sup>96, 107</sup>-dependent relaxations in the main renal artery, a large conduit vessel conducting ~25% of cardiac output<sup>6</sup>, no study so far has thoroughly examined the situation in smaller renal resistance arteries, which may be even more relevant to renal function as they are the key players among all vessels contributing to regulating renal blood flow and perfusion pressure. It is not known whether  $K_v7$ -mediated vasoregulation of small renal resistance arteries depends upon or interferes with endogenous regulation of vascular tone by circulating hormones. We therefore tested the hypothesis that two endogenous vasodilators, the cGMP-dependent ANP and the cAMP-dependent Urocortin, either attenuate or enhance the therapeutically intended vasodilatory effect of the  $K_v7.1$ -specific activator R-L3 and the unspecific  $K_v7.2-5$  activator Retigabine in small renal resistance arteries. Furthermore,  $K_v7$  expression is highly tissue-specific and different  $K_v7.x$  subtypes tend to predominate depending on the location of the blood vessel within the body<sup>248</sup>. In this regard, the renal vasculature appears to be different from other vascular regions: While quantitative expression analysis mostly find KCNQ1<sup>96, 243-245</sup> to predominate in rat renal arteries, other vessels from the coronary, pulmonary, cerebral or musculoskeletal circulation show higher expression of KCNQ4 or KCNQ5<sup>248</sup>. Thus, renovascular  $K_v7.1$  channels are an especially interesting pharmacological target, since inducing dilation by specifically activating  $K_v7.1$  channels would be an elegant way of exclusively improving renal blood flow – thus addressing one majorly important contributing factor in hypertension – without lowering overall blood pressure and thus making sure that the drug effect actually comes to the benefit of renal perfusion while leaving other vascular beds unaffected. However, it is not known whether the  $K_v7.1$  specific activator R-L3 is effective in producing vasodilation not only on a microscopic scale like isolated vessel segments, but also on the whole-organ level. We therefore tested the hypothesis that R-L3 causes specific  $K_v7.1$ -mediated and reversible vasodilation of the entire renal arterial vasculature using a novel isolated perfused rat kidney method.

## 2 METHODS

### 2.1 Animal Model

For all experiments male WISTAR albino rats of the strain RjHan:WI and the genotype  $Tyr^c/Tyr^c$  were used, which are certified as specific pathogen free (SPF) and specific and opportunistic pathogen free (SOPF). Animals were purchased from Janvier Labs, France and delivered at the age of 8 weeks via ISO-9001 certified transport logistics to reduce stress. Upon arrival in the in-house animal facility, animals were given at least one week to acclimatize to local conditions. They were held in IVC cages and had free access to tap water and complete feed pellets V1534-0 from ssniff®, Germany. At the time when used for experiments, animals were 10-12 weeks old. On the day of the experiment the rats were killed by asphyxiation with  $CO_2$  followed by cervical dislocation with a guillotine, upon which death occurred immediately. The treatment of the rats is in agreement with the Guide for the Care and Use of Laboratory Animals (8th edition. National Academies Press (US); 2011.) and legal regulations by the EU (directive 2010/63/EU) and Germany (TierSchG, 2013 (BGBl. I S. 2182) and TierSchVerV, 2013 (BGBl. I S. 3125, 3126)) and was approved by local authorities.

### 2.2 Solutions

When studying arteries *in vitro*, it is important to generate conditions similar to the *in vivo* environment by using solutions that can take over some of the functions blood and interstitial fluid have for the viability of the vessels. We thus used physiological salt solutions (PSS) that imitated physiological conditions with respect to electrolyte concentrations and pH, volatile gases like  $O_2$  and  $CO_2$ , and temperature. In total, four slightly different PSS were used (Table 1). All solutions were either freshly prepared or stored at 4°C and renewed every week.

PSS used for preparation does not contain  $NaHCO_3$  as a pH-buffer because it is not possible to aerate the solution during preparation. Gas bubbles would hinder the view and cause the small isolated vessels to move undesirably. Since  $CO_2$  leaves the  $NaHCO_3$ -buffered solutions to the surrounding air and is thus continuously removed from its equilibrium with protons and bicarbonate, protons are bound into  $H_2O$  and the pH rises. To avoid this, the artificial buffer 4-(2-hydroxyethyl)-1-piperazineethanesulfonic acid (HEPES) which does not need to be aerated was used to maintain the pH. The pH in refrigerated solution was adjusted to 7.3. Oxygenation of the solution occurred through equilibration with the surrounding air. Cooling the solution down to 4°C and its lack of glucose were intended to decrease tissue metabolism and avoid acidosis during the process of preparation.

PSS for myography experiments was used at 37°C and continuously aerated with carbogen (95%  $O_2$  and 5%  $CO_2$ ) to keep pH constant. Before starting and throughout the experiments, pH was repeatedly controlled and adjusted to 7.4 if necessary using HCl or NaOH. EDTA served to chelate traces of heavy ions that might be contained in the water. Once heated, experimental solution was not refrigerated again but discharged.

Modified PSS without  $NaHCO_3$  for the isolated perfused kidney was kept at room temperature during the experiments and only heated while flowing through the perfusion system. The pH was adjusted to 7.55 at room temperature, so that the pH of the solution after passing the heat exchanger would amount to 7.4. Like in myography experiments, the solution was aerated to provide  $O_2$  needed for proper function of the kidney. Calcium-free PSS for viability testing was generated from Modified PSS without  $NaHCO_3$  by adding ethylene glycol-bis( $\beta$ -aminoethyl ether)-N,N,N',N'-tetraacetic acid (EGTA) in a concentration of 2 mM which selectively chelates free  $Ca^{2+}$ , but not  $Mg^{2+}$  ions.

Modified PSS containing 120 mM KCl was used for viability tests in both myography and isolated perfused kidney experiments. Some myography experiments required a solution containing 50 mM

KCl, which was generated by mixing regular experimental solution and 120 mM KCl solution in relations 3:2.

Table 1: Solutions

	Reagents	MW	Conc. [mM]	Source
<b>Preparation solution</b>	NaCl	58,4	145	Carl Roth
	KCl	74,6	4,5	Carl Roth
	NaH <sub>2</sub> PO <sub>4</sub> xH <sub>2</sub> O	137,99	1,2	Merck
	MgSO <sub>4</sub> x7H <sub>2</sub> O	246,48	1	Merck
	CaCl <sub>2</sub> x 2H <sub>2</sub> O	147	0,1	Merck
	EDTA	372,24	0,025	Carl Roth
	HEPES	238,3	5	AppliChem
<b>PSS (for myography)</b>	NaCl	58,4	120	Carl Roth
	NaHCO <sub>3</sub>	84,01	26	Carl Roth
	KCl	74,6	4,5	Carl Roth
	NaH <sub>2</sub> PO <sub>4</sub> x H <sub>2</sub> O	137,99	1,2	Merck
	MgSO <sub>4</sub> x 7H <sub>2</sub> O	246,48	1	Merck
	CaCl <sub>2</sub> x 2H <sub>2</sub> O	147	1,6	Merck
	EDTA	372,24	0,025	Carl Roth
	HEPES	238,3	5	AppliChem
	Glucose	180,16	5,5	Carl Roth
<b>Modified PSS without NaHCO<sub>3</sub> (for isolated kidney)</b>	NaCl	58,4	146	Carl Roth
	KCl	76,6	4,5	Carl Roth
	NaH <sub>2</sub> PO <sub>4</sub> x H <sub>2</sub> O	137,99	1,2	Merck
	MgSO <sub>4</sub> x 7H <sub>2</sub> O	120,4	1	Merck
	CaCl <sub>2</sub> x 2H <sub>2</sub> O	147	1,6	Merck
	EDTA	372,24	0,025	Carl Roth
	HEPES	238,3	5	AppliChem
	Glucose	180,16	5,5	Carl Roth
	<b>Modified PSS with 120mM KCl (for viability tests)</b>	NaCl	58,4	4,5
NaHCO <sub>3</sub>		84,01	26	Carl Roth
KCl		74,6	120	Carl Roth
NaH <sub>2</sub> PO <sub>4</sub> x H <sub>2</sub> O		137,99	1,2	Merck
MgSO <sub>4</sub> x 7H <sub>2</sub> O		246,48	1	Merck
CaCl <sub>2</sub> x 2H <sub>2</sub> O		147	1,6	Merck
EDTA		372,24	0,025	Carl Roth
HEPES		238,3	5	AppliChem
Glucose		180,16	5,5	Carl Roth
<b>Further reagents used</b>	HCl			AppliChem
	NaOH			Carl Roth
	EGTA			Sigma Aldrich
	Aqua dest.			

Conc. = concentration; EDTA = ethylenediaminetetraacetic acid; EGTA = ethylene glycol-bis(β-aminoethyl ether)-N,N,N',N'-tetraacetic acid; HEPES = 4-(2-hydroxyethyl)-1-piperazineethanesulfonic acid; MW = molecular weight; PSS = physiological salt solution

### 2.3 Drugs

Stock solutions were prepared of all drugs according to manufacturer sheets (Table 2) and stored at -20°C. Appropriate dilutions depending on the concentration needed were prepared right before performing the experiment.

When used for myography experiments, the drugs were directly pipetted into the myograph chambers. The myograph chambers have a volume of 5ml. For example, to achieve a concentration of  $10^{-5}$  M in the chamber, a volume of 5  $\mu$ l from a  $10^{-2}$  stock solution was applied. Some drugs were used in multiple concentrations, such as methoxamine for concentration-response relationships and ANP, Urocortin, Retigabine and R-L3 for precontraction experiments. In that case, dilution series were produced using the appropriate solvent H<sub>2</sub>O or dimethyl sulfoxide (DMSO). Special care was taken in protocols using multiple drugs solved in DMSO or precontraction protocols using R-L3 or Retigabine. As DMSO can be cytotoxic at concentrations higher than  $10^{-3}$  M we were careful not to use more than 5  $\mu$ l of DMSO at a time and always applied the same concentration of DMSO in the control channels. Exceptions of this rule were made only in precontraction protocols examining the effect of multiple K<sup>+</sup> channel blockers on ANP- and Urocortin-induced vasorelaxation, where 10  $\mu$ l of DMSO were permitted since the control channel showed no signs of functional damage.

When used for isolated perfused kidney experiments, drugs were applied in two different ways. First, Methoxamine was applied directly into the perfusate in a final concentration of  $3 \cdot 10^{-6}$  M. With approximately 500 ml of perfusate being needed per kidney for one experiment, 150  $\mu$ l of Methoxamine  $10^{-2}$  stock solution were required. Second, drugs were added onto the Methoxamine-induced precontraction by using syringe pumps. Two sizes of syringes were used, 1 ml syringes (Omnifix-F Tuberkulin from B. Braun Melsungen, Germany) and a 100  $\mu$ l Microsyringe (MS\*N100 from Ito Corporation Exmire, Japan). The syringes were filled with stock solutions in concentrations x times higher than the desired concentration and the flow rate of the syringe pumps was set to values x times lower than the flow rate for the kidney perfusion. For example, at a kidney perfusion rate of 3ml/min, the syringe was filled with a  $3 \cdot 10^{-4}$  M stock solution of XE991 and the syringe flow rate was set to 30  $\mu$ l/min, achieving the desired concentration of  $3 \cdot 10^{-6}$  M XE991. Two syringe pumps were used serially connected, so that two drugs could be given at the same time, but independently.

Table 2: Drugs

Drugs	MW	Stock [M]	Conc. [M]	Solvent	Source
Acetylcholine chloride	181.66	$10^{-2}$	$10^{-5}$	H <sub>2</sub> O	Sigma Aldrich
ANP rat	3062.41	$10^{-4}$	$10^{-9}$ - $10^{-7}$	H <sub>2</sub> O	Sigma Aldrich
Barium chloride dihydrate	244.26	$10^{-2}$	$3 \cdot 10^{-5}$	H <sub>2</sub> O	Riedel de Haën
DPO-1	340.44	$10^{-1}$	$10^{-6}$	DMSO	Tocris
Glibenclamide	494	$10^{-2}$	$10^{-6}$	DMSO	Tocris
HMR1556	411.44	$10^{-2}$	$10^{-5}$	DMSO	Tocris
Iberiotoxin	4230.9	$10^{-4}$	$10^{-7}$	H <sub>2</sub> O	Alomone Labs
L-NNA	233,2	$10^{-2}$	$10^{-4}$	H <sub>2</sub> O	Alexis
Methoxamine hydrochloride	247.72	$10^{-2}$	$10^{-8}$ - $10^{-4}$	H <sub>2</sub> O	Sigma Aldrich
Retigabine	303.33	$3 \cdot 10^{-2}$	$3 \cdot 10^{-7}$ - $3 \cdot 10^{-5}$	DMSO	Valeant
R-L3 (L364,373)	397.44	$10^{-2}$	$10^{-8}$ - $10^{-6}$	DMSO	Tocris
Stromatoxin	3792	$10^{-4}$	$10^{-7}$	H <sub>2</sub> O	Alomone Labs
Urocortin rat	4707.26	$10^{-4}$	$10^{-10}$ - $10^{-7}$	H <sub>2</sub> O	Sigma Aldrich
XE991 dihydrochloride	449.37	$10^{-2}$	$3 \cdot 10^{-6}$	H <sub>2</sub> O	Tocris

ANP = atrial natriuretic peptide; conc. = working concentration; DMSO = dimethyl sulfoxide; DPO-1 = (+)-Neomenthyl diphenylphosphine oxide; HMR = N-[(3R,4S)-3,4-Dihydro-3-hydroxy-2,2-dimethyl-6-(4,4,4-trifluorobutoxy)-2H-1-benzopyran-4-yl]-N-methylmetanesulfonamide; L-NNA = NG-Nitro-L-arginine-methyl ester; MW = molecular weight; stock = concentration of the stock solution; XE = 10,10-bis(4-Pyridinylmethyl)-9(10H)-anthracenone dihydrochloride

To avoid high concentrations of DMSO, two strategies were pursued. The first strategy was to use a Microsyringe, allowing higher concentrations of stock solutions and thus smaller amounts of solvent to be given. For example, at a kidney perfusion rate of 3 ml/min, the 100  $\mu$ l microsyringe was filled with a  $10^{-2}$  M stock solution of HMR1556 and the syringe flow rate was set to 3  $\mu$ l/min, achieving a desired concentration of  $10^{-5}$  M HMR1556. The second strategy was to create stock solutions for 1 ml syringes that were diluted in parts with DMSO and in parts with H<sub>2</sub>O. For example, the original stock solution of  $10^{-2}$  M R-L3 solved in DMSO was diluted 1:100 with H<sub>2</sub>O, creating a new syringe stock solution containing  $10^{-4}$  M R-L3 that could be administered in the way as described above while avoiding concentrations of DMSO higher than  $10^{-3}$  M.

## 2.4 Myography

Myography is the study of muscle function. In this thesis, the muscles investigated were smooth muscles in the walls of the renal vasculature and the methodical approach chosen was isometric myography. In isometric myography, the contractile state of a blood vessel can be studied by measuring isometric force exerted by vessels isolated from their original vascular beds and mounted on two parallel wires having a fixed distance, one of which is connected to a force transducer. With this setup, functional aspects like vasoconstriction and vasorelaxation in response to action potentials, electrical stimulation, agonists or antagonists, and to changes in ion concentrations can be studied. Our methodical approach is based on the method first described by Mulvany and Halpern<sup>310, 311</sup> which has been further refined since<sup>312, 313</sup>.

### 2.4.1 The myography setup

All myography experiments were performed on four-chamber wire myographs from Danish Myo Technology A/S, Denmark. Two different generations of the same model myograph were used, the DMT610M and its successor DMT620M. The force readout from the myograph interface was transferred via BNC cables to a data acquisition hardware unit (PowerLab 4/26 and 4/30 from ADInstruments, New Zealand) digitalizing and sampling at 1 kHz, being connected via USB to a PC hard drive with a data acquisition and analysis software (LabChart 7.3.7 from ADInstruments, New Zealand) installed. All four myograph chambers are separately connected to a vacuum gas pump (VP 86 from VWR International, USA) with a suction bottle interposed. Each chamber has its own connection to gas supply, for which carbogen (95% O<sub>2</sub> and 5% CO<sub>2</sub>) was used. Constant temperature of the chambers was guaranteed by an internal heater and thermometer integrated in the Myograph interface. Constant temperature of the experimental solution applied into the chambers was guaranteed by an external circulation thermostat (ED-5 from Julabo, Germany). The force transducers in the myograph chambers were calibrated once a month.

### 2.4.2 Macroscopic preparation

In the following, the steps of preparation for which no microscope was needed are described. All anatomical terms are derived from the *Nomina Anatomica Veterinaria*<sup>314</sup>.

After euthanization the abdominal cavity of the rat was opened via midline laparotomy using surgical forceps and pointed operating scissors. The entire gastrointestinal tract from distal esophagus to distal colon was carefully removed, giving view to the spatium retroperitoneale with the kidneys surrounded by the capsula adiposa. The fascia renalis was opened from the lateral side. The kidneys were elevated from the situs, avoiding direct touching by leaving a small part of the capsula fibrosa adherent to the organ, by which it could be grabbed. The renal artery was truncated close to its branching from the aorta. The organ was immediately transferred to 4°C cold preparation solution in a large petri dish coated with Sylgard polymer, to facilitate immobilization with fixation pins. Using a pointed scalpel, the kidney was split almost in half in the coronal plane, cutting longitudinally into the margo lateralis

of the kidney until it could be flipped open like a book while leaving the hilum intact, and then be pinned into position with cannulas for microscopic preparation.

### 2.4.3 Microscopic preparation

In the following, the steps of preparation for which a microscope was needed are described.

Microscopic preparation was performed under a stereomicroscope (Stemi 2000-C from Zeiss, Germany) with a cold light source (Schott KL750 from Leica, Germany) using fine forceps (No. 5 Inox from Dumont, Switzerland) and fine spring-type scissors (Vannas Capsulotomy Scissors from Geuder, Germany). First, the calices renales and adipose tissue surrounding the pelvis renalis had to be removed to display the venae interlobares underneath which the arteriae interlobares are located. Usually, 3-4 pairs of the arteriae et venae interlobares were observed in every half kidney. Next, the front walls of all the venae interlobares were opened lengthwise so that the arteriae interlobares became visible through the almost transparent rear wall of the vein. The rear wall and the surrounding fat and connective tissue were then carefully loosened from the arteries until they were only attached at their proximal end at the branching from the renal artery and at their distal end where entering the columnae renales to become arteriae interlobares renis. Finally, short vessel segments at a length of 3-4 mm were cut off the arteriae interlobares and transferred to the myograph chambers filled with 4°C preparation solution. This was done with special attention paid not to longitudinally stretch the arteries and not to directly touch the parts which would be mounted onto the myograph wires, in order not to damage the vessel. Only vessels without visible damage were used for experiments and lateral branches were allowed only if sized smaller than 10% of the circumference.

The mounting of the vessel segments onto the stainless steel wires was performed as recommended in the user's manual. The first 20-25 mm piece of wire was fixated at one end to one of the jaws, while the vessel segment was threaded onto the other end, shortened at appropriate length and positioned to fit into the space between the jaws. An optimal length of 2mm was attained in most cases, while at times shorter segments down to 1,8 mm were tolerated. After fixation of the other end of the wire, the second piece of wire was carefully pushed through the vessel lumen and likewise fixated at both ends. Once mounted, remaining blood within the vessel lumen was flushed out using a custom-made plastic Pasteur pipette with fine tip to ensure that all vessels were equally and fully surrounded by PSS. The endothelium was not removed mechanically. The last step under the microscope was to approximate both jaws as close as possible without allowing the two wires to touch and leaving some space for the jaws to expand when heating up. When all four chambers were loaded with vessels they were set on the Myograph interface and slowly warmed up to 37°C. Once target temperature had been reached the preparation solution was replaced with pre-heated PSS. The vessels were given at least 10 minutes to equilibrate before starting Normalization.

The whole process of preparation from euthanization of the rat until setting all four chambers on the Myograph lasted no longer than 60-90 minutes.

### 2.4.4 Principles of measurement

Each myograph chamber contains two jaws holding a wire on which the vessel is mounted. One of them is connected to a micrometer screw, the other to a force transducer. The micrometer is used to set the optimal pretension during the normalization procedure, the force transducer transmits its signal ( $F$  = force) to the data acquisition software which calculates the effective pressure ( $P_i$ ) exerted by the vessel wall according to Laplace's Law as described by Mulvany and Halpern<sup>311</sup>.

The physiological transmural pressure of a vessel *in vivo* may be approximated by the effective pressure  $P_i$  *in vitro*, which is described in the Laplace relation:

$$P_i = 2\pi (T / IC)$$

$P_i$  = effective pressure;  $T$  = wall tension;  $IC$  = internal circumference

The wall tension ( $T$ ) is defined as the circumferential wall force per unit length. It is a sum of active forces generated by smooth muscle, and passive force caused by structural components of the vessel wall and adventitia. In the absence of agonists, only passive force is exerted and at constant passive force the wall tension is inversely proportional to the length of the vessel segment ( $g$ ):

$$T = F / 2g$$

$T$  = wall tension;  $F$  = force;  $g$  = vessel length

The internal circumference ( $IC$ ) of small vessels with sufficiently thin walls when mounted on two myograph wires can be approximated with the following formula, as illustrated in Figure 1.

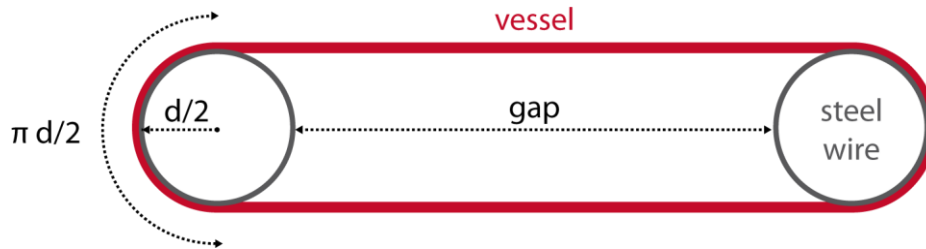


Figure 1: Cross-section of a vessel mounted on two myograph wires

$$IC = (2 \times gap) + (4 \times d/2) + (2 \times \pi d/2)$$

$IC$  = internal circumference;  $gap$  = distance between myograph wires;  $d$  = diameter of myograph wires

Merging the formulas for  $T$  and  $IC$  into the equation of Laplace's Law one can calculate the effective pressure  $P_i$  based on force ( $F$ , which is recorded by the force transducer), the length of the vessel ( $g$ , which is determined under the stereomicroscope during mounting), the diameter of the wires ( $d$ , which is known to be 40  $\mu\text{m}$ ) and the distance between myograph wires ( $gap$ , which is set by the micrometer screw):

$$P_i = 2\pi \times ((F / 2g) / ((2 \times gap) + (4 \times d/2) + (2 \times \pi d/2)))$$

or simply:

$$P_i = 2\pi F \times (gap + d + \frac{1}{2}\pi d) / g$$

This equation can be set equal to the desired  $P_i$  representing the transmural pressure during the normalization procedure, allowing the normalization software to calculate the optimal distance of the myograph wires at which the micrometer screw should be set.

#### 2.4.5 Normalization

Normalization is the procedure of pre-stretching a vessel segment to an internal circumference ( $IC$ ) at which the actin-myosin interaction is at an optimal state in its length/tension relationship of both maximal contact and room to contract, creating a physiological resting tension that enables optimal contractile responses. The goal of normalization is to standardize the vessel circumference in a way that on the one hand, responses to vasoactive agents are maximal, and on the other hand, baseline conditions are set to make results reproducible.

For normalization procedures, the DMT Normalization Module addon for LabChart was used. Normalization starts with both myograph wires almost touching each other, indicating that  $gap = 0$ . The force readout is set to zero before starting measurements. Upon starting, the distance between the jaws is increased stepwise by turning on the micrometer screw. The new  $gap$  value is entered into the software and force is measured for intervals of 90 seconds in a resolution of 0,1 mN and the value then plotted on a passive length/tension graph. The software also plots an isobar line for the target

pressure of 100 mmHg (13,3 kPa). Once a point has reached a force readout above 13,3 kPa, the software calculates the point at which the isobar line is intersected by the parabolic length/tension curve and displays this value as  $IC_{100}$ .

Finally, the  $IC_{100}$  value is multiplied with the normalization factor in order to calculate the optimal *gap* value for active contraction, at which the micrometer screw is subsequently turned back. The normalization factor is the ratio of the IC at which a maximum response to a vasoconstrictor is observed ( $IC_1$ ) divided by the IC at which the transmural wall pressure is 100mmHg ( $IC_{100}$ ).

$$\text{Normalization factor} = IC_1 / IC_{100}$$

The normalization factor has to be determined for each type of vessel. A normalization factor of 0.9 has been established to be appropriate for rat mesenteric arteries by the manufacturer and has been successfully used for rat renal arteries as well<sup>96, 107, 315</sup>. Thus, a normalization factor of 0.9 was chosen for our experiments.

In conclusion, all myography experiments are performed on vessels exposed to a pre-tension that was estimated to correspond to a pre-stretching to 90% of the diameter that can be observed in vessels exposed to wall tensions of 100 mmHg (13.3kPa). Since these calculations are based on passive length/tension relations, it is necessary to stress the importance of a good preparation technique where all connective tissue is accurately removed in order not to distort the normalization procedure.

#### 2.4.6 Viability testing

Viability tests were performed as a standard starting procedure to rule out damage having occurred to the vessels during preparation. This was done at the beginning of each experiment after giving the vessels 10 minutes to equilibrate to the pre-tension established by the normalization procedure. Before the first test, the endothelium was chemically inactivated using  $N^G$ -Nitro-L-arginine-methyl ester (L-NNA), an irreversible inhibitor of endothelial nitric oxide synthase (eNOS) and reversible inhibitor of inducible nitric oxide synthase (iNOS). This measure was repeated several times throughout the experiment prior to every concentration-response relationship or precontraction curve used for data collection.

In total, five viability tests were run. Between two tests the substances or solutions applied were washed out by replacing PSS at least 5 consecutive times at 5 minute intervals.

The first test examined the response to the standard vasoconstrictor Methoxamine, which acts as an agonist to  $\alpha 1$ -adrenoreceptors. Methoxamine was applied for 5 minutes in the highest concentration ( $10^{-5}$  M). The test was deemed successful and the vessels declared viable when the active force measured in response to the vasoconstrictor was at least as high as the passive force measured in the last step of normalization, corresponding to an effective pressure of at 100 mmHg (13,3 kPa) or higher. If a vessel did not meet this requirement, the test was repeated two times. Only if the vessel failed to produce an adequate contraction at the third time was the vessel replaced or the experiment terminated.

The second test examined whether the endothelium had been successfully inactivated. Like in the first test, Methoxamine was applied for 5 minutes at  $10^{-5}$  M, followed by Acetylcholine  $10^{-5}$  M, a vasodilator activating endothelial nitric oxide synthase which was inhibited by L-NNA having been applied priorly. The test was deemed successful if no sustained decrease in the level of contraction was observed within the 3 minutes following application of Acetylcholine. This was the case in all experiments.

The third test evaluated the maximum force generated by the vessels by supplying the strongest contraction stimulus available in form of Modified PSS containing 120 mM  $K^+$  applied simultaneously with Methoxamine  $10^{-5}$  M for 5 minutes. High levels of extracellular potassium substantially decrease  $K^+$  efflux, representing a strong depolarizing stimulus which leads to contraction. The test was deemed

successful when the level of the contraction plateau surpassed the level of the plateau at Methoxamine  $10^{-5}$  M. This was always the case.

In the fourth test, again Methoxamine  $10^{-5}$  M was applied for 5 minutes. The contraction produced was compared to the contraction in the first viability test. If the curves looked similar with regards to shape and height, the test was deemed successful and the force readout prior to and 5 minutes after application of Methoxamine was set as reference for maximum force ( $F_{\max}$ ) for all further experiments performed on the vessels.

The fifth test consisted of a concentration-response relationship (CRR) with Methoxamine as vasoconstrictor. Prior to this, L-NNA was applied again and allowed 10 minutes to exert its effect. Initially, the force readout after 10 minutes was recorded as baseline ( $F_{\text{base}}$ ) wall tension. Methoxamine was then applied in increasing concentrations ( $10^{-8}$  M  $\rightarrow$   $3 \times 10^{-8}$  M  $\rightarrow$   $10^{-7}$  M  $\rightarrow$   $3 \times 10^{-7}$  M  $\rightarrow$   $10^{-6}$  M  $\rightarrow$   $3 \times 10^{-6}$  M  $\rightarrow$   $10^{-5}$  M) and each concentration incubated for 3 minutes. In some protocols using strong vasodilators, two more concentration steps were added up to a maximum of  $10^{-4}$  M. The force readout at each concentration step was recorded to calculate  $\text{pD}_2$ , the negative logarithm of the concentration at which methoxamine causes 50% of its maximum effect ( $\text{EC}_{50}$ ) for later comparison after application of the drugs to be tested.

For each concentration-response relationship or precontraction curve a new baseline was recorded ( $F_{\text{base before } x}$ ). The normalized force ( $F_{\text{norm}}$ ) for any force readout later recorded at a given time point ( $F_x$ ) could then be calculated as

$$F_{\text{norm}} = (F_x - F_{\text{base before } x}) / (F_{\max} - F_{\text{base}}).$$

Since in the above cited Laplace relation all other variables besides F are constant during one experimental series, the effective pressure  $P_i$  is directly proportional to F and consequently relations between the four force readout curves recorded by one myograph may be interpreted as relations between effective pressures exerted by the vessels.

#### 2.4.7 Experimental protocols

The ability of vessels to contract and dilate in response to drugs was investigated using two different types of protocols. The first type consisted of multiple consecutive concentration-response relationships with Methoxamine, prior to which both vasoconstricting or vasodilating drugs could be applied both separately or combined. The second type consisted of sustained precontraction induced by Methoxamine or other vasoconstrictive agents, on top of which vasodilating drugs could be applied in increasing concentrations, thus creating inverse concentration-response relationships.

##### 2.4.7.1 Concentration-response relationship protocols

Protocols using multiple consecutive CRRs allow the study of multiple drugs and how they interact. This can be achieved by only changing one parameter at a time between two consecutive CRRs, allowing to differentiate between the effect of a single drug and the effect of the same drug in combination with another drug (Table 3).

In some experiments, the effect of a 3<sup>rd</sup> drug was studied within the same experiment. This was done by incubating the 3<sup>rd</sup> drug in all four channels prior to incubation with drug 1 and drug 2. This required a 4<sup>th</sup> CRR to be added prior to the 2<sup>nd</sup> CRR, serving as an additional control CRR, at the beginning of which the solvent of the 3<sup>rd</sup> drug was incubated. Such protocols were used to study the effect of ANP resp. Urocortin on HMR1556 and R-L3, with R-L3 being the "3<sup>rd</sup> drug" added in all channels.

In some experiments, a 4<sup>th</sup> CRR was added to examine the effect of different concentrations of one of the two drugs. This was done by incubating the same drug/solvent combination as in the 3<sup>rd</sup> CRR, but with the low concentration of e.g. drug 2 in the 3<sup>rd</sup> and the high concentration in the 4<sup>th</sup> CRR. Such a

protocol was used to examine the effect of ANP on R-L3 and HMR1556, with two concentrations of ANP ( $10^{-8}$  M and  $10^{-7}$  M) being used.

Table 3: Basic structure of a concentration-response relationship protocol

Viability tests (including 1 <sup>st</sup> CRR)	L-NNA $10^{-4}$ M	solvent of drug 1	solvent of drug 2	2 <sup>nd</sup>	washout	solvent of drug 1	solvent of 2 <sup>nd</sup> drug	3 <sup>rd</sup>	washout	Channel 1 (control)
		solvent of drug 1	solvent of drug 2			CRR	solvent of drug 1			<b>drug 2</b>
		<b>drug 1</b>	solvent of drug 2	with		<b>drug 1</b>	solvent of drug 2	with		Channel 3 (drug 1)
		<b>drug 1</b>	solvent of drug 2	Mx		<b>drug 1</b>	<b>drug 2</b>	Mx		Channel 4 (drug 1 + 2)

CRR = concentration-response relationship; L-NNA = N<sup>G</sup>-Nitro-L-arginine-methyl ester; Mx = Methoxamine

#### 2.4.7.2 Precontraction protocols

Two different types of precontraction protocols were used. In the first type, a sustained level of precontraction was induced using the standard vasoconstrictor Methoxamine (in the following called “precontraction plateau”), on top of which a range of dilating or contractile agents were incubated (Table 4). The second type generated a precontraction plateau using a range of different vasoconstrictive agents like Methoxamine, KCl 50 mM or various K<sup>+</sup> channel blockers, which could also be combined in a cocktail, on top of which only one dilating agent was incubated (Table 5). In both types, the first precontraction plateau served as a control with which to compare the vasorelaxation induced by the dilator drug added during the second precontraction plateau.

Table 4: Basic structure of a precontraction protocol using **Methoxamine** for precontraction

Viability tests (including 1 <sup>st</sup> CRR)	L-NNA $10^{-4}$ M	solvent of drug 1	inverse	CRR	washout	solvent of drug 1	inverse	CRR	washout	Channel 1 (control 1)
		<b>drug 1</b>	with			<b>drug 1</b>	with			Channel 2 (drug 1)
		solvent of drug 2	dilator	with		solvent of drug 2	<b>dilator</b>	with		Channel 3 (control 2)
		<b>drug 2</b>	solvent	<b>drug 2</b>		<b>drug 2</b>	<b>drug 2</b>	Channel 4 (drug 2)		

CRR = concentration-response relationship; L-NNA = N<sup>G</sup>-Nitro-L-arginine-methyl ester; Mx = Methoxamine

Methoxamine-induced precontractions usually reached their plateau within 20-30 minutes. The precontraction plateau had to be at constant force for at least 10 minutes before inverse CRRs with solvent or reagent were initiated. Protocols using Methoxamine for precontraction were used to study the effect of dilating agents Retigabine, R-L3, ANP and Urocortin in the presence and absence of XE991 resp. HMR1556.

In the case of Retigabine resp. R-L3, one channel served as Methoxamine-only control, one channel was incubated with HMR1556, and two channels were incubated with XE991 but unequally precontracted with different concentrations of Methoxamine to evaluate whether the level of precontraction played a role for the interaction of XE991 and Retigabine resp. R-L3.

In the case of ANP resp. Urocortin, the Methoxamine-only control channel was left out entirely since the effect of ANP resp. Urocortin on Methoxamine alone had already been examined in protocols described below. Instead, two channels were incubated with XE991 and two with HMR1556, and one of each pair was then dilated using ANP resp. Urocortin.

In the case of ANP, Retigabine and R-L3, the inverse CRRs contained 5 concentration steps, for Urocortin 7 steps were used. Incubation times for each concentration step were 10 minutes for Retigabine and R-L3 and 5 minutes for ANP and Urocortin.

Table 5: Basic structure of a precontraction protocol using **different vasoconstrictive agents** for precontraction

Viability tests (including 1 <sup>st</sup> CRR)	L-NNA 10 <sup>-4</sup> M	1 <sup>st</sup> Precontraction with KCl 50mM	inverse	washout	L-NNA 10 <sup>-4</sup> M	2 <sup>nd</sup> Precontraction with KCl 50mM	inverse	washout	Channel 1 (control KCl)
		1 <sup>st</sup> Precontraction with Mx	CRR			2 <sup>nd</sup> Precontraction with Mx	CRR		Channel 2 (control Mx)
		1 <sup>st</sup> Precontraction with K <sup>+</sup> blockers 1	with dilator			2 <sup>nd</sup> Precontraction with K <sup>+</sup> blockers 1	with dilator		Channel 3 (blockers 1)
		1 <sup>st</sup> Precontraction with K <sup>+</sup> blockers 2	drug solvent			2 <sup>nd</sup> Precontraction with K <sup>+</sup> blockers 2	drug		Channel 4 (blockers 2)

CRR = concentration-response relationship; L-NNA = N<sup>G</sup>-Nitro-L-arginine-methyl ester; Mx = Methoxamine

Protocols using different vasoconstrictive agents for precontraction were used to study the effect of dilating agents ANP resp. Urocortin on contractions produced by various K<sup>+</sup> channel blocker combinations including iberiotoxin, stromatoxin, glibenclamide, DPO-1 and BaCl with XE991 (“K<sup>+</sup> blockers 1”) resp. without (“K<sup>+</sup> blockers 2”) XE991.

Blocker precontractions needed more time to reach their plateau. Usually it took 30-40 minutes, but sometimes up to one hour was required. Many times, strong oscillations occurred ranging up to heights of 50% of the maximum Methoxamine reference. When oscillations did not decrease or disappear, minor concentrations of Methoxamine were used to stabilize the plateau without increasing its level. Before starting inverse CRRs with vasodilators the plateau had to be stable for at least 10 minutes. Vasodilators were always applied simultaneously in all four channels, also when the plateau in the Methoxamine or KCl channel had been reached much earlier. The concentration of Methoxamine was adjusted adequately to generate the same plateau level as induced by KCl 50 mM. In most cases Methoxamine concentrations in the range of 5x10<sup>-7</sup> M to 10<sup>-6</sup> M were required.

#### 2.4.8 Data analysis

All data points obtained by the data acquisition and analysis program (LabChart 7.3.7) were first transferred to Microsoft Excel (2010 and 2016) for basic calculations and analysis.

Data points were obtained in the following way: At most times, vasoconstrictive and vasodilating agents produced a stable plateau which distinctively represented the force readout to be recorded. If after an initial peak the plateau sloped down during Methoxamine CRRs, a representative value of 80-90% of the maximum force was obtained in accordance to the steepness of the slope. If minor

oscillations occurred in precontraction experiments, oftentimes when precontraction was induced with a cocktail of K<sup>+</sup> blockers, a representative average was recorded over longer spans of time (up to 60 seconds) if the plateau of oscillation was horizontal.

The normalized force ( $F_{norm}$ ) values were calculated for all data points within Microsoft Excel data sheets using the above described equation (see: Chapter 2.4.6) and plotted onto dose-response graphs for each channel individually. Mean values and standard error of the mean (SEM) were calculated and displayed in a common graph for all four channels. The following comparisons were made within each series of experiments to guarantee validity of the results:

In all concentration-response relationship protocols, the mean values of  $F_{norm}$  at each concentration step of the 1<sup>st</sup> CRRs during viability testing had to be equal in all four channels resp. experimental groups. This was to serve as an indicator that on average the vessels were equally strong and sensitive to Methoxamine in all four channels, being a necessary requirement to allow comparison of the  $pD_2$  of the 2<sup>nd</sup> CRRs resp. the plateau of the precontraction curves obtained from different channels resp. experimental groups. Analogously, in multiple-CRR protocols testing two or more drugs, mean values of  $F_{norm}$  at each concentration step of the 2<sup>nd</sup> CRR had to be equal in the two channels resp. experimental groups in which the same first drug resp. solvent was applied. This was to serve as an indicator that on average the vessels were equally affected by the first drug, being a necessary requirement to allow comparison of the  $pD_2$  of the 3<sup>rd</sup> (and 4<sup>th</sup>) CRRs with one another and thus be able to draw adequate conclusions on the effect of the 2<sup>nd</sup> drug.

In all precontraction protocols, the mean values of  $F_{norm}$  at the plateau of the 1<sup>st</sup> precontraction curve (using the vasodilator solvent as control), had to be equal to the mean values of  $F_{norm}$  at the plateau of the 2<sup>nd</sup> precontraction curve (using the real vasodilator agent), within the same channel. This equal level of precontraction within one channel was a necessary requirement to draw adequate conclusions on the effect of the vasodilators.

In precontraction protocols using Methoxamine for precontractions, the mean values of  $F_{norm}$  at the plateau of both the 1<sup>st</sup> and 2<sup>nd</sup> precontraction curve after application of the vasoconstrictive drugs (XE991 and HMR) had to be equal in all four channels resp. experimental groups. This equal level of precontraction between channels was a necessary requirement to draw adequate conclusions on the effect of the vasoconstrictors.

In precontraction protocols using KCl 50 mM, Methoxamine and various blockers, it was not possible to generate equal precontraction levels in all four channels, because the blocker combinations in total produced stronger contractions. Instead, the mean precontraction levels of the two channels with K<sup>+</sup> blockers had to be equal, and likewise the mean precontraction levels of KCl 50 mM and Methoxamine. This equal level of precontraction between the two pairs of channels was a necessary requirement to draw adequate conclusions on (i) different effects of the vasodilators between vessels treated with the two K<sup>+</sup> blocker cocktails and (ii) different effects of the vasodilators between vessels treated with KCl and Methoxamine.

Furthermore, in all precontraction protocols, after having demonstrated that average precontraction levels were equal, the force readouts of each inverse CRR concentration step ( $F_{x\ inverse}$ ) were normalized ( $F_{x\ inverse\ norm}$ ) to their corresponding precontraction level ( $F_{precontraction}$ ) and subsequently expressed as a percentage of the precontraction using the formula:

$$F_{x\ inverse\ norm} = (F_{x\ inverse}) / (F_{precontraction}) \times 100$$

## 2.5 Isolated perfused kidney

This isolated perfused kidney method was developed in our laboratory to study the function of vascular smooth muscle in the walls of the renal arterial system on a whole-organ level and thus in a macroscopic and more physiological setting in comparison to myography. In the following, the practical

course of action of the method will be highlighted, while the scientific validation of the method will be elaborated as part of the discussion.

### 2.5.1 Isolated perfused kidney setup

The setup was designed as a flow-rate controlled, no-reperfusion system. A pressure transducer was connected in parallel to the high-pressure part of the system between the perfusion pump and the perfused kidney. Two tube systems of the same design (Figure 2) were connected to one perfusion pump, each separately perfusing one kidney.

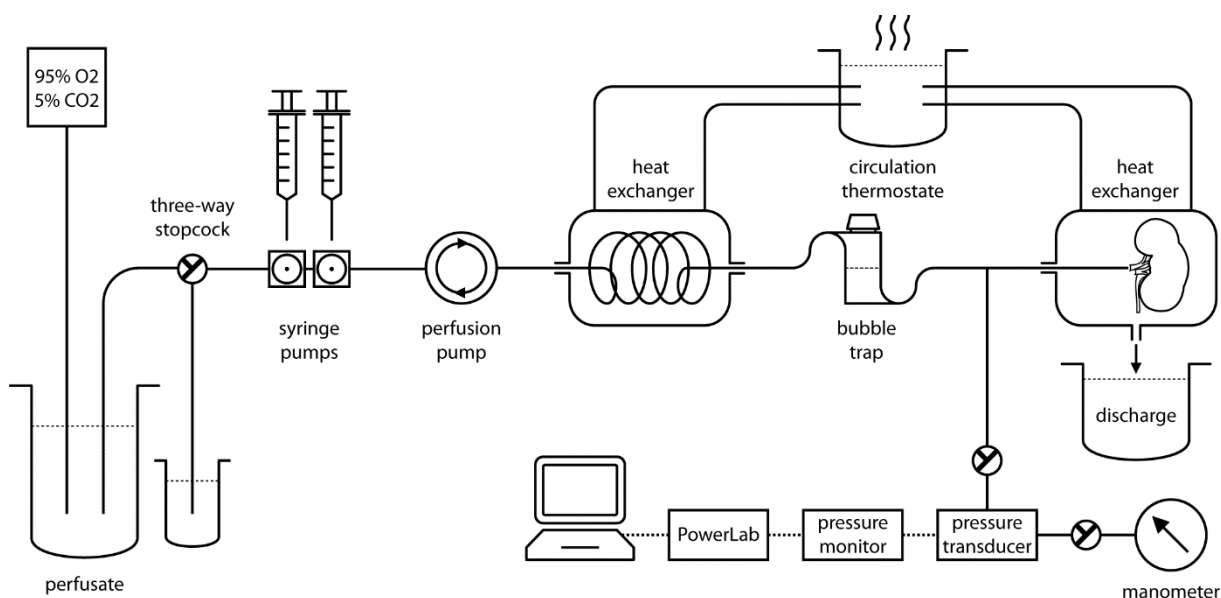


Figure 2: Isolated perfused rat kidney setup

The perfusate was kept in regular laboratory bottles (Wide-mouth rectangular bottles from Nalge Nunc International, USA), but equipped with specially prepared lids containing two holes for the tubes, one allowing carbogen to be administered to the perfusate and one allowing the perfusate to be extracted by the pump. This way the  $pO_2$  of the perfusate was maximized and the loss of  $CO_2$  to the surrounding air was kept at a minimum. This same issue was solved for the two modified solutions used in viability testing, of which only small amounts were needed each day, by using volumetric flasks with long narrow necks (Blaubrand volumetric flask from Brand, Germany). For Details concerning the perfusate solutions, see (Table 1). A three-way stopcock at the entry of the tube system allowed for instantaneous switching between two perfusate solutions.

Drugs were applied using syringe pumps as described above (see: Chapter 2.3). Two syringe pumps (SP100 Microprocessor Controlled Syringe Pump from World Precision Instruments, USA) per kidney were used serially connected.

As a perfusion pump, a roller pump with a 16 roller pump head (Perimax 16/3 Antipuls from Spetec, Germany) was used that generated almost pulse-free perfusion pressures. Pulsatile pressure waves have early proven not to confer any advantage in isolated perfused rat kidney experiments<sup>316</sup>. The flow rate is continuously adjustable in single digit steps from 1-999 speed digits [sd] representing pump head revolutions from < 1 to 33 revolutions per minute (rpm). In our experimental setting, the pump was set on speed digits ranging from 25-800 [sd]. The actual flow rates are further determined by the lumen of the plastic tubes the pump is equipped with and by adjustment of the contact pressure at the roller pump head. In our setup, tubes with an internal circumference of 1,524 mm (PVC Standard double pump tubing 38-0352 from Spetec, Germany) were used. To confirm the flow rates provided by the manufacturer, own measurements were performed by clocking the time needed to pump a certain volume of solution at different speed digits. Considerable deviation of our own measured flow

rates from the flow rates declared in the manufacturer's sheet made a manual calibration necessary. Calibration consisted of repeated measurements at four set speed digits, of which the mean value was calculated. This procedure was performed twice, with and without the perfusion cannula attached (Table 6).

Table 6: Flow rate calibration

Speed digit (perfusion pump)	Flow rate (ml/min) without cannula		Flow rate (ml/min) with cannula attached	
	Mean	SEM	Mean	SEM
<b>100</b>	1,62	0,01	1,63	0,01
<b>200</b>	2,74	0,01	2,67	0,01
<b>400</b>	4,85	0,04	4,84	0,02
<b>800</b>	9,92	0,03	9,88	0,04

The mean values of the four flow rates measured with cannula attached were used to generate a trendline, which could be justified by the strictly linear relation between speed digits and flow rates according to the manufacturer's sheet. Using this trendline, the corresponding flow rates of the other speed digits that were used for pressure-flow relationships in the experiments were calculated (Table 7).

Table 7: Flow rates calculated from calibration for each speed value

Speed digit (perfusion pump)	Flow rate (ml/min) without cannula	Flow rate (ml/min) with cannula attached
<b>25</b>	0,62	0,48
<b>50</b>	0,92	0,78
<b>100</b>	1,51	1,38
<b>200</b>	2,7	2,57
<b>300</b>	3,89	3,76
<b>400</b>	5,08	4,96
<b>600</b>	7,46	7,34
<b>800</b>	9,84	9,72

In a second step we confirmed the flow rate with the cannula attached and an actual rat kidney being mounted and perfused and thus the pump actually creating perfusion pressure remaining to be on average 2,57 ml/min for a speed digit of 200, which is the perfusion rate at which all later experiments following the viability tests on perfused kidneys were performed. Calibration was performed once in the beginning, and a second time when the system was duplicated.

All glass parts (perfusate heating chamber, kidney heating chamber, and air bubble traps) were handcrafted by a local glassblowing company. Both heating chambers were connected via large lumen tubes (Suction tube CH 25 from Oriplast, Germany) to a circulation thermostat (UC-5B from Julabo, Germany) which continually exchanged the heating fluid (Aqua dest). The circulation thermostat was set to a temperature of 42°C, which corresponded to an actual temperature of 37°C measured both on the surface of the heating chambers and in the perfusate itself.

The heating chamber for the perfusate was designed as a spiral-shaped glass tube within a glass container, with the space in between being filled with water when connected the circulation thermostat. The glass tube, containing a volume of approximately 2 ml, allowed for a time span of

approximately 45 seconds for the perfusate to be heated whilst travelling through at the perfusion rate of 2,57 ml/min used during the pharmacological part of the experiments.

The air bubble trap was designed as a small glass cylinder with a volume of 3 ml. Perfusion tubes may be attached to one connecting socket at its top and one at its bottom. Perfusate would flow through the air trap from top to bottom with a screwable lid allowing for release of air and filling of the cylinder with fluid. Air traps had to be filled with perfusate once only at the beginning and last throughout the experiment since refilling of the traps would require stopping the perfusion of the kidney. Air bubbles, which were either sucked in with the perfusate or developed within the perfusion system during passage of the heating chamber would get caught by rising to the top of the bubble trap, slowly filling the glass cylinder with air or gas. Two bubble traps were needed per kidney, since the average gas volume that developed throughout an average four-hour experiment exceeded the volume of one bubble trap. The perfusion pressure within the system was not affected by the amount of air being caught in a trap.

The heating chamber for the kidney was designed as a bell-shaped double-walled container with two connecting sockets for the circulation bath and with an outlet at its bottom for the discharge of used perfusate. The container was positioned with its opening facing obliquely upwards at a 45° angle and a pedestal entered to allow the kidney to be rested upon pedestal and container wall, thus avoiding stretching of the renal artery due to the weight of the kidney when being hung up. With a setup design as a non-reperfusion system, the perfusate flowing from the truncated renal vein immediately left the kidney heating chamber through a hole in its bottom and was discharged, thus avoiding a continuous effect after stopping the administration of a drug.

The pressure transducer (PT-F from Living Systems Instrumentation, USA) was set in parallel to the perfused kidney and connected to a perfusion pressure monitor (PM-4 from Living Systems Instrumentation, USA), which communicated the pressure readout to a data acquisition device (PowerLab 4/26 from ADInstruments, New Zealand) digitalizing and sampling at 1 kHz and transferring the data to a laptop hard drive with a data acquisition and analysis software (LabChart 8.0 from ADInstruments, New Zealand) installed. Two three-way stopcocks attached on both sides of the pressure transducer allowed for switching between monitoring perfusion pressure and performing system pressure calibration. Calibration of the pressure transducer was performed every day before equipping the setup with a kidney. To do so, a fluid-filled container positioned at the height of the pressure transducer would serve as a water level gauge for calibrating 0 mmHg, while an analogue manometer (Big Ben Round from Riester, Germany) was used for calibrating 100 mmHg.

The kidney itself was mounted on a handcrafted perfusion cannula. The cannula was fabricated from a glass capillary (1B200F-4 from World Precision Instruments, USA) using a micropipette puller (PC-10 from Narishige, Japan). The pulling process was interrupted shortly before the two ends of the glass capillary were entirely separated, thus creating an hourglass-shaped capillary. The capillary was manually cut with a glass cutter a short distance beside its narrowest point, creating a slightly biconcave shaped tip (Figure 3). The sharp ends of the cut surface were smoothed with a microforge (Carl Zeiss, Germany) to avoid damage to the wall of the artery.



Figure 3: Biconcave glass cannula used for perfusing the rat kidney

The special design of the perfusion cannula is significant for two main reasons: First, the tying of the renal artery firmly to the narrowest point of the biconcave shaped tip prevented its sliding off the tip up to perfusion pressures above 200mmHg. Second, the relative shortness of the narrowness of tip keeps its intrinsic flow resistance considerably low, allowing for high perfusion rates to be applied

without falsely high perfusion pressures narrowing the validity of measurements during viability testing.

The flow resistance of the cannula was assessed in repeated measures of baseline perfusion pressures at different speed digits with and without the perfusion cannula attached (Table 8). With perfusion pressures of only 4,0 mmHg being produced at a speed digit of 200 (corresponding to the flow rate of 2,57 ml/min used for the pharmacological part of the experiments) even with the perfusion cannula attached, intrinsic resistance was considered neglectable. Two perfusion cannulas with similar intrinsic resistance were produced and used for all experiments.

Table 8: Perfusion pressure with vs. without perfusion cannula attached

Speed digit (perfusion pump)	Perfusion pressure [mmHg] without cannula		Perfusion pressure [mmHg] with cannula attached	
	Mean	SEM	Mean	SEM
<b>100</b>	0,49	0,11	3,13	0,03
<b>200</b>	0,35	0,14	4,04	0,09
<b>400</b>	1,09	0,12	6,30	0,15
<b>800</b>	2,56	0,12	13,90	0,13

### 2.5.2 Macroscopic preparation

Similar to myography experiments, preparation started with midline laparotomy and removal of the entire gastrointestinal tract, displaying the kidneys surrounded by the capsula adiposa in the spatium retroperitoneale. Starting at this point, in total three preparation procedures are described, for the removal of one or two kidneys, and with or without heparinization.

First, in most cases, only one kidney was needed for perfusion experiments. In that case, the right kidney was used due to its favorable more caudal position in the abdomen and because right renal arteries are longer than left ones<sup>317</sup>, which may facilitate mounting onto the perfusion cannula. In a first step the left kidney was removed for myography experiments as described above (see: Chapter 2.4.2). Next, the spatium retroperitoneale was cleared of fat until aorta abdominalis and vena cava were displayed proximally and distally to their junction with the renal artery and vein. The fat surrounding the renal artery was left in place in order not to damage the vessel. Then aorta abdominalis and vena cava were grabbed at their proximal end with anatomical forceps and truncated, first proximally from the point where grabbed, and next distally from the junction with the renal vessels. This way, the kidney could be elevated and removed en bloc with renal vessels and short segments of aorta and vena cava attached, supported only by a few scissor cuts at the margo lateralis to strip the kidney from its capsula adiposa. The kidney was transferred to the same 4°C cold preparation solution as vessels for myography, fixated with pins, and washed several times to clear away blood.

Second, in some cases, both kidneys were needed for perfusion experiments. In that case, additionally to clearing the fat from aorta abdominalis and vena cava, the kidneys itself had to be peeled out of their capsula adiposa while leaving the same protective fat cushion around the renal vessels as mentioned before. The kidneys each had to be flipped to the contralateral side in order to detach their facies dorsalis from the capsula adiposa. This done, both kidneys could be grabbed and elevated by the abdominal vessels and removed en bloc in the same way as described above.

Third, in few cases, heparin had to be infused into the kidneys before removal. This was done with the kidneys still in situ. Again, the abdominal vessels initially had to be cleared from fat, in which case a longer segment of the caudal aorta needed to be displayed. First, the aorta and vena cava were ligated

proximal to their junction with the renal vessels. In case only one kidney was to be used, the vessels of the other kidney were ligated before removal. Second, a ligature around the aorta and vena cava approximately 1 cm distal to their junction with the renal vessels was put into place, but not fastened yet. Third, the distal aorta was punctured with a 27 G cannula attached with 30 mm tubing to a 1 ml syringe (Omnifix-F Tuberkulin from B. Braun Melsungen, Germany) in such a manner that the ligature positioned earlier could easily be fastened over the cannula now positioned within the lumen of the aorta. Fourth, the distal ligature was fastened and the vena cava segment in between the proximal and distal ligatures was incised to permit blood flow exiting the kidney. Finally, the syringe content of 100 I.U. heparin sodium (Heparin-Natrium 25.000 I.E. in 5ml from Ratiopharm, Germany) dissolved in 1 ml Modified PSS without  $\text{NaHCO}_3$  was carefully injected over a time period of at least 30 seconds. Blood flowing from the vena cava incision was observed as confirmation for successful application into the renal vasculature. The remaining preparation was performed as described above.

### 2.5.3 Microscopic preparation

All remaining steps up to connecting the isolated kidney to the perfusion system were performed under the microscope, using the same tools as for myography preparation.

Preparation started with the removal of all perivascular adipose tissue surrounding the arteria renalis and aorta. During this process, the entire vena cava and most of the vena renalis were removed as well, leaving only a short stump of the vena renalis. The ureter was usually not discernable and was thus removed with the fat. The arteria renalis was then truncated as close to the aorta as possible. As an additional step, the capsula fibrosa of the kidney was removed bluntly using two forceps. This was perceived necessary because perfusing the kidney with a colloid-free perfusate might cause organ edema and thus swelling of the kidney, which in turn could cause pressure to rise within the rigid capsula fibrosa to an extent which could possibly affect arterial perfusion pressures. Before mounting the arteria renalis to the perfusion cannula, the cannula had to be thoroughly cleared from air and filled with preparation solution. A fine surgical thread (Ethilon nylon suture 7-0 from Ethicon, USA) was used to tie the artery around the cannula. First, an air knot was tied and pulled over the cannula without fastening. Next, the opening of the arteria renalis was widened and held open with forceps and the cannula was inserted. The air knot was then tightened over the artery on the perfusion cannula, fixating the arteria renalis firmly at the narrowest point of the biconcave tip. Three more surgical knots were added on top to secure the position.



Figure 4: Perfusion cannula connected to renal artery

Only if the artery was at least 2-3 mm long, the kidney could be used for perfusion. Although in about 20-40% of the rats an early division of the arteria renalis into a dorsal and a ventral branch was observed, the common trunk proximal to the division in most cases was sufficiently long. The tip of the cannula was not permitted to be inserted into one of the two branches, but always had to remain in the common trunk, where it maintained a visually controllable distance from the division to ensure that the entire arterial vasculature would be perfused and perfusion pressures thus be comparable.

Preparation took no longer than 30-40 minutes from euthanization of the rat to connecting the isolated kidney to the perfusion system. An additional 5-10 minutes were required in case the kidney was heparinized.

#### 2.5.4 Preparation of the isolated perfused kidney setup

In the following, all necessary preparations to the perfusion system are described. The pressure transducer was calibrated daily as described (see: Chapter 2.5), setting the perfusion pressure readout without the isolated kidney attached to zero. The circulation thermostat was switched on at least 30 minutes before starting experiments to give the heating chambers time to reach 37°C. Perfusate was adjusted to room temperature and gassed with carbogen starting at least 30 minutes before the experiment. After filling the perfusion system with Modified PSS without NaHCO<sub>3</sub> as perfusate, the tubes between the bubble trap and the connecting socket for the perfusion cannula were carefully examined for air bubbles, which had to be removed. The perfusion pump was started at a flow rate below 0,5 ml/min (speed value 25/). Recording of the perfusion pressure was started and as soon as a waveline oscillating tightly around 0 mmHg was observed on the screen, the perfusion cannula was connected to the system. To do this, the kidney had to be carefully lifted from the preparation solution, grabbing the perfusion cannula with the kidney hanging vertically downwards and connecting the cannula to its socket in vertical position, with the kidney resting upon the 45° angled wall of the heating chamber and supported at its margo lateralis by a pedestal priorly inserted into the chamber. In consequence, a steep increase in perfusion pressure was observed in kidneys with intact renal vasculature, reaching a sharp peak followed by an equally steep drop in perfusion pressure, which occurred simultaneously with blood flowing from the vena renalis. The renal artery was then inspected for leaks or jets of perfusate. Only if blood flow was observed immediately and no leak was discovered, the experiment would be concluded.

#### 2.5.5 Viability testing

At the beginning of each experiment, viability tests were performed. Unless otherwise specified, Modified PSS without NaHCO<sub>3</sub> was used as perfusate. Viability testing included (i) examination for complete perfusion by macroscopic appearance, (ii) confirmation of an intact vascular bed using a pressure-flow relationship, (iii) testing for myogenic response by application of calcium-free perfusate at high flow rates and (iv) testing for maximum active vasoconstriction of the renal vasculature by application of Modified PSS containing 120 mM KCl.

Table 9: Viability tests for isolated perfused kidney

<b>Complete perfusion?</b>	<b>Vascular bed intact?</b>	<b>Myogenic response?</b>		<b>Maximum contraction?</b>		<b>Start of experiment</b>
Macroscopic appearance	Pressure-flow relationship	Calcium-free PSS	washout	120 mM KCl PSS	washout	
40 min		5 min	5 min	10 min	10 min	

PSS = physiological salt solution

First, complete perfusion of the entire renal vasculature had to be ascertained in order to warrant comparability of the perfusion pressure readouts to be recorded in our flow-rate controlled setup. Incomplete perfusion of the kidney for example due to blood clots developed during no-flow time in the preparation procedure that obstructed the vessels, thus resulting in a lower cross section of vasculature, would in our flow-rate controlled setup lead to measurement of false-high perfusion pressures. For complete perfusion to be assumed, the entire kidney had to undergo a color change from dark maroon to a spotless pale brown, indicating washout of all blood and thus patency of all major arterial vessels. In case this change in macroscopic appearance did not occur until the end of the pressure-flow relationship, the kidney was declared unviable and the experiment would not be used for data collection.

Second, integrity of the vascular bed and absence of major leaks due to vessel damage during preparation had to be demonstrated, indicated by an adequate rise of perfusion pressure with increasing flow rates. This was ascertained by exposing the kidneys to stepwise increasing flow rates up to a maximum of 9,72 ml/min and monitoring for unreasonably low perfusion pressures in a pressure-flow relationship. Perfusion of the isolated kidney started at a flow rate < 0,5 ml/min and was increased in seven additional steps by setting speed digits corresponding to approximately 0,8 → 1,4 → 2,6 → 3,8 → 5,0 → 7,3 → 9,7 ml/min as calculated above (see: Chapter 2.5.1) with each step lasting 5 minutes. Increasing the flow rate would result in a steep increase in perfusion pressure leveling into a higher horizontal plateau. Data points were collected for each plateau and plotted in a pressure-flow relationship. Only if each increase in flow rate produced a marked increase in perfusion pressure and if at the highest flow rate a perfusion pressure of at least 80 mmHg was obtained would the experiment be continued.

Third, the myogenic response to flow-induced perfusion pressure as an indicator of autoregulation in the renal arterial vasculature was examined. This test was performed subsequently to the pressure-flow relationship, maintaining the maximum flow rate of 9,7 ml/min. After recording pressure for 5 minutes, the regular perfusate was switched for calcium-free perfusate (see: Table 1) by quickly flipping the three-way stopcock, allowing perfusate to be changed without time loss or interrupting perfusion. The calcium-free perfusate was administered for 5 minutes. A deprivation of extracellular calcium would cause inhibition of active vasoconstriction and thus a decrease in perfusion pressure. Next, the calcium-free perfusate was washed out again applying regular perfusate for 5 minutes. Resupply of extracellular calcium thus achieved would reenable active vasoconstriction resulting in another increase in perfusion pressure. Data points were collected at the horizontal plateaus before, during and after application of calcium-free perfusate and plotted in a column diagram. Only if a significant drop in perfusion pressure levelling into a lower horizontal plateau could be recorded as an indicator of an intact myogenic response as a basic requirement for autoregulation being present would the kidney be used for further experiments.

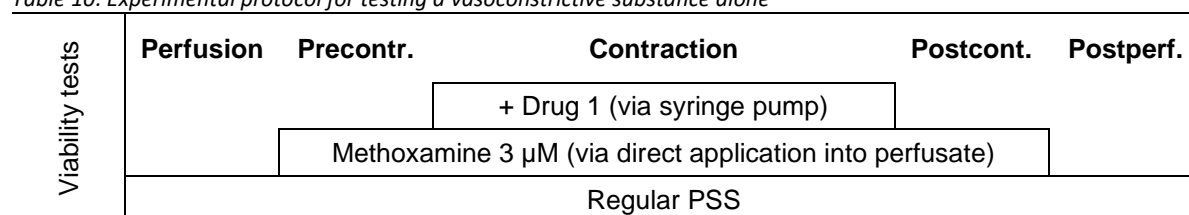
Fourth, the maximum degree of active vasoconstriction in response to 120 mM KCl was examined. To do so, the flow rate first had to be reduced from 9,7 ml/min after 5 minutes washout of calcium-free perfusate to 2,57 ml/min (correlating to a speed digit of 200) in order to reach a new baseline perfusion pressure below 60 mmHg, low enough not to be likely to induce a myogenic response. After reaching a new baseline plateau of perfusion pressure, the regular perfusate was switched for Modified PSS containing 120 mM KCl (see: Table 1) und applied for 10 minutes. High extracellular concentrations of K<sup>+</sup> would represent a strong vasoconstrictive stimulus leading to a marked increase in perfusion pressure. Next, the 120 mM KCl perfusate was washed out applying regular perfusate for at least 10 minutes. Deprivation of the depolarizing stimulus thus achieved would terminate vasoconstriction and perfusion pressure readouts return to the baseline. Data points were collected at the peak of 120 mM KCl-induced pressure increase and at the horizontal plateau before and after application and plotted on a column diagram. Only if active vasoconstriction resulted in an increase of perfusion pressure to absolute values above 160 mmHg and a subsequent drop of a least -120 mmHg back to baseline perfusion pressure could be observed as a sign of functional integrity of the arterial vasculature of the kidney would the kidney be used for further experiments.

#### 2.5.6 Experimental protocols

The ability of the renal arterial vasculature to constrict and dilate in response to drugs was investigated using two types of protocols. In both protocols, viability tests were followed by a brief period of perfusing PSS only at a flow rate of 2,57 ml/min to establish baseline perfusion pressure over at least 5 minutes. Next, precontraction was induced by switching the regular perfusate PSS for PSS preincubated with 3 μM Methoxamine, which was applied for at least 60 minutes until achieving a horizontal plateau before additional drugs were added.

The first type of protocol, applied if only vasoconstrictive drugs like HMR1556 or XE991 were to be tested, then proceeded to continuous application of the drug via syringe pump for at least 20 minutes in the above described manner (see: Chapter 2.3). Upon having been administered for an appropriate time, the application of the drug via syringe pump was stopped while perfusion with Methoxamine was continued to monitor for the occurrence of decrease in perfusion pressure in absence of the vasoconstrictive drug to be examined. Finally, after continuing perfusion with Methoxamine for at least another 30 minutes, the perfusate was switched back to regular PSS to confirm an adequate return of perfusion pressure to the baseline. Data points were collected every 5 minutes, starting 20 minutes before until 20 minutes after initiating application of the vasoconstrictive drug.

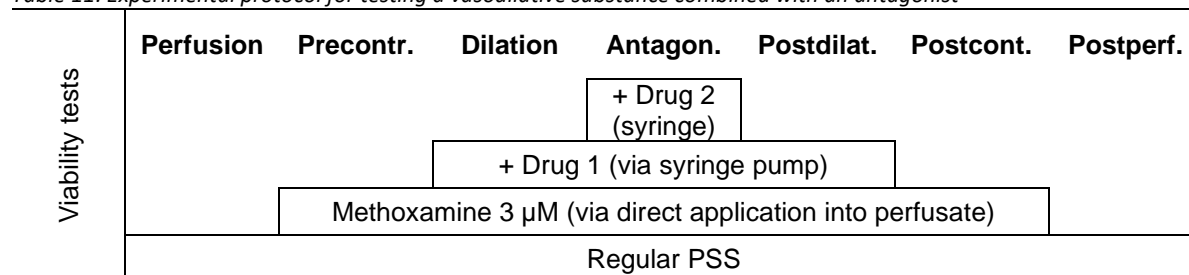
Table 10: Experimental protocol for testing a vasoconstrictive substance alone



Postcont. = post-contraction; Postperf. = post-perfusion; Precontr. = precontraction; PSS = physiological salt solution;

The second type of protocol, applied if a vasodilative drug like R-L3 with an antagonist like HMR155 or XE991 were to be tested, proceeded to continuous application of the vasodilative drug via syringe pump for 20 minutes, followed by the likewise continuous coadministration of the antagonist via a second syringe pump. Afterwards, the application of drugs or Methoxamine was reduced stepwise as described for the first type of protocol, always monitoring for the effect of washout of the substance. Data points were collected every 10 minutes starting at 20 minutes before initiating application of the first drug until 10 minutes after initiating application of the second drug.

Table 11: Experimental protocol for testing a vasodilative substance combined with an antagonist



Antagon. = Antagonization; Postcont. = post-contraction; Postdilat. = post-dilation; Postperf. = post-perfusion; Precontr. = precontraction; PSS = physiological salt solution;

### 2.5.7 Data analysis

All data points obtained by the data acquisition and analysis program (LabChart 8.0) as described above (see: Chapter 2.5.6) were first transferred to Microsoft Excel (2010 and 2016) for basic calculations and analysis.

During viability testing, the raw perfusion pressure readouts in mmHg were used either for direct statistical analysis and graphing or to calculate parameters of viability criteria like the area under the curve for pressure-flow relationships or the delta for the drop or increase in perfusion pressure in response to calcium-free or KCl 120 mM-containing perfusate.

During the actual pharmacological experiments, only raw perfusion pressure readouts in mmHg, subtracted by the baseline perfusion pressure prior to starting precontraction with Methoxamine, were used for direct statistical analysis and graphing without any normalization being necessary. Only for two graphs simple calculations were made, such as for comparison of (i) the degree of vasodilation induced by two different concentrations of R-L3 and (ii) their antagonization by HMR1556. In detail, (i) the delta of the decline in perfusion pressure induced by R-L3 was calculated by subtracting the baseline pressure recorded before application from the pressure readout after 20 minutes of application of R-L3 and then (ii) normalizing the delta of the increase in perfusion pressure induced by coadministration of HMR1556 as a percentage of that R-L3-induced drop in perfusion pressure (see: Figure 64). This same calculation was performed for comparison of the degree of antagonization of R-L3-induced vasodilation by HMR1556 and XE991 (see: Figure 66).

## 2.6 Statistics

GraphPad Prism version 7.03 for Windows (GraphPad Software, La Jolla California USA) was used both for calculating statistics and drawing and formatting graphs. Tables were formatted using Microsoft Word (2016) or Microsoft PowerPoint (2016).

All values are presented as arithmetic mean and standard error of the mean (SEM), with n representing the number of experiments conducted, corresponding to the number of animals used for the series. Significance was assumed at  $p \leq 0.05$ .

The area under the curve (AUC) was calculated for all CRRs and inverse CRRs in myography experiments as well as for pressure-flow relationships during viability testing in isolated perfused kidney experiments.

The negative logarithm of the half maximal effective concentration ( $pD_2$ ) as an expression of Methoxamine sensitivity was estimated from concentration-response curves by fitting the Hill equation using least squares regression as a fitting method

Paired t-tests were used for comparing perfusion pressure at different time points in isolated kidney perfusion experiments.

Unpaired t-tests were used for comparing precontraction levels between two groups in myography experiments as well as for comparison of AUCs in myography experiments.

Ordinary one-way ANOVA was used for comparing precontraction levels between three or more groups in myography experiments.

One-way repeated-measures ANOVA without assuming sphericity and therefore using Geisser-Greenhouse correction was used to separately analyze perfusion pressure amplitudes before and after application of drugs in isolated perfused kidney experiments.

Two-way repeated-measures ANOVA was used for comparing amplitudes of force between both CRRs and inverse CRRs in myography experiments.

Dunnett's multiple comparisons test was performed as a post-hoc test when comparing means of perfusion pressure amplitudes before and after application of drugs in isolated perfused kidney experiments

Pearson's r was calculated for demonstrating a correlation between the level of flow-induced pressure and the magnitude of the myogenic response caused by it in isolated perfused kidney experiments.

### 3 RESULTS

#### 3.1 Validation of the isolated perfused kidney model

The results presented later (see: Chapter 3.6) are the first data collected using this isolated perfused kidney method newly established in our laboratory. For the sake of validation, the following sections will set out the results of the viability tests performed prior to the actual experiments. Data was collected for viability tests including (i) confirmation of an intact arterial vasculature indicated by an appropriate pressure-flow relationship, (ii) testing for an intact myogenic response via calcium-free perfusate and (iii) testing for maximum active vasoconstriction of the renal vasculature via application of Modified PSS containing 120 mM KCl. Furthermore, we present data addressing the question whether kidney viability depends upon possible confounding factors like (a) prolonged cold storage of the kidney in PSS during the process of preparation, (b) usage of heparin prior to the extracorporeal preparation procedure or (c) accidental perfusion with air bubbles. These results will be addressed in detail later as part of the discussion on the validity of the method (see: Chapter 4.1).

The following scatter plot serves as an overview of viability test results and subsequent agonist-induced vasoconstriction with Methoxamine (Figure 5). It represents data derived from all kidneys that were used to collect experimental data in this thesis.

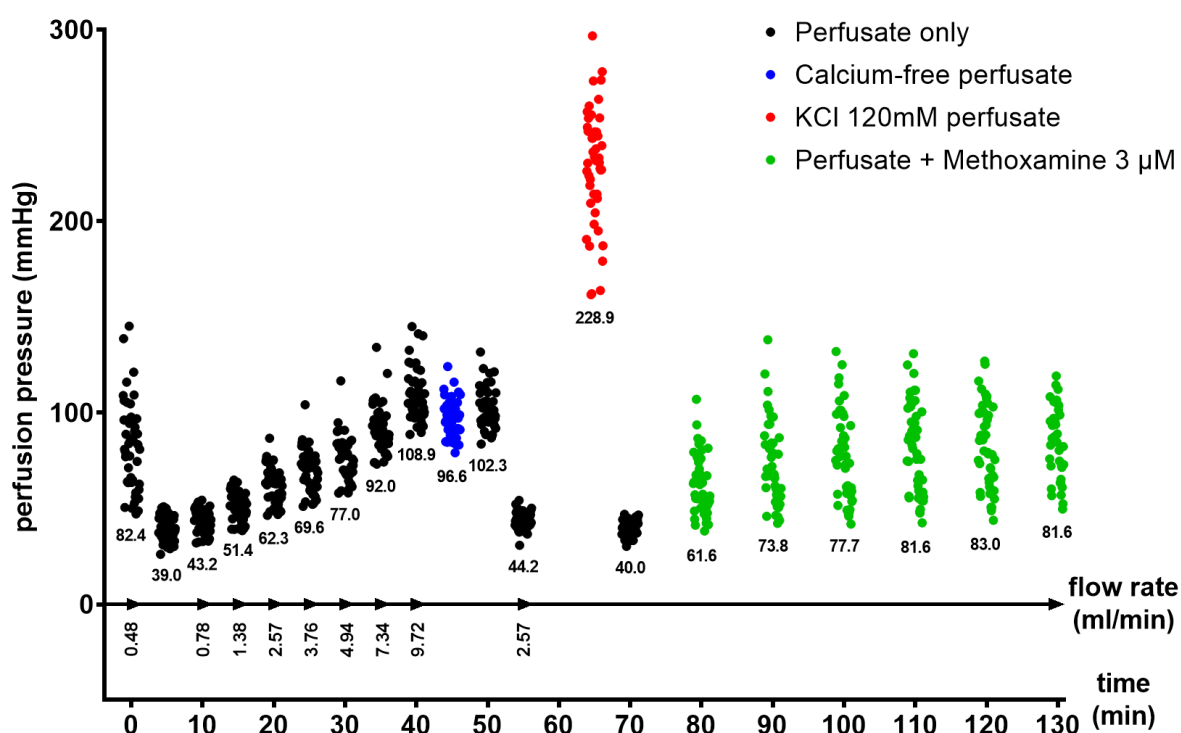


**Figure 5: Viability tests and Methoxamine-induced contraction in isolated perfused rat kidneys**

Time course of viability tests and subsequent precontraction induced by  $3 \mu\text{M}$  Methoxamine performed prior to experiments on Kv7 modulators ( $n=48$ ). Values are presented as original perfusion pressure recordings. Mean values of perfusion pressure readouts are given (in mmHg) below the data point clouds for each time point at which data was collected. The perfusion rate of the isolated kidneys is indicated by the “flow rate” timeline. The type of perfusate used is indicated by the color of the data point clouds as listed in the legend.

Pressure-flow relationships were obtained by stepwise increasing flow rates and typically displayed themselves in form of a steep increase in perfusion pressure leveling into a horizontal plateau of elevated pressure (Figure 6). Out of all 48 experiments used for analysis, the mean perfusion pressure at the maximum flow rate (after 40 minutes), was  $108.9 \pm 2.0$  mmHg (mean  $\pm$  SEM;  $n=48$ ).

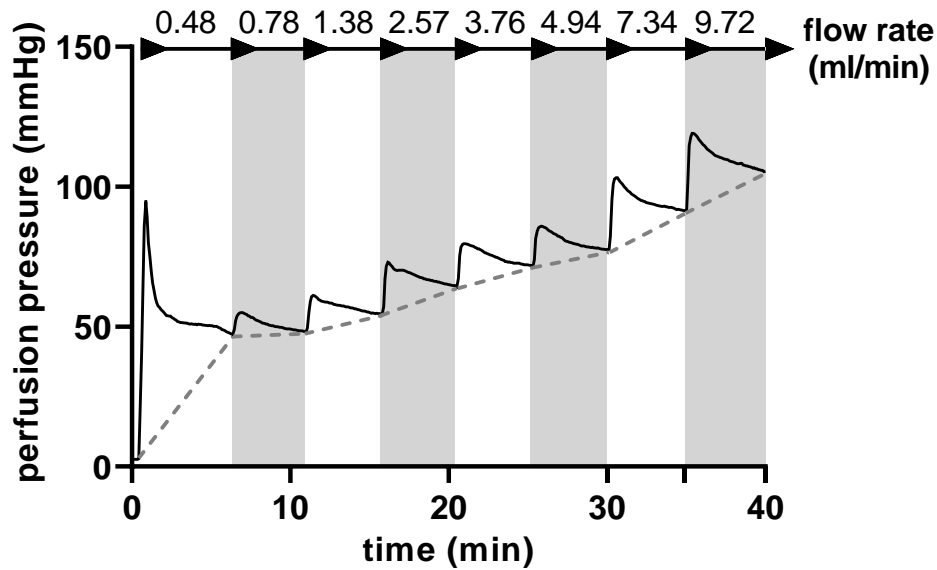


**Figure 6: Pressure-flow relationship indicating an intact arterial vasculature during viability testing of isolated perfused rat kidneys**

Representative recording of flow-induced increases in perfusion pressure immediately after starting perfusion. Values are presented as original perfusion pressure recordings. The perfusion rate of the isolated kidneys is indicated by the “flow rate” timeline. The area under the curve was calculated for each pressure-flow relationship from the data points collected towards the end of the pressure plateau as indicated by the grey dotted line.

Data points collected towards the end of each pressure plateau were used to calculate the area under the curve of the pressure-flow relationships. Having completed all experimental series, a retrospective statistical analysis of these AUC values was performed, finding no differences amongst the kidneys used as part of different experimental series (Figure 6).

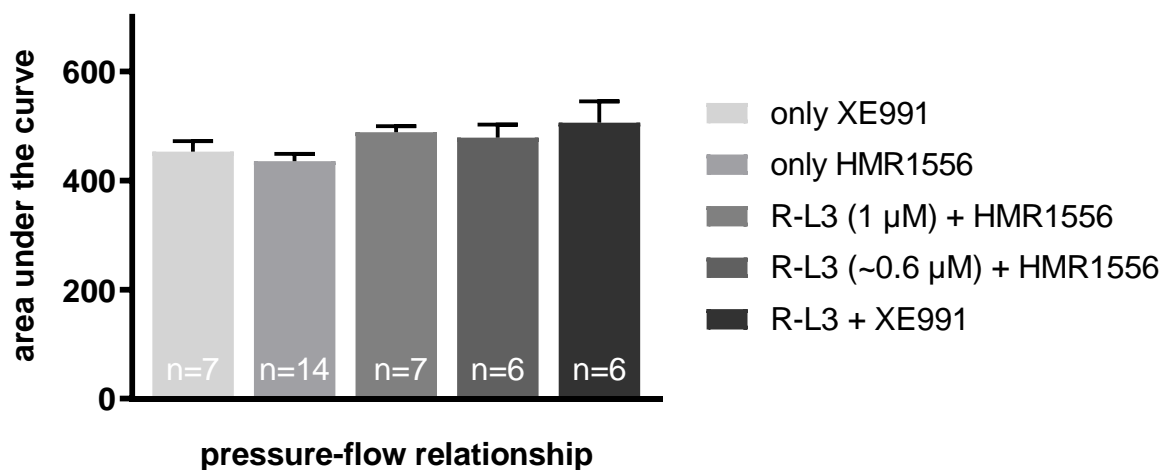


**Figure 7: Pressure-flow relationship in different experimental series during viability testing of isolated perfused rat kidneys**

Area under the curve calculated for each pressure-flow relationship and grouped for experimental series (One-way ANOVA:  $p=0,29$ ). Values are presented as mean  $\pm$  SEM.

Testing for an intact myogenic response at the maximum flow rate occurred by demonstrating the presence of pressure-induced vasoconstriction in form of a steep decrease in perfusion pressure following application of calcium-free perfusate and afterwards a steep increase in perfusion pressure when switching back to regular perfusate (Figure 8).

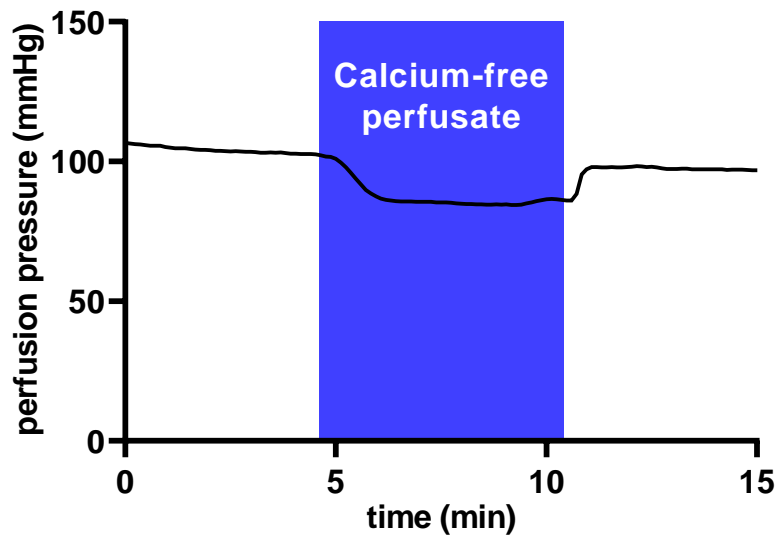


**Figure 8: Effect of calcium-free perfusate indicating an intact myogenic response during viability testing of isolated perfused rat kidneys**

Representative recording of a reversible decrease in perfusion pressure caused by application and weening of calcium-free perfusate. Values are presented as original perfusion pressure recordings. The short delay between change of perfusate and onset of effect is due to the dead space of the tubing system proximal of the perfused kidney.

Data points were collected prior to and towards the end of perfusion with calcium-free solution. Out of all 48 experiments, the average perfusion pressure dropped from  $108.9 \pm 2.0$  mmHg to  $96.6 \pm 1.4$  mmHg in response to calcium free perfusate and rose again to  $102.3 \pm 1.5$  mmHg (mean  $\pm$  SEM; n=48) after washout with regular perfusate (see: Figure 5). Statistical analyses performed for each experimental series found no differences between the deltas of perfusion pressure decreases between experimental series (Figure 9).

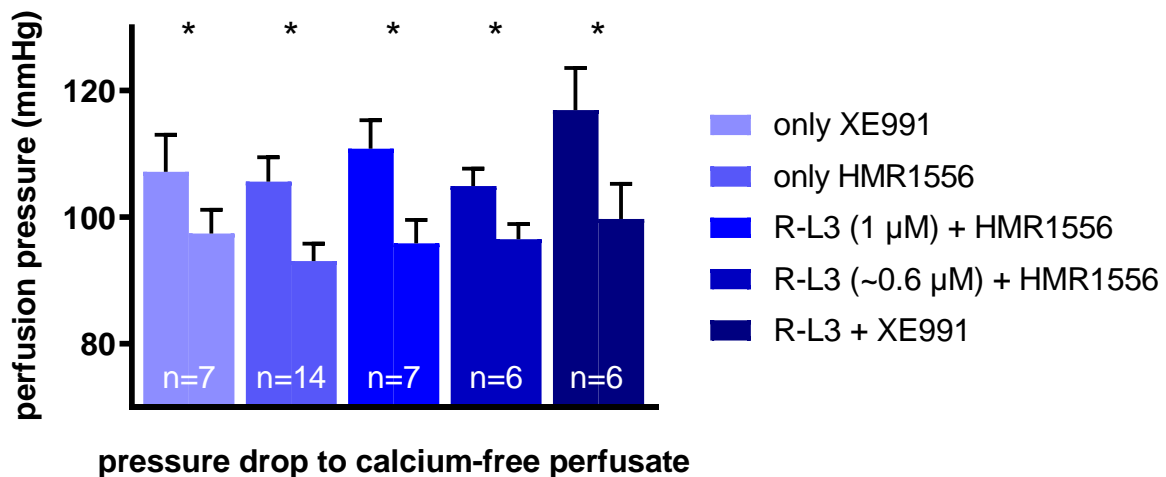


**Figure 9: Effect of calcium-free perfusate in different experimental series during viability testing of isolated perfused rat kidneys**

Perfusion pressure before and towards the end of application of calcium-free perfusate grouped for experimental series (paired Student's t test: \* $p < 0,05$ ). Not visually displayed: statistical comparisons of the Calcium-free induced delta in perfusion pressure (One-way ANOVA:  $p = 0,44$ ). Values are presented as mean  $\pm$  SEM.

Aiming to support the assumption that the pressure drop to calcium-free perfusate was actually due to inhibition of pressure-induced vasoconstriction and thus an indicator of an intact myogenic response, the Pearson correlation coefficient was calculated, revealing a strong correlation between

initial flow-induced perfusion pressure and the delta of perfusion pressure decrease induced by calcium-free perfusate (Figure 10).

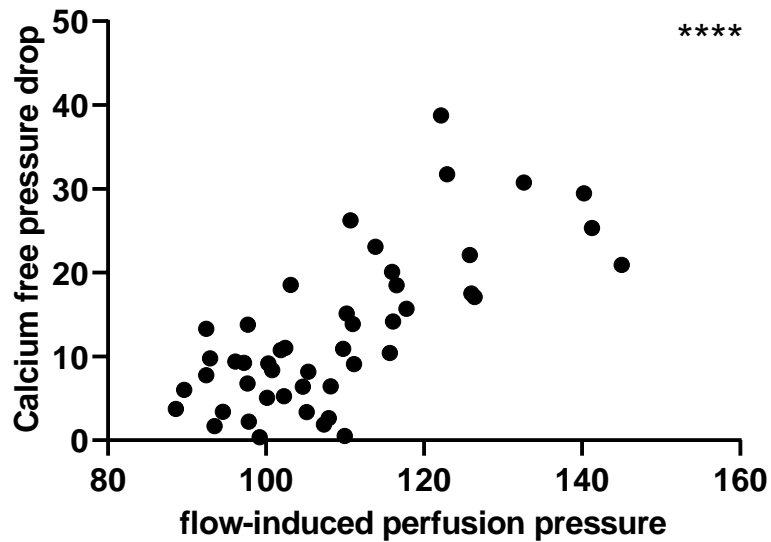


**Figure 10: Correlation between flow-induced perfusion pressure and decrease in perfusion pressure to Calcium-free perfusate in isolated perfused rat kidneys**

Scatter plot of the Calcium-free pressure drop plotted against initial flow-induced perfusion pressure (\*\*\*\* $p < 0,0001$ ; Pearson  $r = 0,71$ ; 95% confidence interval 0,54 to 0,83). Values are presented as original perfusion pressure recordings prior to application of Calcium-free perfusate or the same subtracted by the pressure readout towards the end of application of Calcium-free perfusate.

The maximum active vasoconstriction of the renal vasculature was tested via application of perfusate containing 120 mM KCl. This typically resulted in a marked increase in perfusion pressure that was entirely reversible after switching back to regular perfusate (Figure 11).

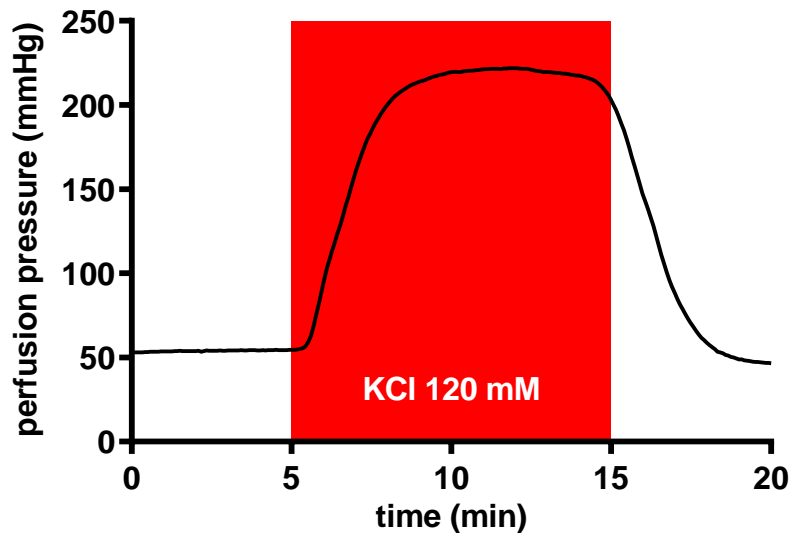


**Figure 11: Effect of KCl initiating maximum active vasoconstriction during viability testing of isolated perfused rat kidneys**  
Representative recording of a reversible increase in perfusion pressure caused by application and weening of perfusate containing 120 mM KCl. Values are presented as original perfusion pressure recordings. The short delay between change of perfusate and onset of effect is due to the dead space of the tubing system proximal of the perfused kidney.

On average, KCl induced increases in perfusion pressure from  $44.2 \pm 0.6$  mmHg to  $228.9 \pm 4.4$  mmHg (mean  $\pm$  SEM;  $n = 48$ ) (see: Figure 5). These data collected at the plateau before and at the peak of

elevated perfusion pressure caused by KCl was also statistically analyzed for groups of experimental series. There was an increase in perfusion pressure in all series and there were no differences among the KCl-induced delta in perfusion pressure between series (Figure 12).

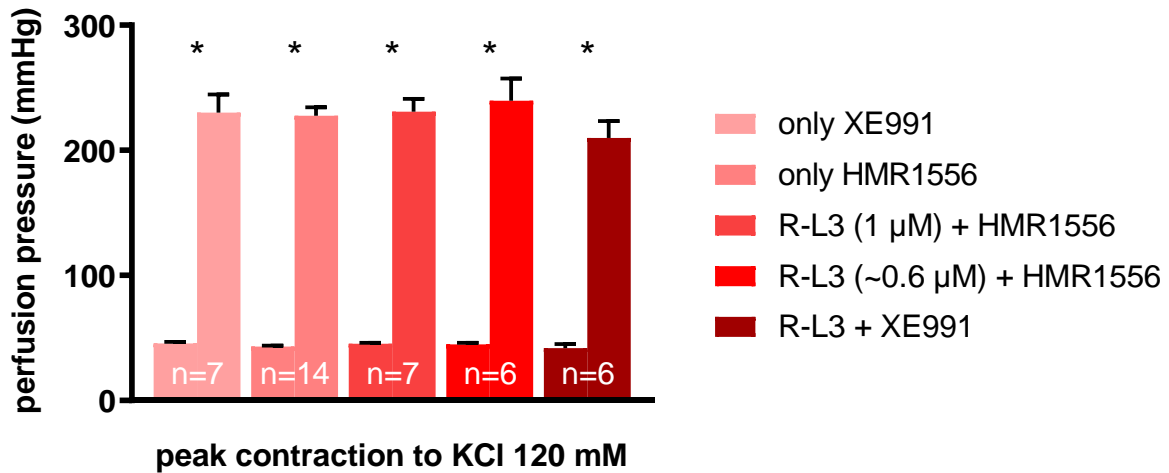


**Figure 12: Effect of KCl 120 mM in different experimental series during viability testing of isolated perfused rat kidneys**  
Perfusion pressure before and after 10 minutes application of perfusate containing 120 mM KCl grouped for experimental series (paired Student's *t* test: \* $p < 0.05$ ). Not visually displayed: statistical comparisons of the KCl 120 mM induced delta in perfusion pressure (One-way ANOVA:  $p = 0,70$ ). Values are presented as mean  $\pm$  SEM.

After finalizing the above described viability tests, perfused kidneys were precontracted by switching to regular perfusate containing Methoxamine at 3  $\mu$ M, which resulted in a gradual but sustained increase in perfusion pressure within usually 40-80 minutes (Figure 13). At this point, the actual experiments on  $K_v7$  modulators started, the results of which will be presented later (see: Chapter 3.6).

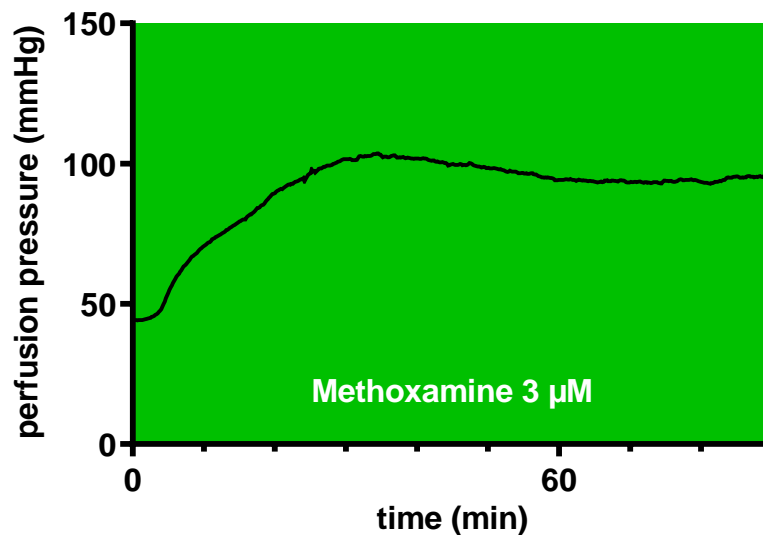


**Figure 13: Effect of Methoxamine initiating agonist-induced vasoconstriction in isolated perfused rat kidneys**  
Representative recording of a sustained increase in perfusion pressure caused by regular perfusate containing 3  $\mu$ M Methoxamine. Values are presented as original perfusion pressure recordings.

To expose a possible influence of renal organ edema caused by long-term perfusion with colloid-free perfusate on baseline perfusion pressure or agonist-induced contraction, we obtained pressure readouts (i) prior to application of Methoxamine; at the peak of Methoxamine-induced contraction both (ii) before wash-in and (iii) after wash-out of  $K_v7$  modulators; and again (iv) at the baseline after

wash-out of Methoxamine. This was done in all experiments except for the series “XE991 only” (see: Figure 59 + Figure 60) and “HMR1556 only” (see: Figure 61), in which experiments were terminated after application of HMR1556 or XE991. Analyses revealed slightly lower baseline perfusion pressures at the end of the experiments, while the maximum perfusion pressure during Methoxamine-induced perfusion pressure increase did not change over the time of the experiment (Figure 14).

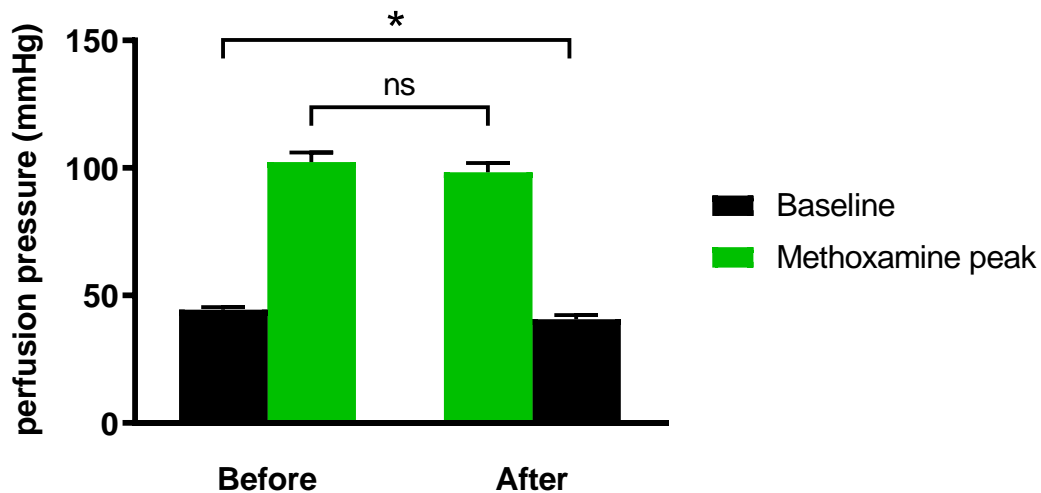


**Figure 14: Effect of long-term perfusion on baseline perfusion pressure and maximum agonist-induced contraction in isolated perfused rat kidneys**

Baseline perfusion pressure before and after the experiment (black) and peak perfusion pressure during application of 3  $\mu$ M Methoxamine before and after wash-in or wash-out of  $K_v7$  modulators (paired Student's *t* test:  $n=27$ ;  $*p<0.05$ ; *ns* = not significant). Baseline perfusion pressure decreased slightly from  $44,5 \pm 0,9$  mmHg to  $40,6 \pm 1,7$  mmHg. Values are presented as mean  $\pm$  SEM.

One possible confounding factor we suspected for influencing isolated perfused kidney viability and thus the ability of the renal vasculature to properly respond to vasoconstrictive or -dilative stimuli or agents was prolonged cold storage. Prolonged cold storage had to occur sometimes during preparation since the capacity to perfuse multiple kidneys simultaneously was limited to the number of perfusion systems and could last up to ~4 hours prior to starting perfusion, as compared to ~30 minutes when starting preparation immediately after cervical dislocation. To evaluate whether cold storage was relevant for viability of the renal arterial vasculature we performed statistical analyses of viability test results between stored and immediately-prepared perfused kidneys. Although the initial perfusion pressure after starting kidney perfusion at a low flow rate was found to be higher in kidneys that had been stored, pressure-flow responses were similar and no differences in peak perfusion pressures induced by either depolarization-induced contraction to 120 mM KCl or by agonist-induced contraction to 3  $\mu$ M Methoxamine were quantifiable (Figure 15).

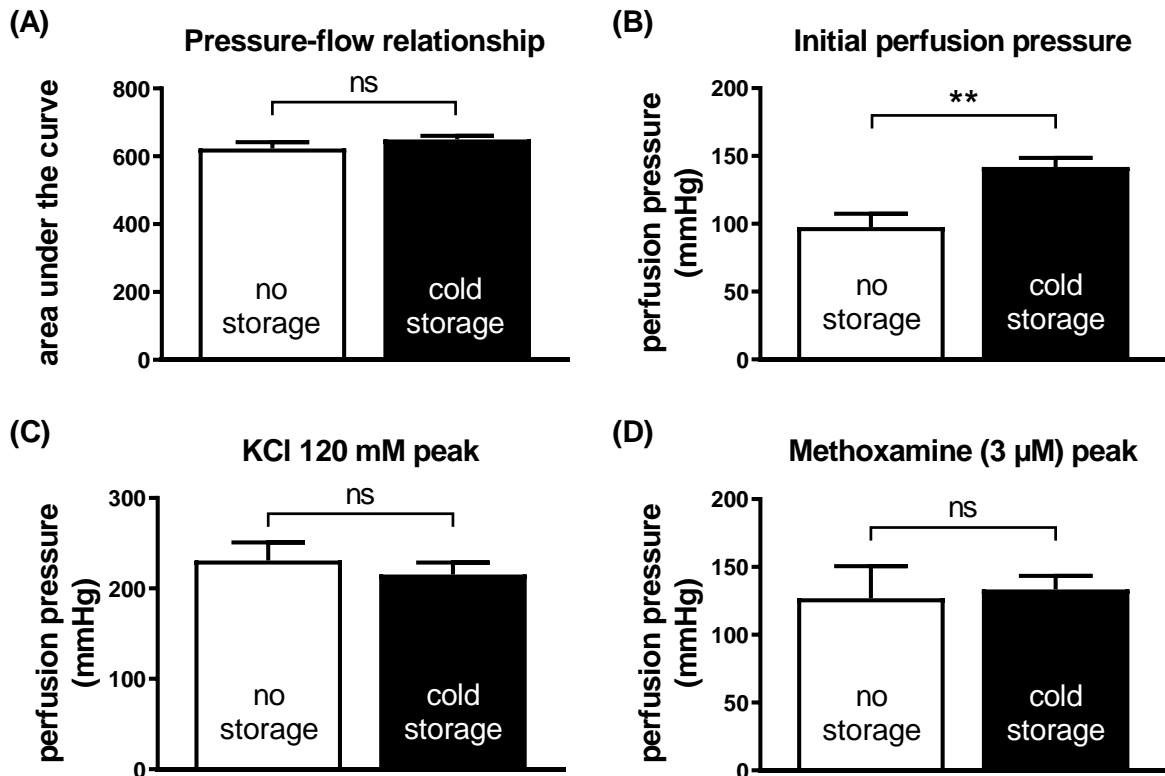


**Figure 15: Effect of prolonged cold storage during preparation on viability tests in isolated perfused rat kidneys**  
 Comparison of perfused kidneys prepared immediately after cervical dislocation (no storage) or stored at 4°C for ~4 hours (cold storage). Values are presented as mean  $\pm$  SEM (unpaired Student's t test:  $n=5$ ;  $**p<0,01$ ; ns = not significant). (A) Area under the curve calculated for pressure-flow relationship (95% confidence interval -23,53 to 76,05). (B) Initial perfusion pressure recording of the pressure peak observed immediately after starting perfusion of the kidneys at a flow rate of ~0,5 ml/min (95% confidence interval 16,71 to 72,01). (C) Original perfusion pressure recording of the pressure peak induced by perfusate containing 120 mM KCl (95% confidence interval -70,75 to 39,73). (D) Original perfusion pressure recording of the pressure peak induced by application of 3  $\mu$ M Methoxamine (95% confidence interval -52,88 to 66,00).

A second possible confounding factor we accounted for was the formation of blood clots in the renal vasculature during no-flow time while preparing the perfused kidneys. Blood clots might influence vascular resistance and thus confound perfusion pressure recordings. We investigated whether intraaortal application of 100 I.U. heparin immediately after laparotomy as has been described (see: Chapter 0) affected the results of viability tests. Evidently, pretreatment with heparin had no effect on either pressure-flow relationships, decreases in perfusion pressure induced by calcium-free perfusate or increases in perfusion pressure induced by perfusate containing 120 mM KCl or 3  $\mu$ M Methoxamine (Figure 16).

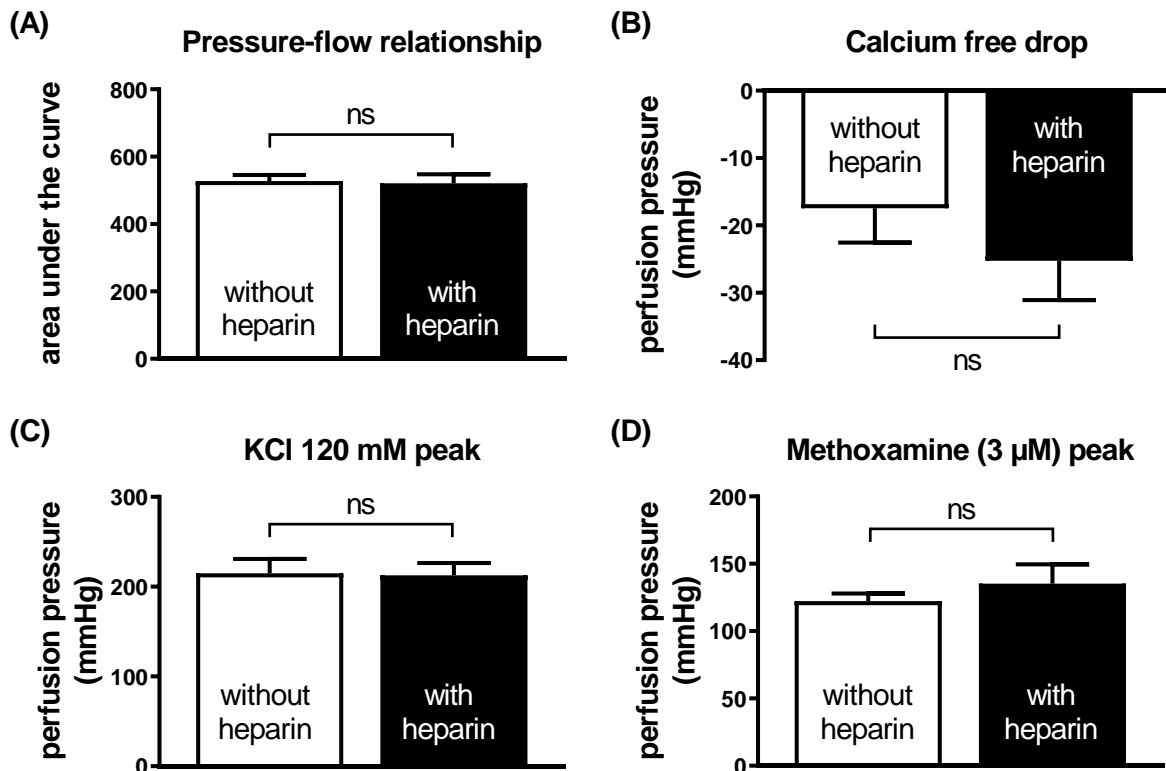


**Figure 16: Effect of heparinization during preparation on viability tests in isolated perfused rat kidneys**

Comparison of perfused kidneys with no postmortal treatment (without heparin) or with intraaortal infusion of 100 I.U. heparin immediately after laparotomy (with heparin). Values are presented as mean  $\pm$  SEM (unpaired Student's *t* test:  $n=7$ ; ns = not significant). (A) Area under the curve calculated for pressure-flow relationship (95% confidence interval -77,58 to 63,75). (B) Original perfusion pressure recording of the pressure drop induced by calcium-free perfusate (95% confidence interval -24,73 to 9,12). (C) Original perfusion pressure recording of the pressure peak induced by perfusate containing 120 mM KCl (95% confidence interval -48,45 to 43,70). (D) Original perfusion pressure recording of the pressure peak induced by application of 3  $\mu$ M Methoxamine (95% confidence interval -20,90 to 46,65).

Thirdly, accidental perfusion with air was a problem we were unable to entirely undermine. Minor air bubbles developed in the final part of the perfusion system tubing between the last bubble trap and the perfusion cannula. This most often occurred towards the end of recording pressure-flow relationships, when flow rates were highest and thus the air-induced effect on perfusion pressure most distinctive. Perfusion with air bubbles typically resulted in either a small hump or a sharp down-and-up spike in perfusion pressure that usually levelled back to previous perfusion pressure levels within 1 minute (Figure 17).

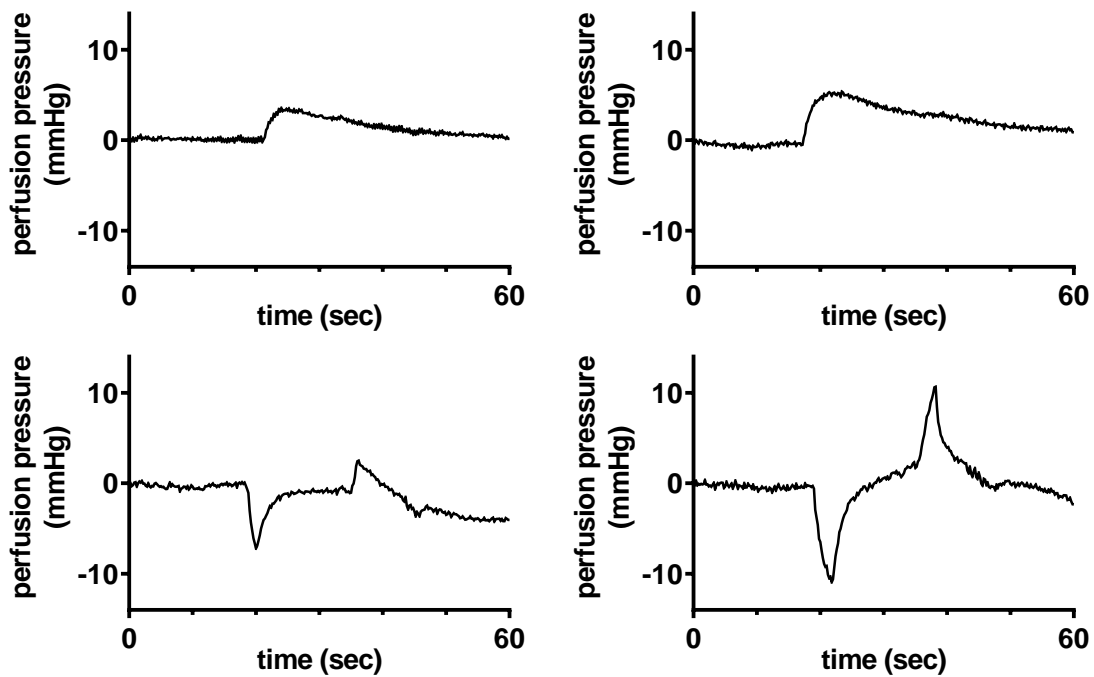


**Figure 17: Examples of accidental perfusion with air bubbles during viability testing of isolated perfused rat kidneys**  
Representative recordings for reversible humps or down-and-up spikes increase in perfusion pressure caused by accidental perfusion with air bubbles recorded at maximum flow rate towards the end of pressure-flow relationships. Values are presented as original perfusion pressure recordings subtracted by pressure readouts at 0 seconds.

Evaluating whether accidental air perfusion affected vasoconstrictive or dilative responses of perfused kidneys in subsequent experiments, no differences were found in pressure-flow relationships, pressure decreases to Calcium-free perfusate or pressure increases to KCl or Methoxamine between the two groups (Figure 18).

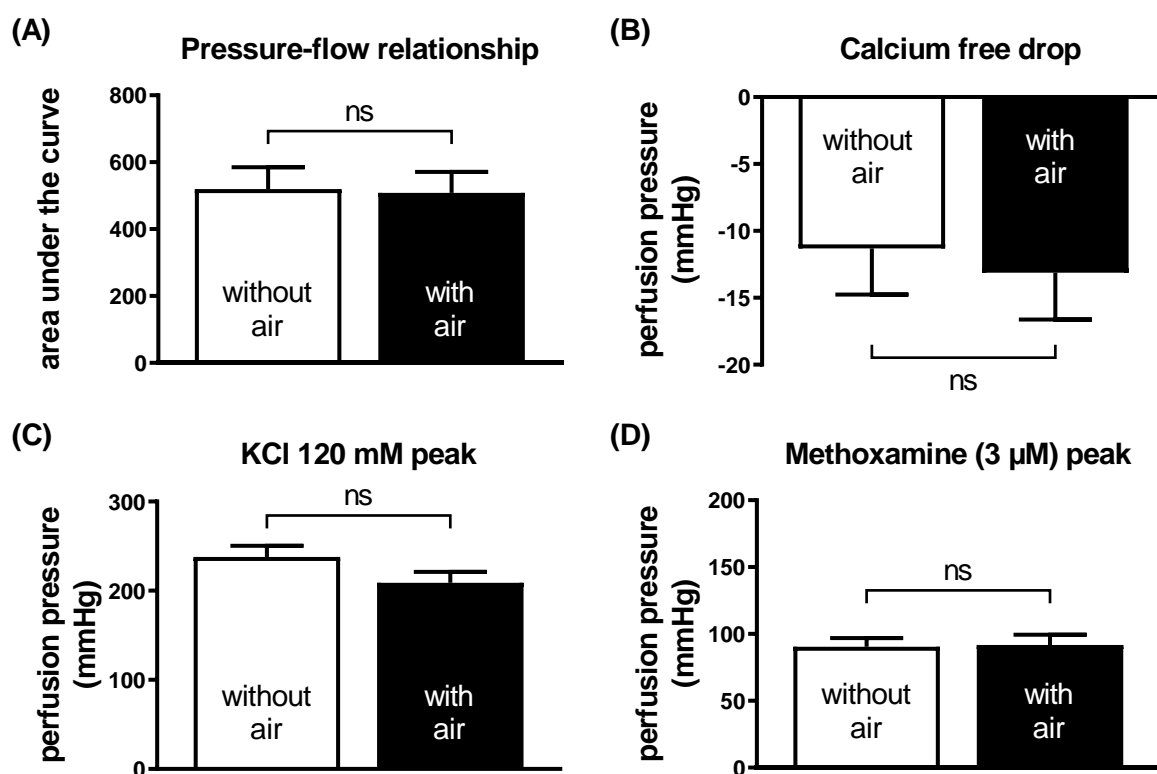


**Figure 18: Effect of accidental perfusion with air bubbles on viability tests in isolated perfused rat kidneys**

Comparison of perfused kidneys in which accidentally air bubbles were dragged and perfused (with air) or in which no accidental air perfusion was observed (without air). Values are presented as mean  $\pm$  SEM (unpaired Student's *t* test:  $n=8$ ; ns = not significant). (A) Area under the curve calculated for pressure-flow relationship (95% confidence interval -205,8 to 183,3). (B) Original perfusion pressure recording of the pressure drop induced by calcium-free perfusate (95% confidence interval -12,36 to 8,73). (C) Original perfusion pressure recording of the pressure peak induced by perfusate containing 120 mM KCl (95% confidence interval -66,33 to 8,23). (D) Original perfusion pressure recording of the pressure peak induced by application of 3  $\mu$ M Methoxamine (95% confidence interval -20,24 to 22,83).

In summary, our results demonstrate that isolated perfused kidney viability tests including (i) pressure-flow relationships for confirmation of an intact arterial vasculature, (ii) pressure decreases to calcium-free perfusate for confirmation of an intact myogenic response, (iii) increases in perfusion pressure to perfusate containing 120 mM KCl for testing of maximum depolarization-induced vasoconstriction and also (iv) increases in perfusion pressure to perfusate containing 3  $\mu$ M Methoxamine for testing agonist-induced vasoconstriction were all unaffected by possible confounding factors like (a) prolonged cold storage during preparation, (b) heparinization as part of the preparation procedure or (c) accidental air perfusion and were furthermore similar when grouped for the experimental series conducted subsequently.

### 3.2 Contribution of $K_v7.2-5$ to agonist-induced renal vasoconstriction

To ascertain the effect of the  $K_v7.2-7.5$  activator Retigabine<sup>249, 273</sup> in context with the pan- $K_v7$  blocker XE991<sup>217, 219, 249, 250</sup> and the selective  $K_v7.1$  activator HMR1556<sup>215, 216</sup> in agonist-induced vasoconstriction of isolated renal small arteries, a series of precontraction experiments was conducted using a protocol with the selective  $\alpha_1$ -adrenoceptor agonist Methoxamine as a precontracting agent (see: Table 4).

Application of Retigabine (0.3-30  $\mu$ M) caused concentration-dependent relaxations of Methoxamine-induced precontractions (Figure 19).

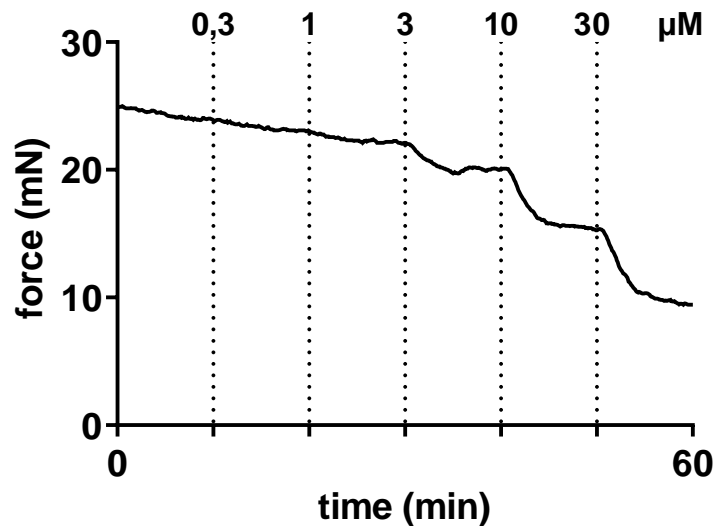


**Figure 19: Effect of Retigabine activating  $K_{v7.2-5}$  channels on agonist-induced contraction in rat renal interlobar arteries**  
Original recording of relaxant responses to Retigabine (0.3 – 30  $\mu\text{M}$ ) in rat renal interlobar artery after precontraction with 0.7  $\mu\text{M}$  Methoxamine.

To exclude the possibility of DMSO being responsible for the dilating effect of DMSO-solved Retigabine we conducted a series of concentration-response relationships comparing the effects of DMSO and Retigabine. We observed a stable plateau of precontraction during administration of DMSO (maximum concentration 1  $\mu\text{l/ml}$ ), compared to which Retigabine induced considerable concentration-dependent relaxations (Figure 20).

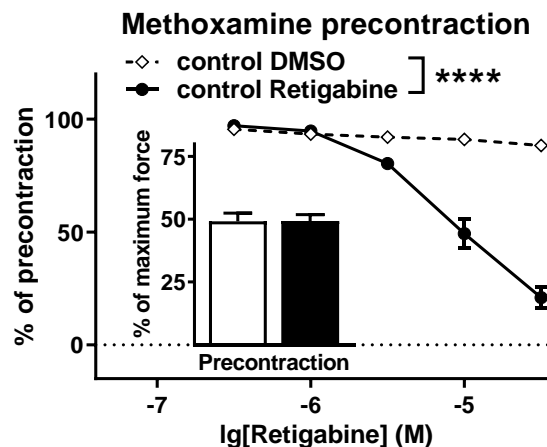


**Figure 20: Effect of  $K_{v7.2-5}$  activation on agonist-induced contraction in rat renal interlobar arteries**  
Concentration-dependent relaxation to Retigabine (0.3 – 30  $\mu\text{M}$ ) normalized to precontraction levels (Two-way repeated-measures ANOVA: \*\*\*\* $p < 0,0001$ ). Arteries were precontracted with Methoxamine to a similar percentage of maximum force (Student's  $t$  test:  $n=9$ ; 95% confidence interval -8,62 to 8,92).

To evaluate whether pan- $K_{v7}$  block with XE991 would prevent relaxations to the  $K_{v7.2-5}$  activator Retigabine, vessels were preincubated with XE991 prior to precontraction and subsequently Retigabine applied as before. We found that Retigabine-induced concentration-dependent relaxations were still observable in the presence of XE991 (Figure 21).

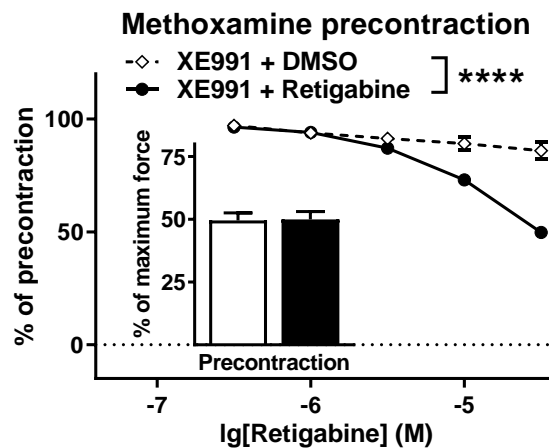


**Figure 21: Effect of  $K_v7.2-5$  activation during  $K_v7$  blockade on agonist-induced contraction in rat renal interlobar arteries**  
 Concentration-dependent relaxation to Retigabine ( $0.3 - 30 \mu\text{M}$ ) normalized to precontraction levels (Two-way repeated-measures ANOVA: \*\*\*\* $p < 0,0001$ ). Arteries were precontracted with Methoxamine to a similar percentage of maximum force (Student's  $t$  test:  $n=9$ ; 95% confidence interval -8,93 to 9,75) and preincubated with  $3 \mu\text{M}$  XE991.

Similarly, we tested the effect of preincubation with the selective  $K_v7.1$  blocker HMR1556 prior to Retigabine CRRs and likewise observed Retigabine-induced concentration-dependent relaxations in the presence of HMR1556 (Figure 22).

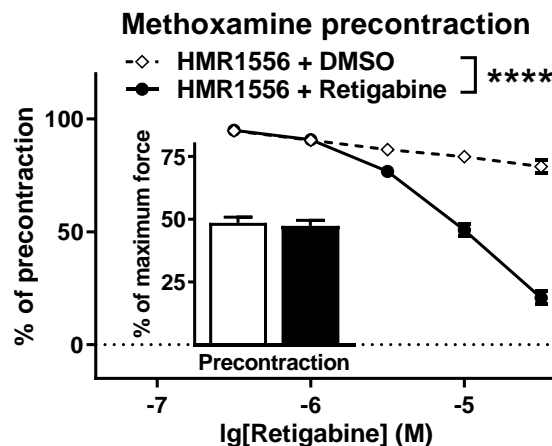


**Figure 22: Effect of  $K_v7.2-5$  activation during  $K_v7.1$  blockade on agonist-induced contraction in rat renal interlobar arteries**  
 Concentration-dependent relaxation to Retigabine ( $0.3 - 30 \mu\text{M}$ ) normalized to precontraction levels (Two-way repeated-measures ANOVA: \*\*\*\* $p < 0,0001$ ). Arteries were precontracted with Methoxamine to a similar percentage of maximum force (Student's  $t$  test:  $n=9$ ; 95% confidence interval -7,88 to 5,56) and preincubated with  $10 \mu\text{M}$  HMR1556.

To discern a possible antagonizing effect of the pan- $K_v7$  blocker XE991 and the selective  $K_v7.1$  blocker HMR1556 on relaxations to the  $K_v7.2-7.5$  activator Retigabine, an additional analysis comparing the above described concentration-response relationships (Figure 20 – Figure 22) was performed. We found that Retigabine-induced concentration-dependent relaxations were reduced by XE991, but not by HMR1556 (Figure 23).

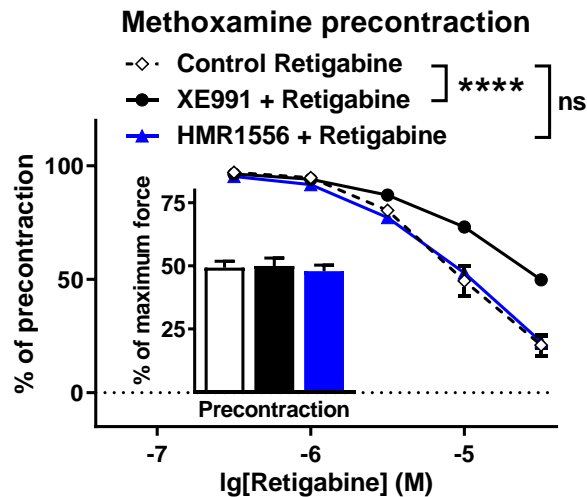


**Figure 23: Effect of  $K_v7.2-5$  activation during  $K_v7$  or  $K_v7.1$  blockade on agonist-induced contraction in rat renal interlobar arteries**

Concentration-dependent relaxation to Retigabine (0.3 – 30  $\mu$ M) normalized to precontraction levels (Two-way repeated-measures ANOVA:  $n=9/9/8$ ; \*\*\*\* $p<0,0001$ ; ns = not significant). Arteries were preincubated with either 3  $\mu$ M XE991 or 10  $\mu$ M HMR1556 and precontracted with Methoxamine to a similar percentage of maximum force (One-way ANOVA:  $n=9/9/8$ ;  $p=0,87$ ).

To test for a dependency of Retigabine-induced relaxations on the level of precontraction, we conducted the above described experiment (Figure 21) in two groups of vessels which were precontracted to either higher or lower tone using different concentrations of Methoxamine. We discovered that the different levels of Methoxamine+XE991-induced precontraction achieved in these experiments did not change the degree by which arteries were relaxed by Retigabine (Figure 24).

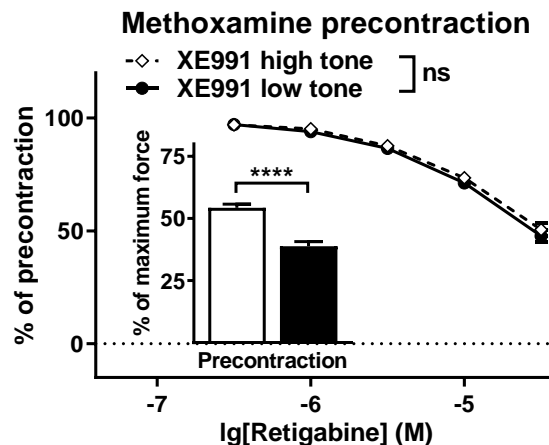


**Figure 24: Effect of  $K_v7.2-5$  activation during  $K_v7$  blockade at different levels of agonist-induced contraction in rat renal interlobar arteries**

Concentration-dependent relaxation to Retigabine (0.3 – 30  $\mu$ M) normalized to precontraction levels (Two-way repeated-measures ANOVA: ns = not significant). Arteries were preincubated with 3  $\mu$ M XE991 and precontracted with Methoxamine to either high tone or low tone (Student's  $t$  test:  $n=9$ ; \*\*\*\* 95% confidence interval -20,44 to -10,44)

To test whether the chronological order in which  $K_v7$  modulators are applied, as well as whether the concentration of XE991 used in our above described experiments (Figure 21 + Figure 24) had been too low to block  $K_v7$  sufficiently, both of which might represent possible reasons for the inability of XE991 to entirely abolish Retigabine-induced relaxations, we conducted additional experiments on

Methoxamine precontractions in which we first applied the maximum concentration of Retigabine used before (30  $\mu$ M) and only afterwards administered XE991 at concentrations of 3  $\mu$ M and subsequently 10  $\mu$ M. We found that Retigabine-induced relaxations were fully antagonized by XE991 at 3  $\mu$ M, and increasing concentration to 10  $\mu$ M did not cause any additional increases in vessel tone (Figure 25).

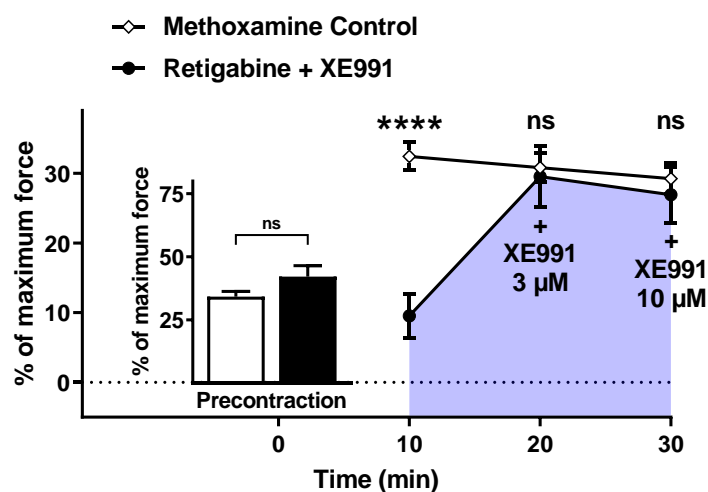


**Figure 25: Effect of  $K_v7$  blockade during  $K_v7.2-5$  activation on agonist-induced contraction in rat renal interlobar arteries**  
Relaxation induced by 30  $\mu$ M Retigabine antagonized over time with 3  $\mu$ M and 10  $\mu$ M XE991 compared to time control (Student's *t* test: \*\*\*\* $p < 0.0001$ ; ns = not significant) in arteries precontracted with Methoxamine to a similar percentage of maximum force (Student's *t* test:  $n=9$ ; ns = not significant; 95% confidence interval -2,19 to 18,11).

In summary, our results demonstrate that Retigabine causes marked vasorelaxations in Methoxamine-precontracted rat renal resistance arteries which are unaffected by the  $K_v7.1$  blocker HMR1556 but diminished by the pan- $K_v7$  blocker XE991 independently of the level of precontraction.

### 3.3 Contribution of $K_v7.1$ to agonist-induced renal vasoconstriction

To determine the role of  $K_v7.1$  in renal resistance artery vasoconstriction, an experimental series similar to the previous one done on Retigabine (see: Chapter 3.2) was conducted using the selective  $K_v7.1$  activator R-L3<sup>213, 318</sup> in context with the pan- $K_v7$  blocker XE991 and the selective  $K_v7.1$  activator HMR1556 on the basis of a Methoxamine precontraction protocol (see: Table 4).

Application of R-L3 produced concentration-dependent relaxations in Methoxamine-induced precontractions. These relaxations differed from the stable plateau of precontraction observed during application of equivalent concentrations of its solvent DMSO (maximum concentration 0.64  $\mu$ l/ml) (Figure 26).

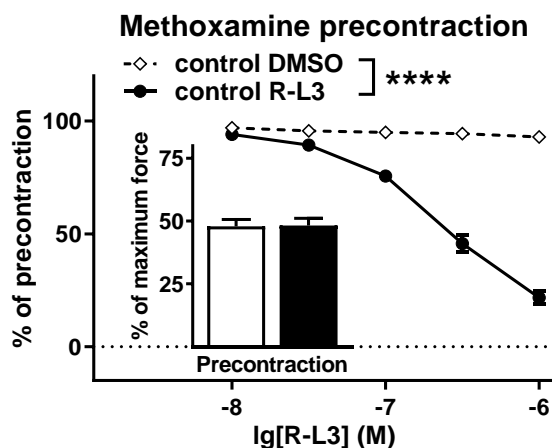


**Figure 26: Effect of  $K_v7.1$  activation on agonist-induced contraction in rat renal interlobar arteries**

Concentration-dependent relaxation to R-L3 (0.01 – 1  $\mu$ M) normalized to precontraction levels (Two-way repeated-measures ANOVA: \*\*\*\* $p < 0,0001$ ). Arteries were precontracted with Methoxamine to a similar percentage of maximum force (Student's  $t$  test:  $n=10$ ; 95% confidence interval -8,10 to 8,75)

To address whether pan- $K_v7$  blockade with XE991 would antagonize the concentration-dependent relaxations induced by R-L3, vessels were preincubated with XE991 prior to Methoxamine precontraction. We found that R-L3-induced relaxations were still observable in the presence of XE991 (Figure 27).

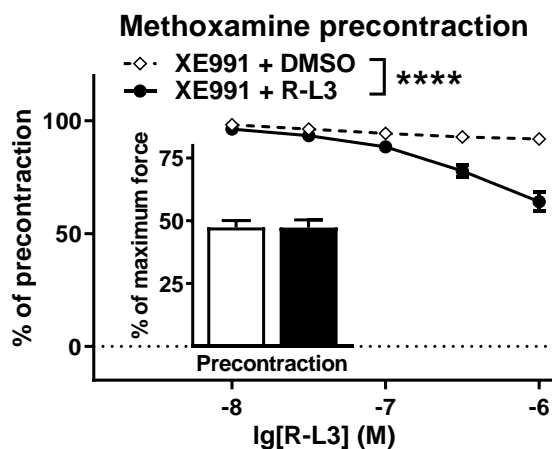


**Figure 27: Effect of  $K_v7.1$  activation during  $K_v7$  blockade on agonist-induced contraction in rat renal interlobar arteries**

Concentration-dependent relaxation to R-L3 (0.01 – 1  $\mu$ M) normalized to precontraction levels (Two-way repeated-measures ANOVA: \*\*\*\* $p < 0,0001$ ). Arteries were preincubated with 3  $\mu$ M XE991 and precontracted with Methoxamine to a similar percentage of maximum force (Student's  $t$  test:  $n=10$ ; 95% confidence interval -8,72 to 8,69).

Analogously, to test whether relaxations to R-L3 would persist in the presence of the  $K_v7.1$  specific blocker HMR1556, vessels were preincubated with HMR1556 prior to Methoxamine precontractions. We likewise observed R-L3-induced concentration-dependent relaxation in the presence of HMR1556 (Figure 28).

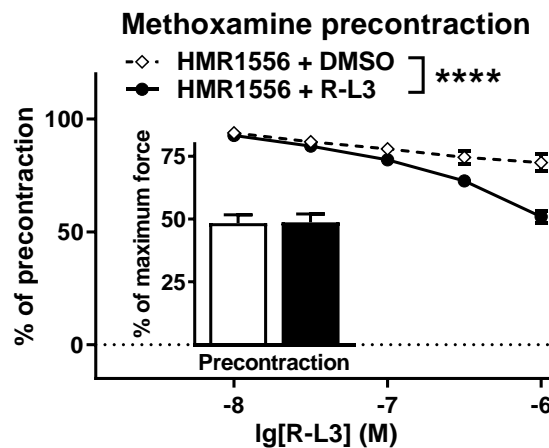


**Figure 28: Effect of  $K_{v7.1}$  activation during  $K_{v7.1}$  blockade on agonist-induced contraction in rat renal interlobar arteries**  
Concentration-dependent relaxation to R-L3 (0.01 – 1  $\mu$ M) normalized to precontraction levels (Two-way repeated-measures ANOVA: \*\*\*\* $p < 0,0001$ ). Arteries were preincubated with 10  $\mu$ M HMR1556 and precontracted with Methoxamine to a similar percentage of maximum force (Student's  $t$  test:  $n=9$ ; 95% confidence interval -9,58 to 10,25).

Aiming to ascertain whether the pan- $K_v7$  blocker XE991 and the selective  $K_{v7.1}$  blocker HMR1556 antagonized relaxations to R-L3, an analysis comparing the above described CRRs was performed (Figure 26 – Figure 28). We established that both XE991 and HMR1556 were effective in reducing R-L3-induced concentration-dependent relaxations (Figure 29).

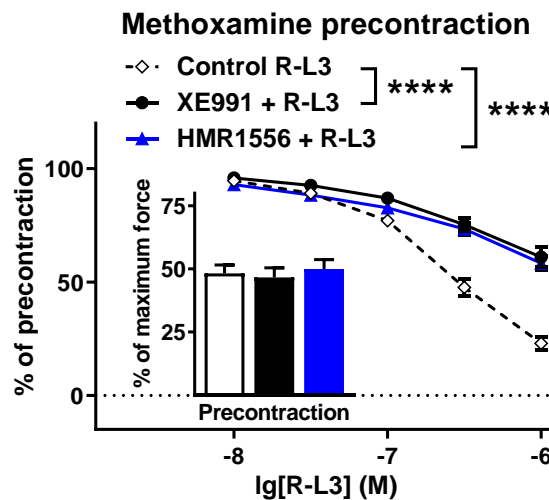


**Figure 29: Effect of  $K_{v7.1}$  activation during  $K_v7$  or  $K_{v7.1}$  blockade on agonist-induced contraction in rat renal interlobar arteries**

Concentration-dependent relaxation to R-L3 (0.01 – 1  $\mu$ M) normalized to precontraction levels (Two-way repeated-measures ANOVA:  $n=8/8/7$ ; \*\*\*\* $p < 0,0001$ ). Arteries were preincubated with either 3  $\mu$ M XE991 or 10  $\mu$ M HMR1556 and precontracted with Methoxamine to a similar percentage of maximum force (One-way ANOVA:  $n=8/8/7$ ;  $p=0,81$ ).

Finally, to differentiate whether the level of agonist-induced precontraction influences the degree by which XE991 diminishes relaxations to R-L3, we performed analogous experiments as earlier with Retigabine (see: Figure 27), having two groups of arteries precontracted to either high or low tone with different concentrations of Methoxamine. We confirmed that different levels of Methoxamine-induced precontraction did not affect the dimension of R-L3-induced relaxations after preincubation with XE991 (Figure 30).

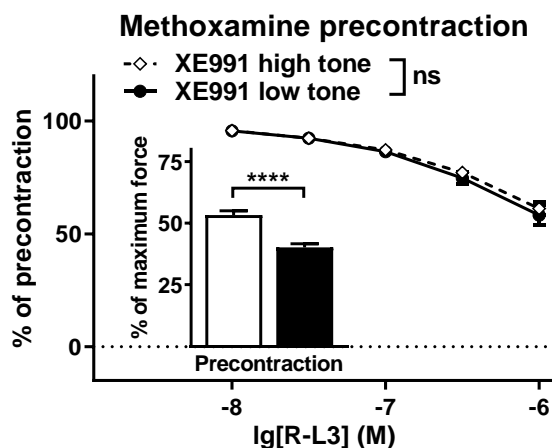


**Figure 30: Effect of  $K_{v7.1}$  activation during  $K_{v7}$  blockade at different levels of agonist-induced contraction in rat renal interlobar arteries**

Concentration-dependent relaxation to R-L3 (0.01 – 1  $\mu$ M) normalized to precontraction levels (Two-way repeated-measures ANOVA: ns = not significant). Arteries were preincubated with 3  $\mu$ M XE991 and precontracted with Methoxamine to either high tone or low tone (Student's *t* test:  $n=10$ , \*\*\*\* 95% confidence interval -18,06 to -8,25).

In summary, our results demonstrate that R-L3 causes marked vasorelaxations in Methoxamine-precontracted rat renal resistance arteries which are diminished by both the  $K_{v7.1}$  blocker HMR1556 and the pan- $K_{v7}$  blocker XE991 independently of the level of precontraction.

### 3.4 Contribution of $K_{v7}$ to the anticontractile effect of ANP in agonist-induced renal vasoconstriction

Endogenous dilators sometimes employ  $K^+$  channels as effectors for their anticontractile effects. In search for interference between the cGMP-dependent vasodilator ANP<sup>319</sup> and  $K_{v7}$  channels in regulating renal artery tone, we performed experiments with a protocol using concentration-response relationships for estimation of  $pD_2$  as an indicator of Methoxamine sensitivity (see: Table 3). By preincubation with ANP and subsequent application of  $K_{v7}$  activators R-L3 or Retigabine or  $K_{v7}$  blockers HMR1556 (in the presence of R-L3) we were able to conduct a detailed functional analysis of  $K_{v7}$  channel contribution to agonist-induced renal resistance artery contractility.

Previous unpublished experiments have shown that XE991 (3  $\mu$ M) increases, while ANP (100 nM) decreases concentration-dependent contractions to Methoxamine in renal interlobar arteries, with their contractile or anticontractile effects, respectively being both unimpaired by the presence of the other. This implicates that elevated Methoxamine sensitivity induced by  $K_{v7}$  block is independent of cGMP-mediated pathways, and that vice versa reduced Methoxamine sensitivity mediated by cGMP-mediated pathways is unaffected by blockade of  $K_{v7}$  channels. To further elucidate the question whether oppositely, the anticontractile effect of  $K_{v7.2-5}$  activation would similarly be independent of ANP-induced vasorelaxation, we first performed concentration-response relationships with Methoxamine after preincubation with either Retigabine, ANP, both substances combined or solvent only for control. We observed that Retigabine (30  $\mu$ M) and ANP (100 nM) both diminish concentration-dependent contractions to Methoxamine, with their decrease being both additive and unimpaired in the presence of the other (Figure 31).

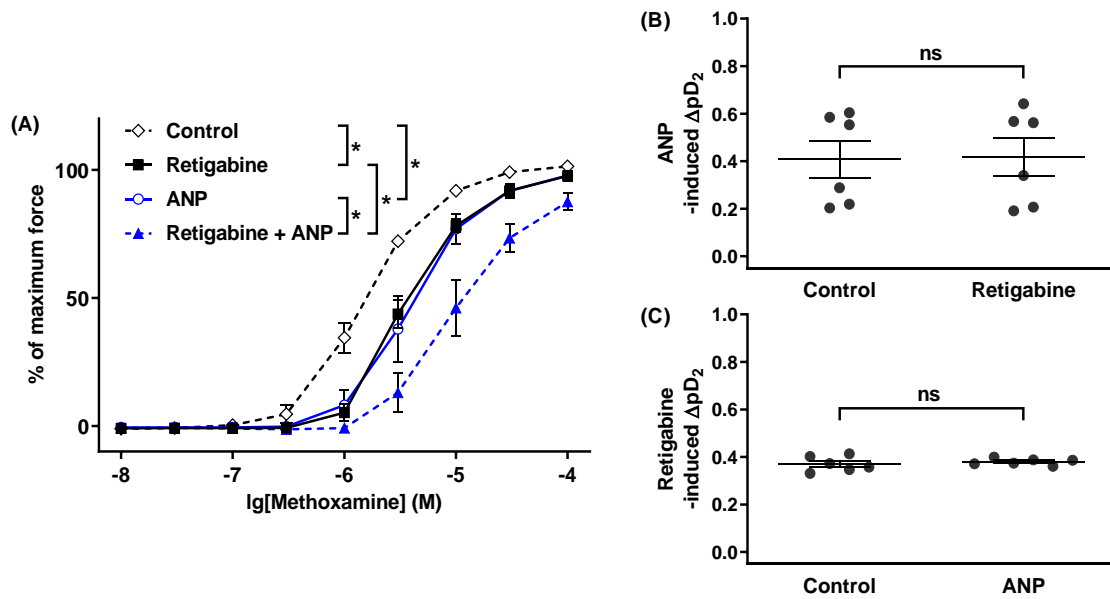


**Figure 31: Functional role of ANP in context with  $K_v7.2-5$  channel activation in rat renal interlobar arteries**

(A) Methoxamine-induced contraction in absence of Retigabine and ANP (control), in presence of 30  $\mu M$  Retigabine only (Retigabine), in presence of 100 nM ANP only (ANP) and in presence of both Retigabine and ANP (Retigabine + ANP) (Two-way repeated measures ANOVA:  $n=6$ ;  $*p<0,05$ ). (B) ANP-induced  $\Delta pD_2$  in absence (control) and in presence of Retigabine (Student's  $t$  test:  $n=6$ ; 95% confidence interval -0,24 to 0,26). (C) Retigabine-induced  $\Delta pD_2$  in absence (control) and in presence of ANP (Student's  $t$  test:  $n=6$ ; 95% confidence interval -0,02 to 0,04).

Next, we examined the anticontractile effect of the  $K_v7.1$  activator R-L3 for interference with ANP-induced vasorelaxation and analogously found that R-L3 (1  $\mu M$ ) and ANP (100 nM) both diminish concentration-dependent contractions to Methoxamine, with their decrease likewise being both additive and unimpaired by the presence of the other (Figure 32).

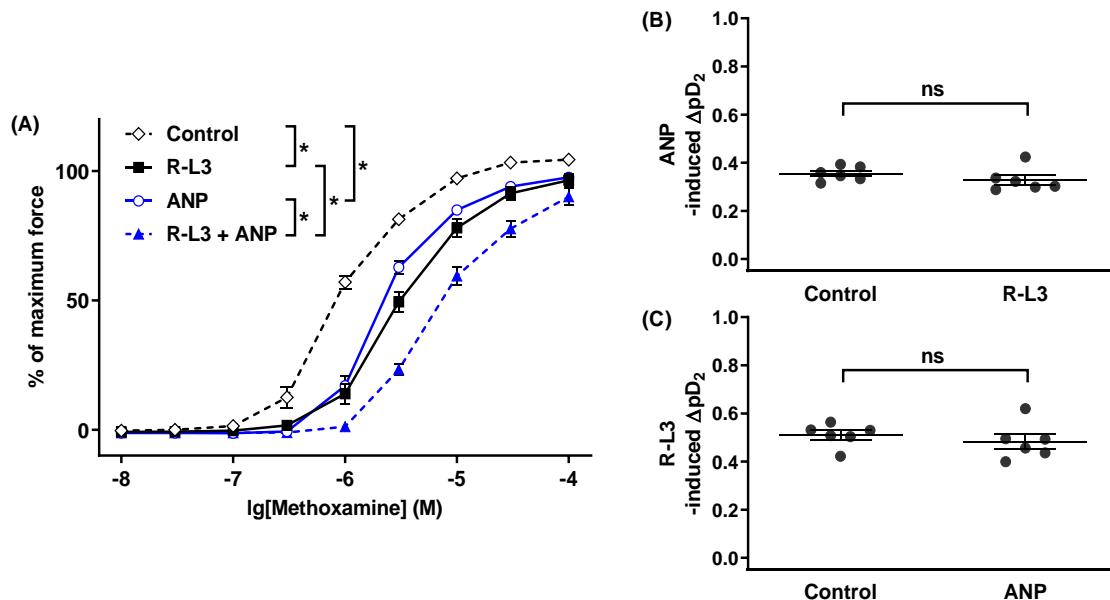


**Figure 32: Functional role of ANP in context with  $K_v7.1$  channel activation in rat renal interlobar arteries**

(A) Methoxamine-induced contraction in absence of R-L3 and ANP (control), in presence of 1  $\mu M$  R-L3 only (R-L3), in presence of 100 nM ANP only (ANP) and in presence of both R-L3 and ANP (R-L3 + ANP) (Two-way repeated measures ANOVA:  $n=6$ ;  $*p<0,05$ ). (B) ANP-induced  $\Delta pD_2$  in absence (control) and in presence of R-L3 (Student's  $t$  test:  $n=6$ ; 95% confidence interval -0,02 to 0,04).

interval -0,079 to 0,026). (C) R-L3-induced  $\Delta pD_2$  in absence (control) and in presence of ANP (Student's *t* test: *n*=6; 95% confidence interval -0,10 to 0,055).

Previous unpublished experiments have demonstrated that application of HMR1556 alone has no effect, whereas HMR is effective in antagonizing R-L3, as indicated by its increase in the contractile response to Methoxamine following preincubation with R-L3. Therefore, we conducted experiments testing the contractile effect of HMR1556 for ANP-dependency after preincubation of all vessels with R-L3. We again confirmed that in the presence of R-L3 (1  $\mu$ M), HMR1556 (10  $\mu$ M) enhanced, while ANP (100 nM) reduced contractile responses to Methoxamine and further demonstrated that the increase or decrease in Methoxamine sensitivity caused by HMR1556 resp. ANP were unimpaired by the absence or presence of one another (Figure 33).

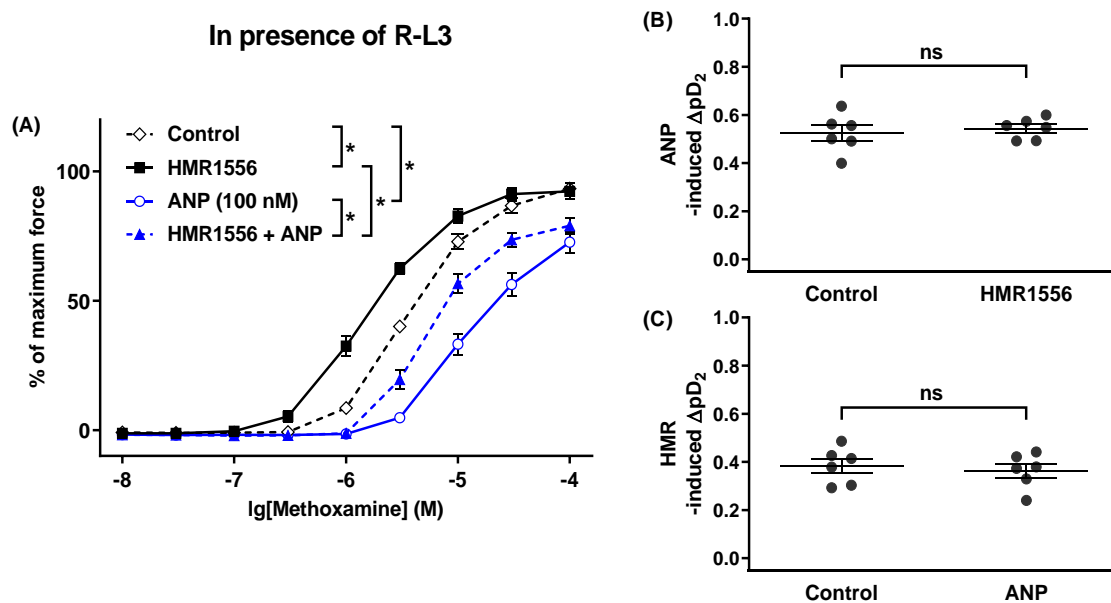


**Figure 33: Functional role of ANP in context with  $K_v7.1$  channel blockade following  $K_v7.1$  activation in rat renal interlobar arteries**

(A) Methoxamine-induced contraction in arteries preincubated with 1  $\mu$ M R-L3 in absence of HMR1556 and ANP (control), in presence of 10  $\mu$ M HMR1556 only (HMR1556), in presence of 100 nM ANP only (ANP) and in presence of both HMR1556 and ANP (HMR1556 + ANP) (Two-way repeated measures ANOVA: *n*=6; \**p*<0,05). (B) ANP-induced  $\Delta pD_2$  in arteries preincubated with 1  $\mu$ M R-L3 in absence (control) and in presence of HMR1556 (Student's *t* test: *n*=6; 95% confidence interval -0,064 to 0,10). (C) HMR-induced  $\Delta pD_2$  in arteries preincubated with 1  $\mu$ M R-L3 in absence (control) and in presence of ANP (Student's *t* test: *n*=6; 95% confidence interval -0,11 to 0,075).

The anticontractile effect of ANP at 100 nM when coadministered with R-L3 was so strong that even in the presence of HMR1556 the maximum contractile response to Methoxamine at the highest concentration (100  $\mu$ M) did not reach the level of the control group (Figure 33). Since by our methods, Methoxamine sensitivity was estimated by fitting concentration-response curves to the Hill equation using least squares regression, the accuracy of the estimate may be reduced in such circumstances. Therefore, to confirm the validity of our results, we conducted another series of the same protocol, only this time with a lower concentration of ANP (30 nM). This as intended brought the maximum contractile response back up to control level, but otherwise confirmed our results (Figure 34).

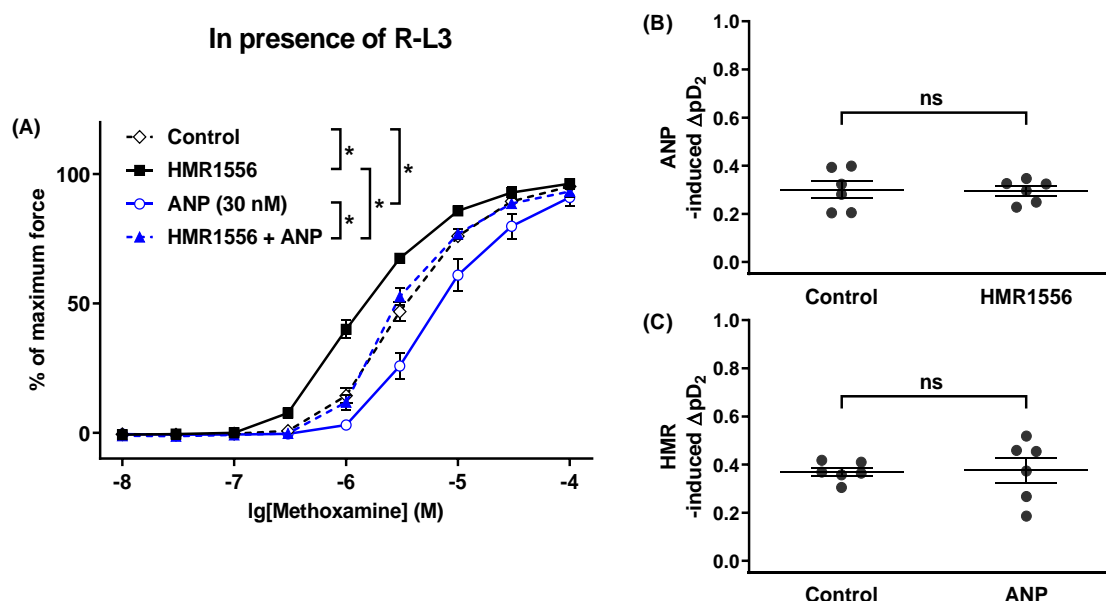


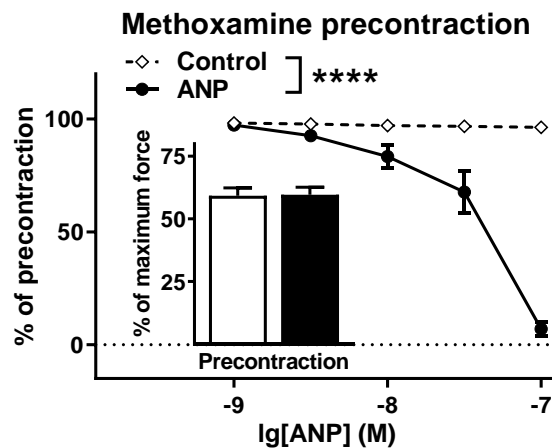
**Figure 34: Functional role of ANP in context with  $K_v7.1$  channel blockade following  $K_v7.1$  activation in rat renal interlobar arteries**

(A) Methoxamine-induced contraction in arteries preincubated with 1  $\mu$ M R-L3 in absence of HMR1556 and ANP (control), in presence of 10  $\mu$ M HMR1556 only (HMR1556), in presence of 30 nM ANP only (ANP) and in presence of both HMR1556 and ANP (HMR1556 + ANP). Two-way repeated measures ANOVA:  $n=6$ ;  $*p<0,05$ . (B) ANP-induced  $\Delta pD_2$  in arteries preincubated with 1  $\mu$ M R-L3 in absence (control) and in presence of HMR1556 (Student's  $t$  test:  $n=6$ ; 95% confidence interval -0,095 to 0,084). (C) HMR-induced  $\Delta pD_2$  in arteries preincubated with 1  $\mu$ M R-L3 in absence (control) and in presence of ANP (Student's  $t$  test:  $n=6$ ; 95% confidence interval -0,12 bis 0,13).

In summary, our results thus far demonstrate that Methoxamine sensitivity of renal resistance arteries is decreased by the  $K_v7.1$  activator R-L3 as well as by the  $K_v7.2-5$  activator Retigabine and is increased by the  $K_v7.1$  blocker HMR1556 in the presence of R-L3, with all of these effects reciprocally being both unaffected by, and itself not affecting, the anticontractile effect caused by preincubation with ANP. We thus provide substantial evidence that on a functional level, both the contractile and the anticontractile effect of  $K_v7$  channels depicted by increased or decreased sensitivity to the vasoconstrictive  $\alpha_1$ -adrenoceptor agonist methoxamine are unaffected by the cGMP-dependent endogenous vasodilator ANP.

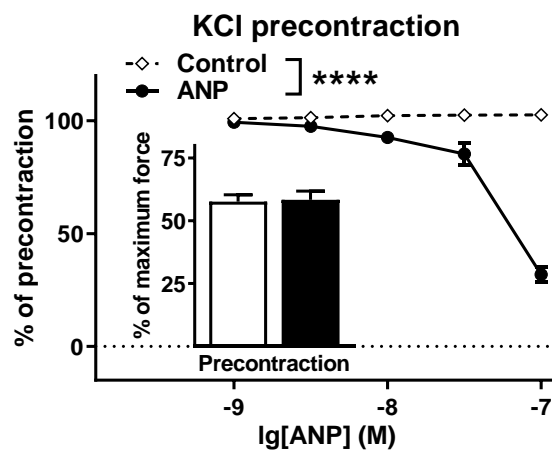
Having demonstrated this, we next conducted experiments following a protocol using either Methoxamine or KCl or various  $K^+$  channel blockers (see: Table 5) to study the concentration-dependent effect of ANP not only on agonist-induced, but also on depolarization-induced vasoconstriction. This way, we were able to investigate the role of  $K_v7$  channels in context with ANP in vessels differentially precontracted through activation of different signaling pathways, allowing us to later draw more detailed conclusions on intracellular signaling of  $K_v7$ - and ANP-mediated modification of renal resistance artery reactivity (see: Chapter 4.4).

First, the effect of ANP on Methoxamine-induced precontraction was examined to ascertain its effectiveness in counteracting agonist-induced vasoconstriction. Agonist-induced vasoconstriction involves a multitude of mechanistic elements, including  $Ca^{2+}$ -dependent and  $Ca^{2+}$ -sensitizing mechanisms (see: Chapter 1.4.2). We found ANP (1-100 nM) to cause marked concentration-dependent relaxations of Methoxamine-precontracted renal interlobar arteries (Figure 35).



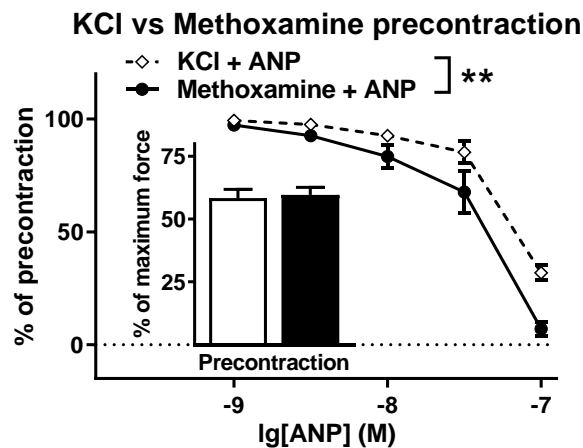
**Figure 35: Effect of ANP on contraction induced by  $\alpha_1$ -adrenoceptor agonist Methoxamine in rat renal interlobar arteries**  
 Concentration-dependent relaxation to ANP (1 – 100 nM) normalized to precontraction levels (Two-way repeated-measures ANOVA: \*\*\*\* $p < 0,0001$ ). Arteries were precontracted with Methoxamine to a similar percentage of maximum force (Student's *t* test:  $n=13$ ; 95% confidence interval -8,53 to 9,29).

Second, the effect of ANP on KCl-induced contraction was studied to evaluate its potential to counteract depolarization-induced vasoconstriction caused by functional elimination of all  $K^+$  channels present. We established that ANP likewise causes concentration-dependent relaxations of renal interlobar arteries precontracted with 50 mM KCl (Figure 36).



**Figure 36: Effect of ANP on contraction induced by KCl in rat renal interlobar arteries**  
 Concentration-dependent relaxation to ANP (1 – 100 nM) normalized to precontraction levels (Two-way repeated-measures ANOVA: \*\*\*\* $p < 0,0001$ ). Arteries were precontracted with 50 mM KCl to a similar percentage of maximum force (Student's *t* test:  $n=13$ ; 95% confidence interval -8,36 to 9,83).

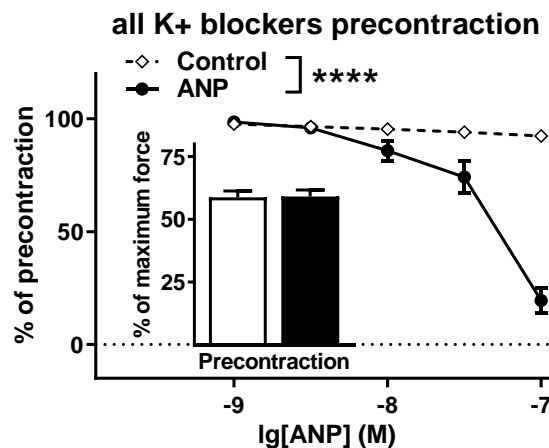
Subsequently, in search for differential effectiveness of ANP in counteracting agonist-induced or depolarization-induced vasoconstriction, a comparison of both responses (Figure 35 + Figure 36) was performed and revealed concentration-dependent relaxation caused by ANP to be more marked in arteries precontracted with Methoxamine than in arteries precontracted with 50 mM KCl (Figure 37).



**Figure 37: Effect of ANP on contraction induced by KCl or  $\alpha_1$ -adrenoceptor agonist Methoxamine in rat renal interlobar arteries**

Concentration-dependent relaxation to ANP (1 – 100 nM) normalized to precontraction levels (Two-way repeated-measures ANOVA:  $**p < 0,01$ ). Arteries were either precontracted with 50 mM KCl or with Methoxamine to a similar percentage of maximum force (Student's t test:  $n=13$ ; 95% confidence interval -8,12 to 10,65).

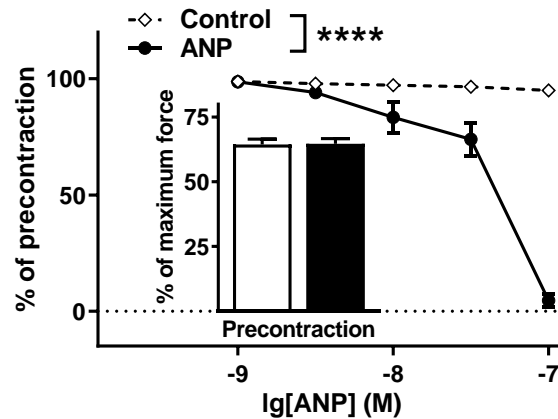
Having demonstrated that ANP is able to relax vasoconstriction induced by KCl and thus via functional elimination of  $K^+$  channels (Figure 36), we proceeded towards investigating the role of  $K_v7$  channels in this process. This was achieved by first testing the effect of ANP on precontraction induced by blockade of all known  $K^+$  channels expressed in the artery's VSMCs, using a cocktail of pharmacological blockers for  $BK_{Ca}$  (iberiotoxin, 0.1  $\mu$ M)<sup>157</sup>,  $K_{ATP}$  (glibenclamide, 1  $\mu$ M)<sup>320</sup>,  $K_{ir2}$  (BaCl, 30  $\mu$ M)<sup>321</sup>,  $K_v1$  (DPO-1, 1  $\mu$ M)<sup>175, 176</sup>,  $K_v2$  and  $K_v4$  (stromatoxin, 0.1  $\mu$ M)<sup>177</sup> and  $K_v7$  (XE991, 3  $\mu$ M). We found that ANP was similarly effective in producing relaxations in precontractions induced by individual pharmacological blockade of all known  $K^+$  channels, specifically including  $K_v7$  blockers (Figure 38).



**Figure 38: Effect of ANP on contraction induced by various  $K^+$  blockers in rat renal interlobar arteries**

Concentration-dependent relaxation to ANP (1 – 100 nM) normalized to precontraction levels levels (Two-way repeated-measures ANOVA:  $****p < 0,0001$ ). Arteries were preincubated with 3  $\mu$ M XE991 and precontracted with blockers for  $BK_{Ca}$  (iberiotoxin, 0.1  $\mu$ M),  $K_{ATP}$  (glibenclamide, 1  $\mu$ M),  $K_{ir2}$  (BaCl, 30  $\mu$ M),  $K_v1$  (DPO-1, 1  $\mu$ M) and  $K_v2$  and  $K_v4$  (stromatoxin, 0.1  $\mu$ M) to a similar percentage of maximum tension (Student's t test:  $n=14$ ; 95% confidence interval -7,14 to 7,86).

In parallel, we applied ANP in arteries precontracted with the same  $K^+$  channel blocker cocktail as before (Figure 38), only this time not including the  $K_v7$  blocker XE991. This likewise resulted in concentration-dependent relaxations to ANP (Figure 39).

all K<sup>+</sup> blockers without XE991 precontraction

**Figure 39: Effect of ANP on contraction induced by various K<sup>+</sup> blockers excluding XE991 in rat renal interlobar arteries**  
 Concentration-dependent relaxation to ANP (1 – 100 nM) normalized to precontraction levels (Two-way repeated-measures ANOVA: \*\*\*\* $p < 0,0001$ ). Arteries were precontracted with blockers for BK<sub>Ca</sub> (iberiotoxin, 0.1  $\mu$ M), K<sub>ATP</sub> (glibenclamide, 1  $\mu$ M), K<sub>ir2</sub> (BaCl, 30  $\mu$ M), K<sub>v1</sub> (DPO-1, 1  $\mu$ M) and K<sub>v2</sub> and K<sub>v4</sub> (stromatoxin, 0.1  $\mu$ M), but not K<sub>v7</sub> to a similar percentage of maximum tension (Student's t test:  $n=14$ ; 95% confidence interval -5,72 to 6,22).

Eventually, to address whether in depolarization-induced vasoconstriction, the anticontractile effect of ANP would differ dependently on K<sub>v7</sub> remaining the only un-blocked K<sup>+</sup> channel as compared to K<sub>v7</sub> being blocked along with all other K<sup>+</sup> channels, we analyzed and compared both of the above concentration-response curves (Figure 38 + Figure 39). Interestingly, no differences were detected, giving no implication for a functionally relevant involvement of K<sub>v7</sub> channels in concentration-dependent relaxations to ANP in depolarization-induced renal resistance artery contraction (Figure 40).

## with vs. without XE991 precontraction

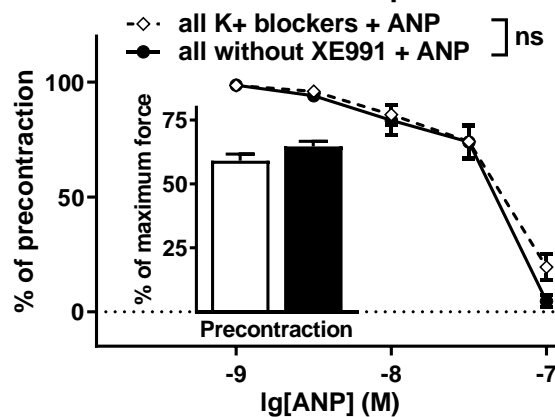


**Figure 40: Effect of ANP on contraction induced by various K<sup>+</sup> blockers including or excluding XE991 in rat renal interlobar arteries**

Concentration-dependent relaxation to ANP (1 – 100 nM) normalized to precontraction levels (Two-way repeated-measures ANOVA: ns  $p=0,35$ ). Arteries were either preincubated with 3  $\mu$ M XE991 (with) or not (without) and precontracted with blockers for BK<sub>Ca</sub> (iberiotoxin, 0.1  $\mu$ M), K<sub>ATP</sub> (glibenclamide, 1  $\mu$ M), K<sub>ir2</sub> (BaCl, 30  $\mu$ M), K<sub>v1</sub> (DPO-1, 1  $\mu$ M) and K<sub>v2</sub> and K<sub>v4</sub> (stromatoxin, 0.1  $\mu$ M) to a similar percentage of maximum tension (Student's t test:  $n=14$ ; 95% confidence interval -1,16 to 12,33).

Having demonstrated that ANP is able to counteract vasoconstriction induced by  $\alpha_1$ -adrenoceptor antagonist Methoxamine (Figure 35), and thus via contractile mechanisms including both

depolarization-mediated  $\text{Ca}^{2+}$  influx and increasing  $\text{Ca}^{2+}$  sensitivity (see: Chapter 1.4.2), we further investigated the role of  $\text{K}_{\text{v}7}$  channels in this process. This was done starting with testing ANP in Methoxamine-induced precontraction of vessels preincubated with pan- $\text{K}_{\text{v}7}$  blocker XE991 (3  $\mu\text{M}$ ), which produced concentration-dependent relaxations (Figure 41).

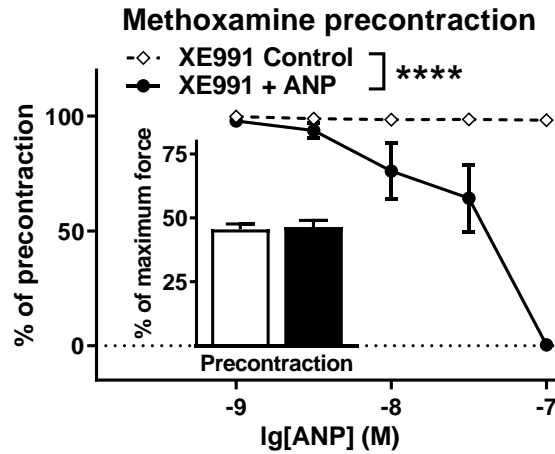


**Figure 41: Effect of ANP during  $\text{K}_{\text{v}7}$  blockade on agonist-induced contraction in rat renal interlobar arteries**

Concentration-dependent relaxation to ANP (1 – 100 nM) normalized to precontraction levels (Two-way repeated-measures ANOVA: \*\*\*\* $p < 0,0001$ ). Arteries were preincubated with 3  $\mu\text{M}$  XE991 and precontracted with Methoxamine to a similar percentage of maximum force (Student's  $t$  test:  $n=8$ ; 95% confidence interval -6,27 to 8,26).

In parallel, ANP was applied to Methoxamine-precontracted arteries that were preincubated with the  $\text{K}_{\text{v}7.1}$  blocker HMR1556 (10  $\mu\text{M}$ ), producing similar concentration-dependent relaxations (Figure 42).

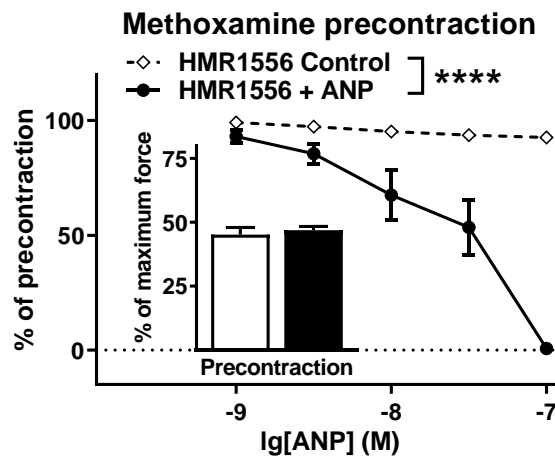


**Figure 42: Effect of ANP during  $\text{K}_{\text{v}7.1}$  blockade on agonist-induced contraction in rat renal interlobar arteries**

Concentration-dependent relaxation to ANP (1 – 100 nM) normalized to precontraction levels (Two-way repeated-measures ANOVA: \*\*\*\* $p < 0,0001$ ). Arteries were preincubated with 10  $\mu\text{M}$  HMR1556 and precontracted with Methoxamine to a similar percentage of maximum force (Student's  $t$  test:  $n=8$ ; 95% confidence interval -5,03 to 8,49).

To establish whether ANP-induced relaxations of Methoxamine-precontracted arteries depend upon  $\text{K}_{\text{v}7}$ , we compared these dose-dependent relaxations in the presence or absence of XE991, demonstrating no difference in the effect of ANP (Figure 43).

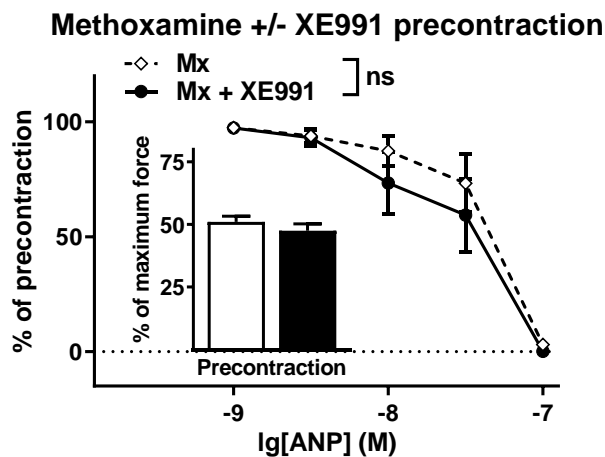


**Figure 43: Effect of ANP with or without  $K_v7$  blockade on agonist-induced contraction in rat renal interlobar arteries**  
 Concentration-dependent relaxation to ANP (1 – 100 nM) normalized to precontraction levels (Two-way repeated-measures ANOVA: ns  $p=0,44$ ). Arteries were preincubated either with or without 3  $\mu$ M XE991 and precontracted with Methoxamine to a similar percentage of maximum force (Student's  $t$  test:  $n=7$ ; 95% confidence interval -11,27 to 4,16).

Finally, to address whether blockade of either all  $K_v7$  or only  $K_v7.1$  specifically would differentially affect ANP-induced relaxations in agonist-induced vasoconstriction, we analyzed and compared the two above results (Figure 41 + Figure 42). There was no difference in the degree by which ANP relaxed Methoxamine precontractions in vessels preincubated with either the  $K_v7.1$ -specific blocker HMR1556 (10  $\mu$ M) or the pan- $K_v7$  blocker XE991 (3  $\mu$ M) (Figure 44).

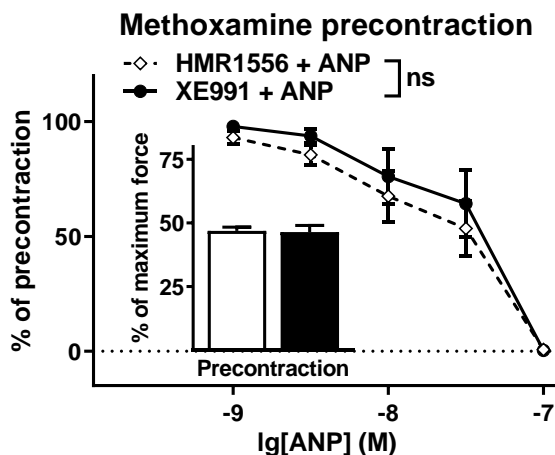


**Figure 44: Effect of ANP during  $K_v7.1$  or  $K_v7$  blockade on agonist-induced contraction in rat renal interlobar arteries**  
 Concentration-dependent relaxation to ANP (1 – 100 nM) normalized to precontraction levels (Two-way repeated-measures ANOVA: ns  $p=0,46$ ). Arteries were preincubated with either 10  $\mu$ M HMR1556 or 3  $\mu$ M XE991 and precontracted with Methoxamine to a similar percentage of maximum force (Student's  $t$  test:  $n=8$ ; 95% confidence interval -6,81 to 6,00).

In summary, our results demonstrate that ANP-induced vasorelaxation in renal interlobar arteries (i) is more marked in Methoxamine- than in KCl-induced precontraction, (ii) does not depend upon  $K_v7$  in depolarization-induced precontraction achieved by pharmacological blockade of VSMC  $K^+$  channels, and (iii) is similarly marked in Methoxamine-induced precontractions when either  $K_v7.1$  or all  $K_v7$  are blocked.

### 3.5 Contribution of $K_v7$ to the anticontractile effect of Urocortin in agonist-induced renal vasoconstriction

As was done for the cGMP-dependent vasodilator ANP, we screened the cAMP-dependent vasodilator Urocortin<sup>88, 322, 323</sup> for interference with  $K_v7$  function in renovascular reactivity, following an analog protocol of concentration-response relationships for calculation of  $pD_2$  as an indicator of Methoxamine sensitivity (see: Table 3), this time incubating Urocortin prior to application of  $K_v7$  activators R-L3 or Retigabine and  $K_v7$  blockers HMR1556 (in the presence of R-L3) or XE991.

Previous unpublished experiments, as mentioned earlier, have shown that XE991 (3  $\mu$ M) increases concentration-dependent contractions to Methoxamine, and furthermore that Urocortin, just like ANP, has an anticontractile effect in renal interlobar arteries. In search for interdependency of these effects we recorded Methoxamine concentration-response relationships after preincubation with either XE991, Urocortin, both substances combined or solvent only for control and calculated changes in  $pD_2$ . We confirmed that XE991 increases, whereas Urocortin decreases Methoxamine sensitivity, and furthermore demonstrated both of these effects were each unimpaired in the presence of the other (Figure 45).

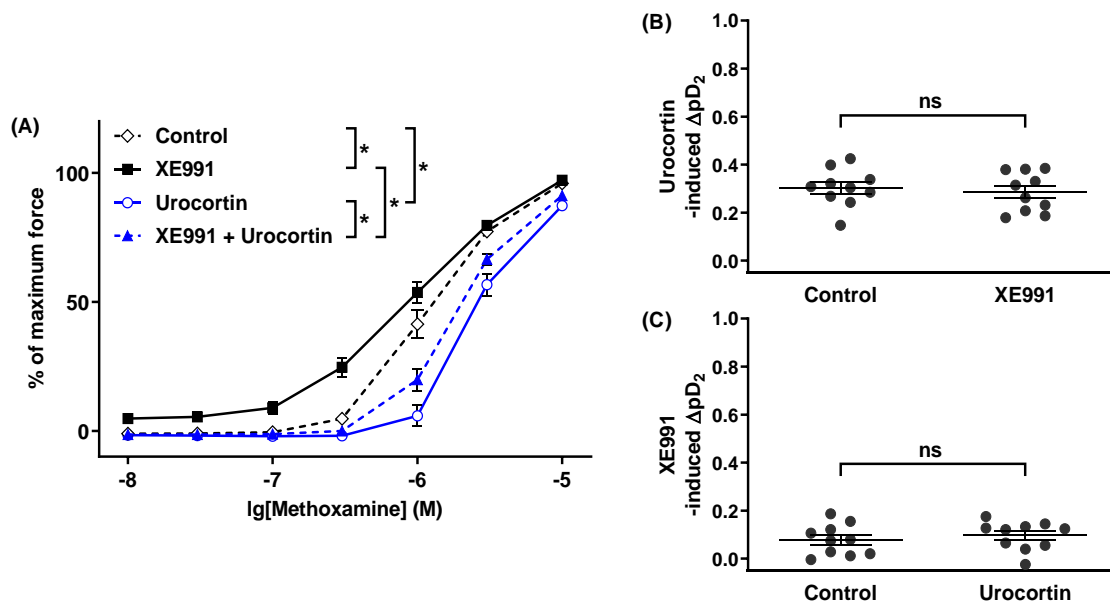


**Figure 45: Functional role of Urocortin in context with  $K_v7$  blockade in rat renal interlobar arteries**

(A) Methoxamine-induced contraction in absence of XE991 and Urocortin (control), in presence of 3  $\mu$ M XE991 only (XE991), in presence of 100 nM Urocortin only (Urocortin) and in presence of both XE991 and Urocortin (XE991 + Urocortin) (Two-way repeated measures ANOVA:  $n=10$ ;  $*p<0,05$ ). (B) Urocortin-induced  $\Delta pD_2$  in absence (control) and in presence of XE991 (Student's  $t$  test:  $n=10$ ; 95% confidence interval -0,094 to 0,06). (C) XE991-induced  $\Delta pD_2$  in absence (control) and in presence of Urocortin (Student's  $t$  test:  $n=10$ ; 95% confidence interval -0,04 to 0,08).

The same was done to examine the anticontractile effect of both the  $K_v7.2-5$  activator Retigabine and the  $K_v7.1$  activator R-L3 for interference with the anticontractile effect of Urocortin, analog to experiments done on ANP (Figure 31 + Figure 32). We demonstrated that Retigabine (30  $\mu$ M) and R-L3 (1  $\mu$ M) as well as Urocortin (100 nM) reduce the concentration-dependent contractile effect of Methoxamine, with their decrease in Methoxamine sensitivity all being both additive and unimpaired in the presence of the other (Figure 46 and Figure 47).

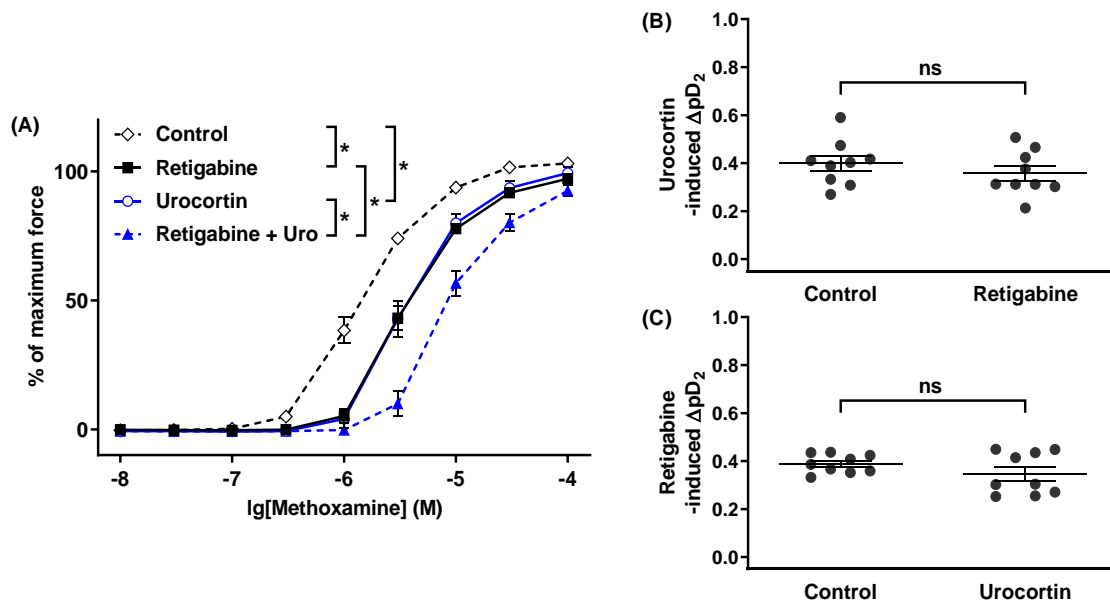


**Figure 46: Functional role of Urocortin in context with  $K_{v7.2-5}$  channel activation in rat renal interlobar arteries**

(A) Methoxamine-induced contraction in absence of Retigabine and Urocortin (control), in presence of  $30 \mu\text{M}$  Retigabine only (Retigabine), in presence of  $100 \text{ nM}$  Urocortin only (Urocortin) and in presence of both Urocortin and Retigabine (Retigabine + Uro) (Two-way repeated measures ANOVA:  $n=9$ ;  $*p<0,05$ ). (B) Urocortin-induced  $\Delta pD_2$  in absence (control) and in presence of Retigabine (Student's  $t$  test:  $n=9$ ; 95% confidence interval  $-0,13$  to  $0,053$ ). (C) Retigabine-induced  $\Delta pD_2$  in absence (control) and in presence of Urocortin (Student's  $t$  test:  $n=9$ ; 95% confidence interval  $-0,11$  to  $0,03$ ).

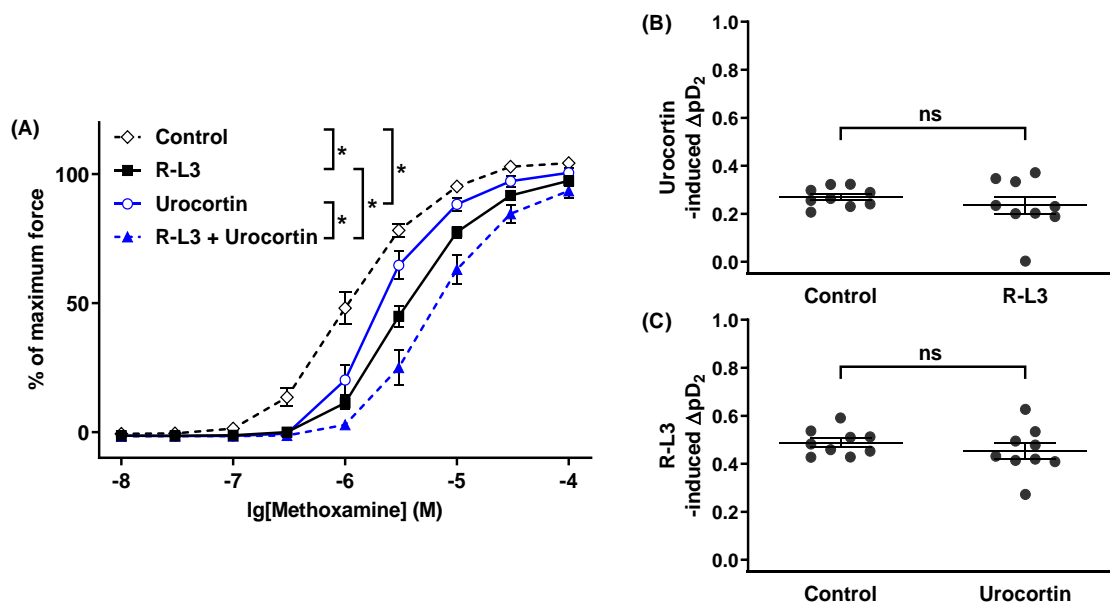


**Figure 47: Functional role of Urocortin in context with  $K_{v7.1}$  channel activation in rat renal interlobar arteries**

(A) Methoxamine-induced contraction in absence of R-L3 and Urocortin (control), in presence of  $1 \mu\text{M}$  R-L3 only (R-L3), in presence of  $100 \text{ nM}$  Urocortin only (Urocortin) and in presence of both R-L3 and Urocortin (R-L3 + Urocortin) (Two-way repeated measures ANOVA:  $n=9$ ;  $*p<0,05$ ). (B) Urocortin-induced  $\Delta pD_2$  in absence (control) and in presence of R-L3 (Student's  $t$  test:  $n=9$ ; 95% confidence interval  $-0,12$  to  $0,05$ ). (C) R-L3-induced  $\Delta pD_2$  in absence (control) and in presence of Urocortin (Student's  $t$  test:  $n=9$ ; 95% confidence interval  $-0,11$  to  $0,04$ ).

Because The  $K_{v7.1}$  blocker HMR1556 exerts its anticontractile effect only in the presence of R-L3, as described earlier (see: Chapter 3.4), testing of HMR1556 for interference with the anticontractile effect

of Urocortin was done after preincubation of all vessels with R-L3. We observed that HMR1556 (10  $\mu$ M) enhanced, while Urocortin (100 nM) reduced the contractile response to Methoxamine (Figure 48). Furthermore, we observed that the increase or decrease in Methoxamine sensitivity caused by Urocortin resp. HMR1556 was unaffected by the absence or presence of the other.

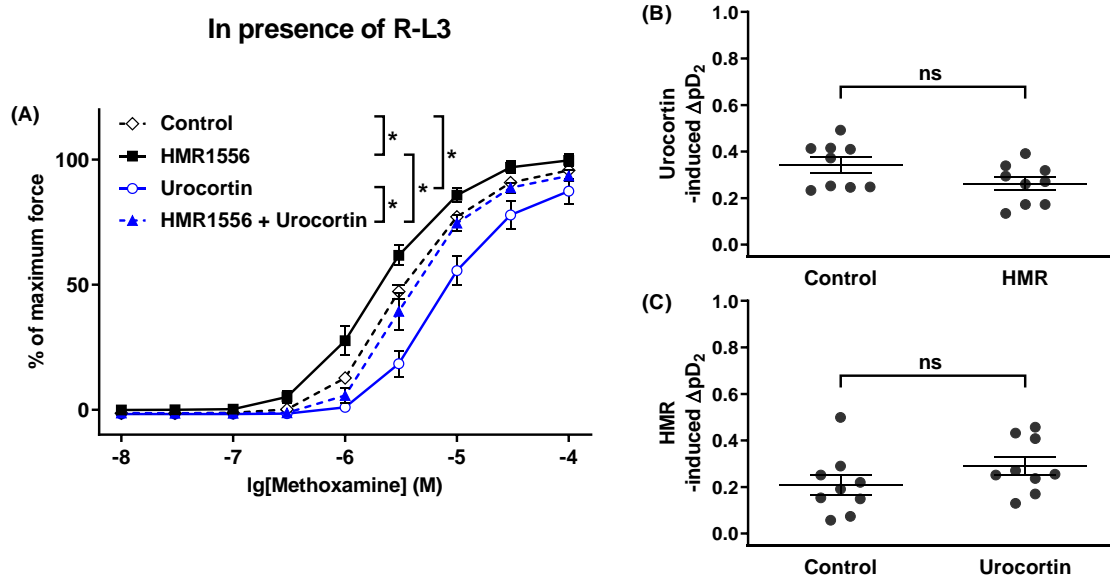


**Figure 48: Functional role of Urocortin in context with  $K_v7.1$  channel blockade following  $K_v7.1$  activation in rat renal interlobar arteries**

(A) Methoxamine-induced contraction in arteries preincubated with 1  $\mu$ M R-L3 in absence of HMR1556 and Urocortin (control), in presence of 10  $\mu$ M HMR1556 only (HMR1556), in presence of 100 nM Urocortin only (Urocortin) and in presence of both HMR1556 and Urocortin (HMR1556 + Urocortin) (Two-way repeated measures ANOVA:  $n=9$ ;  $*p<0,05$ ). (B) Urocortin-induced  $\Delta pD_2$  in arteries preincubated with 1  $\mu$ M R-L3 in absence (control) and in presence of Urocortin (Student's  $t$  test:  $n=9$ ; 95% confidence interval -0,17 to 0,01). (C) HMR-induced  $\Delta pD_2$  in arteries preincubated with 1  $\mu$ M R-L3 in absence (control) and in presence of HMR1556 (Student's  $t$  test:  $n=9$ ; 95% confidence interval -0,04 to 0,214).

In summary, our results demonstrate that Methoxamine sensitivity of renal interlobar arteries is decreased by the  $K_v7.1$  activator R-L3 or by the  $K_v7.2-5$  activator Retigabine and is increased by the  $K_v7.1$  blocker HMR1556 in the presence of R-L3 as well as by the pan- $K_v7$  blocker XE991, with all of these effects reciprocally being both unaffected by, and itself not affecting, the anticontractile effect caused by preincubation with Urocortin.

With all  $K_v7$  activators and blockers displaying no interaction with Urocortin regarding their modulating effect on Methoxamine sensitivity, we next performed a series of precontraction experiments following a protocol with either Methoxamine (see: Table 4) or with KCl and various pharmacological  $K^+$  channel blockers (see: Table 5) to differentiate the concentration-dependent effect of Urocortin in not only agonist-induced but also in depolarization-induced vasoconstriction. As has been elaborated earlier (see: Chapter 3.4), this served to examine the effect of endogenous vasodilators like Urocortin in vessels precontracted by activation of different signal transduction pathways, allowing us to draw conclusions on possible intracellular effects of the cAMP-dependent vasodilator Urocortin in context with  $K_v7$  channel function.

In a first step, we examined the effect of Urocortin on agonist-induced precontraction with Methoxamine as a vasoconstrictor, which acts through both increases in  $[Ca^{2+}]_i$  and increases in  $Ca^{2+}$  sensitivity. We found that Urocortin causes concentration-dependent relaxations of Methoxamine precontractions in renal interlobar arteries (Figure 49).

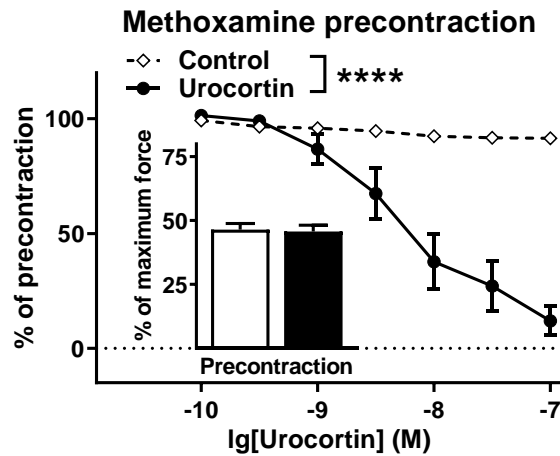


**Figure 49: Effect of Urocortin on contraction induced by  $\alpha_1$ -adrenoceptor agonist Methoxamine in rat renal interlobar arteries**

Concentration-dependent relaxation to Urocortin (0.1 – 100 nM) normalized to precontraction levels (Two-way repeated-measures ANOVA: \*\*\*\* $p < 0,0001$ ). Arteries were precontracted with Methoxamine to a similar percentage of maximum force (Student's t test:  $n=10$ ; 95% confidence interval -7,98 to 6,50).

In parallel, Urocortin was applied during KCl-induced precontraction to evaluate its effectiveness in antagonizing depolarization-induced vasoconstriction due to functional elimination of all  $K^+$  channels. We recorded concentration-dependent relaxations to Urocortin (0.1 – 100 nM) in renal interlobar arteries precontracted with 40 mM KCl (Figure 50).

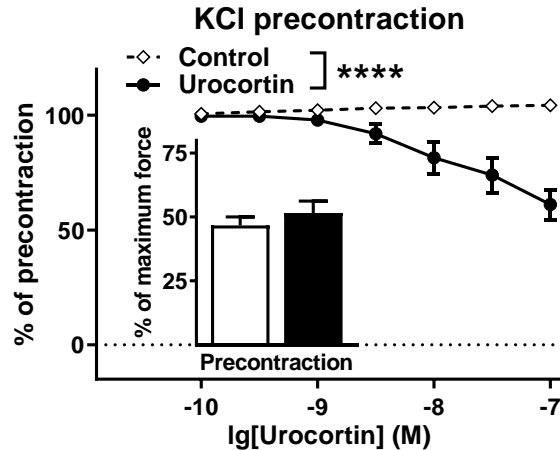


**Figure 50: Effect of Urocortin on contraction induced by KCl in rat renal interlobar arteries**

Concentration-dependent relaxation to Urocortin (0.1 – 100 nM) normalized to precontraction levels (Two-way repeated-measures ANOVA: \*\*\*\* $p < 0,0001$ ). Arteries were precontracted with 40 mM KCl to a similar percentage of maximum force (Student's t test:  $n=10$ ; 95% confidence interval -7,12 to 16,84).

Eventually, to discern differences in the anticontractile effect of Urocortin on agonist-induced versus depolarization-induced vasoconstriction, we analyzed both graphs (Figure 49 + Figure 50), discovering that concentration-dependent relaxation caused by Urocortin were profoundly more marked in arteries precontracted with Methoxamine than with 40 mM KCl (Figure 51).

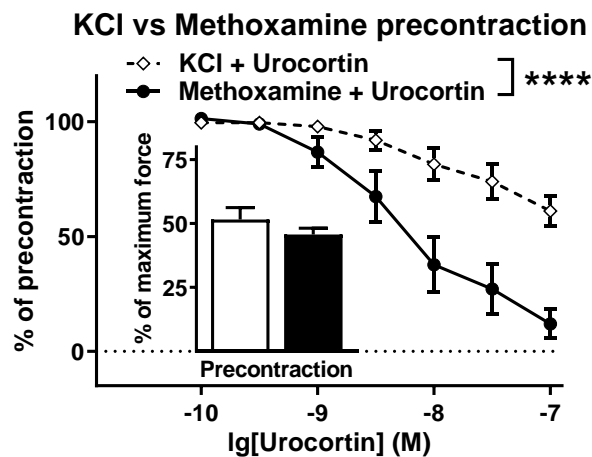


**Figure 51: Effect of Urocortin on contraction induced by KCl or  $\alpha_1$ -adrenoceptor agonist Methoxamine in rat renal interlobar arteries**

Concentration-dependent relaxation to Urocortin (0.1 – 100 nM) normalized to precontraction levels (Two-way repeated-measures ANOVA: \*\*\*\* $p < 0,0001$ ). Arteries were either precontracted with either 40 mM KCl or with Methoxamine to a similar percentage of maximum force (Student's *t* test:  $n=10$ ; 95% confidence interval -16,93 to 5,16).

Having demonstrated that Urocortin is effective in antagonizing precontraction induced by KCl and thus functional elimination of  $K^+$  channels (Figure 50), we further evaluated  $K_v7$  channels for their contribution to this phenomenon. As described before for ANP, we tested the effect of Urocortin on precontraction induced by simultaneous preincubation with pharmacological blockers of the  $K^+$  channel subfamilies known to be expressed in VSMCs, including  $BK_{Ca}$  (iberiotoxin, 0.1  $\mu$ M),  $K_{ATP}$  (glibenclamide, 1  $\mu$ M),  $K_{ir2}$  (BaCl, 30  $\mu$ M),  $K_{v1}$  (DPO-1, 1  $\mu$ M),  $K_{v2}$  and  $K_{v4}$  (stromatoxin, 0.1  $\mu$ M) and  $K_{v7}$  (XE991, 3  $\mu$ M) (for references, see: Chapter 3.4). We established that Urocortin caused concentration-dependent relaxations of precontraction thus created by pharmacological blockade of all known  $K^+$  channels including  $K_{v7}$  (Figure 52).

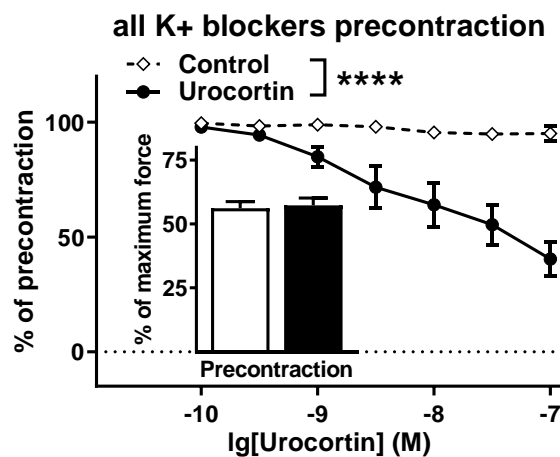


**Figure 52: Effect of Urocortin on contraction induced by various  $K^+$  blockers in rat renal interlobar arteries**

Concentration-dependent relaxation to Urocortin (0.1 – 100 nM) normalized to precontraction levels (Two-way repeated-measures ANOVA: \*\*\*\* $p < 0,0001$ ). Arteries were preincubated with 3  $\mu$ M XE991 and precontracted with blockers for  $BK_{Ca}$  (iberiotoxin, 0.1  $\mu$ M),  $K_{ATP}$  (glibenclamide, 1  $\mu$ M),  $K_{ir2}$  (BaCl, 30  $\mu$ M),  $K_{v1}$  (DPO-1, 1  $\mu$ M) and  $K_{v2}$  and  $K_{v4}$  (stromatoxin, 0.1  $\mu$ M) to a similar percentage of maximum force (Student's *t* test:  $n=8$ ; 95% confidence interval -7,27 to 9,47).

Next, precontraction was induced with the same cocktail of K<sup>+</sup> channel blockers, but this time without the pan-K<sub>v</sub>7 blocker XE991. We demonstrated that such precontraction was likewise relaxed by Urocortin in a concentration-dependent manner (Figure 53).

#### all K<sup>+</sup> blockers without XE991 precontraction

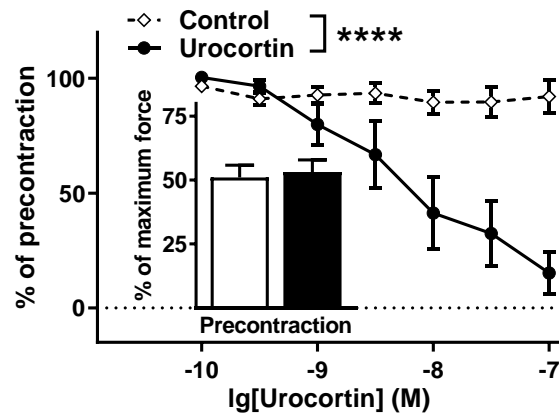


**Figure 53: Effect of Urocortin on contraction induced by various K<sup>+</sup> blockers excluding XE991 in rat renal interlobar arteries**  
Concentration-dependent relaxation to Urocortin (0.1 – 100 nM) normalized to precontraction levels (Two-way repeated-measures ANOVA: \*\*\*\* $p < 0,0001$ ). Arteries were precontracted with blockers for BK<sub>Ca</sub> (iberiotoxin, 0.1  $\mu$ M), K<sub>ATP</sub> (glibenclamide, 1  $\mu$ M), K<sub>ir</sub>2 (BaCl, 30  $\mu$ M), K<sub>v</sub>1 (DPO-1, 1  $\mu$ M) and K<sub>v</sub>2 and K<sub>v</sub>4 (stromatoxin, 0.1  $\mu$ M), but not K<sub>v</sub>7 to a similar percentage of maximum force (Student's t test:  $n=8$ ; 95% confidence interval -12,39 to 16,61).

An analytical comparison of the two graphs (Figure 52 + Figure 53) was undertaken to address whether K<sub>v</sub>7 blockade versus K<sub>v</sub>7 remaining the only un-blocked K<sup>+</sup> channel in the vessel wall would differentially affect Urocortin-induced concentration-dependent relaxations. Notably, no differences were observed, providing no evidence for a contribution of K<sub>v</sub>7 channels in the anticontractile effect of Urocortin during depolarization-induced precontraction (Figure 54).

#### with vs. without XE991 precontraction

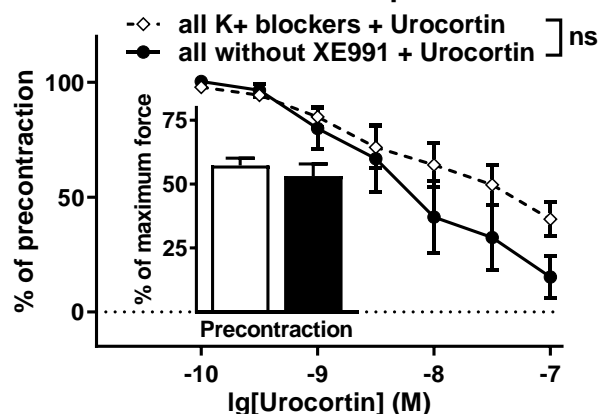


**Figure 54: Effect of Urocortin on contraction induced by various K<sup>+</sup> blockers including or excluding XE991 in rat renal interlobar arteries**

Concentration-dependent relaxation to Urocortin (0.1 – 100 nM) normalized to precontraction levels (Two-way repeated-measures ANOVA:  $ns = p=0,26$ ). Arteries were either preincubated with 3  $\mu$ M XE991 (with) or not (without) and precontracted with blockers for BK<sub>Ca</sub> (iberiotoxin, 0.1  $\mu$ M), K<sub>ATP</sub> (glibenclamide, 1  $\mu$ M), K<sub>ir</sub>2 (BaCl, 30  $\mu$ M), K<sub>v</sub>1 (DPO-1, 1  $\mu$ M) and K<sub>v</sub>2 and K<sub>v</sub>4 (stromatoxin, 0.1  $\mu$ M) to a similar percentage of maximum force (Student's t test:  $n=8$ ; 95% confidence interval -16,06 to 7,79).

Having demonstrated that Urocortin is effective in antagonizing precontraction induced by  $\alpha_1$ -adrenoceptor antagonist Methoxamine and thus via contractile mechanisms including both  $[Ca^{2+}]_i$  increases as well as  $Ca^{2+}$  sensitization (Figure 49), we further investigated whether this process functionally included  $K_v7$  channels. We started by testing Urocortin in Methoxamine-induced precontraction and subsequent preincubation with the pan- $K_v7$  blocker XE991 (3  $\mu$ M), which resulted in concentration-dependent relaxations to Urocortin (Figure 55).

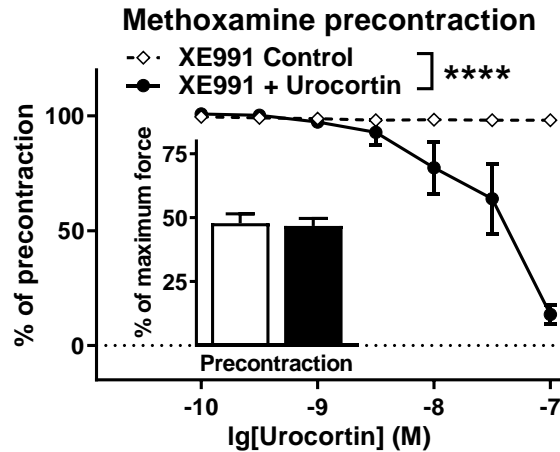


**Figure 55: Effect of Urocortin during  $K_v7$  blockade on agonist-induced contraction in rat renal interlobar arteries**  
Concentration-dependent relaxation to Urocortin (0.1 – 100 nM) normalized to precontraction levels (Two-way repeated-measures ANOVA: \*\*\*\* $p < 0,0001$ ). Arteries were preincubated with 3  $\mu$ M XE991 and precontracted with Methoxamine to a similar percentage of maximum force (Student's  $t$  test:  $n=8$ ; 95% confidence interval -11,03 to 8,88).

In parallel, Urocortin was applied in arteries precontracted with Methoxamine and subsequently preincubated with the  $K_v7.1$  blocker HMR1556 (10  $\mu$ M), which likewise produced concentration-dependent relaxations (Figure 56).

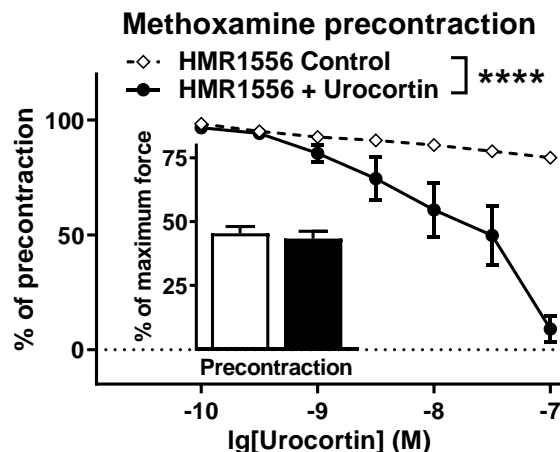


**Figure 56: Effect of Urocortin during  $K_v7.1$  blockade on agonist-induced contraction in rat renal interlobar arteries**  
Concentration-dependent relaxation to Urocortin (0.1 – 100 nM) normalized to precontraction levels (Two-way repeated-measures ANOVA: \*\*\*\* $p < 0,0001$ ). Arteries were preincubated with 10  $\mu$ M HMR1556 and precontracted with Methoxamine to a similar percentage of maximum force (Student's  $t$  test:  $n=8$ ; 95% confidence interval -10,44 to 6,35).

To establish whether Urocortin-induced relaxations of Methoxamine-precontracted arteries depend upon  $K_v7$ , we compared these relaxations in the presence or absence of XE991, demonstrating no difference in the dose-dependent anticontractile effect of Urocortin (Figure 57).

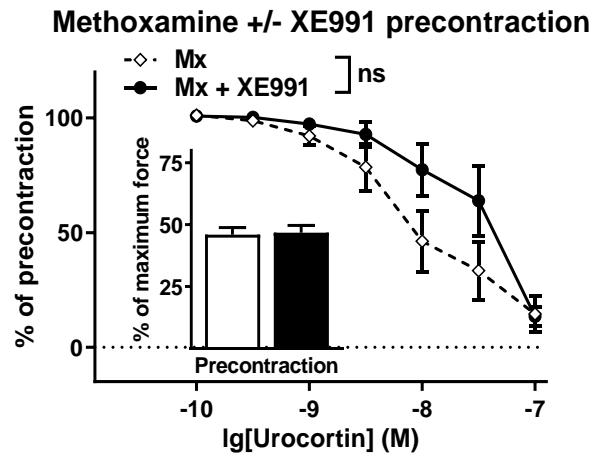


**Figure 57: Effect of Urocortin with or without Kv7 blockade on agonist-induced contraction in rat renal interlobar arteries**  
Concentration-dependent relaxation to Urocortin (0.1 – 100 nM) normalized to precontraction levels (Two-way repeated-measures ANOVA: ns  $p=0,13$ ). Arteries were preincubated either with or without 3  $\mu$ M XE991 and precontracted with Methoxamine to a similar percentage of maximum force (Student's  $t$  test:  $n=8$ ; 95% confidence interval -7,858 to 9,455).

A comparison of the two graphs (Figure 55 + Figure 56), addressing whether in agonist-induced vasoconstriction, Urocortin-induced relaxations would be differently affected by blockade of either all  $K_v7$  or only  $K_v7.1$  channels specifically, revealed no difference. We thus found no evidence for a functionally relevant interaction of  $K_v7$  channels with the cAMP-dependent vasodilator Urocortin in agonist-induced precontractions of renal resistance arteries (Figure 58).

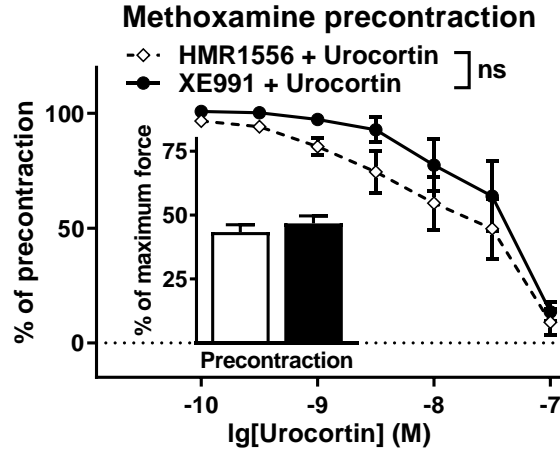


**Figure 58: Effect of Urocortin during  $K_v7.1$  or  $K_v7$  blockade on agonist-induced contraction in rat renal interlobar arteries**  
Concentration-dependent relaxation to Urocortin (0.1 – 100 nM) normalized to precontraction levels (Two-way repeated-measures ANOVA: ns  $p=0,16$ ). Arteries were preincubated with either 10  $\mu$ M HMR1556 or 3  $\mu$ M XE991 and precontracted with Methoxamine to a similar percentage of maximum force (Student's  $t$  test:  $n=8$ ; 95% confidence interval -5,30 to 12,11).

In summary, our results demonstrate that Urocortin-induced vasorelaxation of renal interlobar arteries (i) is more marked in Methoxamine- than in KCl-induced precontraction, (ii) does not depend upon  $K_v7$  channels in depolarization-induced precontraction achieved through pharmacological blockade of VSMC  $K^+$  channels, and (iii) is similar in Methoxamine-induced precontraction when only  $K_v7.1$  is blocked as compared to when all  $K_v7$  are blocked.

### 3.6 Contribution of $K_v7$ to agonist-induced vasoconstriction in isolated perfused kidneys

With isometric tension myography experiments indicating a role for  $K_v7$ , specifically including  $K_v7.1$  channels, in regulating vascular tension in short segments of renal interlobar arteries (see: Chapters 3.2 and 3.3), our next step towards recreating the in vivo circumstances was to conduct renal perfusion pressure measurements in isolated perfused rat kidneys as a more integrative approach. We were thus able to examine  $K_v7$  channel contribution to myogenic tone in the intact renal arterial bed. All following experiments were conducted during perfusion with PSS containing  $\alpha_1$ -adrenoceptor agonist Methoxamine ( $3 \mu\text{M}$ ) to induce a certain degree of agonist-induced vasoconstriction, simulating adrenergic hormones circulating in the blood or being released from efferent intrarenal sympathetic nerves.

We first investigated the effect of the pan- $K_v7$  blocker XE991 on the renal arterial vasculature using the protocol described earlier (see: Table 10). Beforehand, experiments were performed testing XE991 ( $3 \mu\text{M}$ ) over a longer incubation time up to 40 minutes in order to establish how long it took for XE991 to develop its full vasoconstrictive potential. A representative recording is given to demonstrate that this was the case within less than 20 minutes, indicating that further prolongation of the observation period would reveal no additional changes in perfusion pressure (Figure 59).

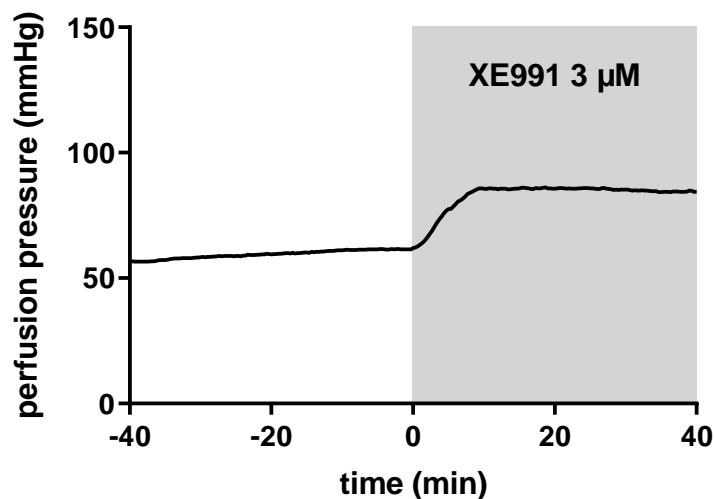


**Figure 59: Representative recording over 40 minutes application of XE991 in Methoxamine-precontracted isolated perfused rat kidneys**

Values are presented as original perfusion pressure recordings subtracted by baseline pressure prior to application of  $3 \mu\text{M}$  Methoxamine.

When applied for 20 minutes, XE991 ( $3 \mu\text{M}$ ) during Methoxamine-induced precontraction caused an increase in renal perfusion pressure which was observed after approximately 5 minutes of application (Figure 60).

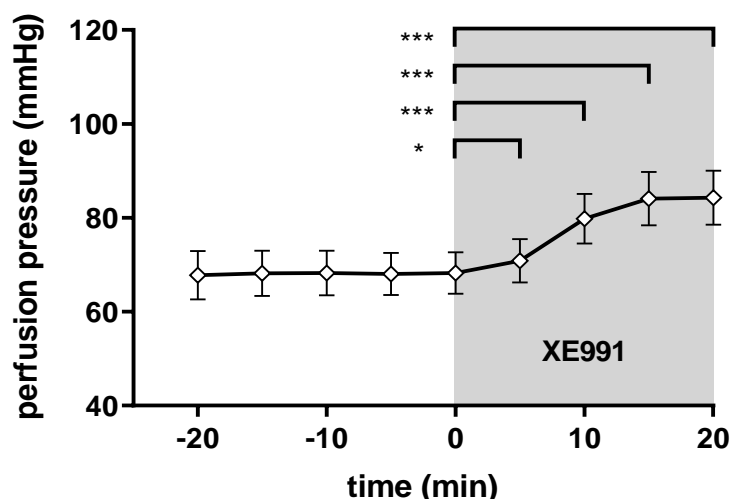


**Figure 60: Effect of XE991 on perfusion pressure in Methoxamine-precontracted isolated perfused rat kidneys**

Time course of perfusion pressure before and during application of 3  $\mu$ M XE991 (XE991) (One-way repeated-measures ANOVA with Geisser-Greenhouse correction, followed by Dunnett's multiple comparisons test:  $n=7$ ; \* $p<0,05$ ; \*\*\* $p<0,001$ ; 95% confidence interval 0,30 to 4,95 at 5 min; 6,60 to 16,61 at 10 min; 9,11 to 22,66 at 15 min; 9,19 to 22,97 at 20 min). Values are presented as mean  $\pm$  SEM of original perfusion pressure recordings subtracted by baseline pressure prior to application of 3  $\mu$ M Methoxamine.

Previous unpublished myography experiments had found no effect of  $K_v7.1$  channel specific blocker HMR1556 on Methoxamine-induced vasoconstriction in isolated renal interlobar artery segments. For independent support, we conducted perfusion experiments to verify these findings on a whole-organ level. We found that in isolated perfused kidneys, application of HMR1556 (10  $\mu$ M) for a minimum of 20 minutes during agonist-induced precontraction did not affect perfusion pressure (Figure 61), confirming that HMR1556 alone has no effect on agonist-induced vasoconstriction.

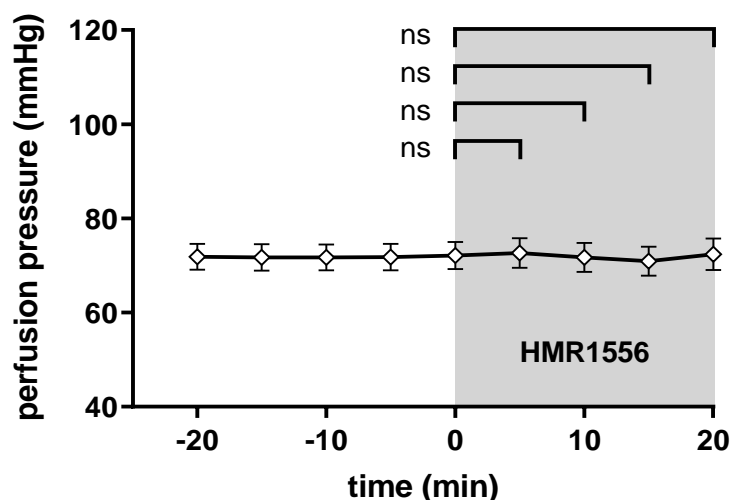


**Figure 61: Effect of HMR1556 on perfusion pressure in Methoxamine-precontracted isolated perfused rat kidneys**

Time course of perfusion pressure before and during application of 10  $\mu$ M HMR1556 (HMR1556) (One-way repeated-measures ANOVA with Geisser-Greenhouse correction, followed by Dunnett's multiple comparisons test:  $n=12$ ; ns = not significant, 95% confidence interval -1,98 to 0,82 at 5 min; -1,53 to 2,31 at 10 min; -0,98 to 3,33 at 15 min; -2,51 to 2,00 at 20 min). Values are presented as mean  $\pm$  SEM of original perfusion pressure recordings subtracted by baseline pressure prior to application of 3  $\mu$ M Methoxamine.

Earlier myography experiments had demonstrated a concentration-dependent (0.01-1  $\mu$ M) anticontractile effect of the  $K_v7.1$  activator R-L3 on Methoxamine-induced precontraction (see: Figure

26) and the ability of the  $K_v7.1$  blocker HMR1556 to diminish these (Figure 29). Thus, we conducted perfusion experiments to test R-L3 using an extended type of protocol as described before (see: Table 11) that allows superfusion of R-L3 with its antagonists HMR1556 or XE991. We started with the highest concentration of R-L3 used in myography experiments ( $1 \mu\text{M}$ ) to examine its maximum effect on Methoxamine-induced renal arterial pressure and to study the effect of coapplication of HMR1556. A profound decrease in perfusion pressure reaching a plateau within 20 minutes of continuous application of R-L3 ( $1 \mu\text{M}$ ) was observed which was partially reversed by HMR1556 ( $10 \mu\text{M}$ ) during coapplication for 10 minutes (Figure 62).

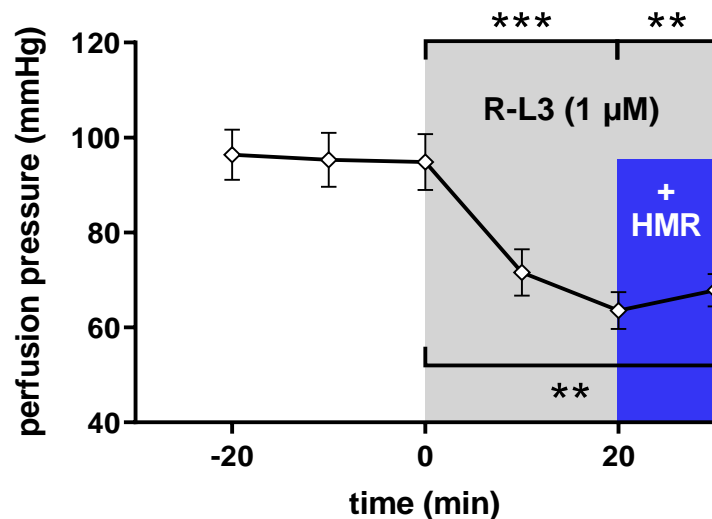


**Figure 62: Effect of R-L3 and HMR1556 on perfusion pressure in Methoxamine-precontracted isolated perfused rat kidneys**  
Time course of perfusion pressure before and during application of  $1 \mu\text{M}$  R-L3 and additional superfusion with  $10 \mu\text{M}$  HMR1556 (HMR) (a-priori paired Student's t test:  $n=7$ ;  $**p<0,01$ ;  $***p<0,001$ ; 95% confidence interval  $-41,19$  to  $-21,31$  from  $0-20$  min;  $1,61$  to  $6,88$  from  $20-30$  min;  $-38,10$  to  $-15,90$  from  $0-30$  min). Values are presented as mean  $\pm$  SEM of original perfusion pressure recordings subtracted by baseline pressure prior to application of  $3 \mu\text{M}$  Methoxamine.

As the maximum concentration of R-L3 we used ( $1 \mu\text{M}$ ) caused a decrease in perfusion pressure only partially antagonized by HMR1556, we aimed to investigate whether the effect of the minimum effective concentration of R-L3 could be completely reversed by HMR1556. To do so, we followed the same protocol, only this time starting with R-L3 at  $0.1 \mu\text{M}$  and successively raising concentrations by  $0.2 \mu\text{M}$  until a distinct decrease in perfusion pressure would be recorded over 10 minutes, to then begin application of HMR1556. Eventually, concentrations of R-L3 used ranged from  $0.3-0.9 \mu\text{M}$  ( $n=6$ ; mean  $\pm$  SEM  $0.6 \pm 0.08 \mu\text{M}$ ). Interestingly, we observed a more marked, but still only partial reversal of the R-L3-induced pressure drop during coapplication of HMR1556 (Figure 63).

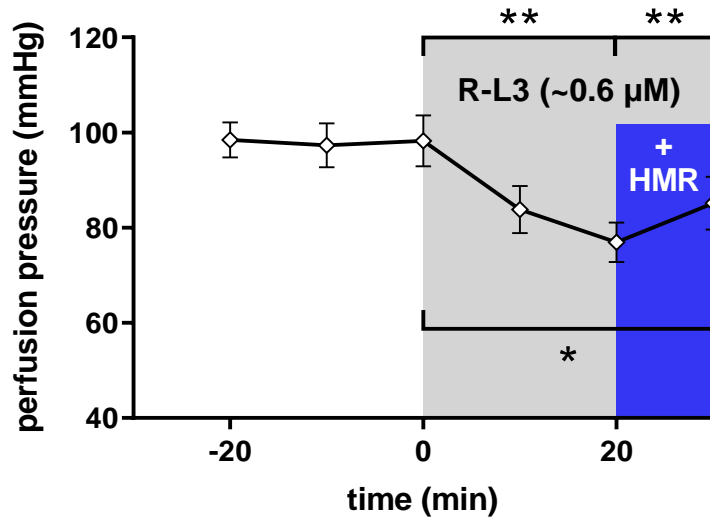


**Figure 63: Effect of minimum effective concentrations of R-L3 and HMR1556 on perfusion pressure in Methoxamine-precontracted isolated perfused rat kidneys**

Time course of perfusion pressure before and during application of minimum effective concentrations of R-L3 (R-L3  $\sim 0.6 \mu\text{M}$ ) and additional superfusion with  $10 \mu\text{M}$  HMR1556 (HMR) (a-priori paired Student's t test:  $n=7$ ;  $*p<0,05$ ;  $**p<0,01$ ; 95% confidence interval  $-30,11$  to  $-12,55$  from  $0-20$  min;  $3,82$  to  $12,59$  from  $20-30$  min;  $-21,56$  to  $-4,68$  from  $0-30$  min). Values are presented as mean  $\pm$  SEM of original perfusion pressure recordings subtracted by baseline pressure prior to application of  $3 \mu\text{M}$  Methoxamine.

To objectify the observed differences in concentration-dependent decreases in perfusion pressure induced by R-L3 and the potential of HMR1556 to antagonize these, the data presented in the two graphs (Figure 62 + Figure 63) were analyzed with regards to precontraction level, R-L3-induced pressure drop and its percentual reversal by HMR1556. We were able to display that at a similar degree of Methoxamine precontraction, the perfusion pressure-decreasing effect of R-L3 at minimum concentrations was approximately 60% of that at maximum concentration (means  $\pm$  SEM  $-21.3 \pm 3.4$  mmHg ( $n=6$ ) vs.  $-33.9 \pm 3.7$  mmHg ( $n=7$ )) and the percentage of that reversed by HMR1556 was almost 4 times higher at minimum concentrations of R-L3 (means  $\pm$  SEM  $42.6 \pm 9.1$  % ( $n=6$ ) vs.  $11.7 \pm 3.6$  % ( $n=7$ )) (Figure 64).

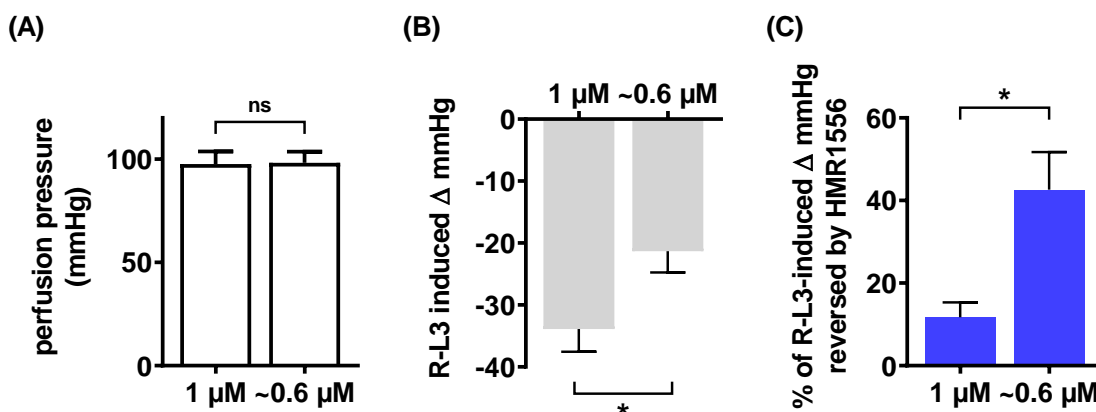


**Figure 64: Effect of HMR1556 on fixed or minimum effective concentrations of R-L3 in Methoxamine-precontracted isolated perfused rat kidneys**

(A) Perfusion pressure during Methoxamine-induced precontraction prior to application of R-L3 at fixed ( $1 \mu\text{M}$ ) or minimum effective concentrations ( $\sim 0.6 \mu\text{M}$ ) (unpaired Student's t test:  $n=6$ ; ns = not significant; 95% confidence interval  $-17,60$  to  $18,93$ ). Values are presented as mean  $\pm$  SEM of original perfusion pressure recordings subtracted by baseline pressure prior to application of  $3 \mu\text{M}$  Methoxamine. (B) R-L3-induced decrease in perfusion pressure in Methoxamine-induced precontraction at fixed ( $1 \mu\text{M}$ ) or minimum effective concentrations ( $\sim 0.6 \mu\text{M}$ ) of R-L3 (unpaired Student's t test:  $n=6$ ;  $*p<0,05$ ; 95% confidence

interval 1,36 to 23,72). Values are presented as mean  $\pm$  SEM of original perfusion pressure recordings subtracted by perfusion pressure recorded prior to application of R-L3 as shown in (A). (C) Percentage of HMR1556-induced reversal of the R-L3 induced decrease in perfusion pressure at fixed (1  $\mu$ M) or minimum effective concentrations ( $\sim$ 0.6  $\mu$ M) of R-L3 (unpaired Student's *t* test: *n*=6; \**p*<0,05; 95% confidence interval 9,12 to 52,70). Values are presented as mean  $\pm$  SEM of original perfusion pressure recordings subtracted by perfusion pressure recorded prior to application of HMR1556 and normalized to R-L3-induced increase in perfusion pressure as shown in (B).

Earlier myography experiments had also demonstrated effectiveness of the pan-K<sub>v</sub>7 blocker XE991 in diminishing R-L3-induced vasorelaxation of Methoxamine-precontracted renal interlobar arteries (see: Figure 29). We therefore conducted perfusion experiments testing the effect of XE991 on R-L3-induced changes in perfusion pressure, again applying the minimum effective concentration of R-L3 as described earlier (Figure 63). In this series, concentrations of R-L3 used ranged from 0.3-1  $\mu$ M (*n* = 6; mean  $\pm$  SEM  $\sim$ 0.6  $\pm$  0.04  $\mu$ M). We observed that the pressure drop following application of R-L3 was again only partially reversed by coapplication of XE991 (Figure 65).

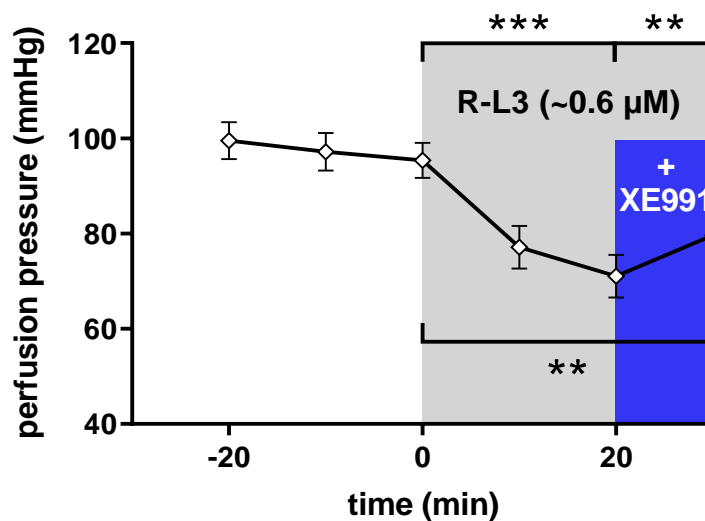


**Figure 65: Effect of minimum effective concentrations of R-L3 and XE991 on perfusion pressure in Methoxamine-precontracted isolated perfused rat kidneys**

Time course of perfusion pressure before and during application of minimum effective concentrations of R-L3 (R-L3  $\sim$ 0.6  $\mu$ M) and additional superfusion with 3  $\mu$ M XE991 (XE991) (a-priori paired Student's *t* test: *n*=6; \*\**p*<0,01; \*\*\**p*<0,001; 95% confidence interval -33,05 to -15,52 from 0-20 min; 4,54 to 12,71 from 20-30 min; -22,82 to -8,51 from 0-30 min). Values are presented as mean  $\pm$  SEM of original perfusion pressure recordings subtracted by baseline pressure prior to application of 3  $\mu$ M Methoxamine.

To discern any possible differences in the degree by which either HMR1556 or XE991 are able to antagonize perfusion pressure decreases induced by minimum effective concentrations of R-L3, the corresponding data (Figure 63 + Figure 65) was analyzed with regards to precontraction level, R-L3-induced pressure drop and its percentual reversal by HMR1556 or XE991. We found no difference in the percentage by which HMR1556 or XE991 reversed the similarly large decrease in perfusion pressure caused by R-L3 in equally strong Methoxamine precontractions (Figure 66).

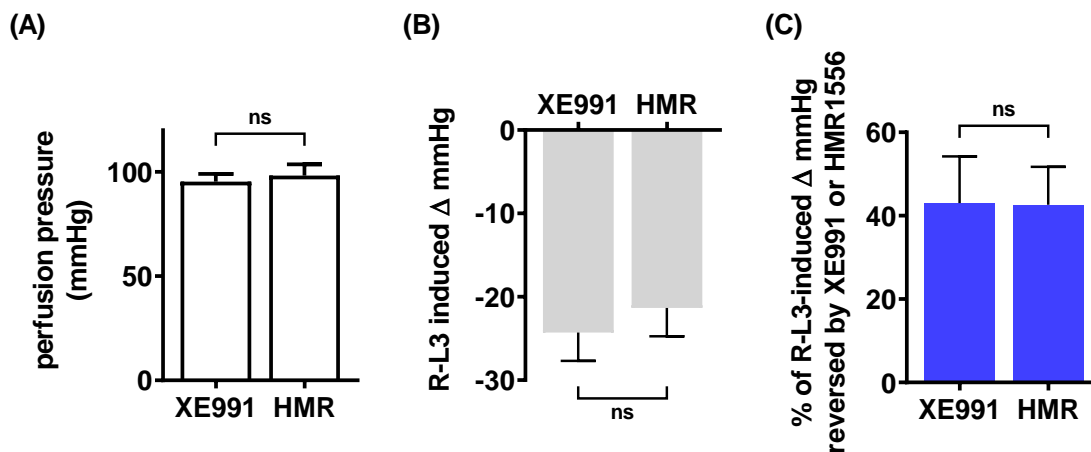


**Figure 66: Effect of XE991 or HMR1556 on minimum effective concentrations of R-L3 in precontracted isolated perfused rat kidneys**

(A) Perfusion pressure during Methoxamine-induced precontraction prior to application of minimum effective concentrations of R-L3 ( $\sim 6 \mu\text{M}$ ) and later  $3 \mu\text{M}$  XE991 (XE991) or  $10 \mu\text{M}$  HMR1556 (HMR) (unpaired Student's *t* test:  $n=6$ ; ns = not significant; 95% confidence interval -11,61 to 17,44). Values are presented as mean  $\pm$  SEM of original perfusion pressure recordings subtracted by baseline pressure prior to application of  $3 \mu\text{M}$  Methoxamine. (B) R-L3-induced decrease in perfusion pressure in Methoxamine-induced precontraction at minimum effective concentrations of R-L3 ( $\sim 6 \mu\text{M}$ ) prior to application of  $3 \mu\text{M}$  XE991 (XE991) or  $10 \mu\text{M}$  HMR1556 (HMR) (unpaired Student's *t* test:  $n=6$ ; ns = not significant; 95% confidence interval -7,80 to 13,71). Values are presented as mean  $\pm$  SEM of original perfusion pressure recordings subtracted by perfusion pressure recorded prior to application of R-L3 as shown in (A). (C) Percentage of reversal of the R-L3 ( $\sim 6 \mu\text{M}$ ) induced decrease in perfusion pressure after application of  $3 \mu\text{M}$  XE991 (XE991) or  $10 \mu\text{M}$  HMR1556 (HMR) (unpaired Student's *t* test:  $n=6$ ; ns = not significant; 95% confidence interval -32,58 to 31,81). Values are presented as mean  $\pm$  SEM of original perfusion pressure recordings subtracted by perfusion pressure recorded prior to application of XE991 or HMR1556 and normalized to R-L3-induced increase in perfusion pressure as shown in (B).

As our results show that the effect of XE991 in reversing R-L3 decreasing pressure was only partial when given 10 minutes to incubate (Figure 65), while XE991 may require up to 20 minutes to develop its full perfusion pressure-increasing effect in Methoxamine precontractions (Figure 60), we more extensively examined whether longer incubation times would reveal full antagonization of the anticontractile effect of R-L3. Subsequent experiments demonstrated that coadministration of XE991 ( $3 \mu\text{M}$ ) for 20 minutes after an initial 20 minute period of R-L3 incubation resulted in a return of perfusion pressure to a level not different than before application of R-L3 (Figure 67). Interestingly, we discovered that the effect of XE991 even persisted for at least 20 minutes after stopping application, although R-L3 was still being administered.

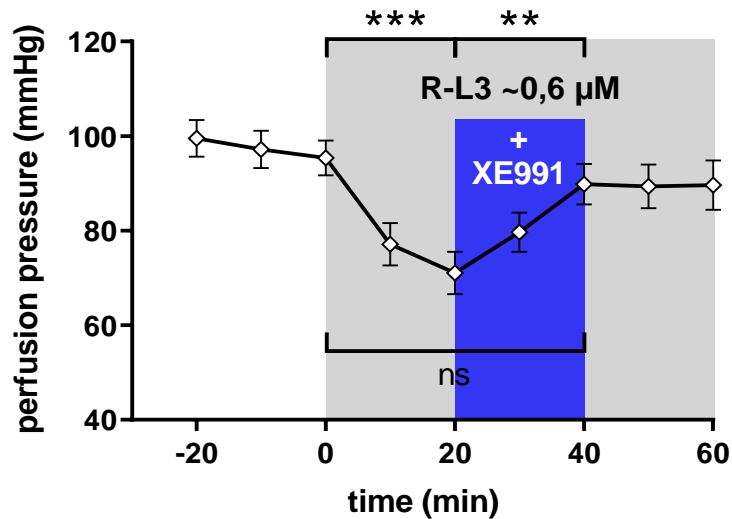


**Figure 67: Effect of minimum effective concentrations of R-L3 before, during and after XE991 superfusion on perfusion pressure in Methoxamine-precontracted isolated perfused rat kidneys**

Time course of perfusion pressure before and during application of minimum effective concentrations of R-L3 (R-L3  $\sim 0.6 \mu\text{M}$ ) and additional superfusion with  $3 \mu\text{M}$  XE991 (XE991) (a-priori paired Student's t test:  $n=6$ ;  $**p<0,01$ ;  $***p<0,001$ ; ns = not significant; 95% confidence interval -33,05 to -15,52 from 0-20 min; 7,10 to 30,41 from 20-40 min; -14,06 to 2,00 from 0-40 min). Values are presented as mean  $\pm$  SEM of original perfusion pressure recordings subtracted by baseline pressure prior to application of  $3 \mu\text{M}$  Methoxamine.

In summary, our results demonstrate that renal perfusion pressure in isolated rat kidneys is increased by the pan- $K_v7$  blocker XE991, but not by the  $K_v7.1$  specific blocker HMR1556. Furthermore, perfusion pressure is decreased by the  $K_v7.1$  activator R-L3 in a concentration-dependent manner which is at least partially reversible by HMR1556 and fully reversible by XE991.

## 4 DISCUSSION

### 4.1 Validating the isolated perfused kidney model

The isolated perfused kidney model described earlier (see: Chapter 2.5) that was used to collect the data presented in Chapters 3.1 and 3.6 represents a novel approach of studying vascular reactivity in our laboratory. Therefore, in the following we will provide a brief discussion on the validity of the method and a listing of its limitations. Special focus is brought to elaborating the background of the viability tests performed (Figure 5 – Figure 13) and the potential confounding factors examined (Figure 14 – Figure 18).

#### 4.1.1 Perfusion flow rate

Since vascular resistance as a depiction of vascular reactivity is the relation of perfusion pressure over flow rate, it is necessary to reflect on those two fundamentally important parameters in our setup. Flow rates that have previously been used for perfusion of rat kidneys tend to vary considerably. Especially earlier studies used lower perfusion rates, starting at 10 ml/min<sup>324, 325</sup>, while flow rates increased with sophisticated perfusion techniques towards 15-20 ml/min<sup>326-328</sup> and eventually 25-40 ml/min<sup>329-331</sup>. However, such high flow rates must be regarded as not physiological, considering that with an average male Wistar rat weighing 350-400 g, its blood volume accordingly amounting to no more than 20-25 ml<sup>332</sup> and its resting cardiac output ranging from ~90-110 ml/min<sup>333</sup>, these high flow rates do not correspond with the ~25% of cardiac output that RBF is typically considered to account for<sup>6</sup>. This is most probably due to the lower viscosity of the perfusate compared to blood, owing mainly to its lack of red blood cells, which may lead to a three- to fivefold increase in the flow rate of the isolated kidney compared to the kidney in vivo<sup>334</sup>. Actually, the flow rate we used for experiments (~3 ml/min) and the maximum perfusion rate used during viability testing (~10 ml/min) more closely resembles values of RBF measured in vivo in ~3 month old Wistar Kyoto rats like ours, which is 2.33 ml/min/100g animal weight<sup>335</sup> or 4.4-5.5 ml/min<sup>336</sup> for one single left kidney, though there appear to be considerable variations depending on the technique used. However, since we used cell-free perfusate, one may object that the flow rates we used appear unphysiologically low. We justify the use of such flow rates by the observation that these were evidently sufficient to generate perfusion pressures averaging ~110 mmHg (see: Figure 5 + Figure 6), which is within the physiological range of renal perfusion pressure in rats<sup>316</sup>. Furthermore, taking into account that in some of the earlier kidney perfusion studies, such flow rates have been successfully used to study renal hemodynamics<sup>324, 325</sup>, we conclude that this usage of supposedly low perfusion rates can be tolerated. With regards to the accuracy of perfusion pressure measurements, we made sure to rule out erroneously measuring high pressures at high flow rates potentially caused by the intrinsic resistance of the perfusion cannula, which is a major confounder in flow-rate controlled perfusion setups<sup>337</sup>, by hand-crafting a low-resistance glass cannula that we initially demonstrated to not produce exceedingly high perfusion pressures without a kidney connected to the perfusion system (see: Chapter 2.5.1).

#### 4.1.2 Viability tests

During viability testing, we demonstrated that the perfused kidneys were able to adequately respond to three different contractile stimuli: (i) flow-induced perfusion pressure, which elicited a myogenic response (see: Figure 8), (ii) KCl, which resulted in depolarization-induced vasoconstriction (see: Figure 12), and (iii) Methoxamine, which caused agonist-induced contraction (see: Figure 13).

(i) The myogenic response is the fastest and quantitatively most influential one of the three mechanisms involved in renal autoregulation of blood flow<sup>338</sup>. Thus, demonstrating an intact myogenic response was essential for demonstrating the functional integrity of the renal arterial vasculature in

our experiments. We did so by recording considerable and reversible decreases in perfusion pressure following application of  $\text{Ca}^{2+}$ -free perfusate (see: Figure 8 + Figure 9), which is a common method to abolish the active contractile component of vascular resistance that has previously been used in perfused kidneys<sup>245</sup>. Data derived from rat hydronephrotic kidney models<sup>339</sup> show that active vasoconstriction as part of the myogenic response starts at perfusion pressures above 60 mmHg<sup>340</sup> and in vivo experiments have found an especially high degree of autoregulatory efficiency at mean arterial pressure between 105-145 mmHg<sup>341</sup>. This corresponds well to the range of perfusion pressure at which we applied  $\text{Ca}^{2+}$ -free perfusate (~105-110 mmHg, see: Figure 8 + Figure 9). We further supported our evidence for an intact myogenic response by showing a strong correlation between the level of flow-induced pressure and the delta by which this was reduced during perfusion with  $\text{Ca}^{2+}$ -free solution (Figure 10), which accords to the higher degree of autoregulatory efficiency at higher pressures described by Arendshorst et al.<sup>341</sup>. Thus, we state that our perfused kidney setup is proficient in keeping the renal vasculature viable enough to show evidence of a properly functioning myogenic response.

(ii) When extracellular NaCl is replaced with equimolar concentrations of KCl, the  $\text{K}^+$  equilibrium potential is shifted so that  $\text{K}^+$  currents across the membrane are inhibited, representing a strong depolarizing stimulus that causes activation of VOCC,  $\text{Ca}^{2+}$  influx and subsequent release from intracellular stores and eventually contraction of blood vessels, which is referred to as electromechanical coupling<sup>19, 342</sup>. KCl has also been successfully used to induce contraction in isolated perfused organ systems<sup>245, 343</sup>. However, to differentiate between active depolarization-induced contraction and contractions as part of myogenic autoregulation, flow rate had to be reduced so that perfusion pressure decreased as can be seen in Figure 5 ( $n=48$ ; mean  $\pm$  SEM  $44.2 \pm 0.6$  mmHg). This was done because in order to obtain passive dynamics, it may be necessary to reduce renal perfusion pressure up to ~40 mmHg<sup>340</sup>. Subsequently, we showed that all perfused kidneys responded to KCl with a marked increase in perfusion pressure ( $n=48$ ; mean  $\pm$  SEM  $228.9 \pm 4.4$  mmHg) (see: Figure 5 + Figure 11). This provides clear evidence for their ability to produce active arterial vasoconstriction. We therefore conclude that our setup depicts kidneys that are capable to respond to electromechanical coupling as a mechanism of contractile stimulation.

(iii) KCl-induced depolarization represents a strong, yet not a very physiological contractile stimulus. By contrast, agonist-induced contraction more closely resembles the in vivo situation, where vasoactive substances are freely circulating in the blood stream. We found in our experiments that Methoxamine, an  $\alpha_1$ -adrenoceptor agonist not taken up by sympathetic nerves<sup>344</sup> that has long been known to contract renal arteries<sup>345</sup>, to produce sustained increases in perfusion pressure (see: Figure 13).

Confirmingly, by demonstrating that our isolated perfused kidney model was successful in depicting three different modes of active vasoconstriction, we argue that it fulfills the necessary requirements to serve as a valid instrument for the study of renal vascular reactivity.

#### 4.1.3 Comparability of kidneys from different rats

In our experiments on  $\text{K}_v7$  modulators, some statistical analyses required comparison of experimental groups of kidneys that were not taken from the same rat. Therefore, to guarantee the validity of our comparison, we screened for differences in viability tests including pressure-flow relationships (see: Figure 7) and responses to  $\text{Ca}^{2+}$ -free (see: Figure 9) or KCl-containing PSS (see: Figure 12) between experimental groups. Additionally, the level of agonist-induced perfusion pressure increases recorded prior to application of  $\text{K}_v7$  modulators was documented whenever comparison between experimental groups were conducted (Figure 64 + Figure 66). With none of these analyses revealing any differences in either of the parameters tested, we may safely assume that comparability is warranted.

#### 4.1.4 Confounding factors

As a benefit of performing viability tests, we were able to rule out three potential confounding factors we initially suspected to influence renal perfusion pressure recordings. As we found no differences in either pressure-flow relationships or the three above mentioned mechanisms of active vasoconstriction between control kidneys and those that had been (a) stored in cold PSS prior to starting perfusion (Figure 15), (b) treated with heparin during the preparation procedure (Figure 16) or (c) accidentally perfused with minor amounts of air (Figure 18), we conclude that these were not relevant to our subsequently conducted perfusion pressure measurements. The only parameter in which we noted a deviation was the initial perfusion pressure, which was higher when kidneys had been exposed to prolonged storage in cold PSS up to ~4 hours. This can easily be explained, since cold temperature represents a reversible contractile stimulus<sup>346</sup>, which is relevant at the moment when the kidney is transferred from the cold PSS, but is soon eliminated by both the heating chamber and the perfusion with warm perfusate. However, perfusion pressures adapted within 5 minutes of perfusion and no variation was seen in the overall comparison of pressure-flow relationships. As it is known from vessel myography experiments that small resistance arteries stored in PSS at 4°C remain viable for up to four days with no altered sensitivity to vasodilators within the first three days<sup>347</sup>, we can be sufficiently sure that the ~4 hours of cold storage our kidneys were exposed are unlikely to affect our perfusion pressure recordings in an undesirable fashion.

#### 4.1.5 Organ edema

One possibly problematic phenomenon of our technique we had to account for was the induction of organ edema following long-term perfusion with colloid-free perfusates. Many isolated perfused kidney models use perfusate to which colloid agents are added, like dextran<sup>324, 325, 348</sup>, bovine serum albumin (BSA)<sup>326, 327</sup>, or even combinations of BSA with dextran<sup>329, 331</sup>. We deferred from doing so, owing to not only simplicity reasons but also to our intention to provide similar experimental conditions in both vessel myography and isolated perfused kidney experiments by using similar PSS and thus avoid unforeseeable interactions of colloids with the K<sup>+</sup> channels we intended to study. However, lack of colloid oncotic agents in the perfusate is known to cause organ edema<sup>349</sup>. To avoid renal edema as a confounder that by increasing intracapsular renal pressure might interfere with arterial perfusion pressure measurements, the capsula fibrosa was removed during microscopic preparation (see: Chapter 2.5.3) so that the kidneys were able to expand their interstitial volume. Additionally, we show that the baseline perfusion pressure actually decreased slightly over the course of the experiment, whereas the contractile response to Methoxamine before and after wash-in or resp. wash-out of the K<sub>v</sub>7 modulators was similar (see: Figure 14). We may thus conclude that our usage of colloid-free perfusate did not produce organ edema to an extent large enough to interfere with our experiments during the time course explored.

#### 4.1.6 Limitations

Besides these majorly important factors that were all accounted for, we in the following provide a list of limitations to our technique that might potentially influence our results:

Venous pressure was not monitored. Venous thrombosis may have occurred during no-flow time in preparation, causing backpressure within the capillary system and producing false-high perfusion pressure readouts.

Venous pO<sub>2</sub> / O<sub>2</sub> saturation was not monitored. The renal parenchyma may have been hypoxic and therefore secreting paracrine vasoactive substances modifying vascular tone.

Cell-free perfusate was used. The low viscosity of cell-free PSS may have altered endothelial function and influenced NO production.

Perfusate temperature was not monitored. Lower perfusate temperatures due to a faster passage of the heating chamber at higher flow rates during pressure-flow relationships may have caused temperature-induced vasoconstriction instead of a myogenic response.

Perfusion rate was not adjusted to kidney weight. Since kidneys were not weighed before starting perfusion, all kidneys were perfused with equal flow rates, which may produce varying responses in differently sized kidneys.

In summary, our isolated perfused kidney technique provides a simple and inexpensive approach of studying renovascular reactivity in response to pharmacological modulators in a setting adequately resembling the *in vivo* situation with flow-induced perfusion pressure initiating a myogenic response and circulating vasoactive substances stimulating agonist-induced vasoconstriction.

#### 4.2 Contribution of $K_v7.2-5$ to agonist-induced renal vasoconstriction

$K_v7$  are a group of  $K^+$  channels more recently discovered to participate in vascular smooth muscle contractility<sup>166</sup>. The current state of knowledge is that activation of  $K_v7$ , i.e. via pharmacological activators like Retigabine or R-L3, enhances  $K^+$  currents, produces membrane hyperpolarization and reduces the probability of voltage-dependent  $Ca^{2+}$  channel opening, thus diminishing vasoconstrictor responses. Blockade of  $K_v7$  on the other hand, i.e. via pan- $K_v7$  blockers like XE991, suppresses  $K^+$  currents and produces membrane depolarization, thus either contracting arteries at rest or enhancing agonist-induced vasoconstriction<sup>123, 183, 300</sup>. Up to date, only a small number of studies have investigated the role of  $K_v7$  in renal arteries<sup>77, 96, 107, 243, 245, 246, 255, 262, 280</sup>. In this thesis, we provide new evidence for a strong anticontractile effect on agonist-induced renal resistance artery vasoconstriction caused by  $K_v7.2-5$  activation.

Retigabine is an antiepileptic drug that has been demonstrated to activate  $K^+$  currents conducted by  $K_v7.2-5$ <sup>249, 252, 253, 273, 274, 350</sup>, but not  $K_v7.1$ , which lacks an essential tryptophan residue required for activation<sup>272, 273, 277</sup>. It causes concentration-dependent relaxations in various rat arteries, including aorta and mesenteric artery<sup>243, 256, 261</sup>, coronary artery<sup>194, 228, 232</sup> cerebral artery<sup>196</sup> and skeletal muscle artery<sup>229</sup>. In humans, Retigabine has been shown to implement vasorelaxation of agonist-induced vasoconstriction in mesenteric and visceral adipose tissue arteries<sup>239</sup> and placental chorionic plate arteries<sup>241</sup>. Specifically in the rat renal vasculature, so far only one study has examined Retigabine, conducting isometric tension myography experiments on the main renal artery and reporting concentration-dependent relaxations in precontraction induced by 3  $\mu M$  Methoxamine<sup>243</sup>. Several other studies have produced similar results using alternative  $K_v7.2-5$  activators like flupirtine, S-1, ML213 or BMS204352<sup>77, 96, 243, 246, 262</sup>. Thus, this thesis is the first report to confirm an anticontractile effect of Retigabine in rat renal resistance arteries, as we demonstrate similar concentration-dependent vasorelaxation in Methoxamine precontractions (Figure 19 + Figure 20).

In renal VSMCs, relative expression analyses of the pore-forming KCNQ mRNA in qPCR experiments have found predominance of KCNQ1, with KCNQ4 and KCNQ5 being readily, KCNQ3 more sporadically and KCNQ2 not at all expressed<sup>96, 243, 244</sup>. Immunodetection has confirmed protein expression for  $K_v7.1$ ,  $K_v7.4$  and  $K_v7.5$  channels<sup>96</sup> in the main renal artery. Pharmacologically,  $EC_{50}$  values of Retigabine for  $K_v7$  activation in heterologous expression systems have been reported to be around  $\sim 1.4 \mu M$ <sup>249</sup>,  $\sim 5.2 \mu M$ <sup>273</sup> or  $\sim 5.9 \mu M$ <sup>274</sup> for  $K_v7.4$  and around  $\sim 3.45 \mu M$ <sup>274</sup> or  $\sim 6.4 \mu M$ <sup>252</sup> for  $K_v7.5$ . Therefore, we conclude that the concentration-dependent (0.3-30  $\mu M$ ) Retigabine-induced relaxations of renal interlobar arteries we observed (Figure 19 – Figure 25) are mainly due to opening of  $K_v7.4$  and  $K_v7.5$ , although an involvement of  $K_v7.3$  cannot be entirely ruled out. More exact functional differentiation of which specific channel contributes most to Retigabine-induced relaxations is currently difficult, as single subunits-specific activators or blockers for  $K_v7.2-5$  are not available. Instead, it is possible to inhibit expression of individual KCNQ subtypes, which has been achieved in main renal arteries, where a role

for  $K_v7.4$  in agonist-induced contractions has been supported by demonstrating enhancement of the contractile effect of Methoxamine after  $K_v7.4$  knockout with either morpholinos<sup>262</sup> or siRNA<sup>96</sup>. Alternatively, the combination of Retigabine with specific  $K_v7.1$  or unspecific pan- $K_v7$  blockers is an approach allowing further insight in  $K_v7$  function.

By doing so, we were able to demonstrate that an involvement of  $K_v7.1$  in the anticontractile effect of Retigabine is unlikely, as we found the  $K_v7.1$ -specific blocker HMR1556 (10  $\mu$ M) unable to diminish Retigabine-induced concentration-dependent relaxations, while the pan- $K_v7$  blocker XE991 was effective in doing so (Figure 23). This is in agreement with findings in mesenteric arteries of KCNQ1 knockout mice, where Retigabine produced regular concentration-dependent relaxations in phenylephrine-precontracted vessels<sup>263</sup>. The only literature we found in opposition to our results, which was a study finding the alternative  $K_v7.1$ -specific blocker chromanol 293B (10  $\mu$ M) to be effective in diminishing retigabine-induced relaxations in rat coronary arteries<sup>194</sup> does not profoundly undermine our findings, because chromanol 293B has been reported to have an  $IC_{50}$  for inhibition of  $K_v7.1$  of 27  $\mu$ M<sup>269</sup>, 41  $\mu$ M<sup>270</sup> or even 67  $\mu$ M<sup>271</sup> and to also inhibit other  $K^+$  channels at similar concentrations<sup>266-268</sup>, which in conclusion does not allow the effect of chromanol 293 to be attributed to  $K_v7.1$  inhibition with enough certainty<sup>300</sup>.

XE991 is a cognitive enhancer that has been shown to block  $K^+$  currents through all  $K_v7.1-5$ , though with differential sensitivity<sup>217, 219, 224, 249-253</sup> and to cause vasoconstriction in various rat arteries, including aorta and mesenteric artery<sup>256, 261</sup>, coronary artery<sup>228, 232</sup>, intrapulmonary artery<sup>226</sup>, cerebral artery<sup>257, 258</sup>, and skeletal muscle artery<sup>229, 234</sup>. In humans, XE991 has been demonstrated to increase both basal arterial tone and agonist-induced contraction in placental chorionic plate arteries<sup>241</sup> and to cause a tonic increase in isometric tension superimposed by phasic contractions in visceral adipose tissue arteries<sup>239</sup>. Specifically in the rat renal vasculature, so far only two studies have tested XE991, reporting it to cause slight contractions ( $\sim 17 \pm 10\%$  of KCl-induced contraction) of the main renal artery at 1  $\mu$ M<sup>255</sup> or to induce dose-dependent vasoconstriction of interlobar arteries at 1-50  $\mu$ M and dose-dependent reductions in RBF in vivo at 0.1-5  $\mu$ M<sup>246</sup>. Thus, we are the first to confirm a contractile effect of XE991 in isolated perfused rat kidneys by demonstrating a sustained increase in perfusion pressure during Methoxamine-induced vasoconstriction (Figure 59 + Figure 60).

*Table 12: Effects of coadministration of the  $K_v7$  blocker XE991 and the  $K_v7.2-5$  activator Retigabine*

Source	Vessel	Precontraction	Conc. XE991	Conc. Reti	Stronger effect	Effect when combined
239	human mesenteric adipose tissue artery	Phenylephrine	10 $\mu$ M	10 $\mu$ M	XE991	contraction
239	human visceral adipose tissue artery	Phenylephrine	10 $\mu$ M	10 $\mu$ M	equal	no dilation
193	murine aorta	Phenylephrine	10 $\mu$ M	20 $\mu$ M	XE991	contraction
193	murine aorta	Phenylephrine	10 $\mu$ M	20 $\mu$ M	equal	no dilation
256	rat mesenteric artery	Methoxamine	10 $\mu$ M	10 $\mu$ M	equal	no dilation
261	rat mesenteric artery	U44619	30 $\mu$ M	10 $\mu$ M	Reti	dilation
255	rat pulmonary artery	none (XE991 only)	1 $\mu$ M	10 $\mu$ M	Reti	dilation
229	rat gracilis muscle artery	5-HT	30 $\mu$ M	10 $\mu$ M	Reti	dilation

*Conc. = concentration; Reti = Retigabine*

Existing data on the effect of combining pan- $K_v7$  blocker XE991 and  $K_v7.2-5$  activator Retigabine is controversial. Intuitively, one would expect the effect of the  $K_v7.2-5$  activator Retigabine to be overridden by the pan- $K_v7$  blocker XE991, which also blocks  $K_v7.1$  channels. However, experiments in human mesenteric and visceral adipose tissue arteries<sup>239</sup>, murine aorta<sup>193</sup>, and rat mesenteric<sup>256, 261</sup>, intrapulmonary, and skeletal muscle artery<sup>229</sup> using different  $G_{q/11}$  coupled agonists for precontraction

(methoxamine, phenylephrine, serotonin, U44619 or none) have sometimes found the contractile effect of XE991, sometimes the anticontractile effect Retigabine to predominate or surpass the other, although mostly using similar concentrations of XE991 (1-30  $\mu\text{M}$ ) or Retigabine (10-20  $\mu\text{M}$ ) (see: Table 12).

In our experiments on Methoxamine-precontracted renal interlobar arteries, (i) preincubation with XE991 (3  $\mu\text{M}$ ) did diminish, but not completely prevent, Retigabine-induced (0.3-30  $\mu\text{M}$ ) concentration-dependent relaxations (Figure 21 + Figure 23), while (ii) relaxations to Retigabine (30  $\mu\text{M}$ ) were completely antagonized, but not surpassed by XE991 (3 or 10  $\mu\text{M}$ ) (Figure 25). These are the first findings on antagonization of XE991 and Retigabine in renal arterial vessels. Three previous reports have studied antagonization of other  $K_v7$  blockers and activators in renal arteries, which also produce seemingly contradictory results: Two studies, both conducted on main renal arteries, report concentration-dependent relaxations of methoxamine-precontracted arteries in response to  $K_v7.2-5$  activators Retigabine (no dosage given) or S-1 (up to 10  $\mu\text{M}$ ) to be completely prevented by prior pan- $K_v7$  block via Linopirdine (10  $\mu\text{M}$ )<sup>96, 243</sup>. Oppositely, a study conducted on renal interlobar arteries reported  $K_v7.2-5$  activator Flupirtine (1-100  $\mu\text{M}$ ) to cause slight relaxations even in arteries precontracted with XE991 (5  $\mu\text{M}$ ) in the absence of other vasoconstrictors<sup>246</sup>. Several explanations appear plausible for such observations:

First, the degree of precontraction and/or the type of vasoconstrictor used may be of relevance, as certain data suggest modulation of  $K_v7$  channel influence on VSM contractility by  $G_{q/11}$  mediated activation of PKC<sup>195, 225, 230, 257, 293</sup>, which is also a pathway involved in  $\text{Ca}^{2+}$  sensitization<sup>16</sup>. According to our results, this is not the case in renal interlobar arteries, since we found different levels of Methoxamine-induced precontraction to have no differential effect on the degree of concentration-dependent relaxations to Retigabine after preincubation with XE991 (Figure 24). In support of our findings is the fact that evidence for PKC involvement in  $K_v7$  influence is either insufficient or contradictory when focusing on the renal vasculature:

On the (i) cellular level, it has been suggested that  $G_{q/11}$  coupled vasoconstrictors mediate VSMC activation by PKC-dependent inhibition of  $K_v7$  channels. This is based mainly on two studies reporting  $G_{q/11}$  coupled vasoconstrictor arginine vasopressin (AVP) to reduce retigabine- or flupirtine-sensitive  $K^+$  currents and thus cause depolarization, which could be reduced by PKC-inhibitors in VSMCs of rat aorta<sup>230</sup> and rat mesenteric artery<sup>225</sup>. Additionally to AVP, other  $G_{q/11}$  coupled vasoconstrictors including serotonin (5-HT) and endothelin-1 (ET-1) have been shown to suppress Retigabine-sensitive  $K_v7$  currents in a manner similar to a direct PKC-inhibitor in rat cerebral artery, though without testing for PKC-dependency<sup>257</sup>. Furthermore, indirect arguments in favor of an involvement of PKC have been made based on the inhibition of AVP-sensitive  $K_v$  currents by XE991 or linopirdine in rat aorta SMCs<sup>230</sup>, the lacking additivity of AVP- and linopirdine- induced depolarization in rat mesenteric artery SMCs<sup>225</sup>, the PKC-dependent inhibition of  $K_v7.5$  currents induced by a DAG-analog in rat A7r5 aortic cells and the reduced extent of AVP-induced depolarization in KCNQ5 knockdown A7r5 cells<sup>293</sup>. More direct proof has been provided by PKC $_{\alpha}$  activation suppressing native  $K_v7$  currents in mesenteric artery SMCs<sup>195</sup>.

On the (ii) whole-vessel level, to our knowledge no direct evidence has been presented for PKC-dependency of  $K_v7$ -mediated regulation of vascular tone. One study examined the effect of PKC inhibitor calphostin in rat mesenteric arteries, finding it to be inefficient in preventing linopirdine-induced contractions in both absence and presence of AVP (n=5), while L-type  $\text{Ca}^{2+}$  channel blocker verapamil (n=3) was effective in doing so<sup>225</sup>. Another study did find PKC activator PMA to mimic the effect of XE991 in producing contractions in rat basilar arteries, but did not investigate whether XE991-induced contractions were PKC-dependent<sup>257</sup>. Nonetheless, indirect support for PKC involvement in vascular reactivity exists in the form of hypotheses based on the above described findings in VSMCs combined with reports of XE991 enhancing AVP-, ET-1- or phenylephrine-induced contractions in murine aorta<sup>193</sup> or rat cerebral arteries<sup>257</sup> as well as reports of retigabine or flupirtine diminishing

AVP-, ET-1, 5-HT- or phenylephrine-induced contractions in murine aorta<sup>193</sup> or rat cerebral arteries<sup>258</sup>. Interestingly, recent evidence suggests a new mechanism of  $G_{q/11}$ -mediated regulation of  $K_v7$  by demonstrating that long-term (> 1h) incubation of angiotensin II can decrease  $K_v7.4$  protein expression without reducing KCNQ4 transcript levels via interaction with HSP90<sup>247</sup>.

In the (iii) renal vessels specifically, PKC-dependency of  $K_v7$ -mediated vascular reactivity has not been demonstrated directly. Nonetheless, various reports of methoxamine- or norepinephrine-induced vasoconstrictions in renal arteries being diminished by Retigabine, Flupirtine, S-1, ML213 or BMS204352<sup>96, 243, 246, 262</sup> or being enhanced by XE991 or linopirdine<sup>77, 96, 246</sup> as well as KCNQ4 knockdown<sup>96, 262</sup> leave open the possibility of a functional relevance of this pathway. Contrarily though, in vivo measurements in rats found angiotensin II- and norepinephrine-induced decreases in RBF to be unaffected by pretreatment with flupirtine (10  $\mu$ M) or XE991 (5  $\mu$ M), giving no implication for a role of  $K_v7$  in  $G_{q/11}$  mediated renal arterial vasoconstriction<sup>246</sup>. Concludingly, our results add to the complexity of the question of  $G_{q/11}$  and PKC activation modulating  $K_v7$  in renal vasoconstriction, in our case rather making an argument against a functional relevance of such a mechanism. Further research is needed, preferably directly testing the effect of PKC inhibitors in context with  $K_v7$  modulators in renal vessels.

Second, the size of the vessels studied may be of relevance, as different vasoconstrictive and vasodilative pathways tend to predominate in differently sized arteries<sup>351, 352</sup>. In context with  $Ca^{2+}$  sensitization, PKC-mediated inhibition of myosin phosphatase (via phosphorylation of CPI-17) is the predominant pathway in small resistance arteries, whereas in large arteries like the aorta, it is ROCK-mediated inhibition of myosin phosphatase (via phosphorylation of MYPT1)<sup>351</sup>. This could help to explain why, in disagreement with our findings on small intrarenal resistance arteries, the anticontractile effect of  $K_v7.2$ -5 activators Retigabine (no concentration given)<sup>243</sup> or S-1 (1-10  $\mu$ M)<sup>96</sup> on Methoxamine precontractions was entirely abolished by preincubation with  $K_v7$  blocker linopirdine (10  $\mu$ M) in the main renal artery, which is a first order branch of the aorta conducting ~25% of cardiac output and thus one of the largest arteries in the body<sup>6</sup>. It could be hypothesized that contractile pathways involving ROCK, but not PKC, may enhance the contractile effect of  $K_v7$  blockers like XE991. Having elaborated above that a modulating effect of PKC on  $K_v7$  remains yet to be established in renal vessels, this hypothesis could give impetus for further research on interactions of ROCK with  $K_v7$  channels in large vessels.

Third, the chronological order in which  $K_v7$  blockers or activators are applied may be important, as XE991 and linopirdine have been found to be state-dependent inhibitors favoring the activated subunit of  $K_v7$ <sup>353</sup> and that therefore their effect on vascular contractility depends upon VSMC  $V_m$  at the time of their application. A study on neuronal  $K_v7$  demonstrated that XE991 (10  $\mu$ M) had a half-inhibition potential for  $K_v7.2$  of  $-51.6 \pm 0.0$  mV, producing near-complete inhibition when applied at potentials more positive than -30 mV, but having no effect in cells held at -70 mV (Greene et al., 2017). Similar results were found for linopirdine. Thus, XE991 and linopirdine preferentially inhibit  $K_v7.2$  at  $V_m$  more depolarized than their activation threshold. This goes in line with the observation in blood vessels that for  $K_v7$  blockers to develop a vasoconstrictive potential, there seems to be a need for a depolarizing stimulus like low concentrations of vasoconstrictors or perfusion pressure, as has been suggested<sup>166</sup> based on data showing variable effects of pan- $K_v7$  blockers in mesenteric arteries<sup>193, 225, 226</sup>. Retigabine (10  $\mu$ M) on the other hand, in the same study on neurons, left-shifted the half-activation voltage of  $K_v7.2$  by -24 mV (from ~-23 mV to -47 mV). Furthermore, Retigabine likewise left-shifted the half inhibition potential of XE991 for  $K_v7.2$  by also -24 mV (from  $-51.6 \pm 0.0$  mV to  $-75 \pm 0.6$  mV)<sup>353</sup>. Measurements of  $V_m$  in renal interlobar and afferent arteriolar VSMC at normal blood pressure have been made in hydronephrotic kidneys, reporting potentials ranging from -55 to -40 mV<sup>118-120, 122, 129</sup>. Half maximum activation thresholds ( $V_{50}$ ) are somewhat different between the  $K_v7.x$  subunits, ranging from -20 mV ( $K_v7.1$  and  $K_v7.4$ ) over -30 mV ( $K_v7.2$ ) down to -40 mV ( $K_v7.3$  and  $K_v7.5$ )<sup>183</sup>. Thus, based on the assumption that results for Retigabine and XE991 on  $K_v7.2$  activation dynamics<sup>353</sup> can be extrapolated for other  $K_v7$  channels, we might draw three conclusions: that (i) after preincubation with Retigabine, XE991 already inhibits  $K_v7$  at more hyperpolarized potentials (ergo, Retigabine enhances

the inhibitory potential of XE991 at less depolarized  $V_m$ ), explaining why in our findings, application of Retigabine prior to XE991 allows XE991 to reverse Retigabine-induced interlobar artery relaxations, returning the force level back to Methoxamine-only control (Figure 25), while vice versa preincubation with XE991 is unable to fully prevent relaxations to Retigabine (Figure 21 + Figure 23); that (ii) in the absence of agonist-induced contraction (ergo, at a not-depolarized  $V_m$ ), XE991 is unable to unfold its full inhibitory potential, explaining why subsequent application of Flupirtine is still able to cause interlobar artery vasodilation<sup>246</sup>; and that (iii) in the presence of agonist-induced contraction (ergo, at more depolarized  $V_m$ ), the inhibitory potential of linopirdine is greater, explaining why subsequent application of Retigabine is not able to cause renal artery vasodilation<sup>96, 243</sup>. The functional relevance of this on a systemic level has yet to be established, as so far, the only existing *in vivo* data showed no significant reduction in RBF when XE991 was administered after flupirtine-pretreatment<sup>246</sup>. Furthermore, in order to make a valid statement on this matter, further research is required on  $K_v7$  activator and inhibitor dynamics with regards to specific  $K_v7.x$  subunits.

Finally, differential sensitivity to XE991 among different KCNQ subunits could play a role in its incomplete antagonization of Retigabine. For example, the proposed existence of homomeric  $K_v7.5$ , which would require much higher doses of XE991 to be blocked, could be of help explaining this phenomenon: For homomeric  $K_v7.5$  channels, the half maximal inhibitory concentration ( $IC_{50}$ ) of XE991 has been reported to range from 61  $\mu M$ <sup>253</sup> or  $\sim 65 \mu M$ <sup>251</sup> up to  $\sim 75 \mu M$ <sup>252</sup>. Meanwhile, the half maximal effective concentration ( $EC_{50}$ ) for  $K_v7.5$  activation by Retigabine is reported to be one order of magnitude lower, ranging from 2.0  $\mu M$ <sup>253</sup> or 3.45  $\mu M$ <sup>274</sup> to 6.4  $\mu M$ <sup>252</sup>. Studies testing antagonization of XE991 and Retigabine always used concentrations of Retigabine sufficiently high for  $K_v7.5$  activation, as did we (0.3-30  $\mu M$ ), but XE991 is mostly used at only 1-10  $\mu M$ <sup>193, 226, 239, 256</sup> or seldomly 30  $\mu M$ <sup>229, 245</sup>, which is not enough to extensively block homomeric  $K_v7.5$  channels. Thus, coapplication of XE991 and Retigabine at such concentrations may result in Retigabine activating all  $K_v7.2-5$ , but XE991 only blocking  $K_v7.1-4$ , which would sum up to a net  $K_v7.5$  activation and thus explain a net anticontractile effect, as we found it in renal resistance arteries (Figure 21 + Figure 23) and as previous studies have done in various other vessels<sup>229, 255, 261</sup>. What might make this argumentation prone to error though, is the circumstance that drug potency may be underestimated, depending on the expression systems they are studied in<sup>248, 354</sup>. Still, as this applies to not only  $K_v7.5$ , but all  $K_v7$  equally, the fact that for the remaining  $K_v7.1-4$ ,  $IC_{50}$  values are reported to be at least one order of magnitude lower while being studied in the same expression systems<sup>217, 219, 249, 250</sup>, does validate the above hypothesis. Provided that homomeric  $K_v7.5$  do exist in the vasculature, this hypothesis may further be supported by the observation that XE991 at 50  $\mu M$  produced 3.5 times larger increases in isometric tension of rat renal interlobar arteries than at 5  $\mu M$ <sup>246</sup>. Opposingly though, studies on the functional assembly of KCNQ subunits as ion channel complexes have tended to find  $K_v7.4/K_v7.5$  heteromers rather than  $K_v7.4$  or  $K_v7.5$  homomers, at least in cerebral<sup>196</sup> and mesenteric<sup>195, 242</sup> artery myocytes. However, this does not rule out the existence of homomeric  $K_v7.5$  channels in renal arteries, though possibly making it less likely. Besides homomeric  $K_v7.5$  channels, another possibility would be a functional role for heteromeric  $K_v7.1/K_v7.5$  channels. Their existence in VSMCs has early been suggested based on bimodal effects of Retigabine in murine portal vein myocytes<sup>238</sup>. More recently, colocalization of  $K_v7.1$  and  $K_v7.5$  subunits has been confirmed morphologically via coimmunoprecipitation in rat aortic myocytes and further indirect support has been provided for functional  $K_v7.1/K_v7.5$  heteromeric channels by demonstrating that when expressed in *Xenopus* oocytes, these were found to be similarly activated by Retigabine as  $K_v7.5$  homomers<sup>194</sup>. The possibility of functionally relevant  $K_v7.1/K_v7.5$  heteromers has also been suggested as an explanation for relaxations induced by both Retigabine and R-L3 being more marked in myocytes isolated from the left coronary artery (LCA) than from the right coronary artery (RCA) with expression of  $K_v7.1$  and  $K_v7.5$ , but not  $K_v7.4$ , being higher in LCA than in RCA myocytes<sup>232</sup>. Unfortunately, no data is available on the sensitivity of  $K_v7.1/K_v7.5$  heteromers to XE991. In case  $K_v7.1/K_v7.5$  heteromers were to require an  $IC_{50}$  of XE991 close to that for  $K_v7.5$  homomers (61-70  $\mu M$ , see above), their existence in renal arteries would be similarly able to explain the predominating effect of Retigabine over XE991. Concludingly, further research is needed on the

pharmacology of  $K_v7.1/K_v7.5$  heteromeric channels in vascular smooth muscle. Also, morphological studies on  $K_v7$  expression and distribution in renal arteries is required, specifically including testing for the existence of both homomeric  $K_v7.5$  and heteromeric  $K_v7.1/K_v7.5$  channels.

For the sake of completeness, it must be noted that data exists suggesting unspecific effects of Retigabine at higher concentrations, leading to relaxations mediated by mechanisms other than  $K^+$  channel activation. This has been documented in form of an anticontractile effect of Retigabine on KCl-induced precontractions in rat pulmonary arteries<sup>255</sup> and rat skeletal muscle arteries<sup>229</sup>. However, this phenomenon was observed at concentration of 100  $\mu$ M Retigabine<sup>229, 255</sup> and is therefore unlikely to be of relevance in our experiments, in which the maximum concentration of Retigabine used was 10-fold lower.

Concludingly, the evidence we found in renal resistance arteries for a strong anticontractile effect of  $K_v7.2-5$  activation in agonist-induced vasoconstriction may well be attributed to  $K_v7.5$ -containing homo- or heteromeric channels, like the already known heteromeric  $K_v7.4/K_v7.5$ , while additionally, we thus provide an argument for a so far unappreciated functional relevance of homomeric  $K_v7.5$  channels or heteromeric  $K_v7.1/K_v7.5$  channels. Furthermore, we argue that (i) our results provide no confirmation for a functional role of  $K_v7$  modulation via a  $G_{q/11}$  mediated, PKC-dependent mechanism and that differential responses to  $K_v7$  modulators in our as well as in existing reports on renal vessels (ii) may be attributed to vessel size or (iii) may hint towards a role for the chronological order or the VSMC  $V_m$  at the point of time at which  $K_v7$  modulators are applied.

#### 4.3 Contribution of $K_v7.1$ to agonist-induced renal vasoconstriction

The role of  $K_v7.1$  in vascular reactivity is so far incompletely understood and currently being discussed controversially<sup>263, 300</sup>. Although vast evidence exists for the expression of KCNQ1 in various rodent blood vessels<sup>96, 166, 193, 208, 223, 225-234, 236-238, 243-245, 255, 256, 258-260, 279</sup> and also for  $K_v7.1$  channel protein presence in VSMC membranes<sup>96, 193, 208, 235, 238, 240</sup>, only few reports make an argument in favor of a functional relevance of these channels<sup>232, 243, 260</sup>. In this thesis, our results in both interlobar artery isometric tension recordings as well as isolated perfused kidney experiments may not suggest a role for  $K_v7.1$  channels in maintaining resting tone of renal resistance arteries, but provide evidence for their functional presence and pharmacological responsiveness in agonist-induced vascular contractility.

R-L3 is a benzodiazepine acting as a partial agonist of  $K_v7.1$  that is reported to either enhance  $K^+$  currents with an  $EC_{50}$  of  $<1 \mu$ M<sup>213</sup> or to have an only small effect at 1  $\mu$ M, but to cause a  $\sim 100\%$  increase in  $K_v7.1$  currents at 10  $\mu$ M<sup>260</sup> in *Xenopus* oocytes. A functional role in arterial contractility has been demonstrated in form of concentration-dependent relaxations of agonist-induced precontraction in murine renal and mesenteric artery<sup>263</sup> as well as in rat aorta, renal, mesenteric, coronary, and intrapulmonary artery<sup>232, 260, 263, 280</sup>, while other studies found R-L3 ineffective in producing relaxations i.e. in rat coronary or cerebral arteries<sup>196, 228, 279</sup>. In the rat renal vasculature specifically, to date only one study has examined the effect of R-L3, finding concentration-dependent (0.1, 0.3 and 1.0  $\mu$ M) relaxations in Methoxamine precontractions of the main renal artery<sup>280</sup>. Additionally, a suggestion for a functional role of  $K_v7.1$  has been made based on the reduced potency of  $K_v7.2-5$  activator Retigabine in the main renal artery compared to mesenteric artery, where  $K_v7.1$  abundance is comparatively low<sup>243</sup>. Thus, our report is the first to confirm an anticontractile effect of R-L3 in rat renal resistance arteries by demonstrating concentration-dependent relaxations in Methoxamine precontractions (Figure 26).

These results require careful consideration, as R-L3 has been argued to be an inappropriate tool for the study of  $K_v7.1$  in mice. This was based on findings of R-L3 producing normal endothelium-

independent relaxations in KCNQ1-knockout mice, producing relaxations in both XE991- and KCl-induced precontractions, and the inability of either HMR1556 or XE991 to reverse R-L3 relaxations<sup>193, 263</sup>. On the other hand, no such results have been published in rat arteries. Nonetheless, doubts have been raised in rat mesenteric arteries that R-L3 indeed primarily acts via  $K_v7.1$  opening, based on the observation that its anticontractile effect in phenylephrine precontractions was reduced by HMR1556 (10  $\mu$ M) in only 3 out of 6, and with a sustained effect in only in 1 out of 6 artery rings, while chromanol 293B (10  $\mu$ M) completely failed to prevent R-L3 relaxations<sup>263</sup>. Our results may help settle such doubts at least for the rat renal vasculature, as we provide profound evidence for a  $K_v7.1$ -specific effect of R-L3: adding to previous unpublished results from our laboratory having found HMR1556 (10  $\mu$ M) to completely abolish and considerably reduce the anticontractile effect of R-L3 (at 1 or 3  $\mu$ M, respectively) on concentration-dependent contractions to Methoxamine which are incidentally confirmed in our experiments on ANP and Urocortin (Figure 32 – Figure 34 and Figure 47 + Figure 48) do we present not only data on renal resistance arteries but also on isolated perfused rat kidneys, demonstrating that R-L3 in Methoxamine precontractions causes marked relaxations of renal resistance arteries as well as decreases in renal perfusion pressure, all of which respond to antagonization by both HMR1556 at 10  $\mu$ M and XE991 at 3  $\mu$ M (Figure 26 – Figure 29 and Figure 62 – Figure 67). Our data support previous reports having found HMR1556 effective in reversing R-L3 induced relaxations in rat thoracic aorta, mesenteric and intrapulmonary arteries<sup>260</sup>. Interestingly though, that study also showed considerable variations in the percentage of reversal, depending on the concentration of R-L3 used. HMR1556 was only able to reduce relaxations to R-L3 at 10  $\mu$ M by  $47.3 \pm 20.6\%$  or  $66.7 \pm 33.3\%$ , but by  $104.2 \pm 5.9\%$  when only 3  $\mu$ M R-L3 were applied. This was interpreted to indicate that in rat aorta and pulmonary arteries, some effects of R-L3 at concentrations above 3  $\mu$ M are not due to stimulation of  $K_v7.1$ <sup>260</sup>. Our results are somewhat similar, although R-L3 was only used at concentrations no higher than 1  $\mu$ M. We found the percentage by which HMR1556 reduced the decrease in perfusion pressure caused by R-L3 at maximum (1  $\mu$ M) or minimum effective concentrations ( $\sim 0.6$   $\mu$ M) to change from  $42.6 \pm 9.1\%$  to  $11.7 \pm 3.6\%$  (Figure 64). Furthermore, we found that HMR1556 and XE991 were equally potent in reversing R-L3 induced decreases in perfusion pressure after 10 minutes (Figure 66). Combining these findings with our observation that in renal interlobar arteries, HMR1556 and XE991 were able to entirely prevent relaxations to R-L3 at concentrations up to 0,1  $\mu$ M, but only diminish relaxations at 0,3  $\mu$ M and 1  $\mu$ M (Figure 29), one may be drawn towards suspecting a mechanism additional to  $K_v7.1$  activation as part of the effect of R-L3. However, we were able to demonstrate that prolonged application of XE991 for 20 minutes resulted in a complete reversal of the pressure-decreasing effect of R-L3, though failing to witness an overshooting contraction as should be expected due to the blockade of the remaining  $K_v7$  subunits by XE991 (Figure 67). Additionally, we showed that different levels of precontraction induced by Methoxamine do not affect the dimension of R-L3-induced relaxations after preincubation with XE991 (Figure 30), providing an argument against an involvement of agonist-induced  $G_{q/11}$ -mediated PKC activation modulating  $K_v7.1$  channels (for a more elaborate discussion, see Chapter 4.2). Thus, to conclude with, although we cannot with absolute certainty rule out an anticontractile mechanism other than  $K_v7.1$  activation contributing to the effect of R-L3, a definite conclusion to be drawn from our results is that R-L3 does exert at least a considerable part of its anticontractile effect via  $K_v7.1$  channels. We may therefore confidently state that  $K_v7.1$  channels do play a functional role in the renal vasculature insofar as when they are pharmacologically activated, they are effective in counteracting agonist-induced renal resistance arterial vasoconstriction.

The next question to be addressed with regards to  $K_v7.1$  function is whether they contribute to resting tension or to agonist-induced vascular tone. To examine this, the effect of specific  $K_v7.1$  blockers on unstimulated or stimulated vessels is of particular interest, as in the case of  $K_v7.1$  contributing to resting or stimulated VSMC  $V_m$ , this blockade would result in an increase in vessel tone.

HMR1556 is a synthetic organic experimental drug initially used for the study of the cardiac  $I_{Ks}$  (KCNQ1/KCNE1) current<sup>264</sup>. HMR1556 has been reported to block native or human cloned  $K_v7.1$

expressed in *Xenopus* oocytes at an  $IC_{50}$  of  $0.54 \mu M$ <sup>216</sup> or  $0.42 \mu M$ <sup>215</sup> respectively and that at  $10 \mu M$  it reduces  $K^+$  currents in  $K_v7.1-$ , but not in  $K_v7.4-$  or  $K_v7.5-$ injected oocytes<sup>96</sup>. Studies testing its effect on resting vessel tone, thus without vasoconstrictive agents added, have uniformly found no effect of HMR1556 in rat coronary<sup>228</sup>, cerebral<sup>196</sup>, mesenteric, intrapulmonary artery and thoracic aorta<sup>260</sup>. Studies testing its effect during active contraction have similarly denied an effect of HMR1556 on either pressurized<sup>245</sup> or methoxamine- and phenylephrine-contracted mesenteric arteries<sup>210, 263</sup>. Furthermore, systemic application of HMR1556 in vivo did not induce vasoconstriction in dogs<sup>264</sup> or affect heart rate, blood pressure or GFR in rats<sup>265</sup>. An even larger number of studies have examined the alternative  $K_v7.1$  blocker chromanol 293B, which in various rodent blood vessels as well as human mesenteric and visceral adipose tissue arteries<sup>239</sup> likewise failed to show any effect on either resting tone or agonist-induced contraction, despite oftentimes within the same study effectively inhibiting  $K_v7.1$  currents<sup>193, 224, 232, 245, 259, 263</sup>. However, no study has done so in renal vessels yet. Our report is therefore the first to confirm the absence of an effect of HMR1556 ( $10 \mu M$ ) on agonist-induced vasoconstriction in the renal vasculature by recording unaltered perfusion pressures in isolated rat kidneys during application of HMR1556 applied for over 40 minutes of observation (Figure 61) whereas, for reference, XE991 distinctly elevated perfusion pressure under the same conditions (Figure 59 + Figure 60). More data in support of this argument is given by previous unpublished experiments from our laboratory, where no contractile effect of HMR1556 ( $10 \mu M$ ) on concentration-dependent contraction to Methoxamine was found, as well as by the results presented in this report, where the pan- $K_v7$  blocker XE991 was coapplied with  $K_v7.2-5$  activator Retigabine, thus leaving only  $K_v7.1$  blocked and not activated. Since we observed persistence of only slightly diminished Retigabine-induced relaxations after preincubation with XE991 (Figure 21 + Figure 23), and found complete antagonization, but no surpassing of the level of pre-Retigabine precontraction when XE991 was applied subsequently to counteract Retigabine-induced relaxations (Figure 25), there is no sign of  $K_v7.1$  blockade enhancing agonist-induced contraction in renal resistance arteries.

As to the question why  $K_v7.1$  apparently do not contribute to setting  $V_m$  or maintain resting vessel tone despite being present in the VSMC membrane, an involvement of the regulatory KCNE subunits has been suggested. Chadha et al.<sup>260</sup> proposed the pore-forming  $K_v7.1$  subunit to associate with the regulatory subunit KCNE4, the gene product of which has been shown to be expressed in various blood vessels including renal arteries<sup>193, 208, 210</sup> and the presence of which is known to effectively silence  $K_v7.1$  activity at physiological  $V_m$ <sup>209, 355, 356</sup>. However, this theory was opposed by Jepps et al.<sup>210</sup>, who found HMR1556 to have no effect on Methoxamine contractions in either KCNE4 knockdown or control mesenteric arteries, although this is what would be expected if  $K_v7.1$  were the predominant binding partner of KCNE4. Instead, the assumption was made that KCNE4 instead interacts with  $K_v7.4$ , as these two proteins co-localized in mesenteric artery myocytes, and KCNE4 knockout both abolished the contractile effect of linopirdine on Methoxamine contractions and reduced  $K_v7.4$  expression in the cell membrane<sup>210</sup>. However, interaction of  $K_v7.1$  with other KCNE subunits seems plausible, since KCNQ1 may assemble with all five KCNE members<sup>182, 184</sup> and all five KCNE genes have been identified in either aorta, renal, mesenteric, femoral, carotid, basilar or cerebral arteries, with no consistent pattern emerging except for KCNE4 being detectable in all vessels<sup>193, 208, 210</sup>. Such interaction of  $K_v7.1$  with KCNE can have numerous consequences on both  $K^+$  currents and pharmacological sensitivity to  $K_v7.1$  modulators. For example, interaction with KCNE1, which corresponds to the slow delayed rectifier current  $I_{Ks}$  in cardiac myocytes<sup>197, 198</sup>, may cause a right-shift of the activation threshold, enhance current amplitudes, slow activation and deactivation<sup>355</sup>, decrease sensitivity to XE991 ~14-fold (Wang et al., 2000), decrease sensitivity to R-L3<sup>213, 214</sup> or increase sensitivity to HMR1556<sup>215, 216</sup>. Oppositely, interaction with KCNE2 can decrease current amplitude and transform  $K_v7.1$  into a voltage-independent channel<sup>205</sup>, while KCNE3 is similarly able to nearly abolish  $K_v7.1$  gating with nearly instant activation, leading to constitutively open channels<sup>207</sup>. KCNE5 again has a similar effect on  $K_v7.1$  as KCNE1, right-shifting the activation threshold by 140 mV towards +40 mV and allowing currents to be conducted only upon strong and continued depolarization<sup>212</sup>. Eventually, while our data may not directly contribute in elucidating the question of KCNE involvement in  $K_v7$  mediated regulation of

vascular tone, we can still provide an argument opposing the previously made suggestion that  $K_v7.1$  tetramers would be expressed, but rendered non-functional by the expression of inhibitory KCNE auxiliary subunits, as has been stated by Haick and Byron<sup>300</sup> as we clearly demonstrate a functional role for  $K_v7.1$  channels in renal resistance arterial contractility. Furthermore, we may point out that since no pharmacological modulators of KCNE are available to date, studying the effect of KCNE subunit knockout in context with the above mentioned  $K_v7$  modulators displaying differential effects in dependence of the presence of KCNE subunits may be a promising direction for future renovascular research.

In summary, we argue that although  $K^+$  currents through  $K_v7.1$  do not appear to be contributing to resting vessel tone and their complex interdependence with the KCNE auxiliary subunits leaves many questions unanswered,  $K_v7.1$  channels represent an interesting therapeutic target as their pharmacological activation by substances like R-L3 is effective and mostly tissue-specific in its relaxation of renal resistance arteries and in its lowering of renal perfusion pressure in a flow-controlled perfusion setup, possibly corresponding to an *in vivo* effect of selectively increasing renal blood flow that could be beneficial in certain forms of renovascular pathology.

#### 4.4 Contribution of $K_v7$ to the anticontractile effect of ANP in agonist-induced renal vasoconstriction

With  $K_v7.1$  being functionally present in renal resistance arteries, but not contributing to resting vessel tone, one assumption to be drawn with regards to their physiological role is that they may be involved in naturally existing vasodilation pathways. Although this has been suggested for  $K_v7.1$  in context with rat arterial vessels a few years back already<sup>260</sup>, only few studies have examined the effect of cyclic nucleotides on  $K_v7.1$  in vascular smooth muscle<sup>77, 107, 196</sup>. This seems surprising, considering that the name for KCNQ channels is originally derived from their characteristic of being  $K^+$  channels gated by cyclic nucleotides. A number of studies in VSMCs have by employing non-specific  $K_v7$  modulators discovered hints towards an involvement of  $K_v7.4$  and/or  $K_v7.5$  channels rather than  $K_v7.1$  channels in various endogenous vasodilator actions that exert their effect via the cyclic nucleotides cGMP, i.e. natriuretic peptides<sup>77</sup>, or cAMP, i.e.  $\beta$  adrenoceptor agonists, adenosine or calcitonin gene-related peptide<sup>96, 97, 107, 196, 228, 259, 262, 280</sup>. In this thesis, we undertook a thorough examination of both cGMP- and cAMP-dependent vasodilator actions in renal resistance arteries in context with all  $K_v7$  channels, specifically including  $K_v7.1$ .

The atrial natriuretic peptide (ANP) is a hormone or paracrine factor that binds to the natriuretic peptide receptor A (NPR-A, also known as NPR1 or GC-A) expressed in VSMCs<sup>319</sup>. In its activated state, it acts as a guanylyl cyclase (GC), generating cGMP from GTP, which in turn may either directly interact with  $K_v7$  channels or exert a variety of effects via stimulation of cGMP-dependent protein kinases (PKG), counteracting  $Ca^{2+}$ -dependent and/or  $Ca^{2+}$ -sensitizing mechanisms of contraction, but not directly phosphorylating MLCK itself<sup>16, 55, 319</sup>. ANP has long been known to cause renal vasodilation, increase RBF, glomerular filtration rate and diuresis and thus reduce arterial pressure<sup>357, 358</sup>, but has only more recently been linked to cardiovascular pathology, as ANP-induced relaxations were shown to be impaired in animal models of diabetes<sup>359</sup> and arterial hypertension<sup>77</sup>. Simultaneously,  $K_v7$  channels have been suggested to be involved in natriuretic peptide vasodilations<sup>77</sup>, which to date is the only published data describing such a phenomenon. Therefore, this thesis is one of the first profound examinations of a possible interdependence of ANP and  $K_v7$  channels with regards to their contribution to vascular reactivity.

Opposite to the above-mentioned study on the main renal artery<sup>77</sup>, our extensive analysis found no evidence of  $K_v7$  channel involvement in ANP-induced vasorelaxation of renal resistance arteries. We report that the anticontractile effect of ANP in renal resistance arteries, as indicated by decreases in Methoxamine sensitivity, does not affect and vice versa is itself unimpaired by the anticontractile effect of both  $K_v7.1$  activation (Figure 32) or  $K_v7.2-5$  activation (Figure 31) as well as by the contractile

effect of both  $K_v7.1$  blockade after previous  $K_v7.1$  activation (Figure 33 + Figure 34) and of pan- $K_v7$  blockade (unpublished data). Furthermore, our results demonstrating that ANP-induced vasorelaxation of precontracted renal interlobar arteries (i) is more marked in  $\alpha_1$ -adrenoceptor agonist-induced than in depolarization-induced precontraction (Figure 35 – Figure 37), (ii) does not depend upon  $K_v7$  channels in depolarization-induced precontraction (Figure 38 – Figure 40), and (iii) is similarly marked in  $\alpha_1$ -adrenoceptor agonist-induced precontraction during blockade of either all  $K_v7$  or only  $K_v7.1$  channels (Figure 41 – Figure 44) all point towards the anticontractile mechanisms of ANP involving either  $Ca^{2+}$  sensitization in a manner independent of  $K_v7$  channels or a  $Ca^{2+}$  dependent mechanism involving  $K^+$  channels other than  $K_v7$ .

Stott et al.<sup>77</sup> have proposed that ANP-evoked relaxation is driven mainly through the activation of vascular  $K_v7.4$  or  $K_v7.5$  channels based on their findings in the main renal artery that ANP-induced relaxations of Methoxamine precontractions were impaired by the pan- $K_v7$  blocker linopirdine (10  $\mu$ M), but not by the  $K_v7.1$ -specific blocker HMR1556 (10  $\mu$ M), and were likewise impaired in arteries from SHRs, in which  $K_v7.4$  protein is reduced<sup>96</sup>. However, no results were presented for confirmation on whether the impairment caused by linopirdine was similarly present or absent in SHR arteries. Neither was there any evaluation done on the signal transduction mechanisms underlying the phenomenologically observed interaction of ANP and the  $K_v7$  blocker. The question remains unanswered whether a direct interaction between the cyclic nucleotide cAMP and the cyclic-nucleotide gated  $K^+$  channels was in fact causing the impairment of ANP-induced relaxations or whether both substances might merely be independently acting upon a common intermediate contractile mechanism, possibly  $Ca^{2+}$  sensitization. Furthermore, it was not shown whether conversely, pharmacological  $K_v7$  activation would enhance, or at all affect the anticontractile effect of ANP. Shedding some more light on these questions, a thorough pharmacological dissection of ANP in context with  $K_v7$  modulators was undertaken as part of this thesis.

By demonstrating that the decrease in Methoxamine sensitivity caused by ANP was reciprocally unaffected by all  $K_v7$  modulators we used (Retigabine at 30  $\mu$ M, R-L3 at 1  $\mu$ M, XE991 at 3  $\mu$ M and HMR1556 at 10  $\mu$ M) (Figure 31 – Figure 34 + unpublished data) we provide strong evidence that a direct interaction is unlikely in renal resistance arteries. It is established that cGMP can activate PKG, which in turn may induce vasorelaxations by decreasing cytosolic  $Ca^{2+}$ , by decreasing  $Ca^{2+}$  sensitivity, or by causing hyperpolarization via activation of  $K_v^-$ ,  $BK_{Ca^-}$  or  $K_{ATP}$ -mediated outward  $K^+$  currents<sup>55</sup> (see: Chapter 1.5.2.1). Several studies have in different arteries also implicated involvement of  $K^+$  channels specifically in ANP-induced vasorelaxations, including  $K_v$ ,  $K_{ATP}$ , or  $BK_{Ca}$  channels<sup>74, 84, 359-361</sup>. Based on our findings however, we conclude that  $K_v7$  in renal resistance arteries are not among the  $K^+$  channels modified by mechanisms downstream of cGMP, since neither the contractile nor the anticontractile effect caused by either activation of  $K_v7.1$  or  $K_v7.2-5$  or blockade of  $K_v7.1$  or all  $K_v7$  was by any means affected by the presence of ANP in agonist-induced contraction (Figure 31 – Figure 34).

Instead, our results suggest that ANP further downstream acts upon  $Ca^{2+}$  sensitization through pathways independent of  $K_v7$  channels. This hypothesis is based on three observations: First (i), ANP-induced vasorelaxation are more marked in Methoxamine- than in KCl-induced precontractions (Figure 35 – Figure 37). By replacing extracellular NaCl with equimolar KCl and thus changing the  $K^+$  equilibrium potential, all  $K^+$  currents are effectively blocked and  $V_m$  is clamped at a depolarized level, allowing to study contraction in an artificial setting characterized by the absence of vasoconstrictive agonist influence<sup>342</sup>. An important first conclusion to be drawn here is that since ANP is effective in producing relaxations in the presence of KCl, at least part of its anticontractile effect must result from mechanisms not involving  $K^+$  channels. KCl causes contraction via MLC phosphorylation in a strictly  $Ca^{2+}$ -dependent manner<sup>362</sup>. This happens initially through a phasic contractile response due to depolarization-induced gating of voltage-operated  $Ca^{2+}$  channels<sup>363</sup> and calmodulin-dependent MLCK activation<sup>364</sup> and subsequently through a tonic contractile response due to phosphorylation of CPI-17 and MYPT1 via activation of the PI3K/Rho/Rho-associated kinase (ROCK) pathway ( $Ca^{2+}$ -induced  $Ca^{2+}$  sensitization)<sup>365</sup>. However, KCl-induced contraction does not involve activation of PKC<sup>92</sup> (for review,

see <sup>366</sup>). Specifically in the renal preglomerular vasculature, Rho kinase inhibition has been demonstrated to reduce depolarization-induced vasoconstriction, though not as effectively as agonist-induced or pressure-induced vasoconstriction <sup>367</sup>. By contrast,  $\alpha$ 1-adrenoceptor agonists like Methoxamine, besides through Rho/ROCK inhibiting MLCP and through  $G_{q/11}$  activating PLC to generate  $IP_3$ , to release  $Ca^{2+}$  and to activate MLCK, also exert a contractile effect via PLC/DAG-mediated activation of PKC <sup>19, 368</sup>. In small resistance arteries altogether, PKC is deemed to play a predominant role in both the initial rising and the late tonic phase of contraction of agonist-induced contraction, whereas the ROCK-MYPT1-mediated  $Ca^{2+}$ -sensitizing pathway is of a lesser significance <sup>351, 369</sup>. However, specifically in the renal preglomerular vasculature, Rho kinase inhibition has been demonstrated to completely abolish agonist-induced vasoconstriction <sup>367</sup>. Thus, in renal resistance arteries, both ROCK and PKC must be considered relevant for agonist-induced vasoconstriction and recognized as central components of  $Ca^{2+}$  sensitization, whereas depolarization-induced vasoconstriction only involves Rho-mediated  $Ca^{2+}$  sensitization (for review, see <sup>6</sup>). Therefore, upon observing more marked small renal resistance artery vasorelaxations in Methoxamine precontractions than in KCl precontractions, we argue that ANP may exert some of its effect via PKC-dependent mechanisms.

Second (ii), the more marked relaxations in Methoxamine precontractions could be explained by the anticontractile effect of ANP relying upon hyperpolarization, possibly as ANP enhances  $K^+$  channel conductance, which is suppressed in KCl-induced contractions. This hypothesis goes in line with the above hypothesis of ANP-induced relaxations being PKC-dependent, since PKC-mediated blockade of  $K^+$  channels (specifically: 4-AP sensitive delayed rectifier  $K^+$  channels) has been proposed as a mechanism contributing to rat preglomerular artery vasoconstriction <sup>370</sup>. If this were the case, and if  $K_{v7}$  were among these channels enhanced by ANP, one would expect a differential effect of ANP on contractions induced by blockade of all  $K^+$  channels compared to blockade of all except  $K_{v7}$ . However, as we examined this in our experiments we found no such difference (Figure 38 – Figure 40), implicating that ANP does not cause relaxations via enhancement of  $K^+$  currents through  $K_{v7}$ . Nonetheless, other  $K^+$  channels may well be involved in ANP-induced relaxations, which may be an interesting question for further research.

Finally (iii), in case the PKC-dependent  $Ca^{2+}$  sensitizing mechanisms activated by Methoxamine were to enable specifically  $K_{v7.4}$  or  $K_{v7.5}$ , but not  $K_{v7.1}$  to counteract ANP-induced relaxations (as indicated by the results of Stott et al. <sup>77</sup> for the main renal artery), one would expect to find a differential effect of ANP in Methoxamine-precontractions after preincubation with  $K_{v7.1}$  specific blocker HMR1556 as compared to preincubation with pan- $K_{v7}$  blocker XE991. Oppositely, our results fail to provide evidence for such circumstances (Figure 41 – Figure 44). We therefore argue that  $K_{v7}$  do not participate in cGMP-mediated anticontractile mechanisms initiated by ANP, independently of whether agonist-induced mechanisms of  $Ca^{2+}$  sensitization involving PKC or depolarization-induced mechanisms of  $Ca^{2+}$ -induced  $Ca^{2+}$  sensitization involving Rho/ROCK are active and contributing to tonic contraction. The discrepancy between our findings and Stott et al. <sup>77</sup> may be explained by differences in  $Ca^{2+}$  sensitizing mechanisms in differently sized vessels <sup>351</sup>. However, as too little is known about the mechanisms by which ANP exerts its anticontractile effect downstream of cGMP, more research is required to elucidate this matter.

In conclusion, we show that the contribution of  $K_{v7}$  to renal resistance artery reactivity in response to vasoconstrictive  $\alpha$ 1-adrenoceptor agonists is independent of the anticontractile effect of the cGMP-coupled vasodilator ANP. ANP may exert its effect in these vessels through modification of  $Ca^{2+}$  sensitization, which likewise does not appear to depend upon  $K_{v7}$  channels. Notably, with the anticontractile effect of the  $K_{v7.1}$  activator R-L3 and of the  $K_{v7.2-5}$  activator Retigabine being unaffected by the presence of ANP, these two substances may be interesting candidates for future pharmacological studies, as they could represent a way to increase renal perfusion independently and additively to the endogenous vasodilator ANP.

#### 4.5 Contribution of $K_v7$ to the anticontractile effect of Urocortin in agonist-induced renal vasoconstriction

Urocortin 1 is an endogenous peptide belonging to the corticotropin-releasing factor (CRF) family that may act in a paracrine or autocrine fashion by binding to the CRF-R2 receptor<sup>87, 371</sup> expressed in VSMCs<sup>372</sup>, which via coupling to different G-proteins may activate various intracellular signaling pathways<sup>373</sup> including activation of adenylyl cyclase (AC) and accumulation of cAMP<sup>88, 322, 374</sup> (for reviews, see<sup>44, 323</sup>). In vivo application of Urocortin in rats dose-dependently reduces mean arterial blood pressure<sup>322, 375-377</sup>. In humans, Urocortin has been found to produce vasodilation in both arteries<sup>372, 378, 379</sup> and veins<sup>380</sup>. Besides vasodilation, recent studies have revealed various biological effects in the cardiovascular system like positive inotropy and lusitropy, cardioprotection against ischemia-reperfusion injury, suppression of the renin-angiotensin system or secretion of ANP, which is why Urocortins and CRF-R2 may be potential therapeutic effectors and targets in coronary heart disease, heart failure or hypertension<sup>323, 381</sup>. No link has been made between the effect of Urocortin and vascular  $K_v7$ , but cAMP signaling has been recently appreciated as regulatory to  $K_v7$  in various vessels<sup>97, 196, 228, 259, 262, 280</sup> including renal arteries<sup>96, 107</sup>. Therefore, we as part of this thesis thoroughly examined Urocortin for a functional interaction with  $K_v7$  in renal resistance arteries.

Overall, the mechanisms of Urocortin-induced relaxations are very complex to understand, which is why a brief outline of its actions and interdependences in context with  $K_v7$  shall be presented prior to the discussion of our results. The Urocortin-induced anticontractile effect may vary between different species, genders, age groups and vascular regions and may differentially involve AC or PKA activation as well as various signaling proteins like PKC, exchange factor directly activated by cAMP (EPAC), A-kinase anchoring proteins (AKAPs) and several more<sup>323</sup>. Further complicating the matter, Urocortin exerts its vasodilative effect not only directly through VSMCs, but also indirectly through endothelial cells. The endothelium-dependent dilations appear to be mediated by NO activating  $Ca^{2+}$ -dependent or  $Ba^{2+}$ -sensitive  $K^+$  channels in a cGMP-dependent manner, as was shown in rat coronary arteries<sup>382</sup> and human internal mammary arteries<sup>379</sup>. For this reason, endothelium removal (in our case achieved chemically with nitric oxide synthase inhibitor L-NNA) is essential to ensure validity of results in myography experiments. It may furthermore be noted that Urocortin-induced endothelium-dependent NO-mediated relaxations are a phenomenon observed in female, but not in male rats<sup>383</sup>. Mediators of the endothelium-independent anticontractile effect of Urocortin that have been identified in rat renal arteries include cAMP, cyclic adenosine diphosphate ribose (cADPR),  $BK_{Ca}$  and RyR in female rats, though not in male rats<sup>383, 384</sup>. In other vessels, the structures and mechanisms employed in Urocortin-induced relaxations include  $K^+$  channels like  $BK_{Ca}$ <sup>88, 379, 385</sup> or  $K_{ir}$ <sup>386</sup> and most notably, the decreasing of  $Ca^{2+}$  sensitivity in a cAMP/PKA-dependent manner<sup>44, 49, 50, 387</sup>. More specifically, it has been shown that in tail arteries, Urocortin causes relaxations (i) with higher potency in KCl- than in agonist-induced precontraction purely through  $Ca^{2+}$  desensitization and not by decreasing  $Ca^{2+}$  itself<sup>387</sup>, (ii) by cAMP-dependently increasing MLCP activity<sup>50</sup> and (iii) without affecting agonist-induced  $Ca^{2+}$  sensitization, possibly due to  $\alpha$ -adrenoceptor mediated inhibition of cAMP generation<sup>44</sup>. Clearly, the situation appears to be different in the renal vasculature, since in our findings, the potency of Urocortin was higher in relaxing agonist-induced than KCl-induced precontractions (Figure 49 – Figure 51). This is in line with the majority of reports made for other vascular beds<sup>88, 385, 386, 388, 389</sup>, in all of which a connection between Urocortin-induced relaxations and cAMP and/or PKA has been demonstrated. However, we were unaware of specific data confirming Urocortin-induced cAMP elevation and PKA activation in renal resistance arteries, which represents a limitation to the interpretation of our findings.

Substantial evidence exists for cAMP involvement in the regulation of vascular  $K_v7$ . Chadha et al.<sup>96</sup> first observed that cAMP elevation induced by  $\beta$ -adrenoceptor agonist isoproterenol (i) enhanced a robust  $K_v$  current sensitive to pan- $K_v7$  blocker linopirdine in renal artery VSMCs, (ii) induced relaxation of methoxamine-precontracted renal arteries that were attenuated by linopirdine (but not by  $K_{ATP}$

blocker glibenclamide or  $K_v1-4$  blocker 4-AP), (iii) caused a smaller degree of renal artery vasorelaxation in KCNQ4 knockdown vessels compared to control vessels and (iv) did not produce relaxations at all in renal arteries from SHR, in which  $K_v7.4$  abundance was reduced, altogether providing consistent evidence for  $K_v7.4$  involvement in  $\beta$ -adrenoceptor responses and an impairment of this mechanism in hypertension. Later, the mechanisms of isoproterenol vasodilations in renal arteries were further defined as being (i) sensitive to PKA inhibition<sup>107</sup> and (ii) capable of increasing  $K_v7.4$  colocalization with A-kinase anchoring protein (AKAP)<sup>107</sup> in a manner dependent on G-protein  $\beta\gamma$  subunits ( $G\beta\gamma$ )<sup>262</sup>.

Interestingly, cAMP-activated pathways appear to differ between vascular beds, since in mesenteric arteries, cAMP-induced vasodilations (i) were sensitive not to inhibition of PKA, but of exchange protein directly activated by cAMP (EPAC)<sup>107</sup> and (ii) were unaffected by inhibition of  $G\beta\gamma$  when isoproterenol was used, but were markedly attenuated when CGRP was used to cause cAMP elevation<sup>262</sup>. In other vascular beds, various studies have identified vasodilators acting through  $G_s$ -protein coupled elevation of intracellular cAMP or direct AC activators to cause vasorelaxations that are dependent on  $K_v7$ <sup>97, 196, 227, 228, 232, 259, 262</sup>. Some of them have further specified the pore-forming subunits to be involved, either favoring  $K_v7.4$ <sup>196, 262</sup> or  $K_v7.5$ <sup>97, 232</sup>, but thus far failed to produce evidence for an involvement of  $K_v7.1$ <sup>107, 196</sup>.

Putting this complex lot of data in context with our findings, it appears that the situation in renal resistance arteries may be different from what has been described for the main renal artery insofar as Urocortin relaxations do not appear to involve  $K_v7$ . In our experiments, the anticontractile effect of Urocortin, represented by a decrease in Methoxamine sensitivity, does not affect and vice versa is itself unimpaired by the anticontractile effect of  $K_v7.2-5$  activation (Figure 46) as well as by the contractile effect of pan- $K_v7$  blockade (Figure 45). Provided that Urocortin acts via cAMP, this is in opposition to the findings in the main renal artery, where cAMP-induced relaxations were attenuated by pan- $K_v7$  blocker linopirdine<sup>96, 107</sup>. This points towards the existence of alternative signaling pathways downstream of cAMP, for which a myriad of possibilities exist, considering that cAMP may activate both PKA and PKG, and furthermore that PKA alone, which is supposed to be involved in the renal artery<sup>107</sup>, offers a wide range of possible targets or mechanisms involved in agonist-induced contraction including the lowering of intracellular  $Ca^{2+}$  and  $Ca^{2+}$  desensitization as well as activation of either type of  $K^+$  channel expressed in VSM ( $K_v$ ,  $BK_{Ca}$ ,  $K_{ATP}$  or  $K_{ir}$ )<sup>55</sup> (see: Chapter 1.5.2.2).

Instead of  $K_v7$  channel involvement in Urocortin-induced decreases of Methoxamine sensitivity, we provide evidence for Urocortin inducing  $Ca^{2+}$  desensitization. We demonstrated that the anticontractile effect of Urocortin is more marked in  $\alpha_1$ -adrenoceptor agonist- than in depolarization-induced precontraction (Figure 49 – Figure 51). Parallel to our argumentation for ANP (see: Chapter 4.4) the conclusions to be drawn from this are that Urocortin (i) induces relaxations at least in part via mechanisms independent of  $K^+$  channels, since it is effective in relaxing KCl-induced contractions; (ii) may exert some of its effect by counteracting PKC-dependent mechanisms of  $Ca^{2+}$  sensitization, since these are involved in Methoxamine- but not in KCl-induced contractions; and (iii) may require hyperpolarization by enhancing  $K^+$  current as another mechanism of relaxation, since it is less effective against KCl-induced contractions, in which all  $K^+$  channels are blocked. Furthermore, we show that in case  $K^+$  channels are responsible for the impairment of Urocortin relaxations in KCl contractions, it is unlikely that these channels are  $K_v7$ , as we found no difference in Urocortin relaxing renal vessels contracted with individual blockade of all vascular  $K^+$  channels compared to when blocking all except  $K_v7$  (Figure 52 – Figure 54). Again, it must be noted that this does specifically not rule out, but rather suggests an involvement of  $K^+$  channels other than  $K_v7$  to contribute in the anticontractile effect of Urocortin. For example, blockade of  $BK_{Ca}$  has been shown to impair Urocortin-induced<sup>88, 379, 385</sup> or cAMP-induced<sup>106, 107</sup> relaxations in non-renal vessels. Eventually, we demonstrate that a role for  $K_v7.4$  or  $K_v7.5$ , but specifically not  $K_v7.1$  channels in cAMP-induced relaxations, as has been proposed for the main renal artery<sup>107, 196</sup>, is unlikely to be functionally relevant in renal resistance arteries, since Urocortin-induced relaxations are similarly marked in  $\alpha_1$ -adrenoceptor agonist-induced precontraction

during blockade of either all  $K_v7$  or only  $K_v7.1$  (Figure 55 – Figure 58). At this point, it must be noted as a minor limitation that the comparison of the effect of Urocortin in the presence or absence of  $K_v7$  blockade with XE991 (Figure 57) was done on vessels taken from different rats and that therefore ruling out the possible existence of a small effect would require confirmation of this data using a different protocol. Since no effect of  $K_v7$  blockade was found in Urocortin relaxations of either agonist-induced (PKC- and ROCK-involving) or depolarization-induced (only ROCK-involving) contractions, we further conclude that the activity or inactivity of PKC-dependent mechanisms of  $Ca^{2+}$  sensitization does not appear relevant to the lacking effect of  $K_v7$ . Nonetheless, it must be noted that with the innumerable effects Urocortin may have on VSMC signaling pathways, it is possible that some minor interaction with  $K_v7$  takes place further downstream which is just too small and not functionally relevant enough to be detected in myography experiments.

To conclude with, in our experiments examining Urocortin as a known cAMP elevating vasodilator, we demonstrate that this agent exerts its anticontractile effect in renal interlobar arteries without functionally employing  $K_v7$  channels.  $Ca^{2+}$  desensitization may play a predominant role in Urocortin relaxations, specifically in counteracting PKC-dependent  $Ca^{2+}$  sensitization. Our results underline the complexity of intracellular and ion channel-dependent signaling mechanisms contributing to vascular reactivity even within closely related arterial beds. Remarkably, our observation that  $K_v7.1$  activator R-L3 and  $K_v7.2-5$  activator Retigabine may exert their anticontractile effect on renal resistance arteries in a manner unaffected by the presence of Urocortin gives further impetus to the potential of these two drugs representing potential therapeutics able to increase renal perfusion independently and additively to the endogenous vasodilator Urocortin.

## 5 SUMMARY

Vascular smooth muscle cell membranes contain potassium channels that by influencing membrane potential importantly contribute to the regulation of arterial tone. The KCNQ gene encodes for 5 different K<sup>+</sup> channel subunits forming homo- or heteromeric K<sub>v</sub>7, which are a family of voltage-dependent K<sup>+</sup> channels functionally expressed in various vascular beds that can be activated by depolarizing stimuli and inactivated upon prolonged depolarization.

In this thesis, the contribution of K<sub>v</sub>7 to the regulation of renal arterial tone was studied, testing the hypotheses that (i) the K<sub>v</sub>7.1-specific activator R-L3 is effective in causing reversible vasodilation of the entire renal arterial vasculature and that (ii) the endogenous vasodilators atrial natriuretic peptide (ANP) and Urocortin either attenuate or enhance the therapeutically intended vasodilatory effect of subunit-specific activation of K<sub>v</sub>7.1 or K<sub>v</sub>7.2-5 in small renal resistance arteries. Isometric wire myography was used to examine the contractile responses of short preglomerular resistance artery segments. A novel isolated perfused rat kidneys setup was introduced to investigate renal perfusion pressure as an indicator of arterial contractility on a whole-organ level.

It was shown that pharmacological activation of K<sub>v</sub>7.2-5 channels produces a strong anticontractile effect in agonist-induced vasoconstriction of renal resistance arteries. Specific activation of K<sub>v</sub>7.1 was found to decrease sensitivity to vasoconstrictive agonists in small interlobar artery segments as well as to decrease perfusion pressure of intact perfused rat kidneys in a manner reversible by specific pharmacological K<sub>v</sub>7.1 channel blockade. Unspecific blockade of all K<sub>v</sub>7 was demonstrated to enhance arterial contractility in both isolated vessels and isolated perfused kidneys, whereas specific blockade of K<sub>v</sub>7.1 was without either of these effects, indicating a contribution of homo- or heteromeric K<sub>v</sub>7.4 and K<sub>v</sub>7.5, but not homomeric K<sub>v</sub>7.1, to resting tone of the renal arterial vasculature.

Experiments on isolated interlobar vessels displayed dose-dependent vasorelaxations in response to the cGMP-coupled hormone ANP and the cAMP-dependent autocrine and paracrine vasodilator Urocortin in both agonist-induced and depolarization-induced vasoconstriction. Further experiments revealed that K<sub>v</sub>7 contribute to vascular reactivity independently of the anticontractile effect induced by both ANP and Urocortin.

The results presented here confirm our first hypothesis that R-L3 is effective in causing reversible vasorelaxation of the entire renal arterial bed, undermining a previously unappreciated role for K<sub>v</sub>7.1 in regulating renal arterial contractility and renal perfusion pressure. By demonstrating the possibility to influence vascular tone through specific K<sub>v</sub>7 modulators independently of both cGMP- and cAMP-dependent endogenous vasodilators and thus negating our second hypothesis, this thesis stresses the importance of K<sub>v</sub>7 as potential therapeutic targets in the treatment of renovascular pathology.

## 6 BIBLIOGRAPHY

1. Nelson, MT, Quayle, JM: Physiological roles and properties of potassium channels in arterial smooth muscle. *Am J Physiol*, 268: C799-822, 1995.
2. Christensen, KL, Mulvany, MJ: Location of resistance arteries. *J Vasc Res*, 38: 1-12, 2001.
3. Guyton, AC, Coleman, TG, Granger, HJ: Circulation: overall regulation. *Annu Rev Physiol*, 34: 13-46, 1972.
4. Guyton, AC, Cowley, AW, Jr., Young, DB, Coleman, TG, Hall, JE, DeClue, JW: Integration and control of circulatory function. *Int Rev Physiol*, 9: 341-385, 1976.
5. Hall, JE: Control of blood pressure by the renin-angiotensin-aldosterone system. *Clin Cardiol*, 14: IV6-21; discussion IV51-25, 1991.
6. Carlstrom, M, Wilcox, CS, Arendshorst, WJ: Renal autoregulation in health and disease. *Physiol Rev*, 95: 405-511, 2015.
7. Gilmore, JP, Cornish, KG, Rogers, SD, Joyner, WL: Direct evidence for myogenic autoregulation of the renal microcirculation in the hamster. *Circ Res*, 47: 226-230, 1980.
8. Navar, LG: Renal autoregulation: perspectives from whole kidney and single nephron studies. *Am J Physiol*, 234: F357-370, 1978.
9. Moore, LC, Casellas, D: Tubuloglomerular feedback dependence of autoregulation in rat juxtamedullary afferent arterioles. *Kidney Int*, 37: 1402-1408, 1990.
10. Pugsley, MK, Tabrizchi, R: The vascular system. An overview of structure and function. *J Pharmacol Toxicol Methods*, 44: 333-340, 2000.
11. Khaddaj Mallat, R, Mathew John, C, Kendrick, DJ, Braun, AP: The vascular endothelium: A regulator of arterial tone and interface for the immune system. *Crit Rev Clin Lab Sci*, 54: 458-470, 2017.
12. Majesky, MW: Vascular Smooth Muscle Cells. *Arterioscler Thromb Vasc Biol*, 36: e82-86, 2016.
13. Sweeney, HL, Houdusse, A: Structural and functional insights into the Myosin motor mechanism. *Annu Rev Biophys*, 39: 539-557, 2010.
14. Brozovich, FV, Nicholson, CJ, Degen, CV, Gao, YZ, Aggarwal, M, Morgan, KG: Mechanisms of Vascular Smooth Muscle Contraction and the Basis for Pharmacologic Treatment of Smooth Muscle Disorders. *Pharmacol Rev*, 68: 476-532, 2016.
15. Kordowska, J, Huang, R, Wang, CL: Phosphorylation of caldesmon during smooth muscle contraction and cell migration or proliferation. *J Biomed Sci*, 13: 159-172, 2006.
16. Somlyo, AP, Somlyo, AV: Ca<sup>2+</sup> sensitivity of smooth muscle and nonmuscle myosin II: modulated by G proteins, kinases, and myosin phosphatase. *Physiol Rev*, 83: 1325-1358, 2003.
17. Somlyo, AV, Somlyo, AP: Electromechanical and pharmacomechanical coupling in vascular smooth muscle. *J Pharmacol Exp Ther*, 159: 129-145, 1968.
18. Schubert, R, Mulvany, MJ: The myogenic response: established facts and attractive hypotheses. *Clin Sci (Lond)*, 96: 313-326, 1999.
19. Somlyo, AP, Somlyo, AV: Signal transduction and regulation in smooth muscle. *Nature*, 372: 231-236, 1994.
20. Khalil, R, Lodge, N, Saida, K, van Breemen, C: Mechanism of calcium activation in vascular smooth muscle. *J Hypertens Suppl*, 5: S5-15, 1987.

21. Adelstein, RS, Sellers, JR: Effects of calcium on vascular smooth muscle contraction. *Am J Cardiol*, 59: 4b-10b, 1987.
22. Amberg, GC, Navedo, MF: Calcium dynamics in vascular smooth muscle. *Microcirculation*, 20: 281-289, 2013.
23. Berridge, MJ: Inositol trisphosphate and calcium signalling. *Nature*, 361: 315-325, 1993.
24. Wirth, A, Benyo, Z, Lukasova, M, Leutgeb, B, Wettschureck, N, Gorbey, S, Orsy, P, Horvath, B, Maser-Gluth, C, Greiner, E, Lemmer, B, Schutz, G, Gutkind, JS, Offermanns, S: G12-G13-LARG-mediated signaling in vascular smooth muscle is required for salt-induced hypertension. *Nat Med*, 14: 64-68, 2008.
25. Webb, RC: Smooth muscle contraction and relaxation. *Adv Physiol Educ*, 27: 201-206, 2003.
26. Cole, WC, Clement-Chomienne, O, Aiello, EA: Regulation of 4-aminopyridine-sensitive, delayed rectifier K<sup>+</sup> channels in vascular smooth muscle by phosphorylation. *Biochem Cell Biol*, 74: 439-447, 1996.
27. Brueggemann, LI, Haick, JM, Cribbs, LL, Byron, KL: Differential activation of vascular smooth muscle Kv7.4, Kv7.5, and Kv7.4/7.5 channels by ML213 and ICA-069673. *Mol Pharmacol*, 86: 330-341, 2014.
28. Minami, K, Fukuzawa, K, Nakaya, Y: Protein kinase C inhibits the Ca<sup>2+</sup>-activated K<sup>+</sup> channel of cultured porcine coronary artery smooth muscle cells. *Biochem Biophys Res Commun*, 190: 263-269, 1993.
29. Leo, MD, Bulley, S, Bannister, JP, Kuruvilla, KP, Narayanan, D, Jaggar, JH: Angiotensin II stimulates internalization and degradation of arterial myocyte plasma membrane BK channels to induce vasoconstriction. *Am J Physiol Cell Physiol*, 309: C392-402, 2015.
30. Schubert, R, Noack, T, Serebryakov, VN: Protein kinase C reduces the K<sub>Ca</sub> current of rat tail artery smooth muscle cells. *Am J Physiol*, 276: C648-658, 1999.
31. Taguchi, K, Kaneko, K, Kubo, T: Protein kinase C modulates Ca<sup>2+</sup>-activated K<sup>+</sup> channels in cultured rat mesenteric artery smooth muscle cells. *Biol Pharm Bull*, 23: 1450-1454, 2000.
32. Crozatier, B: Central role of PKCs in vascular smooth muscle cell ion channel regulation. *J Mol Cell Cardiol*, 41: 952-955, 2006.
33. Ledoux, J, Werner, ME, Brayden, JE, Nelson, MT: Calcium-activated potassium channels and the regulation of vascular tone. *Physiology*, 21: 69-78, 2006.
34. Park, WS, Han, J, Kim, N, Youm, JB, Joo, H, Kim, HK, Ko, JH, Earm, YE: Endothelin-1 inhibits inward rectifier K<sup>+</sup> channels in rabbit coronary arterial smooth muscle cells through protein kinase C. *J Cardiovasc Pharmacol*, 46: 681-689, 2005.
35. Park, WS, Kim, N, Youm, JB, Warda, M, Ko, JH, Kim, SJ, Earm, YE, Han, J: Angiotensin II inhibits inward rectifier K<sup>+</sup> channels in rabbit coronary arterial smooth muscle cells through protein kinase Cα. *Biochem Biophys Res Commun*, 341: 728-735, 2006.
36. Chrissobolis, S, Sobey, CG: Inhibitory effects of protein kinase C on inwardly rectifying K<sup>+</sup>- and ATP-sensitive K<sup>+</sup> channel-mediated responses of the basilar artery. *Stroke*, 33: 1692-1697, 2002.
37. Bonev, AD, Nelson, MT: Vasoconstrictors inhibit ATP-sensitive K<sup>+</sup> channels in arterial smooth muscle through protein kinase C. *J Gen Physiol*, 108: 315-323, 1996.
38. Cole, WC, Malcolm, T, Walsh, MP, Light, PE: Inhibition by protein kinase C of the K(NDP) subtype of vascular smooth muscle ATP-sensitive potassium channel. *Circ Res*, 87: 112-117, 2000.

39. Hayabuchi, Y, Davies, NW, Standen, NB: Angiotensin II inhibits rat arterial KATP channels by inhibiting steady-state protein kinase A activity and activating protein kinase Ce. *J Physiol*, 530: 193-205, 2001.
40. Quinn, KV, Cui, Y, Gibling, JP, Clapp, LH, Tinker, A: Do anionic phospholipids serve as cofactors or second messengers for the regulation of activity of cloned ATP-sensitive K<sup>+</sup> channels? *Circ Res*, 93: 646-655, 2003.
41. Sampson, LJ, Davies, LM, Barrett-Jolley, R, Standen, NB, Dart, C: Angiotensin II-activated protein kinase C targets caveolae to inhibit aortic ATP-sensitive potassium channels. *Cardiovasc Res*, 76: 61-70, 2007.
42. Vanhoutte, PM, Verbeuren, TJ, Webb, RC: Local modulation of adrenergic neuroeffector interaction in the blood vessel wall. *Physiol Rev*, 61: 151-247, 1981.
43. Schubert, R, Lidington, D, Bolz, S: The emerging role of Ca<sup>2+</sup> sensitivity regulation in promoting myogenic vasoconstriction. *Cardiovasc Res*, 77: 8-18, 2008.
44. Pfitzer, G, Lubomirov, LT, Reimann, K, Gagov, H, Schubert, R: Regulation of the crossbridge cycle in vascular smooth muscle by cAMP signalling. *J Muscle Res Cell Motil*, 27: 445-454, 2006.
45. Ringvold, HC, Khalil, RA: Protein Kinase C as Regulator of Vascular Smooth Muscle Function and Potential Target in Vascular Disorders. *Adv Pharmacol*, 78: 203-301, 2017.
46. Puetz, S, Lubomirov, LT, Pfitzer, G: Regulation of smooth muscle contraction by small GTPases. *Physiology*, 24: 342-356, 2009.
47. Wooldridge, AA, MacDonald, JA, Erdodi, F, Ma, C, Borman, MA, Hartshorne, DJ, Haystead, TA: Smooth muscle phosphatase is regulated in vivo by exclusion of phosphorylation of threonine 696 of MYPT1 by phosphorylation of Serine 695 in response to cyclic nucleotides. *J Biol Chem*, 279: 34496-34504, 2004.
48. Nakamura, K, Koga, Y, Sakai, H, Homma, K, Ikebe, M: cGMP-dependent relaxation of smooth muscle is coupled with the change in the phosphorylation of myosin phosphatase. *Circ Res*, 101: 712-722, 2007.
49. Lubomirov, LT, Reimann, K, Metzler, D, Hasse, V, Stehle, R, Ito, M, Hartshorne, DJ, Gagov, H, Pfitzer, G, Schubert, R: Urocortin-induced decrease in Ca<sup>2+</sup> sensitivity of contraction in mouse tail arteries is attributable to cAMP-dependent dephosphorylation of MYPT1 and activation of myosin light chain phosphatase. *Circ Res*, 98: 1159-1167, 2006.
50. Lubomirov, LT, Schubert, R, Gagov, HS, Duridanova, DB, Pfitzer, G: Urocortin decreases phosphorylation of MYPT1 and increases the myosin phosphatase activity via elevation of the intracellular level of cAMP. *Biofizika*, 51: 773-780, 2006.
51. Carvajal, JA, Germain, AM, Huidobro-Toro, JP, Weiner, CP: Molecular mechanism of cGMP-mediated smooth muscle relaxation. *J Cell Physiol*, 184: 409-420, 2000.
52. Moncada, S, Palmer, RM, Higgs, EA: Nitric oxide: physiology, pathophysiology, and pharmacology. *Pharmacol Rev*, 43: 109-142, 1991.
53. Morita, T, Perrella, MA, Lee, ME, Kourembanas, S: Smooth muscle cell-derived carbon monoxide is a regulator of vascular cGMP. *Proc Natl Acad Sci U S A*, 92: 1475-1479, 1995.
54. Maack, T: Receptors of atrial natriuretic factor. *Annu Rev Physiol*, 54: 11-27, 1992.
55. Morgado, M, Cairrao, E, Santos-Silva, AJ, Verde, I: Cyclic nucleotide-dependent relaxation pathways in vascular smooth muscle. *Cell Mol Life Sci*, 69: 247-266, 2012.

56. Tang, KM, Wang, GR, Lu, P, Karas, RH, Aronovitz, M, Heximer, SP, Kaltenbronn, KM, Blumer, KJ, Siderovski, DP, Zhu, Y, Mendelsohn, ME: Regulator of G-protein signaling-2 mediates vascular smooth muscle relaxation and blood pressure. *Nat Med*, 9: 1506-1512, 2003.
57. Osei-Owusu, P, Sun, X, Drenan, RM, Steinberg, TH, Blumer, KJ: Regulation of RGS2 and second messenger signaling in vascular smooth muscle cells by cGMP-dependent protein kinase. *J Biol Chem*, 282: 31656-31665, 2007.
58. Kobayashi, S, Kanaide, H, Nakamura, M: Cytosolic-free calcium transients in cultured vascular smooth muscle cells: microfluorometric measurements. *Science*, 229: 553-556, 1985.
59. Rashatwar, SS, Cornwell, TL, Lincoln, TM: Effects of 8-bromo-cGMP on Ca<sup>2+</sup> levels in vascular smooth muscle cells: possible regulation of Ca<sup>2+</sup>-ATPase by cGMP-dependent protein kinase. *Proc Natl Acad Sci U S A*, 84: 5685-5689, 1987.
60. Cornwell, TL, Pryzwansky, KB, Wyatt, TA, Lincoln, TM: Regulation of sarcoplasmic reticulum protein phosphorylation by localized cyclic GMP-dependent protein kinase in vascular smooth muscle cells. *Mol Pharmacol*, 40: 923-931, 1991.
61. Lincoln, TM, Cornwell, TL: Towards an understanding of the mechanism of action of cyclic AMP and cyclic GMP in smooth muscle relaxation. *Blood vessels*, 28: 129-137, 1991.
62. Mundina-Weilenmann, C, Vittone, L, Rinaldi, G, Said, M, de Cingolani, GC, Mattiazzi, A: Endoplasmic reticulum contribution to the relaxant effect of cGMP- and cAMP-elevating agents in feline aorta. *Am J Physiol Heart Circ Physiol*, 278: H1856-1865, 2000.
63. Furukawa, K, Ohshima, N, Tawada-Iwata, Y, Shigekawa, M: Cyclic GMP stimulates Na<sup>+</sup>/Ca<sup>2+</sup> exchange in vascular smooth muscle cells in primary culture. *J Biol Chem*, 266: 12337-12341, 1991.
64. Furukawa, K, Tawada, Y, Shigekawa, M: Regulation of the plasma membrane Ca<sup>2+</sup> pump by cyclic nucleotides in cultured vascular smooth muscle cells. *J Biol Chem*, 263: 8058-8065, 1988.
65. Komalavilas, P, Lincoln, TM: Phosphorylation of the inositol 1,4,5-trisphosphate receptor. Cyclic GMP-dependent protein kinase mediates cAMP and cGMP dependent phosphorylation in the intact rat aorta. *J Biol Chem*, 271: 21933-21938, 1996.
66. Komalavilas, P, Lincoln, TM: Phosphorylation of the inositol 1,4,5-trisphosphate receptor by cyclic GMP-dependent protein kinase. *J Biol Chem*, 269: 8701-8707, 1994.
67. Schlossmann, J, Ammendola, A, Ashman, K, Zong, X, Huber, A, Neubauer, G, Wang, GX, Allescher, HD, Korth, M, Wilm, M, Hofmann, F, Ruth, P: Regulation of intracellular calcium by a signalling complex of IRAG, IP3 receptor and cGMP kinase Ibeta. *Nature*, 404: 197-201, 2000.
68. Schlossmann, J, Desch, M: IRAG and novel PKG targeting in the cardiovascular system. *Am J Physiol Heart Circ Physiol*, 301: H672-682, 2011.
69. Keef, KD, Hume, JR, Zhong, J: Regulation of cardiac and smooth muscle Ca<sup>2+</sup> channels (Ca<sub>v</sub>1.2a,b) by protein kinases. *Am J Physiol Cell Physiol*, 281: C1743-1756, 2001.
70. Somlyo, AV: Cyclic GMP regulation of myosin phosphatase: a new piece for the puzzle? *Circ Res*, 101: 645-647, 2007.
71. Sauzeau, V, Le Jeune, H, Cario-Toumaniantz, C, Smolenski, A, Lohmann, SM, Bertoglio, J, Chardin, P, Pacaud, P, Loirand, G: Cyclic GMP-dependent protein kinase signaling pathway inhibits RhoA-induced Ca<sup>2+</sup> sensitization of contraction in vascular smooth muscle. *J Biol Chem*, 275: 21722-21729, 2000.

72. Bonnevier, J, Arner, A: Actions downstream of cyclic GMP/protein kinase G can reverse protein kinase C-mediated phosphorylation of CPI-17 and Ca(2)(+) sensitization in smooth muscle. *J Biol Chem*, 279: 28998-29003, 2004.
73. Bolz, SS, Vogel, L, Sollinger, D, Derwand, R, de Wit, C, Loirand, G, Pohl, U: Nitric oxide-induced decrease in calcium sensitivity of resistance arteries is attributable to activation of the myosin light chain phosphatase and antagonized by the RhoA/Rho kinase pathway. *Circulation*, 107: 3081-3087, 2003.
74. Tanaka, Y, Tang, G, Takizawa, K, Otsuka, K, Eghbali, M, Song, M, Nishimaru, K, Shigenobu, K, Koike, K, Stefani, E: Kv channels contribute to nitric oxide- and atrial natriuretic peptide-induced relaxation of a rat conduit artery. *J Pharmacol Exp Ther*, 317: 341-354, 2006.
75. Sathishkumar, K, Ross, RG, Bawankule, DU, Sardar, KK, Prakash, VR, Mishra, SK: Segmental heterogeneity in the mechanism of sodium nitroprusside-induced relaxation in ovine pulmonary artery. *J Cardiovasc Pharmacol*, 45: 491-498, 2005.
76. Cairrao, E, Santos-Silva, AJ, Verde, I: PKG is involved in testosterone-induced vasorelaxation of human umbilical artery. *Eur J Pharmacol*, 640: 94-101, 2010.
77. Stott, JB, Barrese, V, Jepps, TA, Leighton, EV, Greenwood, IA: Contribution of Kv7 channels to natriuretic peptide mediated vasodilation in normal and hypertensive rats. *Hypertension*, 65: 676-682, 2014.
78. Kubo, M, Nakaya, Y, Matsuoka, S, Saito, K, Kuroda, Y: Atrial natriuretic factor and isosorbide dinitrate modulate the gating of ATP-sensitive K<sup>+</sup> channels in cultured vascular smooth muscle cells. *Circ Res*, 74: 471-476, 1994.
79. Miyoshi, H, Nakaya, Y, Moritoki, H: Nonendothelial-derived nitric oxide activates the ATP-sensitive K<sup>+</sup> channel of vascular smooth muscle cells. *FEBS Lett*, 345: 47-49, 1994.
80. Murphy, ME, Brayden, JE: Nitric oxide hyperpolarizes rabbit mesenteric arteries via ATP-sensitive potassium channels. *J Physiol*, 486 ( Pt 1): 47-58, 1995.
81. Wu, CC, Chen, SJ, Garland, CJ: NO and KATP channels underlie endotoxin-induced smooth muscle hyperpolarization in rat mesenteric resistance arteries. *Br J Pharmacol*, 142: 479-484, 2004.
82. Barman, SA, Zhu, S, White, RE: PKC activates BKCa channels in rat pulmonary arterial smooth muscle via cGMP-dependent protein kinase. *Am J Physiol Lung Cell Mol Physiol*, 286: L1275-1281, 2004.
83. Prieto, D, Rivera, L, Benedito, S, Recio, P, Villalba, N, Hernandez, M, Garcia-Sacristan, A: Ca<sup>2+</sup>-activated K<sup>+</sup> (KCa) channels are involved in the relaxations elicited by sildenafil in penile resistance arteries. *Eur J Pharmacol*, 531: 232-237, 2006.
84. Otsuka, K, Tanaka, H, Horinouchi, T, Koike, K, Shigenobu, K, Tanaka, Y: Functional contribution of voltage-dependent and Ca<sup>2+</sup> activated K<sup>+</sup> (BK(Ca)) channels to the relaxation of guinea-pig aorta in response to natriuretic peptides. *J Smooth Muscle Res*, 38: 117-129, 2002.
85. Stockand, JD, Sansom, SC: Role of large Ca(2+)-activated K<sup>+</sup> channels in regulation of mesangial contraction by nitroprusside and ANP. *Am J Physiol*, 270: C1773-1779, 1996.
86. Althoff, TF, Offermanns, S: G-protein-mediated signaling in vascular smooth muscle cells - implications for vascular disease. *J Mol Med*, 93: 973-981, 2015.
87. Lovenberg, TW, Chalmers, DT, Liu, C, De Souza, EB: CRF2 alpha and CRF2 beta receptor mRNAs are differentially distributed between the rat central nervous system and peripheral tissues. *Endocrinology*, 136: 4139-4142, 1995.

88. Schilling, L, Kanzler, C, Schmiedek, P, Ehrenreich, H: Characterization of the relaxant action of urocortin, a new peptide related to corticotropin-releasing factor in the rat isolated basilar artery. *Br J Pharmacol*, 125: 1164-1171, 1998.
89. Barman, SA, Zhu, S, Han, G, White, RE: cAMP activates BKCa channels in pulmonary arterial smooth muscle via cGMP-dependent protein kinase. *Am J Physiol Lung Cell Mol Physiol*, 284: L1004-1011, 2003.
90. Conti, MA, Adelstein, RS: The relationship between calmodulin binding and phosphorylation of smooth muscle myosin kinase by the catalytic subunit of 3':5' cAMP-dependent protein kinase. *J Biol Chem*, 256: 3178-3181, 1981.
91. Rembold, CM: Regulation of contraction and relaxation in arterial smooth muscle. *Hypertension*, 20: 129-137, 1992.
92. Azam, MA, Yoshioka, K, Ohkura, S, Takuwa, N, Sugimoto, N, Sato, K, Takuwa, Y: Ca<sup>2+</sup>-independent, inhibitory effects of cyclic adenosine 5'-monophosphate on Ca<sup>2+</sup> regulation of phosphoinositide 3-kinase C2alpha, Rho, and myosin phosphatase in vascular smooth muscle. *J Pharmacol Exp Ther*, 320: 907-916, 2007.
93. Zieba, BJ, Artamonov, MV, Jin, L, Momotani, K, Ho, R, Franke, AS, Neppl, RL, Stevenson, AS, Khromov, AS, Chrzanoska-Wodnicka, M, Somlyo, AV: The cAMP-responsive Rap1 guanine nucleotide exchange factor, Epac, induces smooth muscle relaxation by down-regulation of RhoA activity. *J Biol Chem*, 286: 16681-16692, 2011.
94. Aiello, EA, Malcolm, AT, Walsh, MP, Cole, WC: Beta-adrenoceptor activation and PKA regulate delayed rectifier K<sup>+</sup> channels of vascular smooth muscle cells. *Am J Physiol*, 275: H448-459, 1998.
95. Dong, H, Waldron, GJ, Cole, WC, Triggle, CR: Roles of calcium-activated and voltage-gated delayed rectifier potassium channels in endothelium-dependent vasorelaxation of the rabbit middle cerebral artery. *Br J Pharmacol*, 123: 821-832, 1998.
96. Chadha, PS, Zunke, F, Zhu, HL, Davis, AJ, Jepps, TA, Olesen, SP, Cole, WC, Moffatt, JD, Greenwood, IA: Reduced KCNQ4-encoded voltage-dependent potassium channel activity underlies impaired beta-adrenoceptor-mediated relaxation of renal arteries in hypertension. *Hypertension*, 59: 877-884, 2012.
97. Mani, BK, Robakowski, C, Brueggemann, LI, Cribbs, LL, Tripathi, A, Majetschak, M, Byron, KL: Kv7.5 Potassium Channel Subunits Are the Primary Targets for PKA-Dependent Enhancement of Vascular Smooth Muscle Kv7 Currents. *Mol Pharmacol*, 89: 323-334, 2016.
98. Aiello, EA, Walsh, MP, Cole, WC: Phosphorylation by protein kinase A enhances delayed rectifier K<sup>+</sup> current in rabbit vascular smooth muscle cells. *Am J Physiol*, 268: H926-934, 1995.
99. Berwick, ZC, Payne, GA, Lynch, B, Dick, GM, Sturek, M, Tune, JD: Contribution of adenosine A(2A) and A(2B) receptors to ischemic coronary dilation: role of K(V) and K(ATP) channels. *Microcirculation*, 17: 600-607, 2010.
100. Dick, GM, Bratz, IN, Borbouse, L, Payne, GA, Dincer, UD, Knudson, JD, Rogers, PA, Tune, JD: Voltage-dependent K<sup>+</sup> channels regulate the duration of reactive hyperemia in the canine coronary circulation. *Am J Physiol Heart Circ Physiol*, 294: H2371-2381, 2008.
101. Heaps, CL, Bowles, DK: Gender-specific K(+) channel contribution to adenosine-induced relaxation in coronary arterioles. *J Appl Physiol*, 92: 550-558, 2002.
102. Heaps, CL, Tharp, DL, Bowles, DK: Hypercholesterolemia abolishes voltage-dependent K<sup>+</sup> channel contribution to adenosine-mediated relaxation in porcine coronary arterioles. *Am J Physiol Heart Circ Physiol*, 288: H568-576, 2005.

103. Li, H, Chai, Q, Gutterman, DD, Liu, Y: Elevated glucose impairs cAMP-mediated dilation by reducing Kv channel activity in rat small coronary smooth muscle cells. *Am J Physiol Heart Circ Physiol*, 285: H1213-1219, 2003.
104. Satake, N, Shibata, M, Shibata, S: The inhibitory effects of iberiotoxin and 4-aminopyridine on the relaxation induced by beta 1- and beta 2-adrenoceptor activation in rat aortic rings. *Br J Pharmacol*, 119: 505-510, 1996.
105. Zhang, Y, Pertens, E, Janssen, LJ: 8-isoprostaglandin E(2) activates Ca(2+)-dependent K(+) current via cyclic AMP signaling pathway in murine renal artery. *Eur J Pharmacol*, 520: 22-28, 2005.
106. Roberts, OL, Kamishima, T, Barrett-Jolley, R, Quayle, JM, Dart, C: Exchange protein activated by cAMP (Epac) induces vascular relaxation by activating Ca<sup>2+</sup>-sensitive K<sup>+</sup> channels in rat mesenteric artery. *J Physiol*, 591: 5107-5123, 2013.
107. Stott, JB, Barrese, V, Greenwood, IA: Kv7 Channel Activation Underpins EPAC-Dependent Relaxations of Rat Arteries. *Arterioscler Thromb Vasc Biol*, 36: 2404-2411, 2016.
108. Friis, UG, Jorgensen, F, Andreasen, D, Jensen, BL, Skott, O: Molecular and functional identification of cyclic AMP-sensitive BKCa potassium channels (ZERO variant) and L-type voltage-dependent calcium channels in single rat juxtaglomerular cells. *Circ Res*, 93: 213-220, 2003.
109. White, R, Bottrill, FE, Siau, D, Hiley, CR: Protein kinase A-dependent and -independent effects of isoproterenol in rat isolated mesenteric artery: interactions with levromakalim. *J Pharmacol Exp Ther*, 298: 917-924, 2001.
110. Orie, NN, Thomas, AM, Perrino, BA, Tinker, A, Clapp, LH: Ca<sup>2+</sup>/calcineurin regulation of cloned vascular K ATP channels: crosstalk with the protein kinase A pathway. *Br J Pharmacol*, 157: 554-564, 2009.
111. Wellman, GC, Quayle, JM, Standen, NB: ATP-sensitive K<sup>+</sup> channel activation by calcitonin gene-related peptide and protein kinase A in pig coronary arterial smooth muscle. *J Physiol*, 507 ( Pt 1): 117-129, 1998.
112. Kleppisch, T, Nelson, MT: Adenosine activates ATP-sensitive potassium channels in arterial myocytes via A<sub>2</sub> receptors and cAMP-dependent protein kinase. *Proc Natl Acad Sci U S A*, 92: 12441-12445, 1995.
113. Quayle, JM, Bonev, AD, Brayden, JE, Nelson, MT: Calcitonin gene-related peptide activated ATP-sensitive K<sup>+</sup> currents in rabbit arterial smooth muscle via protein kinase A. *J Physiol*, 475: 9-13, 1994.
114. Miyoshi, H, Nakaya, Y: Activation of ATP-sensitive K<sup>+</sup> channels by cyclic AMP-dependent protein kinase in cultured smooth muscle cells of porcine coronary artery. *Biochem Biophys Res Commun*, 193: 240-247, 1993.
115. Son, YK, Park, WS, Ko, JH, Han, J, Kim, N, Earm, YE: Protein kinase A-dependent activation of inward rectifier potassium channels by adenosine in rabbit coronary smooth muscle cells. *Biochem Biophys Res Commun*, 337: 1145-1152, 2005.
116. Park, WS, Han, J, Kim, N, Ko, JH, Kim, SJ, Earm, YE: Activation of inward rectifier K<sup>+</sup> channels by hypoxia in rabbit coronary arterial smooth muscle cells. *Am J Physiol Heart Circ Physiol*, 289: H2461-2467, 2005.
117. Hirst, GD, Edwards, FR: Sympathetic neuroeffector transmission in arteries and arterioles. *Physiol Rev*, 69: 546-604, 1989.
118. Loutzenhiser, R, Chilton, L, Trottier, G: Membrane potential measurements in renal afferent and efferent arterioles: actions of angiotensin II. *Am J Physiol*, 273: F307-314, 1997.

119. Buhle, CP, Nobiling, R, Mannek, E, Schneider, D, Hackenthal, E, Taugner, R: The afferent glomerular arteriole: immunocytochemical and electrophysiological investigations. *J Cardiovasc Pharmacol*, 6 Suppl 2: S383-393, 1984.
120. Nelson, MT, Patlak, JB, Worley, JF, Standen, NB: Calcium channels, potassium channels, and voltage dependence of arterial smooth muscle tone. *Am J Physiol*, 259: C3-18, 1990.
121. Sorensen, CM, Braunstein, TH, Holstein-Rathlou, NH, Salomonsson, M: Role of vascular potassium channels in the regulation of renal hemodynamics. *Am J Physiol Renal Physiol*, 302: F505-518, 2012.
122. Salomonsson, M, Brasen, JC, Sorensen, CM: Role of renal vascular potassium channels in physiology and pathophysiology. *Acta Physiol*, 221: 14-31, 2017.
123. Tykocki, NR, Boerman, EM, Jackson, WF: Smooth Muscle Ion Channels and Regulation of Vascular Tone in Resistance Arteries and Arterioles. *Compr Physiol*, 7: 485-581, 2017.
124. Nichols, CG, Lopatin, AN: Inward rectifier potassium channels. *Annu Rev Physiol*, 59: 171-191, 1997.
125. Quayle, JM, McCarron, JG, Brayden, JE, Nelson, MT: Inward rectifier K<sup>+</sup> currents in smooth muscle cells from rat resistance-sized cerebral arteries. *Am J Physiol*, 265: C1363-1370, 1993.
126. Knot, HJ, Zimmermann, PA, Nelson, MT: Extracellular K<sup>(+)</sup>-induced hyperpolarizations and dilatations of rat coronary and cerebral arteries involve inward rectifier K<sup>(+)</sup> channels. *J Physiol*, 492 ( Pt 2): 419-430, 1996.
127. Chilton, L, Loutzenhiser, K, Morales, E, Breaks, J, Kargacin, GJ, Loutzenhiser, R: Inward rectifier K<sup>+</sup> currents and Kir2. 1 expression in renal afferent and efferent arterioles. *J Am Soc Nephrol*, 19: 69-76, 2008.
128. Chilton, L, Smirnov, SV, Loutzenhiser, K, Wang, X, Loutzenhiser, R: Segment-specific differences in the inward rectifier K<sup>+</sup> current along the renal interlobular artery. *Cardiovasc Res*, 92: 169-177, 2011.
129. Chilton, L, Loutzenhiser, R: Functional evidence for an inward rectifier potassium current in rat renal afferent arterioles. *Circ Res*, 88: 152-158, 2001.
130. Troncoso Brindeiro, CM, Fallet, RW, Lane, PH, Carmines, PK: Potassium channel contributions to afferent arteriolar tone in normal and diabetic rat kidney. *Am J Physiol Renal Physiol*, 295: F171-178, 2008.
131. Kurtz, A, Hamann, M, Gotz, K: Role of potassium channels in the control of renin secretion from isolated perfused rat kidneys. *Pflugers Arch*, 440: 889-895, 2000.
132. Magnusson, L, Sorensen, CM, Braunstein, TH, Holstein-Rathlou, NH, Salomonsson, M: Mechanisms of K<sup>(+)</sup> induced renal vasodilation in normo- and hypertensive rats in vivo. *Acta Physiol*, 202: 703-712, 2011.
133. Noma, A: ATP-regulated K<sup>+</sup> channels in cardiac muscle. *Nature*, 305: 147-148, 1983.
134. Ashcroft, SJ, Ashcroft, FM: Properties and functions of ATP-sensitive K-channels. *Cell Signal*, 2: 197-214, 1990.
135. Li, L, Wu, J, Jiang, C: Differential expression of Kir6.1 and SUR2B mRNAs in the vasculature of various tissues in rats. *J Membr Biol*, 196: 61-69, 2003.
136. Bonev, AD, Nelson, MT: ATP-sensitive potassium channels in smooth muscle cells from guinea pig urinary bladder. *Am J Physiol*, 264: C1190-1200, 1993.

137. Jensen, BL, Gambaryan, S, Scholz, H, Kurtz, A: KATP channels are not essential for pressure-dependent control of renin secretion. *Pflugers Arch*, 435: 670-677, 1998.
138. Yamashita, T, Masuda, Y, Kawamura, N, Fujikura, N, Tanaka, S: Comparative study of vasodilator effects of the potassium channel openers NIP-121 and levcromakalim in dogs and rats. *Jpn J Pharmacol*, 68: 145-152, 1995.
139. Uchida, W, Masuda, N, Taguchi, T, Shibasaki, K, Shirai, Y, Asano, M, Matsumoto, Y, Tsuzuki, R, Fujikura, T, Takenaka, T: Pharmacologic profiles of YM934, a novel potassium channel opener. *J Cardiovasc Pharmacol*, 23: 180-187, 1994.
140. Kawata, T, Mimuro, T, Onuki, T, Tsuchiya, K, Nihei, H, Koike, T: The K(ATP) channel opener nicorandil: effect on renal hemodynamics in spontaneously hypertensive and Wistar Kyoto rats. *Kidney Int Suppl*, 67: S231-233, 1998.
141. Sorensen, CM, Giese, I, Braunstein, TH, Holstein-Rathlou, NH, Salomonsson, M: Closure of multiple types of K<sup>+</sup> channels is necessary to induce changes in renal vascular resistance in vivo in rats. *Pflugers Arch*, 462: 655-667, 2011.
142. Loutzenhiser, RD, Parker, MJ: Hypoxia inhibits myogenic reactivity of renal afferent arterioles by activating ATP-sensitive K<sup>+</sup> channels. *Circ Res*, 74: 861-869, 1994.
143. Reslerova, M, Loutzenhiser, R: Renal microvascular actions of calcitonin gene-related peptide. *Am J Physiol*, 274: F1078-1085, 1998.
144. Tang, L, Parker, M, Fei, Q, Loutzenhiser, R: Afferent arteriolar adenosine A<sub>2a</sub> receptors are coupled to KATP in in vitro perfused hydronephrotic rat kidney. *Am J Physiol Renal Physiol*, 277: F926-933, 1999.
145. Brayden, JE, Nelson, MT: Regulation of arterial tone by activation of calcium-dependent potassium channels. *Science*, 256: 532-535, 1992.
146. Nelson, MT, Cheng, H, Rubart, M, Santana, LF, Bonev, AD, Knot, HJ, Lederer, WJ: Relaxation of arterial smooth muscle by calcium sparks. *Science*, 270: 633-637, 1995.
147. Horrigan, FT, Cui, J, Aldrich, RW: Allosteric voltage gating of potassium channels I. Mslo ionic currents in the absence of Ca<sup>2+</sup>. *J Gen Physiol*, 114: 277-304, 1999.
148. Cox, DH, Cui, J, Aldrich, RW: Allosteric gating of a large conductance Ca-activated K<sup>+</sup> channel. *J Gen Physiol*, 110: 257-281, 1997.
149. Perez, GJ, Bonev, AD, Patlak, JB, Nelson, MT: Functional coupling of ryanodine receptors to KCa channels in smooth muscle cells from rat cerebral arteries. *J Gen Physiol*, 113: 229-238, 1999.
150. Harraz, OF, Abd El-Rahman, RR, Bigdely-Shamloo, K, Wilson, SM, Brett, SE, Romero, M, Gonzales, AL, Earley, S, Vigmond, EJ, Nygren, A, Menon, BK, Mufti, RE, Watson, T, Starreveld, Y, Furstenhaupt, T, Muellerleile, PR, Kurjiaka, DT, Kyle, BD, Braun, AP, Welsh, DG: Ca<sub>v</sub>(V)3.2 channels and the induction of negative feedback in cerebral arteries. *Circ Res*, 115: 650-661, 2014.
151. Harraz, OF, Brett, SE, Zechariah, A, Romero, M, Puglisi, JL, Wilson, SM, Welsh, DG: Genetic ablation of Ca<sub>v</sub>3.2 channels enhances the arterial myogenic response by modulating the RyR-BKCa axis. *Arterioscler Thromb Vasc Biol*, 35: 1843-1851, 2015.
152. Zhao, G, Neeb, ZP, Leo, MD, Pachuau, J, Adebisi, A, Ouyang, K, Chen, J, Jaggar, JH: Type 1 IP<sub>3</sub> receptors activate BKCa channels via local molecular coupling in arterial smooth muscle cells. *J Gen Physiol*, 136: 283-291, 2010.

153. Yang, Y, Li, PY, Cheng, J, Cai, F, Lei, M, Tan, XQ, Li, ML, Liu, ZF, Zeng, XR: IP3 decreases coronary artery tone via activating the BKCa channel of coronary artery smooth muscle cells in pigs. *Biochem Biophys Res Commun*, 439: 363-368, 2013.
154. Magnusson, L, Sorensen, CM, Braunstein, TH, Holstein-Rathlou, NH, Salomonsson, M: Renovascular BK(Ca) channels are not activated in vivo under resting conditions and during agonist stimulation. *Am J Physiol Regul Integr Comp Physiol*, 292: R345-353, 2007.
155. Gebremedhin, D, Kaldunski, M, Jacobs, ER, Harder, DR, Roman, RJ: Coexistence of two types of Ca(2+)-activated K<sup>+</sup> channels in rat renal arterioles. *Am J Physiol*, 270: F69-81, 1996.
156. Stockand, JD, Sansom, SC: Large Ca(2+)-activated K<sup>+</sup> channels responsive to angiotensin II in cultured human mesangial cells. *Am J Physiol*, 267: C1080-1086, 1994.
157. Galvez, A, Gimenez-Gallego, G, Reuben, JP, Roy-Contancin, L, Feigenbaum, P, Kaczorowski, GJ, Garcia, ML: Purification and characterization of a unique, potent, peptidyl probe for the high conductance calcium-activated potassium channel from venom of the scorpion *Buthus tamulus*. *J Biol Chem*, 265: 11083-11090, 1990.
158. Prior, HM, Yates, MS, Beech, DJ: Functions of large conductance Ca<sup>2+</sup>-activated (BKCa), delayed rectifier (KV) and background K<sup>+</sup> channels in the control of membrane potential in rabbit renal arcuate artery. *J Physiol Pharmacol*, 511: 159-169, 1998.
159. Fallet, RW, Bast, JP, Fujiwara, K, Ishii, N, Sansom, SC, Carmines, PK: Influence of Ca(2+)-activated K(+) channels on rat renal arteriolar responses to depolarizing agonists. *Am J Physiol Renal Physiol*, 280: F583-591, 2001.
160. Sheldon, JH, Norton, NW, Argentieri, TM: Inhibition of guinea pig detrusor contraction by NS-1619 is associated with activation of BKCa and inhibition of calcium currents. *J Pharmacol Exp Ther*, 283: 1193-1200, 1997.
161. Schubert, R, Nelson, MT: Protein kinases: tuners of the BKCa channel in smooth muscle. *Trends Pharmacol Sci*, 22: 505-512, 2001.
162. Gutman, GA, Chandy, KG, Grissmer, S, Lazdunski, M, McKinnon, D, Pardo, LA, Robertson, GA, Rudy, B, Sanguinetti, MC, Stuhmer, W, Wang, X: International Union of Pharmacology. LIII. Nomenclature and molecular relationships of voltage-gated potassium channels. *Pharmacol Rev*, 57: 473-508, 2005.
163. Gonzalez, C, Baez-Nieto, D, Valencia, I, Oyarzun, I, Rojas, P, Naranjo, D, Latorre, R: K(+) channels: function-structural overview. *Compr Physiol*, 2: 2087-2149, 2012.
164. Kukuljan, M, Labarca, P, Latorre, R: Molecular determinants of ion conduction and inactivation in K<sup>+</sup> channels. *Am J Physiol*, 268: C535-556, 1995.
165. Cox, RH: Molecular determinants of voltage-gated potassium currents in vascular smooth muscle. *Cell Biochem Biophys*, 42: 167-195, 2005.
166. Greenwood, IA, Ohya, S: New tricks for old dogs: KCNQ expression and role in smooth muscle. *Br J Pharmacol*, 156: 1196-1203, 2009.
167. Jackson, WF: KV channels and the regulation of vascular smooth muscle tone. *Microcirculation*, 25, 2018.
168. Hara, Y, Kitamura, K, Kuriyama, H: Actions of 4-aminopyridine on vascular smooth muscle tissues of the guinea-pig. *Br J Pharmacol*, 68: 99-106, 1980.
169. Uchida, Y, Nakamura, F, Tomaru, T, Sumino, S, Kato, A, Sugimoto, T: Phasic contractions of canine and human coronary arteries induced by potassium channel blockers. *Jpn Heart J*, 27: 727-740, 1986.

170. Leblanc, N, Wan, X, Leung, PM: Physiological role of Ca(2+)-activated and voltage-dependent K<sup>+</sup> currents in rabbit coronary myocytes. *Am J Physiol*, 266: C1523-1537, 1994.
171. Gelband, CH, Ishikawa, T, Post, JM, Keef, KD, Hume, JR: Intracellular divalent cations block smooth muscle K<sup>+</sup> channels. *Circ Res*, 73: 24-34, 1993.
172. Knot, HJ, Nelson, MT: Regulation of membrane potential and diameter by voltage-dependent K<sup>+</sup> channels in rabbit myogenic cerebral arteries. *Am J Physiol*, 269: H348-355, 1995.
173. Cox, RH, Fromme, S: Comparison of Voltage Gated K(+) Currents in Arterial Myocytes with Heterologously Expressed K v Subunits. *Cell Biochem Biophys*, 74: 499-511, 2016.
174. Cox, RH, Fromme, S: Functional Expression Profile of Voltage-Gated K(+) Channel Subunits in Rat Small Mesenteric Arteries. *Cell Biochem Biophys*, 74: 263-276, 2016.
175. Lagrutta, A, Wang, J, Fermini, B, Salata, JJ: Novel, potent inhibitors of human Kv1.5 K<sup>+</sup> channels and ultrarapidly activating delayed rectifier potassium current. *J Pharmacol Exp Ther*, 317: 1054-1063, 2006.
176. Tsvetkov, D, Tano, JY, Kassmann, M, Wang, N, Schubert, R, Gollasch, M: The Role of DPO-1 and XE991-Sensitive Potassium Channels in Perivascular Adipose Tissue-Mediated Regulation of Vascular Tone. *Front Physiol*, 7: 335, 2016.
177. Escoubas, P, Diochot, S, Celerier, ML, Nakajima, T, Lazdunski, M: Novel tarantula toxins for subtypes of voltage-dependent potassium channels in the Kv2 and Kv4 subfamilies. *Mol Pharmacol*, 62: 48-57, 2002.
178. Fergus, DJ, Martens, JR, England, SK: Kv channel subunits that contribute to voltage-gated K<sup>+</sup> current in renal vascular smooth muscle. *Pflugers Arch*, 445: 697-704, 2003.
179. Betts, LC, Kozlowski, RZ: Electrophysiological effects of endothelin-1 and their relationship to contraction in rat renal arterial smooth muscle. *Br J Pharmacol*, 130: 787-796, 2000.
180. Gordienko, DV, Clausen, C, Goligorsky, MS: Ionic currents and endothelin signaling in smooth muscle cells from rat renal resistance arteries. *Am J Physiol*, 266: F325-341, 1994.
181. Zou, AP, Fleming, JT, Falck, JR, Jacobs, ER, Gebremedhin, D, Harder, DR, Roman, RJ: 20-HETE is an endogenous inhibitor of the large-conductance Ca(2+)-activated K<sup>+</sup> channel in renal arterioles. *Am J Physiol*, 270: R228-237, 1996.
182. Mackie, AR, Byron, KL: Cardiovascular KCNQ (Kv7) potassium channels: physiological regulators and new targets for therapeutic intervention. *Mol Pharmacol*, 74: 1171-1179, 2008.
183. Barrese, V, Stott, JB, Greenwood, IA: KCNQ-Encoded Potassium Channels as Therapeutic Targets. *Annu Rev Pharmacol Toxicol*, 58: 625-648, 2018.
184. Cooper, EC: Made for "anchorin": Kv7.2/7.3 (KCNQ2/KCNQ3) channels and the modulation of neuronal excitability in vertebrate axons. *Semin Cell Dev Biol*, 22: 185-192, 2011.
185. Delmas, P, Brown, DA: Pathways modulating neural KCNQ/M (Kv7) potassium channels. *Nat Rev Neurosci*, 6: 850, 2005.
186. Hernandez, CC, Zaika, O, Tolstykh, GP, Shapiro, MS: Regulation of neural KCNQ channels: signalling pathways, structural motifs and functional implications. *J Physiol*, 586: 1811-1821, 2008.
187. Brown, DA, Hughes, SA, Marsh, SJ, Tinker, A: Regulation of M(Kv7.2/7.3) channels in neurons by PIP(2) and products of PIP(2) hydrolysis: significance for receptor-mediated inhibition. *J Physiol*, 582: 917-925, 2007.

188. Xu, J, Yu, W, Jan, YN, Jan, LY, Li, M: Assembly of voltage-gated potassium channels. Conserved hydrophilic motifs determine subfamily-specific interactions between the alpha-subunits. *J Biol Chem*, 270: 24761-24768, 1995.
189. Long, SB, Campbell, EB, Mackinnon, R: Crystal structure of a mammalian voltage-dependent Shaker family K<sup>+</sup> channel. *Science*, 309: 897-903, 2005.
190. Schwake, M, Athanasiadu, D, Beimgraben, C, Blanz, J, Beck, C, Jentsch, TJ, Saftig, P, Friedrich, T: Structural determinants of M-type KCNQ (Kv7) K<sup>+</sup> channel assembly. *J Neurosci*, 26: 3757-3766, 2006.
191. Howard, RJ, Clark, KA, Holton, JM, Minor, DL, Jr.: Structural insight into KCNQ (Kv7) channel assembly and channelopathy. *Neuron*, 53: 663-675, 2007.
192. Jentsch, TJ: Neuronal KCNQ potassium channels: physiology and role in disease. *Nat Rev Neurosci*, 1: 21-30, 2000.
193. Yeung, SY, Pucovsky, V, Moffatt, JD, Saldanha, L, Schwake, M, Ohya, S, Greenwood, IA: Molecular expression and pharmacological identification of a role for K(v)7 channels in murine vascular reactivity. *Br J Pharmacol*, 151: 758-770, 2007.
194. Oliveras, A, Roura-Ferrer, M, Sole, L, de la Cruz, A, Prieto, A, Etxebarria, A, Manils, J, Morales-Cano, D, Condom, E, Soler, C, Cogolludo, A, Valenzuela, C, Villarroel, A, Comes, N, Felipe, A: Functional assembly of Kv7.1/Kv7.5 channels with emerging properties on vascular muscle physiology. *Arterioscler Thromb Vasc Biol*, 34: 1522-1530, 2014.
195. Brueggemann, LI, Mackie, AR, Cribbs, LL, Freda, J, Tripathi, A, Majetschak, M, Byron, KL: Differential protein kinase C-dependent modulation of Kv7.4 and Kv7.5 subunits of vascular Kv7 channels. *J Biol Chem*, 289: 2099-2111, 2014.
196. Chadha, PS, Jepps, TA, Carr, G, Stott, JB, Zhu, HL, Cole, WC, Greenwood, IA: Contribution of kv7.4/kv7.5 heteromers to intrinsic and calcitonin gene-related peptide-induced cerebral reactivity. *Arterioscler Thromb Vasc Biol*, 34: 887-893, 2014.
197. Barhanin, J, Lesage, F, Guillemare, E, Fink, M, Lazdunski, M, Romey, G: K(V)LQT1 and Isk (minK) proteins associate to form the I(Ks) cardiac potassium current. *Nature*, 384: 78, 1996.
198. Sanguinetti, MC, Curran, ME, Zou, A, Shen, J, Spector, PS, Atkinson, DL, Keating, MT: Coassembly of K(V)LQT1 and minK (Isk) proteins to form cardiac I(Ks) potassium channel. *Nature*, 384: 80-83, 1996.
199. Jespersen, T, Grunnet, M, Olesen, SP: The KCNQ1 potassium channel: from gene to physiological function. *Physiology*, 20: 408-416, 2005.
200. Vetter, DE, Mann, JR, Wangemann, P, Liu, J, McLaughlin, KJ, Lesage, F, Marcus, DC, Lazdunski, M, Heinemann, SF, Barhanin, J: Inner ear defects induced by null mutation of the isk gene. *Neuron*, 17: 1251-1264, 1996.
201. Neyroud, N, Tesson, F, Denjoy, I, Leibovici, M, Donger, C, Barhanin, J, Faure, S, Gary, F, Coumel, P, Petit, C, Schwartz, K, Guicheney, P: A novel mutation in the potassium channel gene KVLQT1 causes the Jervell and Lange-Nielsen cardioauditory syndrome. *Nat Genet*, 15: 186-189, 1997.
202. Vallon, V, Grahammer, F, Volkl, H, Sandu, CD, Richter, K, Rexhepaj, R, Gerlach, U, Rong, Q, Pfeifer, K, Lang, F: KCNQ1-dependent transport in renal and gastrointestinal epithelia. *Proc Natl Acad Sci U S A*, 102: 17864-17869, 2005.
203. Dedek, K, Waldegger, S: Colocalization of KCNQ1/KCNE channel subunits in the mouse gastrointestinal tract. *Pflugers Arch*, 442: 896-902, 2001.

204. Kunzelmann, K, Bleich, M, Warth, R, Levy-Holzman, R, Garty, H, Schreiber, R: Expression and function of colonic epithelial KvLQT1 K<sup>+</sup> channels. *Clin Exp Pharmacol Physiol*, 28: 79-83, 2001.
205. Tinel, N, Diochot, S, Borsotto, M, Lazdunski, M, Barhanin, J: KCNE2 confers background current characteristics to the cardiac KCNQ1 potassium channel. *Embo j*, 19: 6326-6330, 2000.
206. Roepke, TK, King, EC, Reyna-Neyra, A, Paroder, M, Purtell, K, Koba, W, Fine, E, Lerner, DJ, Carrasco, N, Abbott, GW: Kcne2 deletion uncovers its crucial role in thyroid hormone biosynthesis. *Nat Med*, 15: 1186-1194, 2009.
207. Schroeder, BC, Waldegger, S, Fehr, S, Bleich, M, Warth, R, Greger, R, Jentsch, TJ: A constitutively open potassium channel formed by KCNQ1 and KCNE3. *Nature*, 403: 196-199, 2000.
208. Zhong, XZ, Harhun, MI, Olesen, SP, Ohya, S, Moffatt, JD, Cole, WC, Greenwood, IA: Participation of KCNQ (Kv7) potassium channels in myogenic control of cerebral arterial diameter. *J Physiol*, 588: 3277-3293, 2010.
209. Grunnet, M, Jespersen, T, Rasmussen, HB, Ljungstrom, T, Jorgensen, NK, Olesen, SP, Klaerke, DA: KCNE4 is an inhibitory subunit to the KCNQ1 channel. *J Physiol*, 542: 119-130, 2002.
210. Jepps, TA, Carr, G, Lundegaard, PR, Olesen, SP, Greenwood, IA: Fundamental role for the KCNE4 ancillary subunit in Kv7.4 regulation of arterial tone. *J Physiol*, 593: 5325-5340, 2015.
211. Abbott, GW, Jepps, TA: Kcne4 Deletion Sex-Dependently Alters Vascular Reactivity. *J Vasc Res*, 53: 138-148, 2016.
212. Angelo, K, Jespersen, T, Grunnet, M, Nielsen, MS, Klaerke, DA, Olesen, SP: KCNE5 induces time- and voltage-dependent modulation of the KCNQ1 current. *Biophys J*, 83: 1997-2006, 2002.
213. Salata, JJ, Jurkiewicz, NK, Wang, J, Evans, BE, Orme, HT, Sanguinetti, MC: A novel benzodiazepine that activates cardiac slow delayed rectifier K<sup>+</sup> currents. *Mol Pharmacol*, 54: 220-230, 1998.
214. Yu, H, Lin, Z, Mattmann, ME, Zou, B, Terrenoire, C, Zhang, H, Wu, M, McManus, OB, Kass, RS, Lindsley, CW, Hopkins, CR, Li, M: Dynamic subunit stoichiometry confers a progressive continuum of pharmacological sensitivity by KCNQ potassium channels. *Proc Natl Acad Sci U S A*, 110: 8732-8737, 2013.
215. Lerche, C, Seebohm, G, Wagner, CI, Scherer, CR, Dehmelt, L, Abitbol, I, Gerlach, U, Brendel, J, Attali, B, Busch, AE: Molecular impact of MinK on the enantiospecific block of I(Ks) by chromanols. *Br J Pharmacol*, 131: 1503-1506, 2000.
216. Gogelein, H, Bruggemann, A, Gerlach, U, Brendel, J, Busch, AE: Inhibition of IKs channels by HMR 1556. *Naunyn Schmiedebergs Arch Pharmacol*, 362: 480-488, 2000.
217. Wang, HS, Brown, BS, McKinnon, D, Cohen, IS: Molecular basis for differential sensitivity of KCNQ and I(Ks) channels to the cognitive enhancer XE991. *Mol Pharmacol*, 57: 1218-1223, 2000.
218. Brown, DA, Adams, PR: Muscarinic suppression of a novel voltage-sensitive K<sup>+</sup> current in a vertebrate neurone. *Nature*, 283: 673-676, 1980.
219. Wang, HS, Pan, Z, Shi, W, Brown, BS, Wymore, RS, Cohen, IS, Dixon, JE, McKinnon, D: KCNQ2 and KCNQ3 potassium channel subunits: molecular correlates of the M-channel. *Science*, 282: 1890-1893, 1998.
220. Brown, DA, Passmore, GM: Neural KCNQ (Kv7) channels. *Br J Pharmacol*, 156: 1185-1195, 2009.
221. Kubisch, C, Schroeder, BC, Friedrich, T, Lutjohann, B, El-Amraoui, A, Marlin, S, Petit, C, Jentsch, TJ: KCNQ4, a novel potassium channel expressed in sensory outer hair cells, is mutated in dominant deafness. *Cell*, 96: 437-446, 1999.

222. Kharkovets, T, Hardelin, JP, Safieddine, S, Schweizer, M, El-Amraoui, A, Petit, C, Jentsch, TJ: KCNQ4, a K<sup>+</sup> channel mutated in a form of dominant deafness, is expressed in the inner ear and the central auditory pathway. *Proc Natl Acad Sci U S A*, 97: 4333-4338, 2000.
223. Ohya, S, Sergeant, GP, Greenwood, IA, Horowitz, B: Molecular variants of KCNQ channels expressed in murine portal vein myocytes: a role in delayed rectifier current. *Circ Res*, 92: 1016-1023, 2003.
224. Yeung, SY, Greenwood, IA: Electrophysiological and functional effects of the KCNQ channel blocker XE991 on murine portal vein smooth muscle cells. *Br J Pharmacol*, 146: 585-595, 2005.
225. Mackie, AR, Brueggemann, LI, Henderson, KK, Shiels, AJ, Cribbs, LL, Scrogin, KE, Byron, KL: Vascular KCNQ potassium channels as novel targets for the control of mesenteric artery constriction by vasopressin, based on studies in single cells, pressurized arteries, and in vivo measurements of mesenteric vascular resistance. *J Pharm Exp Ther*, 325: 475-483, 2008.
226. Joshi, S, Balan, P, Gurney, AM: Pulmonary vasoconstrictor action of KCNQ potassium channel blockers. *Respir Res*, 7: 31, 2006.
227. Lee, S, Yang, Y, Tanner, MA, Li, M, Hill, MA: Heterogeneity in Kv7 channel function in the cerebral and coronary circulation. *Microcirculation*, 22: 109-121, 2015.
228. Khanamiri, S, Soltysinska, E, Jepps, TA, Bentzen, BH, Chadha, PS, Schmitt, N, Greenwood, IA, Olesen, SP: Contribution of Kv7 channels to basal coronary flow and active response to ischemia. *Hypertension*, 62: 1090-1097, 2013.
229. Zavaritskaya, O, Zhuravleva, N, Schleifenbaum, J, Gloe, T, Devermann, L, Kluge, R, Mladenov, M, Frey, M, Gagov, H, Fesus, G, Gollasch, M, Schubert, R: Role of KCNQ channels in skeletal muscle arteries and periadventitial vascular dysfunction. *Hypertension*, 61: 151-159, 2013.
230. Brueggemann, LI, Moran, CJ, Barakat, JA, Yeh, JZ, Cribbs, LL, Byron, KL: Vasopressin stimulates action potential firing by protein kinase C-dependent inhibition of KCNQ5 in A7r5 rat aortic smooth muscle cells. *Am J Physiol Heart Circ Physiol*, 292: H1352-1363, 2007.
231. Sedivy, V, Joshi, S, Ghaly, Y, Mizera, R, Zaloudikova, M, Brennan, S, Novotna, J, Herget, J, Gurney, AM: Role of Kv7 channels in responses of the pulmonary circulation to hypoxia. *Am J Physiol Lung Cell Mol Physiol*, 308: L48-L57, 2015.
232. Morales-Cano, D, Moreno, L, Barreira, B, Pandolfi, R, Chamorro, V, Jimenez, R, Villamor, E, Duarte, J, Perez-Vizcaino, F, Cogolludo, A: Kv7 channels critically determine coronary artery reactivity: left-right differences and down-regulation by hyperglycaemia. *Cardiovasc Res*, 106: 98-108, 2015.
233. Hedegaard, ER, Johnsen, J, Povlsen, JA, Jespersen, NR, Shanmuganathan, JA, Laursen, MR, Kristiansen, SB, Simonsen, U, Botker, HE: Inhibition of KV7 Channels Protects the Rat Heart against Myocardial Ischemia and Reperfusion Injury. *J Pharmacol Exp Ther*, 357: 94-102, 2016.
234. Shvetsova, AA, Gaynullina, DK, Tarasova, OS, Schubert, R: Negative feedback regulation of vasocontraction by potassium channels in 10- to 15-day-old rats: Dominating role of Kv 7 channels. *Acta Physiol*: e13176, 2018.
235. Zimmer, J, Takahashi, T, Hofmann, AD, Puri, P: Downregulation of KCNQ5 expression in the rat pulmonary vasculature of nitrofen-induced congenital diaphragmatic hernia. *J Pediatr Surg*, 52: 702-705, 2017.
236. de Jong, IEM, Jepps, TA: Impaired Kv7 channel function in cerebral arteries of a tauopathy mouse model (rTg4510). *Physiol Rep*, 6: e13920, 2018.

237. Jepps, TA, Olesen, SP, Greenwood, IA, Dalsgaard, T: Molecular and functional characterization of Kv 7 channels in penile arteries and corpus cavernosum of healthy and metabolic syndrome rats. *Br J Pharmacol*, 173: 1478-1490, 2016.
238. Yeung, SY, Schwake, M, Pucovsky, V, Greenwood, IA: Bimodal effects of the Kv7 channel activator retigabine on vascular K<sup>+</sup> currents. *Br J Pharmacol*, 155: 62-72, 2008.
239. Ng, FL, Davis, AJ, Jepps, TA, Harhun, MI, Yeung, SY, Wan, A, Reddy, M, Melville, D, Nardi, A, Khong, TK, Greenwood, IA: Expression and function of the K<sup>+</sup> channel KCNQ genes in human arteries. *Br J Pharmacol*, 162: 42-53, 2011.
240. Mills, TA, Greenwood, SL, Devlin, G, Shweikh, Y, Robinson, M, Cowley, E, Hayward, CE, Cottrell, EC, Tropea, T, Brereton, MF, Dalby-Brown, W, Wareing, M: Activation of KV7 channels stimulates vasodilatation of human placental chorionic plate arteries. *Placenta*, 36: 638-644, 2015.
241. Wei, X, Zhang, Y, Yin, B, Wen, J, Cheng, J, Fu, X: The expression and function of KCNQ potassium channels in human chorionic plate arteries from women with normal pregnancies and pre-eclampsia. *PLoS One*, 13: e0192122, 2018.
242. Brueggemann, LI, Mackie, AR, Martin, JL, Cribbs, LL, Byron, KL: Diclofenac distinguishes among homomeric and heteromeric potassium channels composed of KCNQ4 and KCNQ5 subunits. *Mol Pharmacol*, 79: 10-23, 2011.
243. Jepps, TA, Bentzen, BH, Stott, JB, Povstyan, OV, Sivaloganathan, K, Dalby-Brown, W, Greenwood, IA: Vasorelaxant effects of novel Kv 7.4 channel enhancers ML213 and NS15370. *Br J Pharmacol*, 171: 4413-4424, 2014.
244. Ogiwara, K, Ohya, S, Suzuki, Y, Yamamura, H, Imaizumi, Y: Up-Regulation of the Voltage-Gated KV2.1 K(+) Channel in the Renal Arterial Myocytes of Dahl Salt-Sensitive Hypertensive Rats. *Biol Pharm Bull*, 40: 1468-1474, 2017.
245. Schleifenbaum, J, Kassmann, M, Szijarto, IA, Hercule, HC, Tano, JY, Weinert, S, Heidenreich, M, Pathan, AR, Anistan, YM, Alenina, N, Rusch, NJ, Bader, M, Jentsch, TJ, Gollasch, M: Stretch-activation of angiotensin II type 1a receptors contributes to the myogenic response of mouse mesenteric and renal arteries. *Circ Res*, 115: 263-272, 2014.
246. Salomonsson, M, Brasen, JC, Braunstein, TH, Hagelqvist, P, Holstein-Rathlou, NH, Sorensen, CM: K(V)7.4 channels participate in the control of rodent renal vascular resting tone. *Acta Physiol*, 214: 402-414, 2015.
247. Barrese, V, Stott, JB, Figueiredo, HB, Aubdool, AA, Hobbs, AJ, Jepps, TA, McNeish, AJ, Greenwood, IA: Angiotensin II Promotes KV7.4 Channels Degradation Through Reduced Interaction With HSP90 (Heat Shock Protein 90). *Hypertension*, 71: 1091-1100, 2018.
248. Gollasch, M, Welsh, DG, Schubert, R: Perivascular adipose tissue and the dynamic regulation of Kv 7 and Kir channels: Implications for resistant hypertension. *Microcirculation*, 25, 2018.
249. Schroder, RL, Jespersen, T, Christophersen, P, Strobaek, D, Jensen, BS, Olesen, SP: KCNQ4 channel activation by BMS-204352 and retigabine. *Neuropharmacology*, 40: 888-898, 2001.
250. Sogaard, R, Ljungstrom, T, Pedersen, KA, Olesen, SP, Jensen, BS: KCNQ4 channels expressed in mammalian cells: functional characteristics and pharmacology. *Am J Physiol Cell Physiol*, 280: C859-866, 2001.
251. Schroeder, BC, Hechenberger, M, Weinreich, F, Kubisch, C, Jentsch, TJ: KCNQ5, a novel potassium channel broadly expressed in brain, mediates M-type currents. *J Biol Chem*, 275: 24089-24095, 2000.

252. Yeung, SY, Lange, W, Schwake, M, Greenwood, IA: Expression profile and characterisation of a truncated KCNQ5 splice variant. *Biochem Biophys Res Com*, 371: 741-746, 2008.
253. Jensen, HS, Callo, K, Jespersen, T, Jensen, BS, Olesen, SP: The KCNQ5 potassium channel from mouse: a broadly expressed M-current like potassium channel modulated by zinc, pH, and volume changes. *Brain Res Mol Brain Res*, 139: 52-62, 2005.
254. Lerche, C, Scherer, CR, Seebohm, G, Derst, C, Wei, AD, Busch, AE, Steinmeyer, K: Molecular cloning and functional expression of KCNQ5, a potassium channel subunit that may contribute to neuronal M-current diversity. *J Biol Chem*, 275: 22395-22400, 2000.
255. Joshi, S, Sedivy, V, Hodyc, D, Herget, J, Gurney, AM: KCNQ Modulators Reveal a Key Role for KCNQ Potassium Channels in Regulating the Tone of Rat Pulmonary Artery Smooth Muscle. *J Pharmacol Exp Ther*, 329: 368-376, 2009.
256. Jepps, TA, Chadha, PS, Davis, AJ, Harhun, MI, Cockerill, GW, Olesen, SP, Hansen, RS, Greenwood, IA: Downregulation of Kv7.4 channel activity in primary and secondary hypertension. *Circulation*, 124: 602-611, 2011.
257. Mani, BK, O'Dowd, J, Kumar, L, Brueggemann, LI, Ross, M, Byron, KL: Vascular KCNQ (Kv7) potassium channels as common signaling intermediates and therapeutic targets in cerebral vasospasm. *J Cardiovasc Pharmacol*, 61: 51-62, 2013.
258. Mani, BK, Brueggemann, LI, Cribbs, LL, Byron, KL: Activation of vascular KCNQ (Kv7) potassium channels reverses spasmogen-induced constrictor responses in rat basilar artery. *Br J Pharmacol*, 164: 237-249, 2011.
259. Hedegaard, ER, Nielsen, BD, Kun, A, Hughes, AD, Kroigaard, C, Mogensen, S, Matchkov, VV, Frobert, O, Simonsen, U: KV 7 channels are involved in hypoxia-induced vasodilatation of porcine coronary arteries. *Br J Pharmacol*, 171: 69-82, 2014.
260. Chadha, PS, Zunke, F, Davis, AJ, Jepps, TA, Linders, JT, Schwake, M, Towart, R, Greenwood, IA: Pharmacological dissection of K(v)7.1 channels in systemic and pulmonary arteries. *Br J Pharmacol*, 166: 1377-1387, 2012.
261. Schleifenbaum, J, Köhn, C, Voblova, N, Dubrovskaya, G, Zavarirskaya, O, Gloe, T, Crean, CS, Luft, FC, Huang, Y, Schubert, R: Systemic peripheral artery relaxation by KCNQ channel openers and hydrogen sulfide. *J Hypertens*, 28: 1875-1882, 2010.
262. Stott, JB, Barrese, V, Suresh, M, Masoodi, S, Greenwood, IA: Investigating the Role of G Protein betagamma in Kv7-Dependent Relaxations of the Rat Vasculature. *Arterioscler Thromb Vasc Biol*, 38: 2091-2102, 2018.
263. Tsvetkov, D, Kassmann, M, Tano, JY, Chen, L, Schleifenbaum, J, Voelkl, J, Lang, F, Huang, Y, Gollasch, M: Do KV 7.1 channels contribute to control of arterial vascular tone? *Br J Pharmacol*, 174: 150-162, 2017.
264. Towart, R, Linders, JT, Hermans, AN, Rohrbacher, J, van der Linde, HJ, Ercken, M, Cik, M, Roevens, P, Teisman, A, Gallacher, DJ: Blockade of the I(Ks) potassium channel: an overlooked cardiovascular liability in drug safety screening? *J Pharmacol Toxicol Methods*, 60: 1-10, 2009.
265. Pangidis, K: *Wirkung des K+-Kanalblockers HMR 1556 auf die Nierenfunktion bei Ratten*. Med. Dissertation. Institut für Pharmakologie und Toxikologie, Eberhard-Karls-Universität zu Tübingen, 2003.
266. Bachmann, A, Quast, U, Russ, U: Chromanol 293B, a blocker of the slow delayed rectifier K+ current (IKs), inhibits the CFTR Cl- current. *Naunyn Schmiedebergs Arch Pharmacol*, 363: 590-596, 2001.

267. Karle, CA, Bauer, A, Weretka, S, Zitron, E, Abushi, A, Kreye, VA, Schoels, W: Vascular effects of class-III antiarrhythmic drugs: chromanol 293B, but not dofetilide blocks the smooth muscle delayed rectifier K<sup>+</sup> channel. *Basic Res Cardiol*, 97: 17-25, 2002.
268. Lo, YC, Yang, SR, Huang, MH, Liu, YC, Wu, SN: Characterization of chromanol 293B-induced block of the delayed-rectifier K<sup>+</sup> current in heart-derived H9c2 cells. *Life Sci*, 76: 2275-2286, 2005.
269. Lerche, C, Bruhova, I, Lerche, H, Steinmeyer, K, Wei, AD, Strutz-Seebohm, N, Lang, F, Busch, AE, Zhorov, BS, Seebohm, G: Chromanol 293B binding in KCNQ1 (Kv7.1) channels involves electrostatic interactions with a potassium ion in the selectivity filter. *Mol Pharmacol*, 71: 1503-1511, 2007.
270. Busch, AE, Busch, GL, Ford, E, Suessbrich, H, Lang, HJ, Greger, R, Kunzelmann, K, Attali, B, Stuhmer, W: The role of the Isk protein in the specific pharmacological properties of the IKs channel complex. *Br J Pharmacol*, 122: 187-189, 1997.
271. Bett, GC, Morales, MJ, Beahm, DL, Duffey, ME, Rasmusson, RL: Ancillary subunits and stimulation frequency determine the potency of chromanol 293B block of the KCNQ1 potassium channel. *J Physiol*, 576: 755-767, 2006.
272. Main, MJ, Cryan, JE, Dupere, JR, Cox, B, Clare, JJ, Burbidge, SA: Modulation of KCNQ2/3 potassium channels by the novel anticonvulsant retigabine. *Mol Pharmacol*, 58: 253-262, 2000.
273. Tatulian, L, Delmas, P, Abogadie, FC, Brown, DA: Activation of expressed KCNQ potassium currents and native neuronal M-type potassium currents by the anti-convulsant drug retigabine. *J Neurosci*, 21: 5535-5545, 2001.
274. Wang, L, Qiao, GH, Hu, HN, Gao, ZB, Nan, FJ: Discovery of Novel Retigabine Derivatives as Potent KCNQ4 and KCNQ5 Channel Agonists with Improved Specificity. *ACS Med Chem Lett*, 10: 27-33, 2018.
275. Wuttke, TV, Seebohm, G, Bail, S, Maljevic, S, Lerche, H: The new anticonvulsant retigabine favors voltage-dependent opening of the Kv7. 2 (KCNQ2) channel by binding to its activation gate. *Mol Pharmacol*, 67: 1009-1017, 2005.
276. Lange, W, Geißendörfer, J, Schenzer, A, Grötzinger, J, Seebohm, G, Friedrich, T, Schwake, M: Refinement of the binding site and mode of action of the anticonvulsant Retigabine on KCNQ K<sup>+</sup> channels. *Mol Pharmacol*, 75: 272-280, 2009.
277. Schenzer, A, Friedrich, T, Pusch, M, Saftig, P, Jentsch, TJ, Grötzinger, J, Schwake, M: Molecular determinants of KCNQ (Kv7) K<sup>+</sup> channel sensitivity to the anticonvulsant retigabine. *J Neurosci*, 25: 5051-5060, 2005.
278. Seebohm, G, Pusch, M, Chen, J, Sanguinetti, MC: Pharmacological activation of normal and arrhythmia-associated mutant KCNQ1 potassium channels. *Circ Res*, 93: 941-947, 2003.
279. Goodwill, AG, Fu, L, Noblet, JN, Casalini, ED, Sassoon, D, Berwick, ZC, Kassab, GS, Tune, JD, Dick, GM: KV7 channels contribute to paracrine, but not metabolic or ischemic, regulation of coronary vascular reactivity in swine. *Am J Physiol Heart Circ Physiol*, 310: H693-704, 2016.
280. Lindman, J, Khammy, MM, Lundegaard, PR, Aalkjaer, C, Jepps, TA: Microtubule Regulation of Kv7 Channels Orchestrates cAMP-Mediated Vasorelaxations in Rat Arterial Smooth Muscle. *Hypertension*, 71: 336-345, 2018.
281. Elmedyby, P, Calloe, K, Schmitt, N, Hansen, RS, Grunnet, M, Olesen, SP: Modulation of ERG channels by XE991. *Basic Clin Pharmacol Toxicol*, 100: 316-322, 2007.
282. Byron, KL, Brueggemann, LI: Kv7 potassium channels as signal transduction intermediates in the control of microvascular tone. *Microcirculation*, 25, 2018.

283. Wiener, R, Haitin, Y, Shamgar, L, Fernandez-Alonso, MC, Martos, A, Chomsky-Hecht, O, Rivas, G, Attali, B, Hirsch, JA: The KCNQ1 (Kv7.1) COOH terminus, a multitiered scaffold for subunit assembly and protein interaction. *J Biol Chem*, 283: 5815-5830, 2008.
284. Haitin, Y, Attali, B: The C-terminus of Kv7 channels: a multifunctional module. *J Physiol*, 586: 1803-1810, 2008.
285. Zaydman, MA, Cui, J: PIP2 regulation of KCNQ channels: biophysical and molecular mechanisms for lipid modulation of voltage-dependent gating. *Front Physiol*, 5: 195, 2014.
286. Zhang, H, Craciun, LC, Mirshahi, T, Rohacs, T, Lopes, CM, Jin, T, Logothetis, DE: PIP(2) activates KCNQ channels, and its hydrolysis underlies receptor-mediated inhibition of M currents. *Neuron*, 37: 963-975, 2003.
287. Li, Y, Gamper, N, Hilgemann, DW, Shapiro, MS: Regulation of Kv7 (KCNQ) K<sup>+</sup> channel open probability by phosphatidylinositol 4,5-bisphosphate. *J Neurosci*, 25: 9825-9835, 2005.
288. Taylor, KC, Sanders, CR: Regulation of KCNQ/Kv7 family voltage-gated K(+) channels by lipids. *Biochim Biophys Acta Biomembr*, 1859: 586-597, 2017.
289. Zaydman, MA, Silva, JR, Delaloye, K, Li, Y, Liang, H, Larsson, HP, Shi, J, Cui, J: Kv7.1 ion channels require a lipid to couple voltage sensing to pore opening. *Proc Natl Acad Sci U S A*, 110: 13180-13185, 2013.
290. Lousouarn, G, Park, KH, Bellocq, C, Baro, I, Charpentier, F, Escande, D: Phosphatidylinositol-4,5-bisphosphate, PIP2, controls KCNQ1/KCNE1 voltage-gated potassium channels: a functional homology between voltage-gated and inward rectifier K<sup>+</sup> channels. *Embo j*, 22: 5412-5421, 2003.
291. Povstyan, OV, Barrese, V, Stott, JB, Greenwood, IA: Synergistic interplay of Gbetagamma and phosphatidylinositol 4,5-bisphosphate dictates Kv7.4 channel activity. *Pflugers Arch*, 469: 213-223, 2017.
292. Matavel, A, Medei, E, Lopes, CM: PKA and PKC partially rescue long QT type 1 phenotype by restoring channel-PIP2 interactions. *Channels (Austin)*, 4: 3-11, 2010.
293. Mani, BK, Brueggemann, LI, Cribbs, LL, Byron, KL: Opposite regulation of KCNQ5 and TRPC6 channels contributes to vasopressin-stimulated calcium spiking responses in A7r5 vascular smooth muscle cells. *Cell Calcium*, 45: 400-411, 2009.
294. Marx, SO, Kurokawa, J, Reiken, S, Motoike, H, D'Armiento, J, Marks, AR, Kass, RS: Requirement of a macromolecular signaling complex for beta adrenergic receptor modulation of the KCNQ1-KCNE1 potassium channel. *Science*, 295: 496-499, 2002.
295. Potet, F, Scott, JD, Mohammad-Panah, R, Escande, D, Baro, I: AKAP proteins anchor cAMP-dependent protein kinase to KvLQT1/IsK channel complex. *Am J Physiol Heart Circ Physiol*, 280: H2038-2045, 2001.
296. Martelli, A, Testai, L, Breschi, MC, Lawson, K, McKay, NG, Miceli, F, Tagliatela, M, Calderone, V: Vasorelaxation by hydrogen sulphide involves activation of Kv7 potassium channels. *Pharmacol Res*, 70: 27-34, 2013.
297. Kansui, Y, Goto, K, Ohtsubo, T, Murakami, N, Ichishima, K, Matsumura, K, Kitazono, T: Facilitation of sympathetic neurotransmission by phosphatidylinositol-4,5-bisphosphate-dependent regulation of KCNQ channels in rat mesenteric arteries. *Hypertens Res*, 35: 909-916, 2012.
298. Bellocq, C, van Ginneken, AC, Bezzina, CR, Alders, M, Escande, D, Mannens, MM, Baró, I, Wilde, AA: Mutation in the KCNQ1 gene leading to the short QT-interval syndrome. *Circulation*, 109: 2394-2397, 2004.

299. Chen, YH, Xu, SJ, Bendahhou, S, Wang, XL, Wang, Y, Xu, WY, Jin, HW, Sun, H, Su, XY, Zhuang, QN, Yang, YQ, Li, YB, Liu, Y, Xu, HJ, Li, XF, Ma, N, Mou, CP, Chen, Z, Barhanin, J, Huang, W: KCNQ1 gain-of-function mutation in familial atrial fibrillation. *Science*, 299: 251-254, 2003.
300. Haick, JM, Byron, KL: Novel treatment strategies for smooth muscle disorders: Targeting Kv7 potassium channels. *Pharmacol Ther*, 165: 14-25, 2016.
301. Gollasch, M: Vasodilator signals from perivascular adipose tissue. *Br J Pharmacol*, 165: 633-642, 2012.
302. Carr, G, Barrese, V, Stott, JB, Povstyan, OV, Jepps, TA, Figueiredo, HB, Zheng, D, Jamshidi, Y, Greenwood, IA: MicroRNA-153 targeting of KCNQ4 contributes to vascular dysfunction in hypertension. *Cardiovasc Res*, 112: 581-589, 2016.
303. Tano, JY, Schleifenbaum, J, Gollasch, M: Perivascular adipose tissue, potassium channels, and vascular dysfunction. *Arterioscler Thromb Vasc Biol*, 34: 1827-1830, 2014.
304. Kimmelstiel, P, Wilson, C: Inflammatory Lesions in the Glomeruli in Pyelonephritis in Relation to Hypertension and Renal Insufficiency. *Am J Pathol*, 12: 99-106.103, 1936.
305. Moritz, AR, Oldt, MR: Arteriolar Sclerosis in Hypertensive and Non-Hypertensive Individuals. *Am J Pathol*, 13: 679-728.677, 1937.
306. Goldblatt, H, Lynch, J, Hanzal, RF, Summerville, WW: Studies on Experimental Hypertension: I. The Production of Persistent Elevation of Systolic Blood Pressure by Means of Renal Ischemia. *J Exp Med*, 59: 347-379, 1934.
307. Textor, SC, Wilcox, CS: Renal artery stenosis: a common, treatable cause of renal failure? *Annu Rev Med*, 52: 421-442, 2001.
308. Sakakibara, K, Feng, GG, Li, J, Akahori, T, Yasuda, Y, Nakamura, E, Hatakeyama, N, Fujiwara, Y, Kinoshita, H: Kynurenine causes vasodilation and hypotension induced by activation of KCNQ-encoded voltage-dependent K(+) channels. *J Pharmacol Sci*, 129: 31-37, 2015.
309. Morecroft, I, Murray, A, Nilsen, M, Gurney, AM, MacLean, MR: Treatment with the Kv7 potassium channel activator flupirtine is beneficial in two independent mouse models of pulmonary hypertension. *Br J Pharmacol*, 157: 1241-1249, 2009.
310. Mulvany, MJ, Halpern, W: Mechanical properties of vascular smooth muscle cells in situ. *Nature*, 260: 617-619, 1976.
311. Mulvany, MJ, Halpern, W: Contractile properties of small arterial resistance vessels in spontaneously hypertensive and normotensive rats. *Circ Res*, 41: 19-26, 1977.
312. Mulvany, M: Procedures for investigation of small vessels using small vessel myograph. *Aarhus, Denmark: Danish Myo Technology*, 2004.
313. Angus, JA, Wright, CE: Techniques to study the pharmacodynamics of isolated large and small blood vessels. *J Pharmacol Toxicol Methods*, 44: 395-407, 2000.
314. International Committee on Veterinary Gross Anatomical Nomenclature: *Nomina anatomica veterinaria. Sixth edition*. 2017. Online: [www.wava-amav.org/downloads/nav\\_6\\_2017.zip](http://www.wava-amav.org/downloads/nav_6_2017.zip), Stand: 09.11.2019.
315. Stott, JB, Barrese, V, Jepps, TA, Leighton, EV, Greenwood, IA: Contribution of Kv7 channels to natriuretic peptide mediated vasodilation in normal and hypertensive rats. *Hypertension*, 65: 676-682, 2015.
316. Ross, BD: The isolated perfused rat kidney. *Clin Sci Mol Med Suppl*, 55: 513-521, 1978.

317. Yoldas, A, Dayan, MO: Morphological characteristics of renal artery and kidney in rats. *Sci World J*, 2014: 468982, 2014.
318. Seebohm, G, Pusch, M, Chen, J, Sanguinetti, MC: Pharmacological activation of normal and arrhythmia-associated mutant KCNQ1 potassium channels. *Circ Res*, 93: 941-947, 2003.
319. Potter, LR, Abbey-Hosch, S, Dickey, DM: Natriuretic peptides, their receptors, and cyclic guanosine monophosphate-dependent signaling functions. *Endocr Rev*, 27: 47-72, 2005.
320. Gribble, FM, Reimann, F: Pharmacological modulation of K(ATP) channels. *Biochem Soc Trans*, 30: 333-339, 2002.
321. Schubert, R, Krien, U, Wulfsen, I, Schiemann, D, Lehmann, G, Ulfig, N, Veh, RW, Schwarz, JR, Gago, H: Nitric oxide donor sodium nitroprusside dilates rat small arteries by activation of inward rectifier potassium channels. *Hypertension*, 43: 891-896, 2004.
322. Vaughan, J, Donaldson, C, Bittencourt, J, Perrin, MH, Lewis, K, Sutton, S, Chan, R, Turnbull, AV, Lovejoy, D, Rivier, C, et al.: Urocortin, a mammalian neuropeptide related to fish urotensin I and to corticotropin-releasing factor. *Nature*, 378: 287-292, 1995.
323. Rademaker, MT, Richards, AM: Urocortins: Actions in health and heart failure. *Clin Chim Acta*, 474: 76-87, 2017.
324. Weiss, C, Passow, H, Rothstein, A: Autoregulation of flow in isolated rat kidney in the absence of red cells. *Am J Physiol*, 196: 1115-1118, 1959.
325. Vandongen, R, Peart, WS, Boyd, GW: Adrenergic stimulation of renin secretion in the isolated perfused rat kidney. *Circ Res*, 32: 290-296, 1973.
326. Bowman, RH: Gluconeogenesis in the isolated perfused rat kidney. *J Biol Chem*, 245: 1604-1612, 1970.
327. Scholz, H, Kaissling, B, Inagami, T, Kurtz, A: Differential response of renin secretion to vasoconstrictors in the isolated perfused rat kidney. *J Physiol*, 441: 453-468, 1991.
328. Scholz, H, Gotz, KH, Hamann, M, Kurtz, A: Differential effects of extracellular anions on renin secretion from isolated perfused rat kidneys. *Am J Physiol*, 267: F1076-1081, 1994.
329. Wang, J, Nation, RL, Evans, AM, Cox, S: Isolated rat kidney perfused with dextran and bovine serum albumin: a stable model for investigating renal drug handling. *J Pharmacol Toxicol Methods*, 49: 105-113, 2004.
330. Georgiev, T, Iliev, R, Mihailova, S, Hadzhibozheva, P, Ilieva, G, Kamburova, M, Tolekova, A: The isolated perfused kidney models-certain aspects. *Trakia J Sci*, 9: 82-87, 2011.
331. Chang, HH, Choong, B, Phillips, A, Loomes, KM: Isolated perfused rat kidney: a technical update. *Exp Anim*, 62: 19-23, 2013.
332. Lee, HB, Blaufox, MD: Blood volume in the rat. *J Nucl Med*, 26: 72-76, 1985.
333. Coleman, TG: Cardiac output by dye dilution in the conscious rat. *J Appl Physiol*, 37: 452-455, 1974.
334. Maack, T: Physiological evaluation of the isolated perfused rat kidney. *Am J Physiol*, 238: F71-78, 1980.
335. Hsu, CH, Slavicek, JM: The effect of renal perfusion pressure on renal vascular resistance in the spontaneously hypertensive rat. *Pflugers Arch*, 393: 340-343, 1982.
336. Flemming, B, Arenz, N, Seeliger, E, Wronski, T, Steer, K, Persson, PB: Time-dependent autoregulation of renal blood flow in conscious rats. *J Am Soc Nephrol*, 12: 2253-2262, 2001.

337. Loutzenhiser, R, Horton, C, Epstein, M: Flow-induced errors in estimating perfusion pressure of the isolated rat kidney. *Kidney Int*, 22: 693-696, 1982.
338. Just, A: Mechanisms of renal blood flow autoregulation: dynamics and contributions. *Am J Physiol Regul Integr Comp Physiol*, 292: R1-17, 2007.
339. Loutzenhiser, RD: In situ studies of renal arteriolar function using the in vitro-perfused hydronephrotic rat kidney. *Int Rev Exp Pathol*, 36: 145-160, 1996.
340. Cupples, WA, Loutzenhiser, RD: Dynamic autoregulation in the in vitro perfused hydronephrotic rat kidney. *Am J Physiol Renal Physiol*, 275: F126-130, 1998.
341. Arendshorst, WJ, Finn, WF, Gottschalk, CW: Autoregulation of blood flow in the rat kidney. *Am J Physiol*, 228: 127-133, 1975.
342. Bolton, TB: Mechanisms of action of transmitters and other substances on smooth muscle. *Physiol Rev*, 59: 606-718, 1979.
343. Fésüs, G, Dubrovskaya, G, Gorzelniak, K, Kluge, R, Huang, Y, Luft, FC, Gollasch, M: Adiponectin is a novel humoral vasodilator. *Cardiovasc Res*, 75: 719-727, 2007.
344. Trendelenburg, U, Maxwell, RA, Pluchino, S: Methoxamine as a tool to assess the importance of intraneuronal uptake of l-norepinephrine in the cat's nictitating membrane. *J Pharmacol Exp Ther*, 172: 91-99, 1970.
345. Hashimoto, K, Kumakura, S: The pharmacological features of the coronary, renal, mesenteric and femoral arteries. *Jpn J Physiol*, 15: 540-551, 1965.
346. Grant, R: Physiological effects of heat and cold. *Annu Rev Physiol*, 13: 75-98, 1951.
347. McIntyre, CA, Williams, BC, Lindsay, RM, McKnight, JA, Hadoke, PW: Preservation of vascular function in rat mesenteric resistance arteries following cold storage, studied by small vessel myography. *Br J Pharmacol*, 123: 1555-1560, 1998.
348. Jia, L, Li, X, Shao, C, Wei, L, Li, M, Guo, Z, Liu, Z, Gao, Y: Using an isolated rat kidney model to identify kidney origin proteins in urine. *PLoS One*, 8: e66911, 2013.
349. Guyton, AC, Granger, HJ, Taylor, AE: Interstitial fluid pressure. *Physiol Rev*, 51: 527-563, 1971.
350. Dupuis, DS, Schroder, RL, Jespersen, T, Christensen, JK, Christophersen, P, Jensen, BS, Olesen, SP: Activation of KCNQ5 channels stably expressed in HEK293 cells by BMS-204352. *Eur J Pharmacol*, 437: 129-137, 2002.
351. Kitazawa, T, Kitazawa, K: Size-dependent heterogeneity of contractile Ca<sup>2+</sup> sensitization in rat arterial smooth muscle. *J Physiol*, 590: 5401-5423, 2012.
352. Dippold, RP, Fisher, SA: Myosin phosphatase isoforms as determinants of smooth muscle contractile function and calcium sensitivity of force production. *Microcirculation*, 21: 239-248, 2014.
353. Greene, DL, Kang, S, Hoshi, N: XE991 and Linopirdine Are State-Dependent Inhibitors for Kv7/KCNQ Channels that Favor Activated Single Subunits. *J Pharmacol Exp Ther*, 362: 177-185, 2017.
354. Grissmer, S, Nguyen, AN, Aiyar, J, Hanson, DC, Mather, RJ, Gutman, GA, Karmilowicz, MJ, Auperin, DD, Chandy, KG: Pharmacological characterization of five cloned voltage-gated K<sup>+</sup> channels, types Kv1.1, 1.2, 1.3, 1.5, and 3.1, stably expressed in mammalian cell lines. *Mol Pharmacol*, 45: 1227-1234, 1994.
355. Jespersen, T, Grunnet, M, Olesen, S-P: The KCNQ1 potassium channel: from gene to physiological function. *Physiology*, 20: 408-416, 2005.

356. McCrossan, ZA, Abbott, GW: The MinK-related peptides. *Neuropharmacology*, 47: 787-821, 2004.
357. Burnett, JC, Jr., Granger, JP, Opgenorth, TJ: Effects of synthetic atrial natriuretic factor on renal function and renin release. *Am J Physiol*, 247: F863-866, 1984.
358. Aalkjaer, C, Mulvany, MJ, Nyborg, NC: Atrial natriuretic factor causes specific relaxation of rat renal arcuate arteries. *Br J Pharmacol*, 86: 447-453, 1985.
359. Marrachelli, VG, Centeno, JM, Miranda, I, Castello-Ruiz, M, Burguete, MC, Jover-Mengual, T, Salom, JB, Torregrosa, G, Miranda, FJ, Alborch, E: Diabetes impairs the atrial natriuretic peptide relaxant action mediated by potassium channels and prostacyclin in the rabbit renal artery. *Pharmacol Res*, 66: 392-400, 2012.
360. Matsumoto, T, Watanabe, S, Yamada, K, Ando, M, Iguchi, M, Taguchi, K, Kobayashi, T: Relaxation Induced by Atrial Natriuretic Peptide Is Impaired in Carotid but Not Renal Arteries from Spontaneously Hypertensive Rats Due to Reduced BKCa Channel Activity. *Biol Pharm Bull*, 38: 1801-1808, 2015.
361. Zhang, S, Geng, X, Zhao, L, Li, J, Tian, F, Wang, Y, Fan, R, Feng, N, Liu, J, Cheng, L, Pei, J: Cardiovascular and renal effect of CNAAC: An innovatively designed natriuretic peptide. *Eur J Pharmacol*, 761: 180-188, 2015.
362. Sakurada, S, Takuwa, N, Sugimoto, N, Wang, Y, Seto, M, Sasaki, Y, Takuwa, Y: Ca<sup>2+</sup>-dependent activation of Rho and Rho kinase in membrane depolarization-induced and receptor stimulation-induced vascular smooth muscle contraction. *Circ Res*, 93: 548-556, 2003.
363. Sato, K, Ozaki, H, Karaki, H: Changes in cytosolic calcium level in vascular smooth muscle strip measured simultaneously with contraction using fluorescent calcium indicator fura 2. *J Pharmacol Exp Ther*, 246: 294-300, 1988.
364. Wilson, DP, Sutherland, C, Walsh, MP: Ca<sup>2+</sup> activation of smooth muscle contraction: evidence for the involvement of calmodulin that is bound to the triton insoluble fraction even in the absence of Ca<sup>2+</sup>. *J Biol Chem*, 277: 2186-2192, 2002.
365. Mita, M, Tanaka, H, Yanagihara, H, Nakagawa, J, Hishinuma, S, Sutherland, C, Walsh, MP, Shoji, M: Membrane depolarization-induced RhoA/Rho-associated kinase activation and sustained contraction of rat caudal arterial smooth muscle involves genistein-sensitive tyrosine phosphorylation. *J Smooth Muscle Res*, 49: 26-45, 2013.
366. Mills, RD, Mita, M, Walsh, MP: A role for the Ca(2+)-dependent tyrosine kinase Pyk2 in tonic depolarization-induced vascular smooth muscle contraction. *J Muscle Res Cell Motil*, 36: 479-489, 2015.
367. Nakamura, A, Hayashi, K, Ozawa, Y, Fujiwara, K, Okubo, K, Kanda, T, Wakino, S, Saruta, T: Vessel- and vasoconstrictor-dependent role of rho/rho-kinase in renal microvascular tone. *J Vasc Res*, 40: 244-251, 2003.
368. Davis, MJ, Hill, MA: Signaling mechanisms underlying the vascular myogenic response. *Physiol Rev*, 79: 387-423, 1999.
369. Minneman, KP: Alpha 1-adrenergic receptor subtypes, inositol phosphates, and sources of cell Ca<sup>2+</sup>. *Pharmacol Rev*, 40: 87-119, 1988.
370. Kirton, CA, Loutzenhiser, R: Alterations in basal protein kinase C activity modulate renal afferent arteriolar myogenic reactivity. *Am J Physiol*, 275: H467-475, 1998.
371. Hillhouse, EW, Grammatopoulos, DK: The molecular mechanisms underlying the regulation of the biological activity of corticotropin-releasing hormone receptors: implications for physiology and pathophysiology. *Endocr Rev*, 27: 260-286, 2006.

372. Wiley, KE, Davenport, AP: CRF2 receptors are highly expressed in the human cardiovascular system and their cognate ligands urocortins 2 and 3 are potent vasodilators. *Br J Pharmacol*, 143: 508-514, 2004.
373. Adao, R, Santos-Ribeiro, D, Rademaker, MT, Leite-Moreira, AF, Bras-Silva, C: Urocortin 2 in cardiovascular health and disease. *Drug Discov Today*, 20: 906-914, 2015.
374. Kageyama, K, Furukawa, K, Miki, I, Terui, K, Motomura, S, Suda, T: Vasodilative effects of urocortin II via protein kinase A and a mitogen-activated protein kinase in rat thoracic aorta. *J Cardiovasc Pharmacol*, 42: 561-565, 2003.
375. Parkes, DG, Weisinger, RS, May, CN: Cardiovascular actions of CRH and urocortin: an update. *Peptides*, 22: 821-827, 2001.
376. Abdelrahman, AM, Syyong, HT, Tjahjadi, AA, Pang, CC: Analysis of the mechanism of the vasodepressor effect of urocortin in anesthetized rats. *Pharmacology*, 73: 175-179, 2005.
377. Chen, J, Tao, J, Zhang, R, Xu, Y, Soong, T, Li, S: Urocortin inhibits mesenteric arterial remodeling in spontaneously hypertensive rats. *Peptides*, 30: 1117-1123, 2009.
378. Leitch, IM, Boura, AL, Botti, C, Read, MA, Walters, WA, Smith, R: Vasodilator actions of urocortin and related peptides in the human perfused placenta in vitro. *J Clin Endocrinol Metab*, 83: 4510-4513, 1998.
379. Chen, Z-W, Huang, Y, Yang, Q, Li, X, Wei, W, He, G-W: Urocortin-induced relaxation in the human internal mammary artery. *Cardiovasc Res*, 65: 913-920, 2005.
380. Sanz, E, Monge, L, Fernandez, N, Martinez, MA, Martinez-Leon, JB, Dieguez, G, Garcia-Villalon, AL: Relaxation by urocortin of human saphenous veins. *Br J Pharmacol*, 136: 90-94, 2002.
381. Walczewska, J, Dzieza-Grudnik, A, Siga, O, Grodzicki, T: The role of urocortins in the cardiovascular system. *J Physiol Pharmacol*, 65: 753-766, 2014.
382. Yao, X, He, GW, Chan, FL, Lau, CW, Tsang, SY, Chen, ZY, Huang, Y: Endothelium-dependent and -independent coronary relaxation induced by urocortin. *J Card Surg*, 17: 347-349, 2001.
383. Sanz, E, Fernández, N, Monge, L, Climent, B, Diéguez, G, García-Villalón, AL: Relaxation by urocortin of rat renal arteries: effects of diabetes in males and females. *Cardiovasc Res*, 58: 706-711, 2003.
384. Sanz, E, Monge, L, Fernández, N, Climent, B, Diéguez, G, Garcia-Villalón, AL: Mechanisms of relaxation by urocortin in renal arteries from male and female rats. *Br J Pharmacol*, 140: 1003-1007, 2003.
385. Huang, Y, Chan, FL, Lau, CW, Tsang, SY, Chen, ZY, He, GW, Yao, X: Roles of cyclic AMP and Ca<sup>2+</sup>-activated K<sup>+</sup> channels in endothelium-independent relaxation by urocortin in the rat coronary artery. *Cardiovasc Res*, 57: 824-833, 2003.
386. Chan, Y, Yao, X, Lau, C, Chan, F, He, G, Bourreau, J-P, Huang, Y: The relaxant effect of urocortin in rat pulmonary arteries. *Regul Pept*, 121: 11-18, 2004.
387. Lubomirov, L, Gagov, H, Petkova-Kirova, P, Duridanova, D, Kalentchuk, VU, Schubert, R: Urocortin relaxes rat tail arteries by a PKA-mediated reduction of the sensitivity of the contractile apparatus for calcium. *Br J Pharmacol*, 134: 1564-1570, 2001.
388. Seçilmis, MA, Özü, ÖY, Emre, M, Büyükafsar, K, Kiroglu, OE, Ertug, P, Karatas, Y, Önder, S, Singirik, E: Urocortin induces endothelium-dependent vasodilatation and hyperpolarization of rat mesenteric arteries by activating Ca<sup>2+</sup>-activated K<sup>+</sup> channels. *Tohoku J Exp Med*, 213: 89-98, 2007.

389. Smani, T, Domínguez-Rodríguez, A, Hmadcha, A, Calderón-Sánchez, E, Horrillo-Ledesma, A, Ordóñez, A: Role of Ca<sup>2+</sup>-independent phospholipase A2 and store-operated pathway in urocortin-induced vasodilatation of rat coronary artery. *Circ Res*, 101: 1194-1203, 2007.

## 7 APPENDIX

Table 13: Statistics for myography experiments following concentration-response relationship protocols (see: Table 3)

Figure:	Experiment description:	n	Drug added:					
31	CON vs. RETI/ANP vs. MIX	6		CON/RETI	CON/ANP	RETI/MIX	ANP/MIX	
			1. CRR	none	>0,9999	0,4491	0,4491	>0,9999
			2. CRR	solvent	0,6492	0,8726	0,5567	>0,9999
			3./4. CRR	RETI/ANP/MIX	<b>0,0008</b>	<b>0,0134</b>	<b>0,0088</b>	<b>0,0329</b>
32	CON vs. R-L3/ANP vs. MIX	6		CON/R-L3	CON/ANP	R-L3/MIX	ANP/MIX	
			1. CRR	none	>0,9999	0,8305	0,8305	>0,9999
			2. CRR	solvent	>0,9999	0,4212	0,3453	0,7582
			3./4. CRR	R-L3/ANP/MIX	<b>0,0001</b>	<b>&lt;0,0001</b>	<b>0,0016</b>	<b>&lt;0,0001</b>
33	CON vs. HMR/ANP(-7) vs. MIX (in the presence of R-L3)	6		CON/HMR	CON/ANP	HMR/MIX	ANP/MIX	
			1.CRR	none	0,4937	0,8551	0,6333	0,6063
			2.CRR	HMR	0,468	0,7239	0,5044	0,2544
			3.CRR	R-L3 (all), ANP (-7)	<b>0,0008</b>	<b>&lt;0,0001</b>	<b>&lt;0,0001</b>	<b>0,0027</b>
34	CON vs. HMR/ANP(3-8) vs. MIX (in the presence of R-L3)	6		CON/HMR	CON/ANP	HMR/MIX	ANP/MIX	
			1.CRR	none	0,4937	0,8551	0,6333	0,6063
			2.CRR	HMR	0,468	0,8512	0,7622	0,2109
			3.CRR	R-L3 (all), ANP (3-8)	<b>0,0004</b>	<b>0,0147</b>	<b>0,0003</b>	<b>0,0155</b>
44	CON vs. XE/URO vs. MIX	10		CON/XE	CON/URO	XE/MIX	URO/MIX	
			1. CRR	none	0,7756	0,633	0,8721	0,7674
			2. CRR	XE	<b>0,0081</b>	0,7726	0,7981	<b>0,0465</b>
			3. CRR	URO	<b>0,0022</b>	<b>&lt;0,0001</b>	<b>&lt;0,0001</b>	<b>0,0207</b>
45	CON vs. RETI/URO vs. MIX	9		CON/RETI	CON/URO	RETI/MIX	URO/MIX	
			1. CRR	none	>0,9999	0,7109	0,7109	>0,9999
			2. CRR	solvent	0,8267	0,8188	0,5943	0,9005
			3./4. CRR	RETI/URO/MIX	<b>&lt;0,0001</b>	<b>0,0001</b>	<b>0,0003</b>	<b>0,0022</b>
46	CON vs. R-L3/Uro vs. MIX	9		CON/R-L3	CON/URO	R-L3/MIX	URO/MIX	
			1. CRR	none	>0,9999	0,6884	0,6884	>0,9999
			2. CRR	solvent	>0,9999	0,6674	0,6674	>0,9999
			3./4. CRR	R-L3/URO/MIX	<b>&lt;0,0001</b>	<b>0,0041</b>	<b>0,0258</b>	<b>0,0014</b>
47	CON vs. HMR/URO(-7) vs. MIX (in the presence of R-L3)	9		CON/HMR	CON/URO	HMR/MIX	URO/MIX	
			1. CRR	none	0,7474	0,6884	0,99	0,5155
			2. CRR	HMR	0,3285	0,2816	0,8359	0,8287
			3. CRR	URO (-7)	0,6468	0,0001	0,0005	0,7392
			4. CRR	R-L3 (all)	<b>0,0055</b>	<b>0,002</b>	<b>0,0014</b>	<b>0,0263</b>

Two-way repeated-measures ANOVA was used for statistical analysis. ANP = atrial natriuretic peptide; CON = control; CRR = concentration-response relationship; HMR = HMR1556; MIX = application of both drugs; RETI = Retigabine; URO = Urocortin; XE = XE991;

Table 14: Statistics for myography experiments following precontraction protocols (see: Table 4 and Table 5)

Figure:	Experiment description:	Drug added:				
20 – 25	Retigabine precontraction		CON/XE	CON/HMR	LO/HI	
			(n = 9)	(n = 9)	(n = 9)	
		1. CRR	none	0,7764	0,6431	0,3889
		1. PRC	solvent	0,8335	0,0337	0,4458
		2. PRC	Retigabine	<b>0,0018</b>	0,8484	0,4895
26 – 30	R-L3 precontraction		CON/XE	CON/HMR	LO/HI	
			(n = 10)	(n = 10)	(n = 10)	
		1. CRR	none	0,6597	0,6182	0,7188
		1. PRC	solvent	0,4920	0,0812	0,6268
		2. PRC	R-L3	<b>&lt;0,0001</b>	<b>0,0001</b>	0,6536
35 – 43	ANP precontraction		KCl/Mx	ALL/no XE	HMR/XE	
			(n = 13)	(n = 14)	(n = 8)	
		1. CRR	none	0,7303	0,1559	0,8377
		1. PRC	solvent	0,7471	0,0826	0,6240
		2. PRC	ANP	<b>0,0075</b>	0,3518	0,4612
48 – 56	Urocortin precontraction		KCl/Mx	ALL/no XE	HMR/XE	
			(n = 12)	(n = 10)	(n = 8)	
		1. CRR	none	0,1103	0,7383	0,9027
		1. PRC	solvent	0,2962	0,3119	0,2363
		2. PRC	Urocortin	<b>0,0010</b>	0,2586	0,1637

Two-way repeated-measures ANOVA was used for statistical analysis. ALL = precontraction induced by all K<sup>+</sup> channel blockers; ANP = atrial natriuretic peptide; CON = control; CRR = concentration-response relationship; HI = high level of Methoxamine-induced precontraction; HMR = HMR1556; no XE = precontraction induced by all K<sup>+</sup> channel blockers without XE991; KCl = KCl-induced precontraction; LO = low level of Methoxamine-induced precontraction; MIX = application of both drugs; Mx = Methoxamine-induced precontraction; PRC = precontraction curve; URO = Urocortin; XE = XE991;

## 8 CURRICULUM VITAE

### PERSONALIEN

Name und Vorname: Felix Stocker  
Geburtsdatum: 27.03.1992  
Geburtsort: Berchtesgaden  
Familienstand: ledig  
Vater: Andreas Stocker  
Mutter: Dorothee Reuter-Stocker

### SCHULISCHER WERDEGANG

09/2002 – 07/2008 Europäisches Gymnasium Berchtesgaden  
08/2008 – 07/2009 Bourne High School, Massachusetts, USA  
08/2009 – 05/2011 Europäisches Gymnasium Berchtesgaden  
02.05.2011 Abitur

### UNIVERSITÄRER WERDEGANG

WS 2011/12 Beginn des Studiums der Humanmedizin an der Universität Heidelberg  
04.09.2013 1. Abschnitt der Ärztlichen Prüfung  
13.10.2016 2. Abschnitt der Ärztlichen Prüfung  
14.11.2018 3. Abschnitt der Ärztlichen Prüfung

### BERUFLICHER WERDEGANG

seit 04/2019 Assistenzarzt in der Klinik und Poliklinik für Chirurgie,  
Klinikum rechts der Isar der Technischen Universität München

## 9 DANKSAGUNG

Mein erster Dank gilt Prof. med. Rudolf Schubert, für die Überlassung des interessanten Themas, die Möglichkeit, dieses in einem professionellen Umfeld zu bearbeiten, und die exzellente Betreuung in allen Aspekten von der Versuchsdurchführung bis zur Verfassung der Dissertationsschrift.

Einen weiteren Dank möchte ich Stephanie Braun, Dr. Nadine Schmid und Dr. Olga Zavaritskaya aussprechen, für ihre erstklassige Einarbeitung und Mitbetreuung. Für die immer angenehme und bereichernde Zusammenarbeit im Labor danke ich meinen Laborgenossen und Studienkollegen sehr herzlich. Besonders danken möchte ich unserer Laborleiterin Frau Camela Jost, für ihre tatkräftige Hilfe bei den vielen kleinen und großen praktischen Hürden.

Ein großer Dank geht an meine Familie, für ihre Unterstützung in all den Herausforderungen, die eine solche Arbeit außerhalb des Fachlichen mit sich bringt.